Peat compaction in deltas

Nederlandse Geografische Studies / Netherlands Geographical Studies

ISSN 0169-4839

Netherlands Geographical Studies 395

Peat compaction in deltas

Implications for Holocene delta evolution

Sanneke van Asselen

Utrecht 2010

Koninklijk Nederlands Aardrijkskundig Genootschap
Faculteit Geowetenschappen Universiteit Utrecht

This publication is identical to a dissertation submitted in partial fulfilment of the requirements for the degree of Doctor of Philosophy at Utrecht University, The Netherlands.
The public defence of the dissertation took place on June 16, 2010.

Promotores

Prof. dr. H. Middelkoop	Utrecht University
Prof. dr. E.A. Koster	Utrecht University

Co-promotor

Dr. E. Stouthamer	Utrecht University

Examination committee

Prof. dr. N.D. Smith	University of Nebraska-Lincoln
Prof. dr. M.R. Gibling	Dalhousie University
Prof. dr. S.B. Kroonenberg	Delf University of Technology
Prof. dr. M.J. Wassen	Utrecht University
Dr. B. Makaske	Wageningen University

ISBN 978-90-6809-438-1

Graphic design, cartography and figures:
GeoMedia (Faculty of Geosciences, Utrecht University)

Cover: The Cumberland Marshes in Canada. Photo by Sanneke van Asselen.

Printed in The Netherlands by A-D Druk b.v. – Zeist

Contents

Figures

Tables

Preface

When I started this PhD research, in fact, I didn't know much about deltas and peat compaction. Until then, I had mainly done research in (Alpine) geomorphology and soil erosion. I was surprised that my new colleagues could actually see relief in seemingly flat grasslands in the distal part of the Rhine-Meuse delta in The Netherlands. But, during the course of my PhD research, the same people have increasingly made me enthusiastic for delta research, and have taught me a lot. Without them, I could never have finished this thesis, for which I am very grateful.

First of all, I would like to thank my co-promotor Esther Stouthamer. Esther, I was your first PhD candidate to supervise, and in my opinion you've done a great job! Besides reviewing all of my manuscripts, discussing results and research ideas, giving support for organizing and carrying out fieldworks, etc., we could also talk about other things in life, which I much appreciated. My two promotores Ward Koster and Hans Middelkoop are also thanked for carefully reviewing manuscripts and fruitful discussions.

Of course, many thanks to my roommates. I have spent most of the time with Nelleke van Asch sitting opposite of me. Thanks for the many laughs (I will certainly miss those!), discussions and for putting things into perspective, the way you can do so nicely ('boeiend'). My other roommates Ate Visser, and later on Joachim Rozemeijer, are also thanked a lot for their enjoyable company. You were great roommates!

But also my other colleagues, especially from the first floor where the majority of the 'Gruppo Fluvial' had their office, are thanked for their pleasant company and willingness to help out with anything. Ingwer Bos, who I met in the first year of the study Physical Geography at the University of Amsterdam, many thanks for your always great company and help while we were studying, doing many fieldworks together, during our PhD, but also in life besides study and work. Gilles Erkens, well-dressed smooth talker from Amsterdam, I have very much enjoyed to work (and do things besides work) with you. Kim Cohen, thanks for all of your help and giving asked or unasked, but always helpful, advice. Wim Hoek, always running around doing a million things at the same time, but always willing to help out or make a (sometimes..) funny joke, many thanks for that! I would like to thank Nelleke, Joachim and Marc Hijma for all the walks and nice conversations in the botanical garden during lunch time. Furthermore, I would specifically like to mention Henk Berendsen, Esther Stouthamer, Marc Gouw, Roy Frings, Willem Toonen and Jan Peeters, all members of the 'Gruppo Fluvial'. All other colleagues from the Department of Physical Geography are also thanked for all conversations about nearly anything in the coffee corner. You all contributed to a very pleasant working atmosphere, which I much appreciate.

This research involved quite some fieldwork, which I could not have done alone. First a special word for Chris Roosendaal. Chris, you have helped me during each of my fieldworks and we have even devised a new peat sampler together (and published an article!). Many thanks for this, and for your optimistic view of life and great humor, which brought many nice moments. Furthermore, I wish to thank Ingwer, Willem, Kim, Esther, Wim, Joachim, Gary Carriere and Norman Smith, all of whom have helped me enormously during fieldworks.

Data collected during fieldworks were analyzed in the laboratory. For this I was supported especially by Wim, for which I am very thankful. Hanneke Bos and Nelleke are thanked for selecting botanical macrofossils for radiocarbon dating. Evert Wielsma helped with sampling two peat cores from the Rhine-Meuse delta.

Theo van Asch, Gerard Kruse, Henk Kruse, Evert den Haan and Meindert Van are thanked for their input regarding the geotechnical aspects of this research. Peat is not an easy matter, but the many discussions with you, and lessons I learned from you, have helped me a lot with understanding (a bit) the geotechnical behavior of peat.

I could not have done the modeling part of this research without the help of Derek Karssenberg, thanks for that! Also, Kor de Jong, Theo van Asch and Gerard Kruse are thanked for setting up an earlier version of the new peat compaction model.

Besides my colleagues I would like to thank my family, that is, Otto, Corrie, Bram and Marieke. You have always been there for me and have always supported me. Not only with my PhD research, but with everything that comes in life. For that, I am very grateful. But also my family-in-law, Lonneke and Nuno, and of course my nephew Marnix, thank you for all the good and valuable times we have had (and will have) together!

Finally, I wish to thank everyone that has given me some distraction from this research, which was oh-so important for me. Dear friends, thanks for drinking a glass of whine, or a cup of tea, somewhere in the Woestduinstraat or elsewhere in Amsterdam, while having conversations about everything. Thanks for making home-made pizza while 'complaining' about life, or go ice-skating during working-time in the Botshol. And of course, I have had a great time during tour-skiing trips in the Alps and in Norway, including the never-to-forget trips to the mountains in (sometimes) crappy cars or vans. I very much enjoyed cycling tours, climbing and mountaineering trips in the Alps, or just for a weekend in Belgium or Germany. And not to forget making travels in beautiful far-away countries, lying awake at night in a tent with bears walking around, or drinking maté somewhere in South America. I loved it all, many thanks! And enjoy reading the remaining part of this thesis!

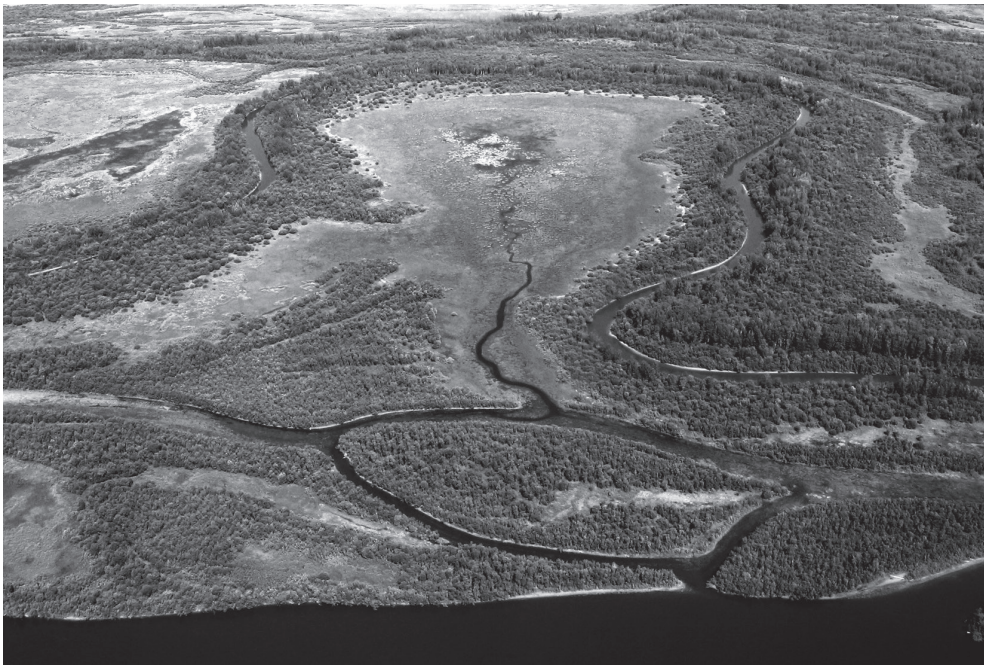

1 General introduction

1.1 Context

The formation and evolution of deltas is basically controlled by sediment supply and the provision of accommodation space, which are both variable in time and space. The balance between these two main controls determines the tendency to either delta progradation or drowning, and is affected by numerous processes, making deltas highly dynamic systems (Day and Giosan, 2008). Sediment supply is affected by factors controlling river discharge and sediment yield, such as climate, human impact and erodibility of sediments and rocks in the upstream drainage basin of a river. The provision of accommodation space is controlled by the rate of base-level rise (e.g., forced by eustatic sea-level rise) and land subsidence due to tectonics, isostasy and sediment compaction. Many deltaic successions include substantial amounts of peat, which is the most compressible soil type. Therefore, peat compaction is expected to be an important contributor to total subsidence in deltas, and therewith, to the provision of accommodation space. This thesis focuses on subsidence due to natural compaction of peat in fluvial-deltaic settings.

By local and/or regional provision of additional accommodation space, subsidence due to peat compaction likely influences temporal and spatial sedimentation patterns in deltas, and with that, the natural evolution of deltaic systems. Understanding such processes is essential for interpreting alluvial archives and for predicting delta evolution. To study the peat compaction process in fluvial-deltaic settings it is necessary to collect spatial and temporal field data from present-day deltas containing peat, which are formed during the Holocene. Hence, Holocene timescales should be considered when studying the effect of peat compaction in deltas. Moreover, it is important to study subsidence due to peat compaction because many deltas are densely populated (close to half a billion people currently live on or near deltas) and are increasingly threatened by pressures that enhance the risk of delta drowning, such as artificial drainage, hydrocarbon and groundwater extraction, reduced sediment supply and eustatic sea-level rise (e.g., Ericson et al., 2006; Syvitski, 2008; Blum and Roberts, 2009; Syvitski et al., 2009). A better understanding of processes leading to land subsidence, such as peat compaction, will support the development of sustainable delta management plans. These are indispensable for protecting delta systems, and therewith, their inhabitants and their valuable wetland ecosystems that usually support a high biodiversity.

Furthermore, Holocene deltas may be used as analogues of ancient deltaic sequences. The alluvial architecture of these ancient sequences is likely influenced by peat compaction, through its control on sedimentation patterns and by post-depositional distortion of the original stratigraphy. This is important information for e.g., the exploration of natural resources, and for the interpretation of sedimentary archives regarding past changes in the amount of accommodation space, which influences delta formation (Diessel et al., 2000; Gibling et al., 2004; Davies et al., 2005).

1.2 Problem definition

In spite of the potentially large effects of subsidence due to peat compaction on Holocene delta evolution and alluvial architecture (e.g., Michaelsen et al., 2000; Rajchl and Uličný, 2005), they have never been studied in detail. There are only few field studies that have estimated

local amounts of subsidence due to peat compaction. These estimates are averaged over long time periods, often millennia (e.g., Bloom, 1964; Haslett et al., 1998; Törnqvist et al, 2008). Alternatively, compaction rates are estimated using empirical and numerical models (e.g., Den Haan, 1994; Haslett et al., 1998; Kruse, 1998; Paul and Barras, 1998; Sheldon and Retallack, 2001; Massey et al., 2006; Meckel et al., 2007). Especially numerical models are valuable tools for understanding and predicting peat compaction through time in Holocene deltaic sequences of various compositions. Existing peat compaction models are however mostly inadequate for considering Holocene timescales and the spatial complexity of deltaic successions. An important problem in current peat compaction modeling is the estimation of geotechnical parameters of different types of peat. The loose and heterogenic character of peat requires special sampling devices that induce minimum disturbance of the peat sample, and enable extracting relatively large samples (Lefebvre et al., 1984). However, geotechnical parameters of peat are usually estimated based on short-duration compression tests and laboratory analysis of few small-in-volume peat samples in an already compressed state. Such analyses are unlikely to be applicable for accurately modeling peat compaction on Holocene timescales. Another shortcoming of current peat compaction models is that the applied empirical relations, for example between depth and porosity, are mostly derived from ancient deeply-buried sediments (Sclater and Christie, 1980). Such relations are likely not applicable to Holocene peat, which occurs at shallow depths and has very distinctive geotechnical properties, e.g. regarding the permeability and compressibility, compared to clastic sediments (Mesri and Ajlouni, 2007). Finally, time-dependent compaction, independently of loading conditions, is often not included in current compaction models, whereas this is considered to cause substantial compaction in peat layers (Den Haan, 1994), and therewith additional accommodation space.

Hence, there is a need for a detailed field-based investigation of temporal and spatial patterns in the amount and rate of subsidence due peat compaction in deltas, and factors influencing such patterns should be specified. Such information can subsequently be used to evaluate effects of peat compaction on delta evolution and to improve peat compaction modeling.

1.3 Objectives and approach

Previous studies in the fluvial-dominated part of the Holocene Rhine-Meuse delta, which is one of the main study areas of this research, have resulted in detailed palaeogeographic reconstructions of Holocene delta evolution (Berendsen and Stouthamer, 2001). Additionally, factors controlling fluvial style (Törnqvist, 1993a; Makaske, 1998), alluvial architecture (Gouw, 2007) and the avulsion history (Stouthamer, 2001) have been studied in detail. Furthermore, the influence of different factors, such as tectonics (Cohen, 2003) and sediment supply (Erkens, 2009), on delta evolution have been investigated. In these studies, peat compaction has been acknowledged to be another important factor controlling the evolution of the Rhine-Meuse delta, which contains substantial amounts of peat, for example because it creates additional accommodation space for fluvial deposition. But, this has never been studied in detail. Above mentioned studies offered a good starting point to quantify peat compaction and evaluate effects of peat compaction on Holocene delta evolution, as were the main objectives of this research. Furthermore, this research contributes to improving existing 3D process-based alluvial

architecture models (e.g., Karssenberg and Bridge, 2008), which presently do not accurately describe effects of peat compaction.

More specifically, three objectives have been formulated:

(1) Quantify the amount and rate of subsidence due to peat compaction in Holocene alluvial sequences based on field data.
(2) Develop a numerical peat compaction model, calibrated with field data, to predict temporal and spatial variations in subsidence due to peat compaction within deltas.
(3) Evaluate the effect of subsidence due to peat compaction on spatial and temporal sedimentation patterns in deltaic settings, and therewith on delta evolution.

To achieve these objectives, first, literature was reviewed to give a detailed overview of the peat compaction process, presumed and potential effects of peat compaction on delta evolution, and methods to measure subsidence due to peat compaction based on field data and models (chapter 2). Next, field studies were carried out in the Cumberland Marshes (Canada), the Rhine-Meuse delta (The Netherlands) and the Biebrza National Park (Poland; Fig. 1.1). One of the used field methods required sampling uncompacted surface peat from field settings, for which a new peat sampler was devised (chapter 3). The study area in the Cumberland Marshes has experienced minimum human influence, and was recently (~135 years ago) invaded by an avulsion of the Saskatchewan River, which partly covered a Late Holocene fen peat layer with an alluvial

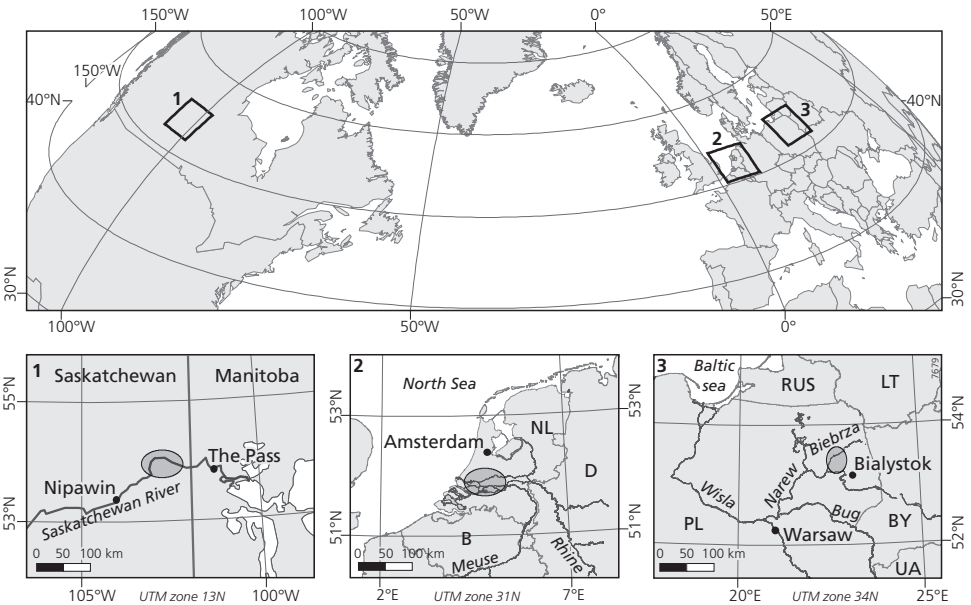

Figure 1.1. Locations of the three study areas (shaded areas in detail maps below): (1) the Cumberland Marshes (Canada), (2) the Rhine-Meuse delta (The Netherlands), and (3) the Biebrza National Park (Poland).

sediment layer of variable thickness (up to ~3 m; Smith et al., 1989, 1998). This setting allowed studying natural peat compaction on relatively short timescales of decades to centuries (chapter 4). Peat compaction occurring on millennial timescales were studied in the Rhine-Meuse delta, for which an extensive field dataset was already available (e.g., Berendsen and Stouthamer, 2001; chapter 5). Care should be taken regarding human influences in this area, which at present is largely cultivated. For example, groundwater table lowering for land reclamation has caused peat oxidation and additional peat compaction. The Biebrza National Park offered an excellent setting to sample different types of uncompacted surficial fen peat, of the same type as occur in the subsurface of the Rhine-Meuse delta (chapters 3 and 5).

Field data were used to (1) quantify the amount and rate of subsidence due to peat compaction in different deltaic settings, with associated boundary conditions, at different temporal scales, essentially based on dry bulk density and organic-matter content measurements of compacted and uncompacted peat, and based on the reconstruction of initial levels of peat formation (methods described in chapter 2-5), and (2) determine the most important factors influencing peat compaction in deltaic settings. Furthermore, field data obtained from the Cumberland Marshes were used to calibrate a new numerical peat compaction model (chapter 6). This model was used to predict spatial and temporal variations in the amount and rate of subsidence due to peat compaction in different Holocene deltaic settings. Altogether, field data obtained from the different study areas, and results of the modeling study, were used to evaluate effects of subsidence due to peat compaction on spatial and temporal sedimentation patterns in deltaic environments. The main results of chapter 2-6, its implications, and directions for future research are synthesized in chapter 7.

2 Effects of peat compaction on delta evolution: a review on processes, responses, measuring and modeling

Van Asselen, S., Stouthamer, E. and Van Asch, Th.W.J., 2009. Effects of peat compaction on delta evolution: a review on processes, responses, measuring and modeling. Earth Science Reviews 92, 35-51. Reprinted with permission (Elsevier B.V.).

Abstract

Peat is most compressible of all natural soils. Compaction of peat layers potentially leads to substantial amounts of land subsidence. Peat is common in many distal parts of Holocene deltas, which are often densely populated. It is known that land subsidence due to peat compaction may have serious societal implications in such areas, since it may cause damage to construction works and lead to land inundation. Effects of peat compaction on the natural evolution of deltas are however poorly understood, whereas this might be an important control on delta evolution at both local and regional scales.

The main objective of this paper is to review current knowledge concerning the peat compaction process and its effect on delta evolution in Holocene settings, and to identify gaps in this knowledge. An overview is given regarding: (1) the compaction process, (2) presumed and potential effects of peat compaction on delta evolution, (3) field methods to quantify peat compaction and (4) numerical models to calculate the amount and rate of peat compaction.

Peat compaction and formation influence channel belt elevation, channel belt geometry and channel belt configuration. Last-mentioned aspect mostly concerns the influence of peat compaction on avulsion, which is one of the most important processes controlling delta evolution. Interactions between peat compaction, peat formation and avulsion have seldom been studied and remain unclear, partly because factors such as peat type, organic-matter content, sediment sequence composition and groundwater table fluctuations are so far not taken into account. Peat compaction and formation potentially influence avulsion because (1) a decrease in accommodation space created by peat compaction underneath a channel causes superelevation and/or an increase in lateral migration, (2) the high cohesiveness of peat banks inhibits lateral migration, which increases bed aggradation, decreases sediment transport capacity and hence increases crevassing frequencies, which possibly evolve into an avulsion, although the low regional gradient in peatlands will hinder this, and (3) peat compaction and oxidation in flood basins following groundwater table lowering leads to relief amplification of channel belts. At delta scale, variations in compaction rates might stimulate the occurrence of avulsions. To quantify effects of peat compaction on delta evolution, and to determine the relative importance of different factors involved, field research should be combined with numerical models describing peat compaction and formation. The model should be validated and calibrated with field data.

Keywords: peat compaction, delta evolution, quantifying compaction, numerical compaction models.

2.1 Introduction

The evolution of deltas is largely controlled by (1) sediment supply and discharge, (2) substrate composition and topography, (3) base-level fluctuations, (4) climate and (5) vertical land movements. The last-mentioned process may be due to tectonics, isostasy and compaction of unconsolidated sediments. Compaction is a process by which the porosity of sediment is reduced, and involves micro-biological (e.g., organic matter decay), hydro-chemical (e.g., silica solution, cementation, clay dehydration) and physical processes (e.g., settlement, pore water expulsion), acting at different stages during the vertical accumulation within one system (e.g., Allen, 1999; Fig. 2.1). This paper focuses on physical processes causing compaction, occurring at shallow depths (0-10^1 m below surface) in Holocene fluvial-deltaic settings.

Especially in distal parts of modern deltas, which are often densely populated, peat is common. Because peat has the highest compaction potential of all natural soils, compaction of peat potentially leads to substantial amounts of land subsidence. This may result in many societal implications including damage to construction works and relative sea-level rise causing e.g. coastal wetland loss and land inundation. In areas reclaimed for agriculture or habitation, land inundation often requires artificial lowering of the groundwater table. In such situations, compaction and oxidation of peat above the groundwater table leads to even more land subsidence, and hence, ongoing lowering of the groundwater table is needed to prevent inundation. Groundwater extraction for economic purposes also increases subsidence rates (Abidin et al., 2001; Chen et al., 2003; Ericson et al., 2006; Rodolfo and Siringan, 2006; Teatini et al., 2006).

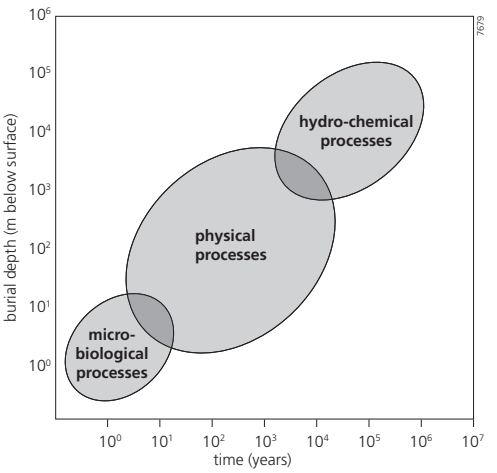

Figure 2.1. Dominant processes leading to compaction at different burial depths and timescales.

The effect of peat compaction on the natural evolution of Holocene fluvial-deltaic environments, and hence on the alluvial architecture, is poorly understood however. Alluvial architecture is defined as the geometry, proportion and spatial distribution of different types of fluvial deposits in an alluvial succession (Allen, 1978; Leeder, 1978). A detailed understanding of the alluvial architecture is vital for e.g. exploration of natural resources (oil, gas, water, metals) and for construction works, which need a solid incompressible substrate. A principal factor controlling alluvial architecture is avulsion (Bridge and Leeder, 1979; Smith et al., 1989; Stouthamer, 2001), which is a natural process by which a channel belt is abandoned in favor of a new course. Although Gouw (2007) recognized compaction as a factor influencing alluvial architecture in the Mississippi delta and the Rhine-Meuse delta, our knowledge about its role is still limited.

The main objective of this paper therefore is to review current knowledge concerning the peat compaction process and its effect on delta evolution at Holocene timescales, and to identify gaps in this knowledge. Therewith, this paper serves as a starting point for future research regarding effects of peat compaction in Holocene fluvial-deltaic settings.

2.1.1 The compaction process

Compaction is one of the most important processes leading to vertical land subsidence, besides processes as isostasy and tectonics (e.g., Kooi and De Vries, 1998; Shennan and Horton, 2002). Also, it is the first step in lithification, the process in which unconsolidated sediments are converted into sedimentary rocks. After the sediments have been compacted, cementation by dissolved minerals transforms loose sediment into rock. In some environments cementation may occur prior to or simultaneously with compaction. In such situations, cementation may influence the compaction potential as pore space is filled with cement, which finally leads to less subsidence due to (mechanical) compaction (Clari and Martire, 1996). In peat however, this will be uncommon.

Compaction does not always lead to *subsidence*. This can be illustrated by considering a situation in which a uniform peat layer overlies an incompressible subsurface (Fig. 2.2). In this scenario, it is assumed that peat growth can keep up with the rate of groundwater table rise. Close to the incompressible surface the pressure exerted by the thick overlying sediment

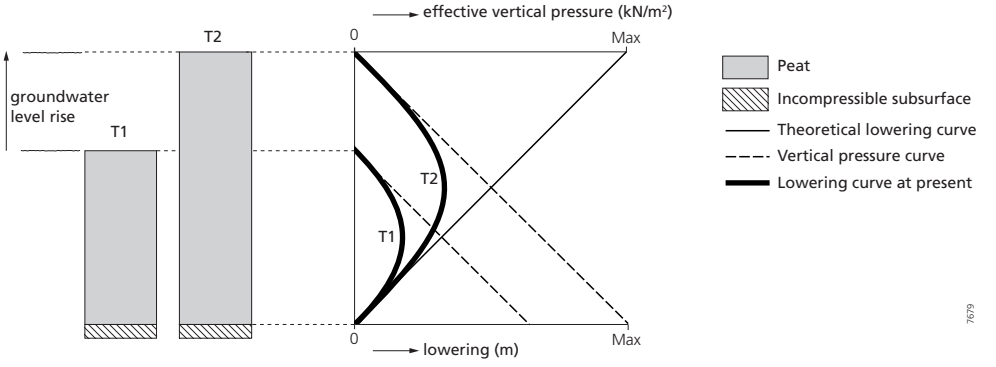

Figure 2.2. Vertical lowering within a sequence, due to peat compaction. For a uniform sediment sequence maximum lowering occurs in the middle of the sequence. It is assumed that peat accumulation keeps up with groundwater level rise.

sequence (expressed in vertical effective stress, see section 2.1.4) is greatest, so the amount of compaction will be high, but the amount of subsidence is close to zero since the underlying substrate is incompressible (assuming there are no other causes of subsidence). For a uniform sediment sequence, the maximum amount of lowering therefore occurs in the middle of the sequence. At this point, an optimum exists for the amount of compressible sediment below this point and the load above this point. A similar lowering profile is described by compaction models of e.g., Pizzuto and Schwendt (1997), Paul and Barras (1998) and Massey et al. (2006), and is shown by field data from the Rhine-Meuse delta (unpublished).

Although physical processes are considered to be most important regarding compaction at Holocene timescales, some biological and chemical processes can be important as well, as is outlined in the following sections.

2.1.2 Compaction due to biological processes

Considering compaction of peat, a significant amount of the volume reduction may occur during the peat formation phase, mainly due to *micro-biological processes*. In principal, peat formation is initiated in wet environments with low mineral input where production of organic matter exceeds decay. The balance between production and decay of organic matter determines the peat accumulation rate. This balance is primarily controlled by the decay rate (largely a result of microbial decomposition), which is influenced by temperature, water content, oxygen supply, microbial and soil animal population and plant material (Charman, 2002). Because these factors are highly variable (spatially and temporally), the production and decay rates, and therewith the rate of volume reduction due to biological processes, are also highly variable (for an overview of peat accumulation, production and decay rates is referred to Charman (2002)). A clear distinction can be made though between rates in the acrotelm (top soil layer which is at least seasonally aerated) and the catotelm (permanently waterlogged): productivity and decay will be highest in the acrotelm, because in this zone conditions for plant growth and soil fauna are most favorable.

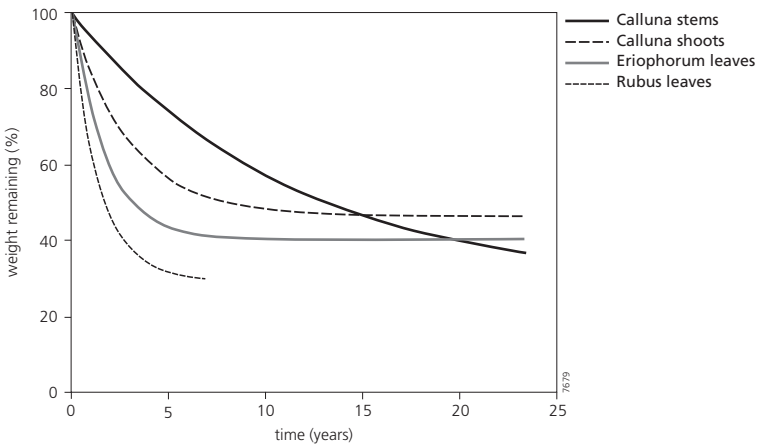

Figure 2.3. Percentage of litter weight remaining with time (from Latter, 1998).

Latter et al. (1998) demonstrated, based on litter bag experiments on a peat bog in upland Britain, that the rate of biomass loss is highest during the first couple of years (Fig. 2.3). The rate depends on the type of litter, although after 23 year the percentage of the initial weight remaining for all litter types was similar (about 40-50%).

2.1.3 Compaction due to chemical processes

Oxidation of organic matter is considered to be an important chemical process leading to volume reduction of a soil layer, and hence to land subsidence (e.g., Gambolati et al., 2003). The amount of biomass loss due to oxidation will be highest in the acrotelm. The depth of this zone may be enlarged by natural or artificial groundwater table lowering. For example, in the Netherlands, floodbasins were artificially drained for agriculture ('polders') since approximately 1000 AD, while the main rivers consecutively were embanked (Fig. 2.4). This has induced significant land subsidence in the floodbasins due to oxidation and compaction, which led to additional groundwater table lowering and hence further land subsidence, causing huge problems in this densely populated area.

Schothorst (1977) studied subsidence of peat soils in the western Netherlands. At different experimental fields, groundwater tables were maintained at different levels, ranging from 0.25 to 1.00 m below the surface. After 6 years surfaces had subsided up to 10 cm (16.7 mm/yr). The highest amount of subsidence occurred at sites where the groundwater table was relatively low. Based on periodic altitude measurements of metal disks placed at regular intervals in vertical peat sections, Schothorst (1977) concluded that on average 65% of the total subsidence was due to shrinkage caused by increased moisture tensions and oxidation of organic matter in the layer

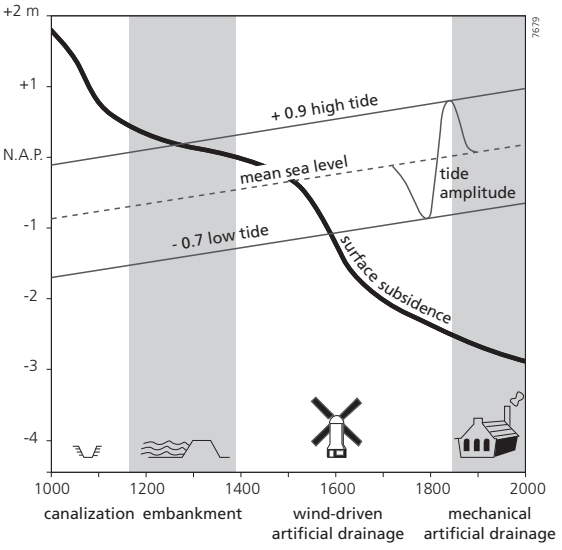

Figure 2.4. Subsidence of a peat surface in The Netherlands as a result of canalization, embankments and artificial drainage since 1000 AD (after Berendsen, 2000).

above groundwater table, and about 35% was attributed to compaction of the layer below the groundwater table due to a decrease of the hydrostatic pressure.

Another study in a Dutch polder (Beuving and Van den Akker, 1996) demonstrated that a groundwater table kept for 25 years at 0.3-0.35 m below the surface led to subsidence of 0.167 m (6.7 mm/year). A groundwater table kept at 0.70 m below the surface for the same time period led to 0.396 m subsidence (15.8 mm/year).

2.1.4 Compaction due to physical processes

Compaction caused by physical processes can be explained by changes in *effective stress* (σ'), which is defined as the difference between the total stress (σ) and the pore water pressure (*u*) (Eq. 2.1; Fig. 2.5; Terzaghi, 1943).

$$\sigma' = \sigma - u \tag{2.1}$$

During compaction, soil particles are packed more closely together which results in a decreased porosity and increased bulk density. Equation 2.1 implies that an increase in total stress and/or a decrease in pore pressure causes an increase in effective stress and hence induces compaction. In natural situations, the total stress imposed on a sediment layer is increased due to loading by active deposition. Pressure induced by heavy machinery and construction works also increase the total stress.

A decrease of the pore water pressure is in natural situations caused by groundwater table lowering e.g., due to sea level lowering or evaporation. A human-induced decrease of the pore water pressure can be the result of artificial groundwater table lowering for land reclamation and withdrawal of drinking water, oil and gas in older deltaic sequences (e.g., Kooi and De Vries, 1998).

The physical compaction process can be subdivided into compression and consolidation (e.g., Paul and Barras, 1998; GeoDelft, 2003). *Compression* is the instantaneous decrease in soil volume due to a stress-dependent rearrangement of the internal sedimentary structure. *Consolidation* is the volume reduction of a soil due to the time-dependent expulsion of overpressured pore water, occurring while the sediment structure approaches a new equilibrium at an extra applied load. In fine-grained sediments with low permeability, such as clay and peat, dissipation of excess pore pressure might take considerable time. The time-duration of the consolidation process is called the *hydrodynamic period* (or primary compression). After this period the soil continues to settle, which is called *secondary compression* (sometimes indicated as *creep*). Causes of secondary compression are not completely understood (GeoDelft, 2003). Possible explanations are (1)

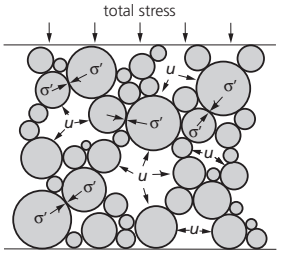

Figure 2.5. Schematic representation of the effective stress (σ' = total stress (σ) – pore water pressure (*u*)) in a soil. The total stress is the weight of the overlying soil and external load per square meter above a certain level in the soil.

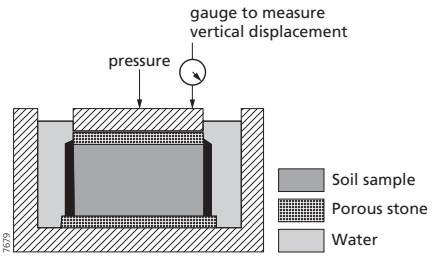

Figure 2.6. Schematic representation of an oedometer, in which one-dimensional compression can be measured, resulting from increasingly applied vertical pressure.

long-term deformation of the thin water layer that coat clay particles, due to high pressures on the soil mass, or (2) expulsion of excess pore water pressure from extremely small voids, which was not expelled during the hydrodynamic period. The start of secondary compression is also a topic of debate; some researchers believe it starts after the hydrodynamic period has ended (e.g., Terzaghi, 1943), while others think it occurs directly after loading and continues for a very long time (e.g., Buisman, 1940; Bjerrum, 1967; for a detailed discussion see Den Haan, 1994).

In geotechnical studies, compressibility characteristics of sediments are usually determined with *oedometer* tests (Fig. 2.6). One of the most important assumptions made in oedometer tests is that there is no lateral strain (only vertical compaction) and that the sediment is considered to be homogeneous.

Soil behaves differently under conditions of loading, unloading and subsequent reloading, which is visualized in the stress-strain figure resulting from an oedometer test (Fig. 2.7). The maximum effective stress a sample has experienced in the soil is called the *preconsolidation stress* (σ'_c). A sample taken from the soil will first experience a load release, following the relaxation curve b-c in Figure 2.7 (gradient C_1). During reloading, settlement will follow the same curve in the opposite direction (recompression curve c-d) until the preconsolidation stress is reached. Soils in conditions represented by these curves are considered to be overconsolidated, which means that the soil has been subject to an effective pressure greater than the pressure of the

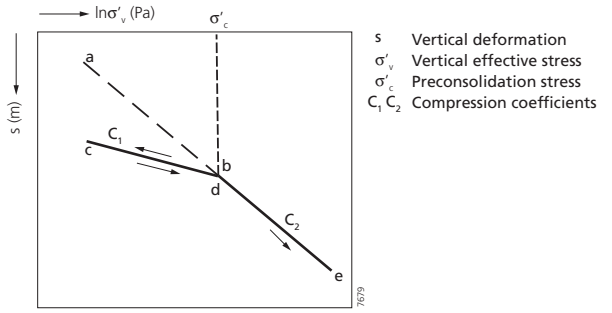

Figure 2.7. Schematized stress-strain diagram (after GeoDelft, 2003). Soils subjected to load release or to reloading follow curve b-c-d, soils subjected to higher stresses than they have experienced before follow curve a-b-e.

present overburden. Further loading of a sample beyond the preconsolidation stress results in a higher compressibility (steeper slope of the stress-strain line; C_2); curve a-b-e is called the *virgin compression line*. Soils in such conditions are indicated as normally consolidated.

During loading overpressured pore water is expelled and mineral grains are rearranged, fractured and distorted by compression. During unloading the soil takes up water again, but the fractured and rearranged soil matrix will not recover to its initial state. This explains why the volume change is less for un- and reloading (less steep gradient) compared to loading of normally consolidated soils.

2.1.5 Compaction potential of different soil types

A soil is composed of organic matter, minerals and pore space, which is filled with air (gasses) and/or water. The compaction potential of a specific soil depends on the following factors:

(1) *Initial porosity*. Soils with a high initial porosity have a higher compaction potential than soils with a low initial porosity.
(2) *Water content* (percentage of pores that are filled with water). Water acts to decrease friction between soil particles, which makes moist soil easier to compact compared to dry soil. However, if a soil is too wet, water carries part of the load of the soil, which will lead to a lower compaction potential.
(3) *Soil texture* (percentage of sand, silt and clay). Soils with particles of about the same size compact less than soils consisting of particles with variable size. In the last case, small particles can fill pores between larger particles making the soil denser.
(4) *Organic-matter content*. Organic matter is often used to improve the fertility of a clastic (agricultural) soil. This also makes the soil more resistant against compaction since the soil structure is improved. However, natural organic soils such as (clayey) peat have a high compaction potential due to its low mineral content and high initial porosity. Most likely, the clastic content and type of peat-forming plant species (e.g., wood, herbal plants or mosses) will influence the compaction potential.

In general, sands and gravels are nearly incompressible, clays compact to a moderate degree and peat is highly compressible (Allen, 1999). Land subsidence due to compaction is largely controlled by the spatial distribution of deposits with different soil textures, overlying load, compaction response time (hydrodynamic delay) of sediment layers (Kooi and De Vries, 1998) and groundwater table fluctuations.

2.2 Effects of peat compaction and formation on delta evolution

2.2.1 Effects on surface topography

A well-known effect of differential compaction of lithologically diverse sediment sequences is distortion of the original stratigraphy, and of the surface topography (e.g., Allen, 1999; 2000; Amorosi and Milli, 2001). In a situation of groundwater table lowering, compaction and oxidation of peat may lead to:

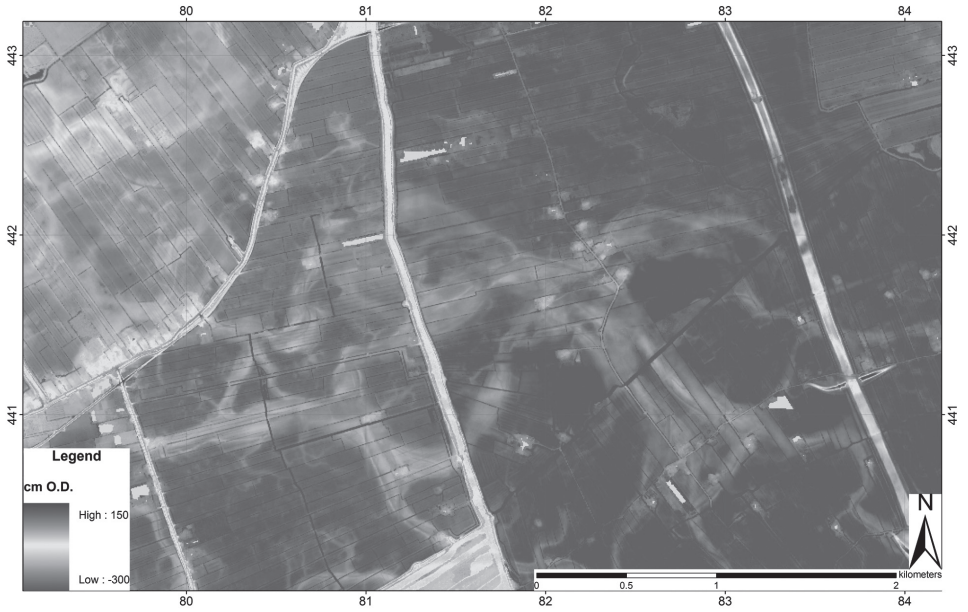

Figure 2.8. Digital Elevation Model (DEM; 5 m resolution). Levees appear as ridges in the landscape after compaction of peat and clay in the floodbasins (near Rotterdam, western Netherlands) (Rijkswaterstaat-AGI, 2005). See also Berendsen and Volleberg (2007). For color version of this figure, see page 177.

(1) *Amplification of the surface topography*. In general, channel and natural-levee deposits consist of sand and silt, while further away from the channel (in the floodbasin) peat and clay dominate the sediment sequence. Because peat and clay are more compressible, land subsidence due to compaction and oxidation of peat is greater in the floodbasins. Consequently, the elevation of the channel belts is amplified (Fig. 2.8).

(2) *Relief inversion*. This occurs for example in intertidal areas. Initially, tidal creeks incise in peat and clay deposits and form low-lying channels. After abandonment, the sand-filled channels appear as ridges in the landscape since sand is less susceptible to compaction and oxidation than peat and clay deposits in the surrounding floodbasin (Fig. 2.9; Vos and Van Heeringen, 1997; Berendsen, 2005; Spijker, 2005).

2.2.2 Geometry of channel and natural levee deposits

Subsidence due to compaction of peat creates accommodation space for (e.g., fluvial) deposition, thereby increasing sedimentation rates, as was demonstrated by a field study of Haslett et al. (1998). Results of a modeling study of Allen (1999) supported this idea. Peat underlying a river channel will be compacted (if not eroded) due to the load of channel deposits. Provided that the sediment load of the river is sufficiently high, accommodation space created by peat compaction will be filled by increased within-channel sedimentation. This leads to vertical aggrading river channels (e.g., Michaelsen et al., 2000; Rajchl and Uličný; 2005) with a low width/depth ratio. Similarly, peat compaction beneath natural levees can result in thick natural levees.

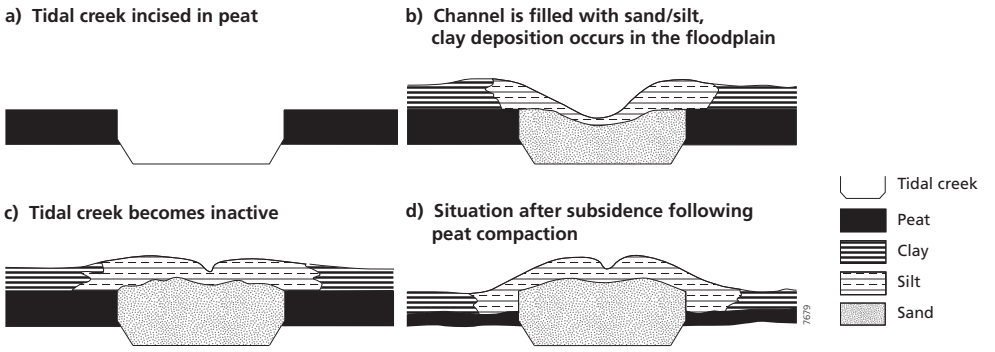

Figure 2.9. Schematic representation of relief inversion of tidal creeks (after Berendsen, 2005).

The geometry of river channels is also affected by the high cohesiveness of a peat substrate, besides other factors as stream power and aggradation rate (Törnqvist, 1993b; Makaske, 1998, 2001; Gouw and Berendsen, 2007). A cohesive subsoil (like peat), low stream power and a high aggradation rate (e.g., due to sea level rise) are favorable conditions for the development of channels with a low width/depth ratio. According to Gouw and Berendsen (2007) bank stability caused by river dissection of a peat substrate was the dominating factor leading to relatively deep and narrow channels in the Holocene Rhine-Meuse delta. Low sediment supply may be an additional factor leading to laterally stable channels. Contrary, if an incising channel encounters an intercalated peat layer it will first erode to the depth of the peat layer, which then due to its resistance prevents further vertical incision resulting in channels with a high width/depth ratio (Smith and Pérez-Arlucea, 2004; Fig. 2.11 mechanism 4).

2.2.3 Avulsion

Avulsion is regarded as one of the most important processes influencing delta evolution, and hence, alluvial architecture. The occurrence of avulsion is influenced by climate, tectonics, base-level change, discharge variations, substrate composition, human influence and local factors such as ice and log jams (Stouthamer and Berendsen, 2000). The influence of peat compaction and formation on avulsion has seldom been investigated. The few existing conceptual sedimentary models concerning this topic are based on exposures of old sediment sequences presently comprising coal layers (Michaelsen et al., 2000; Rajchl and Uličný; 2005). These sequences show the end-product of numerous processes that have acted over a long time period. Partly based on these studies, ignoring the difference in time scale, potential influences of peat compaction on avulsion in Holocene settings are derived:

(1) When a river invades a peatland, accommodation space is created by peat compaction underneath the channel, which initially leads to vertical aggradation. Through time, the rate of accommodation space created by peat compaction, due to loading by channel belt deposits, decreases. This results in a greater tendency for lateral migration, a higher sinuosity and a decrease in downstream channel slope (Rajchl and Uličný, 2005). As a result, the river becomes more prone to avulsion (Fig. 2.11: mechanism 1). The resulting alluvial architecture at floodplain scale is shown in Figure 2.10.

(2) The combination of the high cohesiveness of river banks consisting of peat, low stream power and low regional gradients in peatlands inhibits lateral migration of rivers (Fig. 2.11: mechanism 2). Instead, bed aggradation is favored, which reduces channel flow and sediment transport capacity (Stouthamer and Berendsen, 2007). This results in frequent crevassing of the main channel, which is an important mechanism initiating avulsion (Smith et al., 1989). However, it should be noted that due to the low regional gradients common in peatlands, crevasses often fail to evolve into an avulsion. The occurrence of either mechanism 2 or mechanism 1 depends on the balance between the rate of accommodation space created by peat compaction (v_{as}) and the sediment load of the river. A relatively low v_{as} and high sediment load will favor mechanism 2. The v_{as} is influenced by the weight of overlying deposits and peat type, ignoring other causes of creating accommodation space.

(3) In a situation of groundwater table lowering, floodbasin subsidence due to compaction and oxidation of peat above the groundwater table induces superelevation of the channel belt (Fig. 2.11: mechanism 3; see also section 2.2.1). Superelevation of a channel or channel belt above the floodplain, and the associated increase in the cross-valley slope (s_{cv})/down-channel slope (s_{dc}) ratio, increases the risk of avulsion (e.g., Heller and Paolo, 1996; Stouthamer and Berendsen, 2007). The s_{cv}/s_{dc} ratio is by some authors regarded as one of the most important controls on avulsion (e.g., Törnqvist and Bridge, 2002). Field data from the Mississippi River floodplain showed however that gradient advantages are not fully responsible for the occurrence of avulsion (Aslan et al., 2005; Stouthamer and Berendsen, 2007).

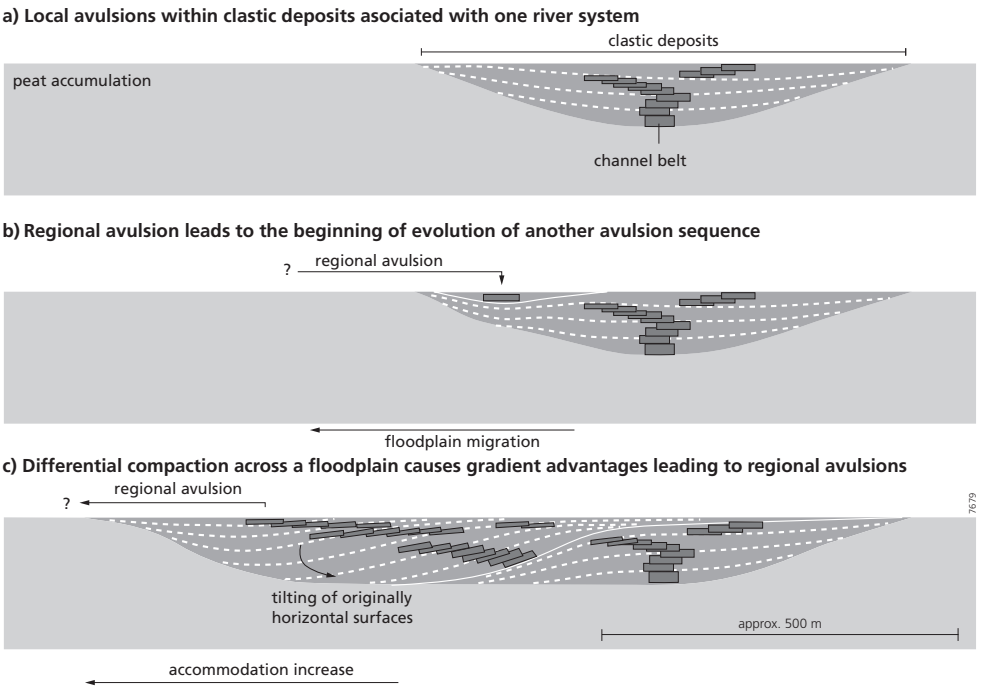

Figure 2.10. Schematic cross section representing the evolution of clastic deposits on top of compacting peat according to Rajchl and Uličný (2005).

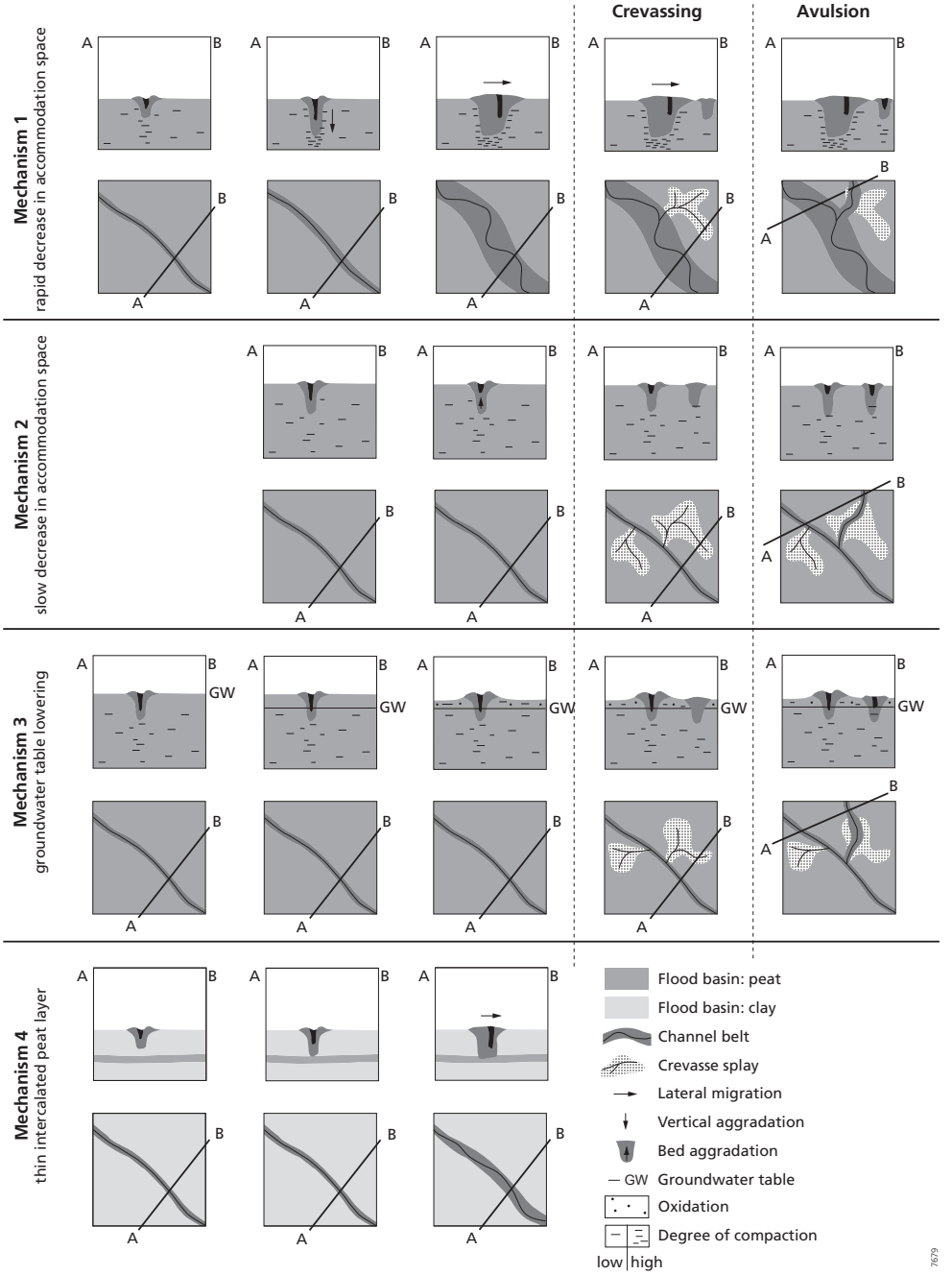
Crevassing
Avulsion
Mechanism 1
rapid decrease in accommodation space
Mechanism 2
slow decrease in accommodation space
Mechanism 3
groundwater table lowering
Mechanism 4
thin intercalated peat layer
A
B
GW
Flood basin: peat
Flood basin: clay
Channel belt
Crevasse splay
Lateral migration
Vertical aggradation
Bed aggradation
GW Groundwater table
Oxidation
Degree of compaction
low high
7679

(4) At a larger temporal and spatial scale, variations in compaction rate across the floodplain influences regional topography, which potentially leads to a shift of the river system to a formerly uninvaded part of the floodplain. Different compaction rates might occur due to for example variations in thickness and composition of the Holocene sediment sequence and peat type. Furthermore, the low regional gradient of peatlands causes a sudden drop in channel belt gradient at the point where the river enters the peatland, resulting in deposition of relatively coarse clastics at these sites. These conditions favor the occurrence of regional (nodal) avulsions at the edges of peatlands (e.g., Morozova and Smith, 2000; Rajchl and Uličný; 2005).

Conceptual models regarding the influence of peat compaction on avulsion do not address the influence of factors such as peat type (plant composition), organic-matter content of the peat, sediment sequence composition, sediment load and river discharge, and rate of fluvial sedimentation on the amount and rate of compaction in different fluvial settings. Plant composition influences peat structure, which might affect the compaction potential, and the resistance of a peat substrate to fluvial erosion. Organic material is more compressible than clastic material, so a high organic-matter content probably leads to a higher compaction potential. Loading by fluvial deposits will lead to compaction of underlying peat, but the amount of compaction will depend on the thickness and composition of the overlying clastic sediment layer, and of the depositional environment.

Detailed field studies in modern floodplain areas are needed to determine and quantify the relative importance of such factors on peat compaction and hence on the evolution of fluvial-deltaic environments.

2.3 Field methods to quantify peat compaction

2.3.1 Dry bulk density

The dry bulk density of unconsolidated sediments generally increases due to compaction following external loading (e.g., Craig, 1987; Kruse, 1998) or groundwater fluctuations (Kool et al., 2006; Whittington and Price, 2006). Bird et al. (2004) found relations between the bulk density, texture and organic-matter content of uncompacted peat samples and used these to calculate the uncompacted bulk density of compacted Holocene sediments (Table 2.1). In this way, the amount of subsidence due to compaction could be calculated. Both the compacted and uncompacted sediment samples were taken from mangrove regions (intertidal zone; enhanced compaction may occur during low tides) along the coast of Singapore. The percentage of compaction for three mangrove sediment sequences (in which a peat layer underlies a clastic

⇦ *Figure* 2.11. Schematic representation of possible influences of peat compaction and formation on river behavior. Crevassing, and hence possibly avulsion, may be initiated by an increased tendency for lateral migration due to a decrease in the rate of accommodation space created by peat compaction (mechanism 1), by bed aggradation and the associated lower sediment transport capacity, caused by the high cohesive peat banks (mechanism 2) and by superelevation of the channel belt due to peat compaction and oxidation in floodbasins following groundwater table lowering (mechanism 3). Mechanism 4 shows that an intercalated peat layer may lead to channel belts with a high width/depth ratio.

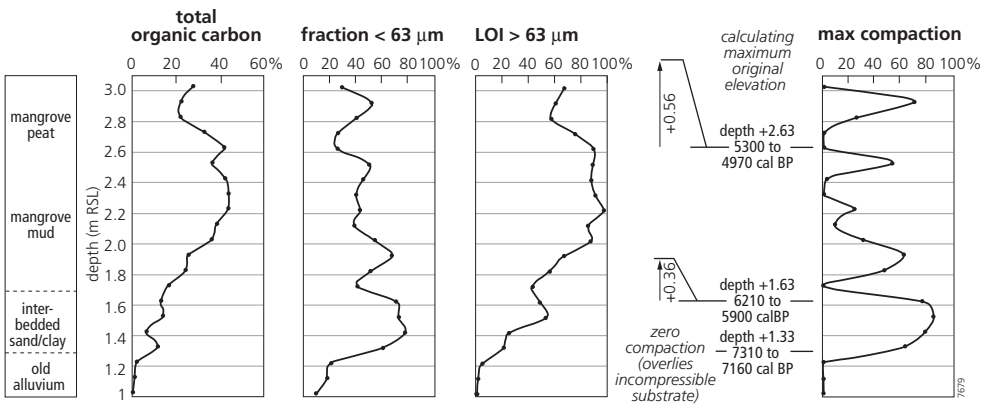

Figure 2.12. Total organic carbon (%), fraction < 63 μm (%), LOI of fraction > 63 μm (%) and amount of compaction (%) plotted against depth for a core taken in a mangrove environment near Singapore (from Bird et al., 2004).

sediment layer of up to ~9 m, partly due to recent landfill material) calculated over 10 cm intervals ranged from 0 to 67%. Based on their results they concluded that organic rich and/or fine grained sediments were more susceptible to compaction than inorganic sands. However, a closer examination of their results shows that peaks in the percentage of compaction especially seem to correlate with peaks in the fraction <63 μm and less with the organic-matter content (Fig. 2.12).

The amount of compaction calculated over 10 cm intervals sometimes drops to zero, though the LOI (loss on ignition) of the >63 μm fraction is >80%. This seems very unlikely as high organic peat is highly compressible. Furthermore, their sampling technique probably caused some disturbance of the sediments, which might have influenced their results; a PVC tube of 3.8 cm in diameter was pushed into the sediment surface. Peat often has a loose structure, and peat characteristics are highly variable, for example due to the inclusion of wood fragments. Field studies on physical properties of soils have shown that dry bulk densities of different peat types from different areas vary in the range of 0.01 to 0.4 g/cm^3 (e.g., Brandyk et al., 2002; Price et al., 2005; Whittington and Price, 2006). Moreover, Price et al. (2005) investigated relationships between the compressibility of peat, bulk density, fiber content and the state of peat decomposition, expressed by the 'Von Post number'. The only significant correlation they found was between virgin compressibility and bulk density at one location (in one core).

To take into account the heterogeneity of peat characteristics, sufficiently large samples should be taken when determining peat characteristics such as dry bulk density and organic-matter content. Furthermore, it is vital not to disturb the peat structure during sampling. Special sampling devices should be used, such as the block sampler of Lefebvre et al. (1984). This device takes cylindrical shaped block samples by using sharp cutting blades, which rotate while moving down to carefully cut the fibers in the peat. The Wardenaar corer is another device that may be used for taking relatively undisturbed peat samples (Wardenaar, 1987). This corer consists of two rectangular boxes with sharp cutting edges at the lower ends. The two halves can be pushed

into the soil alternatingly to take relatively undisturbed peat cores of 10x10x100 cm. A modified Wardenaar corer with larger dimensions (15x15x100 cm) and a serrated cutting edge was developed by Givelet et al. (2004). Buttler et al. (1998) developed a peat sampler consisting of two concentric tubes, whereby the outer one is used as a cutter and the inner one as a collector. This sampler extracts cores of 13.3 cm in diameter and up to 70 cm long.

Provided that a suitable peat sampling device is used, it is suggested here that relations between the dry bulk density of compacted and uncompacted peat could be used to estimate the decompaction height of compacted Holocene peat layers. Note that only bulk density values of peat of the same type can be compared.

2.3.2 Lithostratigraphy, basal peat and ^{14}C dating

Basal peat is formed directly on an incompressible substrate, and therefore, does not subside due to compaction. By dating basal peat and the peat profile in floodbasins, which is susceptible to subsidence due to compaction, isochrones can be constructed (Fig. 2.13). The amount of subsidence due to compaction can now be calculated by assuming the initial level of peat formation is at the same altitude as the isochronous dated basal peat.

Haslett et al. (1998) used this method to estimate the amount of compaction at Somerset Levels, Britain (Fig. 2.14, Table 2.1). Three ^{14}C dated peat samples confirmed the top of the peat layer was isochronous. The minimum altitude of the original peat surface was estimated based on its maximum present altitude (distance 40 m in Fig. 2.14), where the peat is regarded as basal peat. The maximum difference between this altitude and the present minimum altitude of the top of the peat layer (distance 120 m in Fig. 2.14) indicated maximum subsidence due to compaction of 2.22 m (of a peat layer with an assumed original thickness of 4 m).

Bloom (1964; Table 2.1) used the same method in a tidal marsh in Connecticut, USA, and found that in 7000 years the peat layer had compacted to 13 to 44% of its original thickness.

Based on ^{14}C dating and an assumed initial level of peat formation, that was related to past mean sea level, Törnqvist et al. (2008; Table 2.1) calculated compaction rates of up to 5 mm/year on millennium-scale. On shorter timescales (10^2-10^3 years) they estimated rates of 10 mm/year. A linear relationship between compaction rate and overburden thickness was found.

The method described in this section can also be used to investigate relations between the amount of compaction and fluvial deposition patterns, for example by constructing a

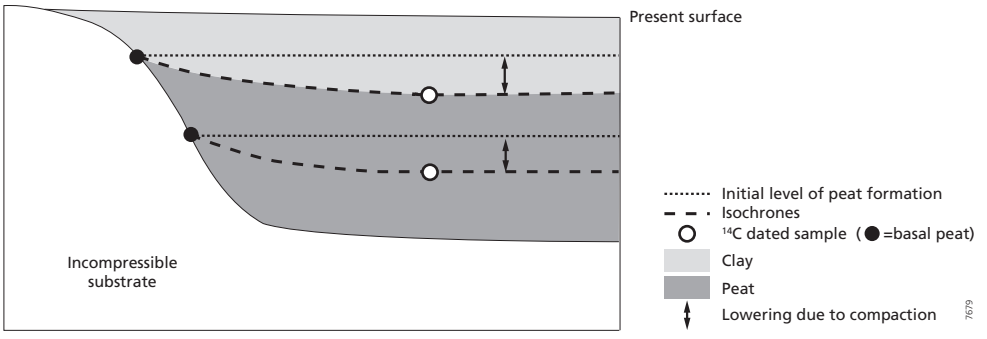

Figure 2.13. Schematic representation of using stratigraphic cross sections and ^{14}C dating of (basal) peat to estimate the amount subsidence due to compaction.

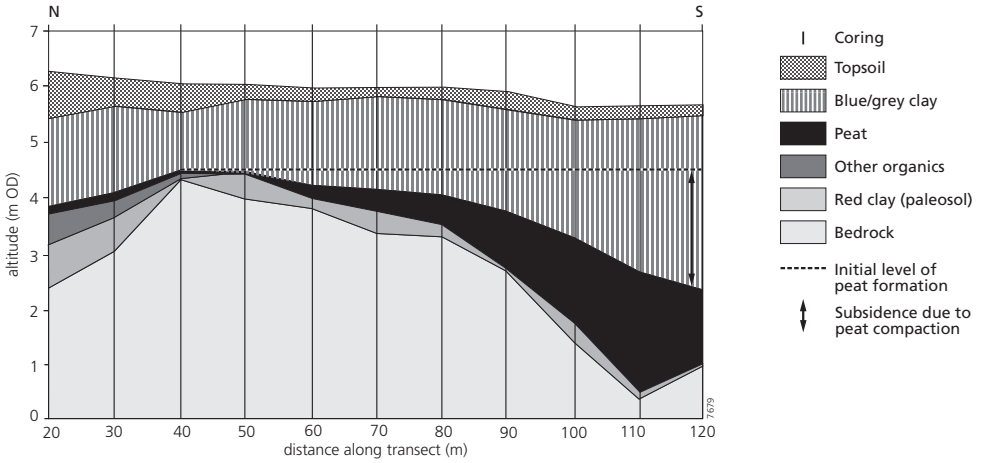

Figure 2.14. Using a stratigraphic cross section to calculate the amount of subsidence due to peat compaction. The initial level of peat formation is estimated based on its maximum present altitude, at a site where it directly overlies incompressible bedrock. After Haslett et al. (1998).

cross section from a channel belt towards the flood basin. To determine changes in boundary conditions through time, a detailed understanding of the palaeogeographical development of the investigated area is needed, which requires detailed logging of many cores. The altitude of ^{14}C dates and surface topography should be measured accurately, which requires the use of leveling or differential (d)GPS for measuring surface elevation.

2.3.3 Measuring surface elevation change

Surface elevation changes are measured by e.g., conventional leveling, (d)GPS surveys, high resolution Digital Elevation Models (DEMs) and Sedimentation Erosion Tables (SET, see Boumans and Day, 1993; Fig. 2.15).

Last-mentioned technique measures elevation changes from a fixed level above the surface. Vertical accretion is measured as the rate of sedimentation above marker horizons. The difference between accretion and elevation change is used to calculate the amount of shallow subsidence. The rate of compaction of newly deposited sediments can be determined by installing a second set of marker horizons after the start of measurements (Cahoon et al., 2000).

Using this technique, Cahoon et al. (1995, 2000; Table 2.1) measured vertical accretion and surface elevation change in salt marshes in Louisiana, Florida and North Carolina, USA, using feldspar marker horizons, which are easily distinguishable from the surrounding sediments. The objective of their study was to calculate the amount and rate of subsidence of the upper 5 m of soil. After two years, they had measured total vertical accretion by sediment deposition and plant production ranging from 7.7 to 51.9 mm (3.85 to 25.95 mm/yr) and total subsidence due to compaction of 4.5 up to 49.0 mm (2.25 to 24.5 mm/yr). At each site, surface elevation change was significantly lower than vertical accretion, due to compaction. This was also found by Rogers et al. (2006; Table 2.1), who applied the same method at ten different sites in salt-marshes and mangroves in southeast Australia. After three years of measuring, compaction rates varied considerably between the different sites, with values of up to 11.62 mm/yr. Differences in

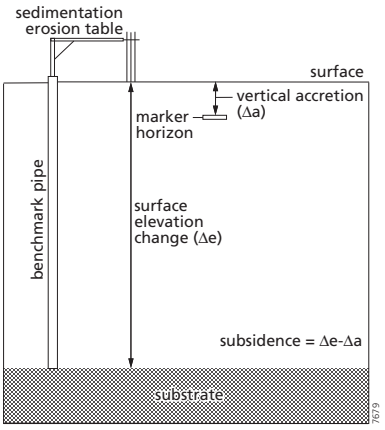

Figure 2.15. Schematic representation of a Sedimentation Erosion Table (SET) and marker horizons. Shallow subsidence is calculated as vertical accretion minus elevation change. Adapted after Cahoon et al. (2000).

compaction rates between sites were attributed to different bulk densities, mineral and organic-matter contents, rainfall and plant production rate.

Abidin et al. (2001; Table 2.1) used leveling and GPS surveys to estimate land subsidence rates in Jakarta, Indonesia. Based on leveling surveys, up to 800 and 1600 mm subsidence for the periods 1982-1991 (mean rate of 89 mm/yr) and 1991-1997 (mean rate of 267 mm/yr) respectively was measured. Based on a GPS survey 200 mm of subsidence for the period of 1997-1999 (mean rate of 100 mm/yr) was calculated. Thus, on average, the highest rates of subsidence occurred in the period 1991-1997. Comparison with hydrological data (registered groundwater extraction and piezometric level measurements) showed that the amount of subsidence was strongly related with the amount of groundwater extraction.

The amount of land subsidence may also be estimated by comparing altitudes of high resolution DEMs, representing former and present surface topographies. Laser altimetry or radar images may be used to compute such high resolution DEMs and detect changes in surface topography (e.g., Galloway et al., 1998; Fig. 2.8; Table 2.1).

In conclusion, high-precision techniques are available to monitor surface elevation changes. Highest accuracies (mm precision) are attained by using conventional leveling, SET and differential GPS. The drawback of such techniques is that elevation changes only over short timescales are measured. Still, such surveys are useful as they give insight into the rate of processes leading to subsidence. Using high resolution DEMs and GPS surveys for surface elevation change measurements result in 10^0-10^1 cm-precision.

2.3.4 Deformation of logs

Rough estimates of peat compaction were made by Kaye and Barghoon (1964; Table 2.1), who determined the minimum amount of peat compaction from the distortion of buried logs, which were assumed to originally have been circular in cross section. They estimated compaction of peat layers of about 25-43% of its original thickness. Stout and Spackman (1989; Table 2.1) used the same method and estimated minimum average compaction of peat by 21%.

This method does not give accurate estimates of the amount of peat compaction. First of all, only minimum compaction can be estimated, as probably considerable compaction of peat has

Table 2.1. Overview of field methods used to quantify peat compaction.

Method		Study site	Measured amount of compaction	Over-burden	Subsidence rate (due to compaction)	Accuracy	Spatial scale	Time scale	Source
Relation bulk density with LOI/texture		Intertidal zone coast Singapore	0-67%;* (calculated for 10 cm intervals)	Up to 9 m; variable composition	-	Intermediate	Small	Large	Bird et al. (2002)
Stratigraphic cross sections and ^{14}C dating of basal peat		SW Britain, Connecticut (USA), Mississippi Delta (USA)	13-55%**	Up to 3.16 m; clay	5 mm/yr	High	Intermediate	Large	Haslett et al. (1998); Bloom (1964); Törnqvist et al. (2008)
Surface elevation measurements	Surface Elevation Table	Salt marshes Louisiana, Florida and North Carolina (USA)	-	-	2.25-24.5 mm/yr (mean rates; upper 5 m)	High	Small	Small	Cahoon et al. (1995, 2000); Rogers et al. (2006)
	Levelling/GPS survey	Jakarta, Indonesia	-	-	80-267*** mm/yr (mean rates)	Low	Intermediate	Small	Abidin et al. (2001)
	High resolution DEMs	Coachella Valley, California (USA)			Up to 90 mm/yr*	High	Large	Small	Galloway et al. (1998)
Deformation of logs		Boston (Kaye and Barghoon), Florida (Stout and Spackman)	20-45%**	Up to few meters	-	Low	Small	Large	Kaye and Barghoon (1964); Stout and Spackman (1989)

* Compaction = volume reduction/decompacted thickness.
** Compaction = present thickness/original thickness.
*** High rates due to artificial groundwater extraction.

taken place before flattening of the logs occurs. Furthermore, the assumption that the tree trunk and the surrounding peat have the same compressibility will introduce significant errors in the calculated amount of compaction.

2.4 Compaction models

Another method used to quantify the amount and rate of compaction is by the use of empirical and numerical models. Examples of such models are presented and discussed in the following sections.

2.4.1 Empirical models

Empirical models are based on results from experiments and observations. Empirical compaction models are often based on porosity-depth relations. There are numerous porosity-depth equations, but it is not the aim of this paper to review all of these, especially since many of these equations were constructed for (deeply buried) clastic sediments and not for peat. Some that do account for compaction of peat are discussed here.

Sheldon and Retallack (2001) developed a porosity-depth equation for nonmarine sediments such as floodplain sediments and peat. This equation was based on porosity-depth equations for deeply-buried sediments of Sclater and Christie (1980) and of Baldwin and Butler (1985):

$$C = \frac{-S_i}{\left(\left(F_0 / e^{Dk}\right) - 1\right)} \tag{2.2}$$

where C is the compaction as a fraction of the original thickness, S_i is the initial solidity (= 1-F_0), F_0 is the initial porosity, D is the burial depth and k is an empirically derived constant. Values for k were determined using empirical relationships with the initial porosity, valid for marine sediments (Sclater and Christie, 1980). Thus, a required parameter in this model is the initial solidity of the sediment under consideration, which was calculated using the dry bulk density and the solid bulk density. Sheldon and Retallack (2001) used S_i = 0.06 (F_0 = 0.94) and k = 2.09 to calculate compaction of peat. Using these values, the compaction ratio becomes 0.85 at 5 meter and 0.75 at 10 meter depth (85% and 75% respectively of the original thickness).

Allen (1999) used a simple empirical equation, based on experimental research of Skempton (1970), to estimate the amount of compaction in coastal mudflats and marshes:

$$T = \left(T_0 - T_{\min}\right)e^{-kH} + T_{\min} \tag{2.3}$$

where T is the final thickness of a sediment layer, T_0 the thickness at the time of deposition, T_{min} the limiting thickness (zero porosity), k the empirical compressibility of the layer, and H the thickness of the sediment overburden, assumed to fill the accommodation space to the height determined by sea level at that time. Values of k for each type of sediment were estimated by solving the formula with field data. A bulk density for the initial and most compacted state was assumed to estimate T_0 and T_{min} respectively. To quantify the effect of accommodation space

provided by compaction on deposition rate, the deposition-rate enhancement factor (*DEF*) was used:

$$DEF = \frac{\Delta S_{\min} + \Delta S_{org}}{\Delta M} = 1 + \frac{\Delta P}{\Delta M} \tag{2.4}$$

where ΔS_{min} is the added thickness of mineral sediment, ΔS_{org} the thickness of organic material, ΔM the change in relative sea level and ΔP the lowering of the surface due to compaction. Thus, following this equation, changes in accommodation space are determined by changes in sea level (or another local base level) and by compaction. Assuming a steady sea-level rise of 1.5 mm/yr, the *DEF* gradually increases in a sequence formed over 15 periods of silt deposition (Fig. 2.16a; one period equals 667 years). In Figure 2.16b 3 periods of peat accumulation are followed by 12 periods of silt deposition. In this case, the *DEF* first rapidly increases due to a high rate of creation of accommodation space by peat compaction. Continued peat compaction enhances silt deposition, but after about 6 periods the *DEF* has recovered again.

Fokkens (1970) set up an empirical relation based on compression tests on a large number of peat samples. Using an empirical relation between the organic-matter content and the specific gravity of the solids (Den Haan and El Amir, 1994) the following empirical equation was used to estimate the amount of settlement:

$$\frac{\Delta h}{h} = \frac{w_i - w_u}{w_i + n + mN} \tag{2.5}$$

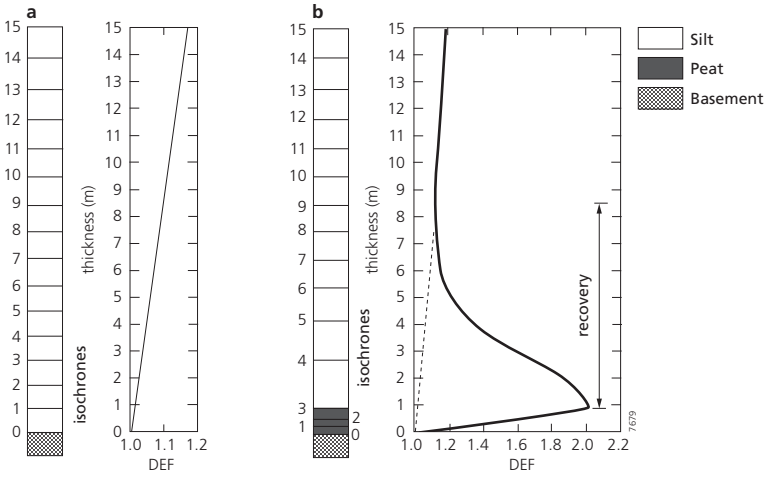

Figure 2.16. The deposition-rate enhancement factor (*DEF*) used to quantify the effect of accommodation space provided by compaction on deposition rate. In (a) the *DEF* gradually increases in a sequence formed over 15 periods of silt deposition (one period equals 667 years), (b) shows the effect of 3 periods of peat accumulation followed by 12 periods of silt deposition. The *DEF* first rapidly increases due to high rate of creation of accommodation space by peat compaction. Continued peat compaction enhances silt deposition, but after about 6 periods the *DEF* has recovered again. After Allen (1999).

where Δh is the amount of subsidence (m), h is the initial layer thickness (m), w_i is the initial water content, w_u is moisture content after compression, N is the organic-matter content (determined by LOI test; N = weight organic matter in soil sample/weight solid fraction of soil sample) and m and n are fitted parameters (see also Kruse, 1998).

2.4.2 Geotechnical models

Most compaction models however, are based on geotechnical theory, which basically describes stresses occurring in soil. The most important law used in such models is Terzaghi's principle of effective stress (σ'), which is the stress between soil particles (Eq. 2.1). Different kinds of geotechnical compaction models exist: models that only describe one-dimensional (vertical) compression, three-dimensional models, models describing consolidation (pore water expulsion), models that distinguish between primary and secondary compression. Furthermore, a distinction can be made between backward and forward modeling. A backward modeling approach starts from the compacted state and estimates the decompaction correction. A forward modeling approach calculates the amount of compaction starting from the uncompacted state.

Models describing one-dimensional compression

Many compaction models describe only one-dimensional (vertical) compression, and are based on Terzaghi's law (Eq. 2.1). Necessary model parameters, such as compression coefficients (slope of stress/strain curve; see section 2.1.4), are often determined from oedometer test results.

For example, Paul and Barras (1998) developed a simple one-dimensional compression model, using a backward modeling approach (Fig. 2.17). Massey et al. (2006) used the same model to calculate the decompaction correction for 10 to 15 meters thick Holocene sediments in southern UK. In the model, the sediment sequence is first divided into layers of 0.1-0.2 m thick, for each of which the volume reduction is calculated according to the stress increase the layer has experienced. The total subsidence due to compaction is the sum of these volume changes. Figure 2.17 shows that the increase in effective stress (P_0 to P_1) following sediment loading, causes subsidence of sample S of ΔH. The effective stress was calculated based on Terzaghi's law of effective stress (Eq. 2.1), for which the pore water pressure was calculated from the depth of a sample below the water table (assumed 1 m below surface) and the total stress was calculated based on the weight and thickness of the sequence overlying the sample. As outlined before, peat may show a high variability concerning its geotechnical characteristics. Consequently, it may be difficult to determine the compression index from oedometer tests. Therefore, the compression index (slope of the compression line in Fig. 2.17) of peat was calculated using a correlation with the liquid limit (the water content at which a soil changes from a liquid state to a plastic state). However, the relation used was originally derived from results from clastic sediments (Skempton, 1944), which therefore introduced a significant uncertainty into the model calculations.

Other one-dimensional compaction models also describe fluid flow. Groundwater flow in porous sediments is usually modeled assuming Darcy's law, in which flow velocity is a function of the permeability of the sediment and of the gradient of the water table. Furthermore, besides assuming Terzaghi's law of effective stress (Eq. 2.1), changes in effective stress are often modeled using porosity – effective stress relations (e.g., Kooi, 1997; Kooi and De Vries, 1998; Meckel et al., 2007), or using void-ratio – effective stress relations (Audet, 1996; Pizutto and Schwendt, 1997; Tovey and Paul, 2002; Gutierrez and Wangen, 2005). Void ratio is defined as the ratio

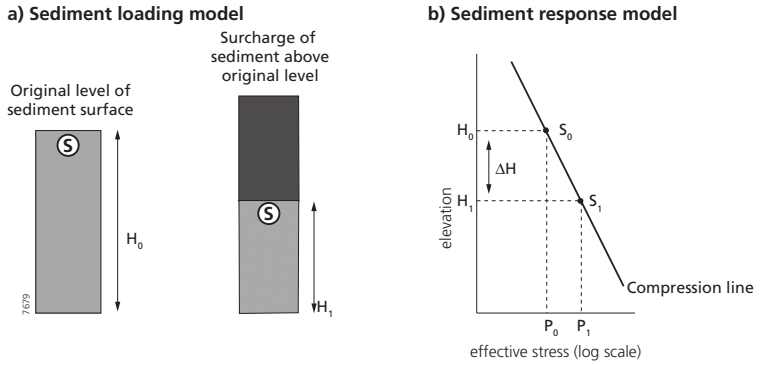

Figure 2.17. Calculating the decompacted thickness of a sediment layer using the model of Paul and Barras (1998). The original height H_0 of a sample S is lowered to height H_1, after an increase of the effective stress from P_0 to P_1, due to the load of the added sediment layer. ΔH depends on the ratio of effective stresses (P_0 to P_1) and the slope of the compression line (=compression index).

between the volume of voids and the volume of solids. Oedometer tests show that the void ratio is linearly related to the logarithm of the effective vertical stress (Skempton, 1944):

$$\sigma'_v = \sigma_{100} \exp_{10} \left(\frac{e_{100} - e}{C_c} \right) \tag{2.6}$$

$$e_{100} - e = C_c \frac{\ln \sigma'_v}{\ln \sigma_{100}}$$

where, σ_{100} is a reference value for σ'_v (usually 100 kPa), e_{100} is the void ratio at σ'_v = 100 kPa and C_c is the compression index.

Based on calculations used in the model of Kooi (1997), Meckel et al. (2007) used a forward modeling approach to model sedimentation and subsequent compaction rates of stochastically generated sediment sequences with different thicknesses, sedimentation rates and lithological composition. Highest compaction rates were found in stratigraphies with a high proportion of peat layers that are loaded with high bulk density lithologies such as sand.

Three-dimensional models

In environments that are severely influenced by tectonics or by increased stresses resulting from artificial constructions such as dykes, lateral deformations can be important (e.g., Lefebvre et al., 1984). To model three-dimensional deformation in deep buried fine-grained sedimentary basins, Pouya et al. (1998) introduced a mechanical constitutive model. In Holocene peatlands in deltaic settings however, lateral strain will be of minor importance compared to vertical strain.

One-dimensional models describing primary and secondary compression

Secondary compression was not considered in previous mentioned models. Especially in peat however, secondary compression causes a considerable part of total compaction, and therefore should be taken into account.

Terzaghi (1943) described primary and secondary compression with the following equation:

$$s = h\frac{C_c}{1+e_0}\log\frac{\sigma'_v + \Delta\sigma'_v}{\sigma'_v} + hC_\alpha \log t \tag{2.7}$$

where s is the settlement (Δh), h is the layer thickness, C_c the primary compression index, e_0 the initial void ratio, C_α the secondary compression index and t the time in days. The second term ($hC_\alpha \log t$) describes secondary settlement, which is independent of the vertical stress and occurs after the hydrodynamic period has ended.

Contrary, in the model of Buisman-Koppejan (described in Den Haan, 2003) secondary compression is dependent on the effective stress. It is assumed that primary and secondary compression both start directly after loading. Compression is calculated using the equation:

$$s = h\left(\frac{1}{C_p} + \frac{1}{C_s}\log t\right)\ln\frac{\sigma'_v + \Delta\sigma'_v}{\sigma'_v} \tag{2.8}$$

where C_p and C_s are the primary and secondary compression coefficients of Buisman-Koppejan respectively. In this model, the rate of secondary compression (settlement) is dependent on previous effective stress increases ('superposition rule'). Ranges of values for C_p and C_s for three types of soil are presented in Table 2.2. Mean values resulting from oedometer tests on peat samples from the western part of The Netherlands, taken from different depths (Kruse, 2004) are shown in Table 2.3.

However, it appeared from long-duration compression tests that the secondary compression rate was not dependent on the effective stress after all. Actually, Bjerrum (1967) already found that creep(=secondary compression)-strain rates are constant in a plot of strain versus the natural logarithm of vertical effective stress. Such lines are called creep isotaches. The *a,b,c-isotach model* uses this concept and was developed by Den Haan (1994) to improve modeling of compaction of soft soils like peat. In this model, natural strain (ε^H) instead of linear strain (ε^C) is used to

Table 2.2. Range of values for primary (suffix p) and secondary (suffix s) compression coefficients of Buisman-Koppejan, for conditions before and after the preconsolidation stress (suffix 1 and 2 respectively; from Locher and De Bakker, 1993).

Soil type	C_{p1}	C_{s1}	C_{p2}	C_{s2}
Peat	10-150	25-1000	4-30	14-140
Clay	20-300	60-2500	7-125	30-300
Sand	80-800	70-3500	140-140	40-1250

Table 2.3. Values for compression parameters resulting from 7 oedometer tests on peat samples taken from western Netherlands (Kruse, 2004).

	C_{p1}	C_{s1}	C_{p2}	C_{s2}
Average	19.52	110.85	5.08	26.30
Maximum	24.01	210.40	5.61	43.18
Minimum	12.33	48.98	4.43	13.05

better describe large compressions. For large compressions, ε^C tends to 1, but ε^H tends to infinity (Fig. 2.18). Natural strain is described as:

$$\varepsilon^H = -\int_{h=h_0}^{h=h} \frac{-dh}{h} = -\ln\frac{h}{h_0} = -\ln(1-\varepsilon^c) \tag{2.9}$$

Natural strain is incrementally defined, whereas linear strain is a differential measure. Above approximately 10% compression the difference between linear and natural strain becomes noticeable, and therefore in highly compressible soils like peat, the use of natural strain is of advantage (Den Haan and Edil, 1993).

Another difference with most other compaction models is that the *a-b-c isotach model* uses intrinsic time. Intrinsic time is described as the time which would have been necessary to achieve the present volume, assuming that the present stress had been applied immediately to the soil in its freshly deposited state (Den Haan and Edil, 1993). Intrinsic time (τ) is defined as:

$$\tau = t - t_r \tag{2.10}$$

where t_r is a time constant. In the *a,b,c-isotach* model, three main parameters are used (*a*, *b* and *c*) to describe soil compressibility (Fig. 2.19). Direct compression, following an increase in effective stress, is described by parameter *a*:

$$\varepsilon_d^H = a\ln\left(\frac{\sigma'_v}{\sigma'_{vp}}\right) \tag{2.11}$$

The slope of the creep isotaches as shown in Figure 2.19 is given by parameter *b*. The vertical distance between two lines is given by parameter *c* if their rates differ by a factor exp(1). The reference isotach starts at the preconsolidation stress (σ_{vp}') and is characterized by a reference creep strain rate ($\dot{\varepsilon}_{s,ref}^H$). The creep isotaches are described by:

$$\dot{\varepsilon}_s^H = \dot{\varepsilon}_{s,ref}^H \exp\left(\frac{(b-a)\ln\left(\frac{\sigma'}{\sigma'_{vp}}\right) - \varepsilon_s^H}{c}\right) \tag{2.12}$$

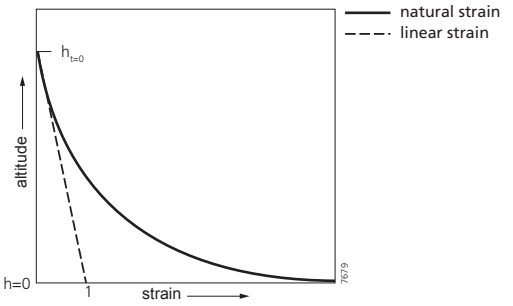

Figure 2.18. Graphical interpretation of linear and natural strain (from Den Haan, 1994).

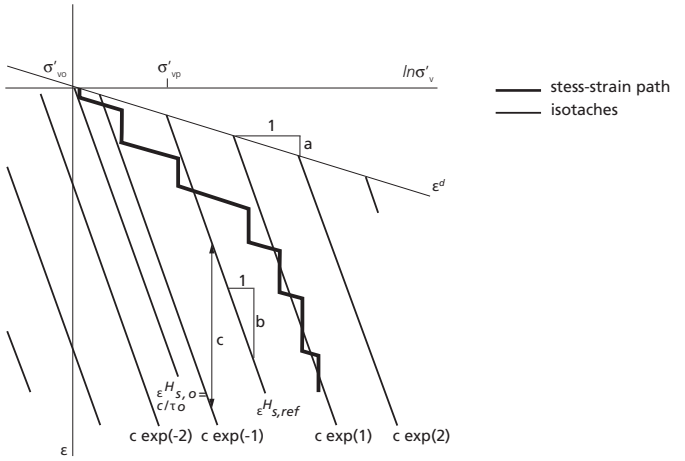

Figure 2.19. Stress-strain-creep strain rate relationships according the a-b-c-isotach model (Den Haan, 1994). Creep isotaches are shown with slope *b* and vertical distance *c*. Initial conditions are represented by effective stress σ'_{vo} with creep strain rate $\varepsilon^{H}_{s,o}$. The line representing direct compression (ε^{d}) has slope gradient *a*. σ'_{vp} is the preconsolidation stress. See text for further explanation.

The creep rate is related to the intrinsic time by:

$$\dot{\varepsilon}^{H}_{s} = \frac{c}{\tau} \tag{2.13}$$

Total rate of strain is calculated using:

$$\dot{\varepsilon}^{H} = \dot{\varepsilon}^{H}_{d} + \dot{\varepsilon}^{H}_{s} \tag{2.14}$$

Values for parameters *a*, *b* and *c* resulting from tests on peat samples taken from western Netherlands (Kruse, 2004) are presented in Table 2.4. These values correspond with other values found in literature (Den Haan, 1994).

The model takes into account reduced pore volume during consolidation, leading to reduced permeability and increased stiffness of the soil. The outflow of pore water is modeled using Darcy's law.

Table 2.4. Values for compression parameters *a*, *b* and *c* used in the a,b,c-isotach model, derived from compression tests on peat samples taken from different depths (Kruse, 2004).

	a	*b*	*c*
Mean	0.062	0.32	0.022
Maximum	0.083	0.34	0.034
Minimum	0.044	0.30	0.013

2.4.3 Discussion peat compaction models

According to Den Haan (2003), the a,b,c-isotach model is currently most realistic for modeling compaction of soft soils like peat since it (1) takes into account secondary compression, (2) uses natural strain instead of linear strain, which better describes large compressions in soft soils, and (3) creep rate is a function of effective stress and strain.

The model can still be improved however, as for example stress distributions in soil are not accurately described, which is necessary though when describing e.g., lateral stresses occurring as a result of artificial constructions. Currently, the model uses Boussinesq's (1885) theory to describe stresses in soil, in which a linear relationship between the applied stress and the resulting strain is assumed using the Poisson ratio. In the plain of the maximum vertical and minimum horizontal applied stress, this parameter is defined as the ratio between the strain in vertical direction to the strain in horizontal direction. Boussinesq's theory assumes that the soil is an isotropic, homogenous linear elastic material, and that the stress distribution is the same in different soil types. Soils however rarely meet these conditions, and stress distributions will vary between different soil types. For example, considering natural levee and crevasse splay deposits next to a channel belt, the vertical effective stress will be highest close to the channel where the levee is thickest, and the applied stress will distribute differently through the sand of the channel and the floodplain deposits (peat and clay).

Besides choosing the most suitable compaction model, another difficulty in modeling peat compaction is to determine the highly variable geotechnical characteristics of peat (Magnan, 1993; Termaat and Topolnicki, 1993). This is the result of a combination of factors, such as the type of organic material (e.g., wood, sedge or reed peat), clastic content and the chemical and biological evolution of the organic matter with time (degree of decomposition).

To overcome the problem of determining compression parameters of peat samples, Paul and Barras (1998) and Massey et al. (2006) used a relation between the compression index and the liquid limit. This correlation usually underestimates the compression index for very soft materials and will probably vary between different peat types. Pizzuto and Schwendt (1997) also stressed that their organic samples could not be used in oedometer tests due to the high contents of large organic debris (e.g., wood fragments). They estimated model parameters for organic deposits by model calibration. However, parameters obtained from model calibration are not very reliable as different combinations of parameters may lead to the same results.

Another solution to take into account the variability of peat is using relatively large samples in oedometer tests, since larger samples are representative for a larger volume of peat soil. Normally, samples of about 6 cm in diameter and 2 cm in height are used. For peat, samples of about 20 cm in diameter and 8 cm in height might give more reliable results. A disadvantage of using larger samples in oedometer tests is that it takes much longer before all pore water is expelled (long consolidation time), so testing will be more time-consuming (Lefebvre et al., 1984).

Peat compaction in alluvial architecture models

Alluvial architecture models are used by geologists and reservoir engineers to understand and predict the spatial distribution and geometry of (sandy) channel belts (e.g., Leeder, 1978; Bridge and Leeder, 1979; Mackey and Bridge, 1995; Karssenberg and Bridge, 2008). Until now, compaction processes are not, or only in a simplified form, incorporated in such models.

In the two-dimensional process-based alluvial architecture model of Bridge and Leeder (1979) fine-grained overbank deposits are compacted using a polynomial equation based on porosity-depth curves of Baldwin (1971) and Rieke and Chilingarian (1974; Fig. 2.20). However, these porosity-depth curves were based on data derived from marine sediments, which may not be applicable to alluvial sediments, and especially not to peat. Mackey and Bridge (1995) used a different expression to simulate porosity changes with depth, allowing for higher near-surface porosities, and for a faster porosity reduction near the surface (Alternate Shale Curve in Fig. 2.20).

Many Holocene deltas contain peat, which is highly sensitive to compaction and thereby influences alluvial architecture, as is outlined in this paper. Present alluvial architecture models can be greatly improved by incorporating peat compaction and peat formation. For modeling peat compaction it is suggested to use the a,b,c-isotach model as a basis for reasons mentioned above. Initially, peat formation in an aggrading system can simply be modeled by assuming it keeps up with the groundwater table rise.

Including peat compaction and formation might for example affect the ratio between cross-valley (s_{cv}) and down-valley (s_{dv}) gradient, which is often used in alluvial architecture models as an important factor controlling the occurrence of avulsion (e.g., Mackey and Bridge, 1995; Karssenberg and Bridge, 2008). Although it has been proved that this is not the only control on avulsion (Aslan et al., 2005; Stouthamer and Berendsen, 2007), some suggestions were made in section 2.2 about how peat formation and compaction affect this ratio. However, considering

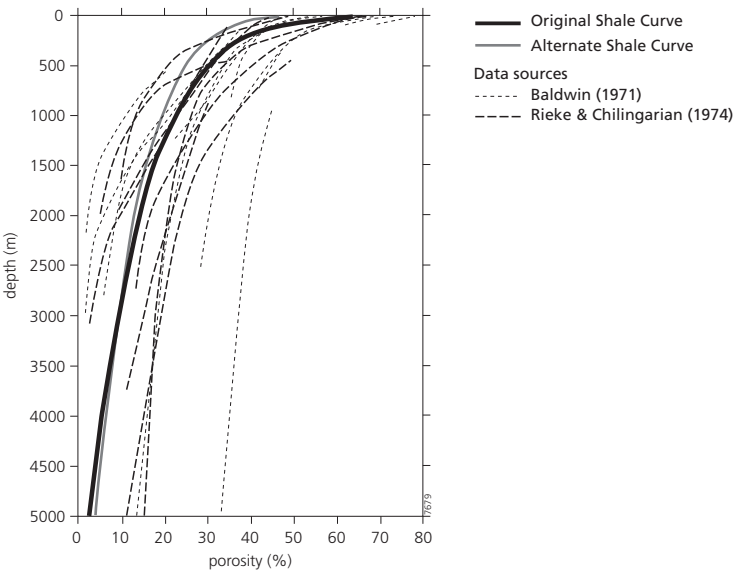

Figure 2.20. Porosity-depth curves, with data from Baldwin (1971; short dashed lines) and Rieke and Chilingarian (1974; long dashed lines). The Original Shale Curve is the best fit to these data. The Alternate Shale Curve more closely approximates the rapid loss of porosity near the surface in alluvial sediments (Anderson, 1991, in: Mackey and Bridge, 1995).

a situation of groundwater table rise, as is common in most Holocene deltas, the s_{cv}/s_{dv} ratio will not increase as long as peat formation in the floodbasin can keep up with the rise of the water table. When peat bogs develop further away from the river, the ratio might even decrease. Furthermore, peat compaction underneath fluvial deposits initially leads to subsidence, thereby creating accommodation space for increased fluvial deposition. If the sedimentation rate keeps up with subsidence due to peat compaction, it is thought that the s_{cv}/s_{dv} ratio will not greatly alter. Overall, it is thought that incorporating peat compaction and formation into alluvial architecture models will decrease avulsion probability. In such environments avulsions most likely occur due to random crevassing during periods of high discharge.

2.5 Conclusions

Peat compaction and formation are key processes in delta evolution, especially in distal parts with relatively high accommodation rates where thick peat layers are formed in the flood basins. The way and magnitude by which peat compaction and formation influence delta architecture strongly depend on the temporal and spatial scale. Peat compaction and formation influence the following aspects of delta evolution:

(1) *Channel belt elevation*. In a situation of groundwater table lowering, subsidence due to compaction and oxidation of peat above the groundwater table in floodbasins leads to relief amplification of sandy channel belts or inversion of former creeks filled with sand. Relief amplification might lead to avulsion.
(2) *Channel belt geometries.* Vertical aggradation, resulting in channel belts with low width/depth ratios, is favored by (I) the high cohesiveness of peat inhibiting bank erosion and (II) peat compaction beneath a channel belt creating accommodation space for fluvial deposition. Contrary, if a relatively thin peat layer is intercalated in between less cohesive sediments, an incising channel will first erode to the depth of the peat layer, which due to its high resistance prevents further vertical incision resulting in channels belts with a high width/depth ratio.
(3) *Channel belt configuration and distribution of fluvial deposits*. A decrease in the rate of accommodation space created by peat compaction beneath a channel belt increases the tendency for lateral migration and hence, the channel becomes more prone to avulsion. The combination of a high bank stability, low regional gradients and low stream power in peatlands favors crevassing, which is an important mechanism initiating avulsion. At a larger scale, invasion of a river system onto a new part of a floodplain is stimulated by (I) variations in compaction rate across a floodplain and (II) a sudden drop in gradient a river experiences where it enters a peatland causes higher rates of clastic deposition at the edges of peatlands, which stimulates the occurrence of nodal avulsions.

The third mentioned aspect is still mainly a hypothesis. The influence of peat compaction and formation on delta evolution is influenced by many factors such as peat type, organic-matter content, sediment sequence composition and groundwater table fluctuations, which so far are seldom taken into account. To determine the relative importance of these factors and to quantify the influence of peat compaction and formation on different aspects of delta evolution, field

research should be combined with numerical models describing peat compaction and formation. To calibrate and validate such a model field data is needed, including lithological data, time control, and groundwater table reconstructions, all at delta scale. The Rhine-Meuse delta dataset contains this kind of data and therefore would be a suitable dataset for calibration and validation.

Acknowledgements

This paper greatly benefited from the critical and constructive reviews by Whitney Autin and Marta Pérez-Arlucea. We thank Ward Koster, Kim Cohen and Hans Middelkoop for commenting on earlier drafts of this paper. Henk Kruse and Gerard Kruse (GeoDelft/Deltares) are thanked for explaining the *a,b,c-isotach* model of Den Haan (1994). This research was funded by the Netherlands Organization for Scientific Research – Earth and Life Sciences (NWO-ALW, project 814.01.014) and Utrecht University, Faculty of Geosciences.

3 A new method for determining the bulk density of uncompacted peat from field settings

Van Asselen, S. and Roosendaal, C., 2009. A new method for determining the bulk density of uncompacted peat from field settings. Journal of Sedimentary Research 79, 918–922.
Reprinted with permission (Society for Sedimentary Geology).

Abstract

A new method for determining the bulk density of uncompacted surficial peat from field settings is presented. Most importantly, a new peat sampler was developed to ensure minimum disturbance of the peat sample. The main benefits of the new device are (1) from the moment of field sampling, the peat sample remains undisturbed in an inner collecting liner, which has a fixed volume and fits perfectly in an outer cutting tube, until the sample is ready to be analyzed in a laboratory, (2) the risk of fracturing or disturbing the sample during lifting it to the surface is significantly reduced by using a vacuum pump or hose to reduce suction at the base of the peat core, and (3) the razor-sharp cutting edge of the outer tube easily cuts through all kinds of fibers by short rotational movements. Furthermore, sufficiently large samples can be extracted, thereby accounting for the heterogeneous character of peat. The device is relatively light and easy to operate, which is a great advantage in the often remote and difficult-to-access peatlands. The sampler was successfully used during test trials on different types of fen peat in the Biebrza National Park, Poland.

Keywords: peat sampler, compaction, dry bulk density, loss on ignition.

3.1 Introduction

Recently formed peat has a very loose and heterogeneous structure; it often contains different kinds of plant remains and may consist partly of a living root mat. Therefore, sampling modern peat without disturbing the peat structure or inducing compaction is difficult. Extracting undisturbed and uncompacted peat samples is needed, however, for determining physical (e.g., bulk density, porosity, organic-matter content, fiber content) and chemical properties (e.g., nutrient concentrations) of peat (Clymo, 1988; Buttler et al., 1998), which is important information for, e.g., carbon storage, ecological and hydrological studies. Furthermore, determination of physical properties of peat is essential with regard to understanding and predicting compactional behavior of peat soils (e.g., Lefebvre et al., 1984), from both a geological and an engineering perspective. Peat is most compressible of all natural soils, and hence, peat compaction potentially leads to vast amounts of subsidence. In populated areas, this may lead to damage to constructions and land inundation. In natural environments, subsidence due to

peat compaction creates accommodation space for either fluvial deposition or peat accumulation, thereby influencing the evolution of, for example, wetlands and alluvial plains (Van Asselen et al., 2009).

An important physical property regarding peat compaction is the dry bulk density. The dry bulk density, and initial porosity, of modern peat depends mainly on (1) organic-matter content, (2) grain-size distribution of the inorganic content, and (3) plant species composition. During compaction initial pore volume is reduced and dry bulk density increases. So, for a specific peat type, changes in dry bulk density reflect changes in the degree of peat compaction. The dry bulk density of uncompacted peat can therefore be used to estimate the amount of compaction of buried peat, which often has higher dry bulk densities (e.g., Bird et al., 2004; Van Asselen et al., 2009). A precondition for this method is that the uncompacted peat sample should be of the same type as the compacted peat sample, meaning they should have similar organic-matter content, texture of the inorganic content, and plant species composition. Furthermore, it is essential to accurately determine the dry bulk density of modern peat, which requires sampling of a fixed volume of peat from field settings without disturbing or compacting the peat. For this purpose, a new peat sampler, presented in this paper, was developed. The main features of the sampler that ensure minimum disturbance of the peat sample are: (1) it consists of an outer cutting tube and an inner collecting liner; the peat sample remains inside the liner with fixed volume until it has been transported to the laboratory for further analyses, (2) a manual vacuum pump or hose is used to reduce suction at the base of the peat core, which prevents fracturing of the core during lifting it to the surface, and (3) the razor-sharp cutting edge of the outer tube easily cuts through all kinds of fibers by short rotational movements. Further details of the sampler are described in the next sections.

3.2 Construction and usage

The peat sampler consists of an outer stainless steel tube and an inner PVC liner which collects the peat sample (Fig. 3.1). The liner fits perfectly in the outer tube, and the inner surface is perfectly smooth (Fig. 3.2a). The sharp cutting edge of the outer tube has sinuous teeth, which easily cut through all kinds of plant remains without disturbing the internal peat structure of the sample. Fibers like wood and thick reed stems do take a little more sawing time. The sampling device is brought downward into a peat substrate by small back-and-forth rotational sawing

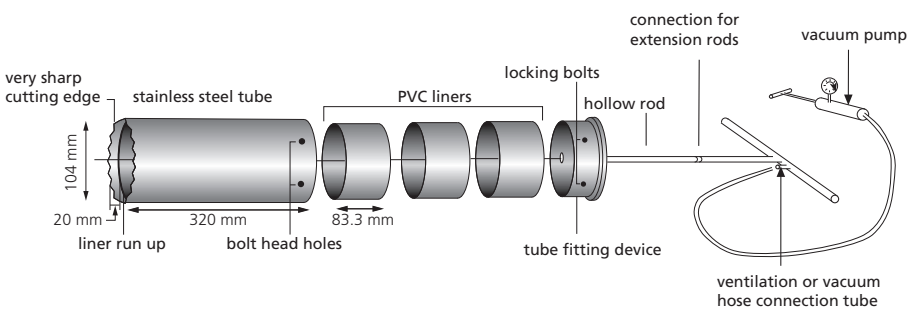

Figure 3.1. Schematic representation of the peat sampler.

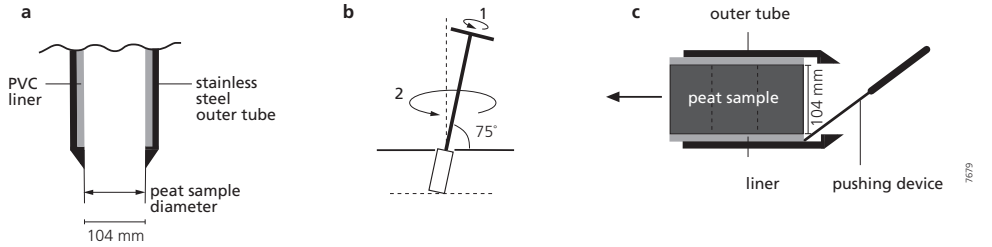

Figure 3.2. a) The liner fits perfectly in the outer tube. b) Before lifting the peat sampler it is turned around its axis and simultaneously twisted at an angle of ~75° with the surface. c) The liner with sample is removed from the outer tube by pushing against the liner using a pushing device. Not to scale.

movements (±1 cm), without exerting any extra downward pressure. During coring, displaced air inside the peat sampler is ventilated through hollow extension rods (Fig. 3.1).

To detach the peat sample from the underlying peat substrate, the sampler is first turned around its axis several times before it is positioned at an angle of maximum 75°, at which position it is turned several times more (Figs. 3.2b, 3.3a). Positioning the sampler at an angle while turning enlarges the borehole. This allows air to flow down along the sides of the peat sampler until the depth of the groundwater table, which makes it easier to lift the sampler to the surface because suction from the sides of the sampler is reduced. Lifting a peat sample to the surface is difficult, because suction in commonly highly saturated peat often causes disruption of fracturing of the sample.

Suction at the base of the peat sample is further reduced by using a manual vacuum pump connected to the hollow rods (Figs. 3.1, 3.3a), which creates a partial vacuum inside the sampler. At the same time, if necessary, air can be blown directly under the sampler using a ~2 cm diameter pipe or hose. The lower end of the pipe or hose was brought down to the desired depth

Figure 3.3. a) Coring in a wet fen: the corer is turned to detach the peat sample while using a vacuum pump to create a partial vacuum inside the sampler. b) The corer with fitting device and extension rod still attached, stabilized in a three-sided cradle. For color version of this figure, see page 177.

Figure 3.4. Individual liners are separated by using a very thin and sharp knife. The liners are stabilized in the sample cradle. For color version of this figure, see page 178.

under the sampler by digging out the peat enclosing the sampler by hand. Field observations indicated that in many cases blowing additional air under the sample was very effective to further reduce the risk of fracturing while lifting the sampler to the surface.

Once the peat sampler is lifted to the surface, the outer tube with the collecting liner and peat sample inside is easily detached from the tube fitting-device with extension rod by turning the bolts clockwise inside (Fig. 3.1), while stabilizing the sampler in a three-sided cradle (Fig. 3.3b). The liner is removed from the outer tube by pushing against the edge of the liner using a pushing device (Fig. 3.2c). During the entire procedure of lifting and removing the liner, the peat sample inside the liner is not disturbed.

The liner consists of three parts, each 83.3 mm in length (= 250 mm/3) and 104 mm in diameter (volume = 708 cm^3), which are held together using strong water-resistant tape. After removing the liner from the outer tube, the three-sided sample cradle is used to stabilize the liner while separating the three parts using a very thin and sharp knife (Fig. 3.4), which ensures that minimum pressure is induced while separating the peat samples. Because the outer cutting tube is 2 cm longer than the liner (Fig. 3.1), the peat core is detached approximately 2 cm below the bottom of the lower liner. The extending part of the core, which most likely has experienced some disturbance during detachment, is removed using the sharp knife. The individual liners with the peat samples are canned with hardtop caps and sealed with foil for protection against deformation and desiccation during transportation to the laboratory.

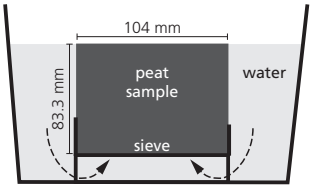

Figure 3.5. Peat samples are placed on a sieve in a bucket of water for saturation.

The same borehole can be used again, to sample deeper buried peat. However, the top sample of the second core is most often disturbed due to the rotational movements used to detach the first core. Therefore, only the middle and bottom sample of the second (or even deeper) core are used for laboratory analyses. To obtain samples at continuous depth intervals, a second borehole in close proximity to the first one may be pre-drilled to a depth shallower than the length of the liner (255 mm), from which sampling starts. This procedure enables extracting samples from each desired depth. A maximum depth of 70 cm was attained during test trials of this sampler.

3.3 Laboratory analyses

The peat samples are first saturated with water to determine the wet bulk density. The peat samples, still inside the collecting liners, are put on top of a sieve in a bucket of water (Fig. 3.5). The sieve mesh width is 280 µm, which prevents loss of sample material. The water level in the bucket is at the same level as the upper edge of the liner. After a couple of hours the samples are close to saturation and are weighed to determine the wet bulk density (WBD = $mass_{sat}/volume_{liner}$). Next, a pie-shaped subsample is cut from the large saturated sample (Fig. 3.6). On average 0.02% mass loss (of ca. 800 g) is introduced by cutting the subsample. This was calculated by measuring the mass of the large sample before cutting, and the cumulative mass of the two parts after cutting (mass loss = $(mass_{before\ cutting} - mass_{after\ cutting})/mass_{before\ cutting} \cdot 100\%$). The large sample is described regarding the size and kinds of fibers in the peat, such as roots, reed, sedge, and wood fragments. Both samples are dried at 105°C for at least 22 hours and weighed afterwards to determine the dry bulk density (DBD = $mass_{dry}/volume_{large\ or\ small\ sample}$). The volume of the large and subsamples are determined assuming that the ratio between the volume of the subsample and the large sample is the same as the ratio between the weight of the subsample and the large sample. In other words, the sample is considered to be homogeneous. The small

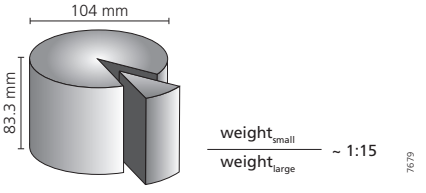

Figure 3.6. A pie-shaped subsample is cut from the large sample. The small sample is burned to determine loss on ignition.

subsamples (on average 5 g dry weight) are burned for four hours at 550°C to determine loss on ignition (LOI = ($mass_{dry}$ – $mass_{burned}$)/$mass_{dry}$), which is used as a measure of the organic-matter content.

3.4 Discussion

The device presented in this paper has several important advantages regarding extracting undisturbed surficial peat samples from field settings compared to other peat samplers. Firstly, the cylindrical shape and razor-sharp sinuous cutting teeth allow to easily cut and saw all kinds of plant materials by short rotational movements. Rectangular-shaped peat samplers (e.g., Digerfeldt, 1966; Cuttle and Malcom, 1979; Fenton, 1980; Wardenaar, 1987; Glew et al., 2001; Givelet et al., 2004) can only be pushed down, thereby likely disturbing the structure of modern peat.

An important advantage of the new device compared to other cylindrical peat samplers, such as the "Hiller sampler" (SCPS, 1961), piston corers (Wright et al., 1984; Glew et al., 2001), the "Russian sampler" or "Macauly samplers" (Jowsey, 1965; Guenet and Reille, 1988), is that it consists of an outer cutting tube and an inner PVC collecting liner with a fixed volume. Peat samples extracted using coring devices that consist of one piece need to be removed from the coring device for further analyses, which inevitably causes some disturbance and/or compaction of the peat sample. It is also difficult to accurately extract a fixed volume of peat from such peat cores. Furthermore, corers such as the "Macauly sampler" are relatively small in diameter (5 cm), which causes disturbance of a large part of the peat sample due to friction between the corer wall and the peat. Also, peat cores with a small diameter might not be representative of heterogeneous peat. Hargis and Twilley (1994) developed a piston corer from which the cutting head can be removed from the cylinder that collects the core. In this case, the peat core remains inside the cylinder, but because it is sectioned to create subsamples for further analyses it cannot be used repeatedly.

Clymo (1988) and Buttler et al. (1998) developed and used a cylindrical-shaped peat sampler consisting of a cutting and collecting tube. These devices have some features, however, that potentially induce disturbance and/or compaction during coring. Clymo's cutting device is first brought down to the desired depth by small up-and-down and rotational movements. Then, the cutting device is removed and a PVC tube is pushed down to enclose the peat core. Buttler et al. (1998) brought down the cutting device and collecting tube consecutively, a few centimeters at a time. So, in both methods, the peat core is prone to some compaction before the collecting tube is pushed down, because it stands freely in the borehole or in the outer tube, and hence is not supported by surrounding peat or an inner coring wall. Also, removing the cutting tube and pushing down the PVC liner likely causes friction at the sides of the peat sample and thereby disturbs the peat structure. The two tubes of the device presented in this paper are brought down simultaneously, and therefore avoids this possible source of compaction or disturbance of peat.

Lifting a peat core to the surface often causes disruption or fracturing of the peat core. To ascertain that the core remains inside the collecting tube, Buttler et al. (1998) constructed a 1-2 mm collar at the lower inside wall of the cutting tube. This, however, may cause some friction with the peat sample during the coring process. Furthermore, especially in very wet peatlands suction from the base of the peat core may be very high, in which case the relatively small

collars may not prevent fracturing. Clymo (1988) used a rather complicated way of detaching and lifting the peat core, which requires well-developed coring skills and more time. In the new device presented in this paper the liner fits perfectly in the outer tube and the inner surface is perfectly smooth. Furthermore, some simple but very efficient techniques, such as using the manual vacuum pump or a pipe or hose to blow air below the peat core, reduce suction from the base of the peat core, which effectively prevents disruption and fracturing during the lifting process.

The peat sample remains undisturbed in the liner from the moment of field sampling until further analysis in the laboratory. In contrast, Buttler et al. (1998) used a steel piston to push the peat core out of the collecting tube into another PVC tube. Because the liner of the new device consists of three equal parts, different volumes can be extracted; depending on the purpose of the study, the three liners can be separated or left in one piece. Because the dry bulk density of peat can be highly variable (Lefebvre et al., 1984), for example due to the inclusion of larger wood fragments, sufficiently large samples should be taken that are representative of larger volumes of peat soil. Too large samples are not practical either, because these are difficult to obtain from the field, and for many experimental tests it takes a long time to analyze very large samples in a laboratory. Therefore, medium-sized peat samples (~1 dm^3) are most favorable for determining bulk density.

The new device is designed for sampling in fens, where peat generally is highly saturated. However, field experiments indicated that the device can also be used in less saturated peat. Furthermore, the sampling device was designed to be as light as possible and can be transported and operated by two persons. This is of great advantage in peatlands, which are often remote and difficult to access.

The method described in this paper was applied in the southern part of the Biebrza National Park, N.E. Poland, which is a wetland that has experienced minimum human disturbance (Żurek, 1984; Oświt, 1993). Different types of fen peat were sampled, including reed, sedge and wood peat. Results showed that the organic-matter content of all samples approximates 90%.

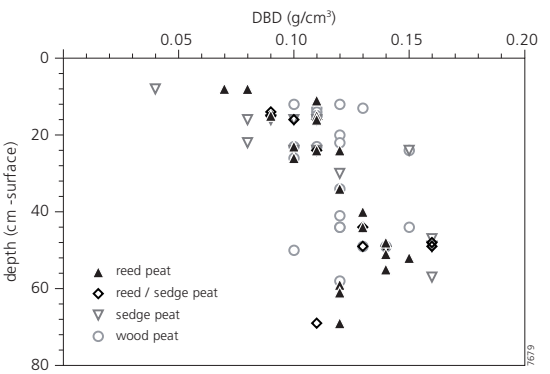

Figure 3.7. Dry bulk density (DBD) of 72 fen peat samples, obtained from the Biebrza National Park (Poland), plotted against depth.

Table 3.1. Calculating the dry bulk density based on the mass density of different texture classes and porosity estimates. The mass densities of organic matter, clay, and silt + sand are indicated in italics in the column headings.

Organic-matter content (%) *1470 kg/m³*	**Clastics – total content (%)**	**Clays (%)** *2700 kg/m³*	**Silt + sand (%)** *2650 kg/m³*	**Mass density* (kg/m³)**	**Porosity (%)**	**Dry bulk density (g/cm³)**
90.0	10	60.0	40.0	1539.5	95.0	0.08
90.0	10	60.0	40.0	1539.5	85.0	0.23
80.0	20	60.0	40.0	1615.9	95.0	0.08
80.0	20	60.0	40.0	1615.9	85.0	0.24

* Mass density = $1/((f_{org}/1470) + (f_{class} \cdot f_{clay}/2700) + (f_{class} \cdot f_{silt+sand}/2650))$, with f = fraction.

The dry bulk density ranges from 0.04 to 0.16 g/cm^3 among the different peat types; the lowest values are measured at shallowest depths (Fig. 3.7). These values indicate the high variability of the dry bulk density of peat. Even wider ranges (0.02 to 0.4 g/cm^3) are found in other field studies (see Brandyk et al., 2002). Clymo (1988) and Buttler et al. (1998), who used cylindrical-shaped peat samplers, determined the dry bulk density of undisturbed high-organic *Sphagnum* peat, which ranged from 0.02 g/cm^3 in the top of the acrotelm to 0.1 g/cm^3 in the underlying catotelm. Our results show on average higher values for fen peat, which is most likely due to a different plant species composition, which influences initial porosity and dry bulk density.

Alternatively, the dry bulk density can be assessed based on calculated mass densities of different texture compositions and initial porosity estimates (Poelman, 1975). Dry bulk densities of high-organic peat calculated based on this method range from 0.08 to 0.24 g/cm^3, depending mainly on the initial porosity (Table 3.1).

The dry bulk densities of uncompacted fen peat, as determined using the method presented in this paper, are within the range of previously published or calculated (Table 3.1) dry bulk densities. However, the validity of the new method can be accurately determined only when different peat samplers are applied in the same study area, which requires extensive fieldwork, which was not possible during this study. Still, the qualitative comparison with other peat samplers (first part of the discussion) strongly implies that using this device introduces minimum disturbance of the sample, and hence, determined dry bulk densities are a close approximation of actual field dry bulk densities.

Acknowledgements

We thank Esther Stouthamer and Kim Cohen for their suggestions for designing the new peat sampler and for their assistance during field campaigns. Esther Stouthamer is also thanked for reviewing earlier drafts of this manuscript. This research was funded by the Netherlands Organization for Scientific Research – Earth and Life Sciences (NWO-ALW, project 814.01.014) and Utrecht University, Faculty of Geosciences.


World's
Most
Dangerous
Road

4 Factors controlling peat compaction in alluvial floodplains: a case study in the cold-temperate Cumberland Marshes, Canada

Van Asselen, S., Stouthamer, E. and Smith, N.D., 2010. Factors controlling peat compaction in alluvial floodplains: a case study in the cold-temperate Cumberland Marshes, Canada. Journal of Sedimentary Research 80, 155-166.
Reprinted with permission (Society for Sedimentary Geology).

Abstract

Subsidence due to peat compaction may have important implications in alluvial floodplains, because it leads to wetland loss, land inundation, and damage to buildings and infrastructure. Furthermore, it potentially influences spatial and temporal river sedimentation patterns, and hence the evolution of alluvial floodplains. As the vast majority of peatlands occur in cold temperate regions, alluvial plains situated in such areas are most susceptible to these implications. To determine which locations within alluvial floodplains are most vulnerable to high amounts of compaction-induced subsidence, it is necessary to quantify compaction and to identify which factors influence the amount and rate of peat compaction. For this, we carried out field work in the Cumberland Marshes (east-central Saskatchewan, Canada) guided by the following two questions: (1) how much peat compaction has occurred over the past decades to centuries, and (2) which factors control the amount and rate of peat compaction at the same timescale. To address these questions, we used methods involving construction of stratigraphic cross sections, organic-matter content and bulk-density measurements, and radiocarbon dating. A new sampling device was devised to sample uncompacted peat in the field. Results show that peat layers have compacted up to 43% within a few centuries, with compaction rates of up to 6.08 mm/yr. The dominant factors influencing peat compaction are: (1) organic-matter content, (2) stress imposed on a peat layer, and, to a lesser extent, (3) plant species composition. In an alluvial setting, crevasse splays and natural levees are sites that are most susceptible to high amounts of peat compaction at short timescales (10^0-10^2 years). Sheet-like splay deposits initially compact underlying peat uniformly, whereas differential compaction commonly occurs beneath natural levees due to lateral variations in sediment thickness. Subsidence due to peat compaction creates additional accommodation space and hence locally enhances floodplain sedimentation rates.

Keywords: subsidence, peat compaction, alluvial floodplain, Cumberland Marshes.

4.1 Introduction

Many modern alluvial floodplains contain thick peat layers, in particular those located in (cold) temperate climatic settings above 45° N, where most peatlands are found (Charman, 2002). Because peat is most compressible of all natural soils (Allen, 1999), compaction of peat layers potentially leads to substantial amounts of subsidence. This may have important consequences in alluvial settings. For example, in populated areas, subsidence due to compaction may cause damage to buildings and infrastructure. In coastal areas, it may accelerate relative sea-level rise, resulting in wetland loss and land inundation (e.g., Long et al., 2006; Törnqvist et al., 2008). Furthermore, peat compaction creates accommodation space for fluvial deposition, and in this way is an important factor controlling spatial and temporal fluvial deposition patterns in deltas and floodplains (e.g., Allen, 1999; Michaelsen et al., 2000; Rajchl and Uličný, 2005; Day and Giosan, 2008; Van Asselen et al., 2009).

To assess the impact of peat compaction, it is necessary to quantify the amount and rate of peat compaction in Holocene alluvial successions. So far, this has mainly been done using empirical or geotechnical models (for an overview see Van Asselen et al., 2009). Results of such modeling studies need to be verified with field data. However, only a few field studies have attempted to quantify peat compaction in Holocene strata. Basically two methods have been used in these studies: (1) the amount of compaction is calculated from estimates of the initial dry bulk density, derived from relations between the dry bulk density of uncompacted peat samples and physical characteristics such as organic-matter content (Bird et al., 2004), and (2) the amount of compaction is estimated using radiocarbon-dated basal peat samples to reconstruct initial levels of peat formation of currently subsided peat samples (Bloom, 1964; Haslett et al., 1998; Törnqvist et al., 2008). Both methods have been used to quantify compaction of peat layers formed in tidal marshes buried by marine deposits during transgression, on millennial timescales. Törnqvist et al. (2008) applied the second method to calculate peat compaction in the Mississippi delta and found a significant relationship between overburden thickness and compaction rate.

In this study, both methods are used to quantify peat compaction in the Cumberland Marshes (CM), a cold temperate wetland in the interior of Canada, on short temporal (10^1-10^2 yr) and small spatial scales (10^0-10^1 m^2). The study site was recently (~135 years ago) invaded by an avulsion of the Saskatchewan River (Smith et al., 1998), which led to alluvial deposition over a peat layer that started to form up to approximately 3000 years ago (Morozova and Smith, 2003). This setting allowed us to (1) quantify peat compaction occurring over decades to centuries and (2) identify and evaluate the factors controlling the amount and rate of peat compaction on the same timescales. Regarding the second objective, (1) variations in stress imposed by deposits overlying the peat layer and (2) peat type (organic-matter content and plant species composition) were recorded at high spatial resolution.

4.2 Geographical setting

The Cumberland Marshes, also referred to as the Saskatchewan River Delta (Dirschl, 1972), are located on the border of the provinces of Saskatchewan and Manitoba, Canada (Fig. 4.1). The Marshes are situated in the western margin of the lacustrine plain of the former glacial

Lake Agassiz (Schreiner, 1983; Morozova and Smith, 1999), downstream of a sharp gradient reduction of the Saskatchewan River, whose drainage basin extends from the continental divide in the Canadian Rocky Mountains to Lake Winnipeg (Fig. 4.1). Alluvial deposition began around 8700-8200 cal yr BP, following withdrawal of glacial Lake Agassiz (Morozova and Smith, 1999). In the subsequent millennia, alluvial aggradation resulted in numerous avulsions of the Saskatchewan River (Morozova and Smith, 1999, 2000), which resulted in episodic redistribution of alluvial sedimentation. The most recent avulsion occurred in the 1870s (Smith et al., 1989; Smith et al., 1998), which initiated the formation of a progradational alluvial wedge in the northwestern part of the Cumberland Marshes. This avulsion affected about 500 km^2 of former peatland, an area which is now characterized by anastomosing channels, splay complexes, wetlands, and shallow lakes. The alluvial wedge overlies a layer of peat typically a few decimeters to over 1 m in thickness. Most peat-forming vegetation in the area receives nutrients from mineral soils, transported by groundwater and rivers, which results in formation of predominantly fen peat. In some isolated localities, however, where plants receive nutrients only from atmospheric deposition, nutrient-poor conditions prevail, and consequently bogs are present (Dirschl, 1972). Hence, in this study, fens and bogs are distinguished based on the main water source at the time of formation, which influences the nutrient status and thereby the main peat-forming vegetation (Birks and Birks, 1980; Charman, 2002). The organic-matter content of peat depends on factors that control the amount of inorganic sediments received by floodbasins, such as distance to an active channel, presence of alluvial ridges that act as barriers to floodbasin deposition, and channel abandonment (Davies-Vollum and Smith, 2008).

The substrate underlying the peat layer consists of predominantly fine-grained floodbasin deposits of previous main channels of the Saskatchewan River and smaller tributaries (Smith et al., 1998). In the area of the current avulsion belt, these sediments are typically found about 2 to 4 m below the surface mainly as stiff, well-compacted, gray silt and silty clay (mud). The high stiffness and the presence of concretions and oxidation stains indicate soil formation during which the sediment has been compacted. Furthermore, silt and clay are much less compressible than peat (Locher and De Bakker, 1990; Mesri and Ajlouni, 2007). For these reasons, the substrate is assumed to be essentially incompressible at centennial timescales.

The Cumberland Marshes region has a daily mean temperature of 18°C for July and -23°C for January, and the mean duration of the frost-free period is about 102 days. Mean annual precipitation is 433 mm, of which about 270 mm falls during the growing season (Dirschl and Coupland, 1972).

4.3 Methods

4.3.1 Site selection

Four study sites were selected to represent different environmental settings (Fig. 4.1). In the North Angling Channel (NAC) and Muskeg Lake Splay (MLS) sites, the peat layer is overlain by crevasse-splay deposits. The Mossy River (MR) and James Bond River (JBR) sites were selected because the peat is overlain by variably thick natural-levee deposits and, at greater distance from the channel, by either thin clayey floodbasin deposits (JBR) or no overburden at all (MR).

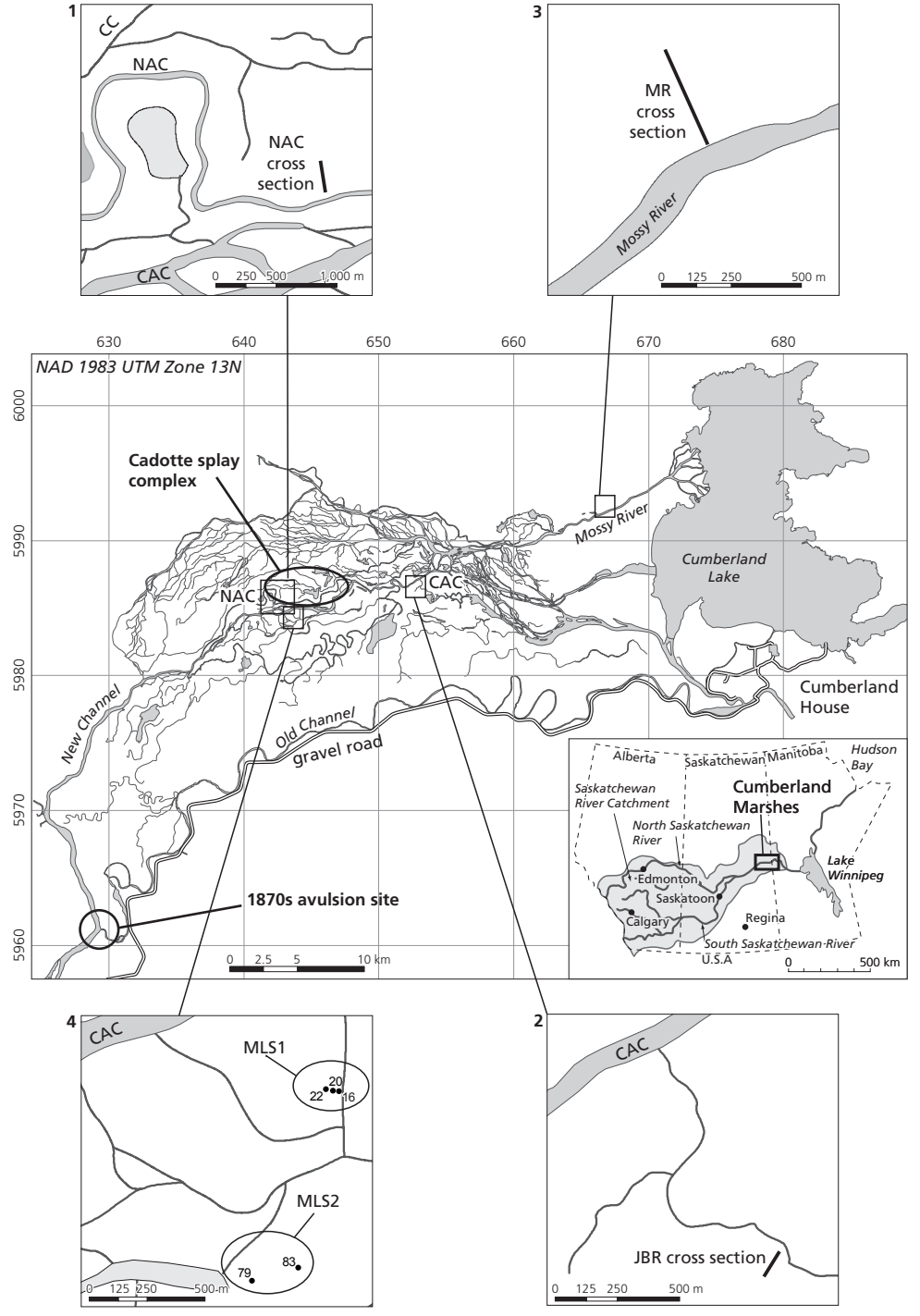
1
CC
NAC
NAC cross section
CAC
0 250 500 1,000 m
3
MR cross section
Mossy River
0 125 250 500 m
630
640
650
660
670
680
NAD 1983 UTM Zone 13N
6000
5990
5980
5970
5960
Cadotte splay complex
NAC
CAC
Mossy River
Cumberland Lake
Cumberland House
New Channel
Old Channel
gravel road
1870s avulsion site
0 2.5 5 10 km
Alberta
Saskatchewan
Manitoba
Hudson Bay
Saskatchewan River Catchment
Cumberland Marshes
North Saskatchewan River
Lake Winnipeg
Edmonton
Saskatoon
Calgary
Regina
South Saskatchewan River
U.S.A
0 500 km
4
CAC
MLS1
20
22
16
MLS2
83
79
0 125 250 500 m
2
CAC
JBR cross section
0 125 250 500 m

⇦ *Figure* 4.1. Location of the Cumberland Marshes and the four study sites. 1 = North Angling Channel (NAC), 2 = James Bond River (JBR), 3 = Mossy River (MR), 4 = Muskeg Lake Splay (MLS). CAC = Centre Angling Channel, CC = Cadotte Channel, H = Horseshoe, dots labelled with coring numbers indicate sampling locations in the MLS (after Smith and Pérez-Arlucea 1994; Morozova and Smith 2000).

4.3.2 Cross sections

Stratigraphic cross sections were constructed to gain insight into the palaeogeographic development of a specific site. Cross sections were oriented perpendicular to the main flow direction, running from the trunk channel towards the floodbasin. In total, six cross sections distributed over the four study sites were constructed, based on logged borehole data retrieved with Edelman and (mainly) gouge augers. Coring depth was determined by the depth of the mud substrate beneath the peat, typically 2-4 m below the surface. Spacing between coring sites was determined based on surface relief and was usually in the range of 2-10 m. Each core was logged at 10-cm intervals for sediment texture, organic-matter content, color, plant remains, oxidation/reduction characteristics, calcium carbonate content, and other relevant properties such as the occurrence of shell fragments, concretions, and sediment-layer transitions (cf. Berendsen and Stouthamer, 2001).

4.3.3 Quantifying peat compaction

The amount of peat compaction was determined by two different methods: (1) measuring changes in dry bulk density (ρ_{dry}) with depth, and (2) where possible, by reconstructing initial elevations of peat formation and isochrones using AMS radiocarbon dating.

During compaction, pore volume decreases and ρ_{dry} increases. Hence, changes in ρ_{dry} of buried peat, compared to the ρ_{dry} of surface peat, which is generally in an uncompacted state, can be used to estimate the relative amount of compaction. A prerequisite for this method is that the compacted and uncompacted samples should be of the same peat type, i.e., they should have a similar plant species composition and organic-matter content. Accordingly, changes in ρ_{dry} were measured at different core sites within the same peat layer. Sampling locations were determined based on variations of thickness and type of alluvial deposits overlying the peat layer. Peat samples were taken at 5-cm intervals directly from a 3-cm-wide gouge auger using a 1 cm x 1 cm x 5 cm sampler. The core was first cut lengthways in half using a thin stretched wire so that the inner part of the core could be sampled. Each 5 cm^3 peat sample was dried at 105°C and weighed on an electronic scale (accuracy of 0.01 g) to determine dry bulk density (ρ_{dry} = dried weight/5 cm^3). The samples were subsequently heated at 550°C for 4 hours to determine loss on ignition (LOI = (dried weight – ashed weight/dried weight)·100%). For determining dry bulk density, the greatest error is introduced by the use of the 5 cm^3 field sampler. It is estimated that the error in volume may be up to 10% (5±0.5 cm^3). According to standard rules of error propagation, the fractional uncertainty in the bulk density calculations is 10%.

Surface peat generally has a very loose structure and heterogeneous plant species composition that may consist partly of a living root mat, which makes it difficult to extract an undisturbed peat sample with fixed volume. Using the gouge auger in combination with the 5 cm^3 sampler introduces significant disturbance and compaction of surficial peat samples. Therefore, we devised a new coring device that takes sufficiently large samples (708 cm^3) to account for the high variability and to minimize disturbance of the fragile structure of peat during sampling (e.g., Lefebvre et al., 1984; Buttler et al., 1998; Givelet et al., 2004). Details

concerning the construction and field application of this sampler are described in Van Asselen and Roosendaal (2009). The uncompacted peat sample was dried at 105°C to determine dry bulk density. To determine LOI, a subsample over the entire length of the large sample was removed and separately dried at 105°C. The dried subsample was further subdivided to meet the capacity of the crucibles, in which they were burned for 4 hours at 550°C.

The ρ_{dry} and LOI data of uncompacted peat samples were used to establish an equation to calculate the uncompacted dry bulk density ($\rho_{dry,uncomp}$) of the compacted peat samples, based on its LOI. Based on a Dutch classification system of peat soils, samples with a LOI >20% are regarded as peat (De Bakker and Schelling, 1966). The data were best described using a nonlinear regression:

$$\rho_{dry,uncomp} = a e^{bLOI} \tag{4.1}$$

in which *a* and *b* are parameters that may differ for different peat types (see section 4.4.2). The $\rho_{dry,uncomp}$ was subsequently used to calculate the decompacted thickness (h_{decomp}) of each 5 cm^3 sample ignoring lateral strain ($h_{decomp}=(\rho_{dry,comp}/\rho_{dry,uncomp})\cdot 5$). Percentage of compaction is expressed as the ratio between the thickness reduction a 5 cm^3 sample has experienced ($h_{red} = h_{decomp} - 5$) and the calculated decompacted thickness of a 5 cm^3 peat sample:

$$\text{compaction} = \frac{h_{red}}{h_{decomp}} \times 100\% \tag{4.2}$$

The decompacted thickness of a peat layer was calculated by summing the decompacted thicknesses calculated for each 5 cm. Like with the 5 cm^3 samples, compaction percentage of a peat layer was calculated using Equation 4.2.

Constructing isochrones and initial levels of peat formation for estimating the amount of peat compaction requires detailed vertical time control. For this, peat samples of 1-2 cm thickness were extracted from the gouge auger using depth intervals of up to 20 cm. The samples were treated with a 5% KOH solution, after which they were washed and wet-sieved over a 150 µm mesh. Next, macrofossils of terrestrial vegetation were selected from the residue using a microscope and submitted for AMS dating. The radiocarbon dates were calibrated using Oxcal 4.1 (Bronk Ramsey, 2001) with the INTCAL04 calibration curve (Reimer et al., 2004) and the *Sequence* deposition model, which assumes that deposition occurs in a specific order, i.e., age increases with depth (Bronk Ramsey, 2008).

Dated peat that directly overlies the compacted mud substrate is assumed not to have experienced any subsidence due to compaction. The elevation of such basal peat samples is used to reconstruct the level of initial peat formation at a certain time. The elevation of peat samples of the same age that experienced subsidence due to compaction is used to estimate the amount of compaction (Fig. 2.13). A precondition of this method is that the incompressible substrate underlying the peat layer has significant relief, which allows basal peat samples to be taken at different depths.

4.3.4 Compaction rates

Compaction rates were calculated by dividing the calculated volume reduction by the time of initiation of clastic deposition overlying the peat layer as determined by AMS radiocarbon

dating of the top of the peat layer. Hence, it is assumed that the peat layer did not significantly compact until it was loaded by fluvial deposits. In this way, maximum compaction rates are calculated, inasmuch as some of the total compaction might have occurred before the start of sediment loading due to microbiological processes (e.g., decay of organic matter), chemical processes (e.g., oxidation and shrinkage above the groundwater table), and self-weight (Allen, 1999; Van Asselen et al., 2009). Compaction due to self-weight is of minor importance in this study because the high-organic peat has a low mass density and consists largely of water (approximately 90% for uncompacted peat). Furthermore, in our study sites the water table is at or near the surface during most of the frost-free season, and hence, compaction due to biological and chemical processes is likely to be much less then compaction caused by loading. This was supported by field observations; extremely wet conditions prevailed in the summer season, and investigated peat layers were generally poorly decomposed. Also, peat layers without overburden were visually less compacted. Analyses of such peat layers showed that the dry bulk density is in the same range as the dry bulk density of uncompacted surface peat (see section 4.4.2; Fig. 4.7a, core MR130). The calculated compaction rates are average values; higher rates might for example occur shortly after loading.

Similarly, average peat accumulation rates could be estimated by dividing the thickness of the peat layer by the duration of peat accumulation (= dated base of peat layer minus dated top of peat layer). Accumulation rate based on the present thickness includes both peat formation and compaction processes, whereas the rate based on the calculated decompacted thickness is corrected for compaction.

The amount and rate of peat compaction in cold-temperate settings may be affected by frost, which is therefore a possible source of error in our calculations. Frost may lead to small seasonal changes in surface elevation due to expansion (freezing) and collapse (ice melt) of pores (Roulet, 1991; Petrone et al., 2008). Because this process is largely reversible, it does not significantly alter the total amount of compaction on longer time periods (decades or more). The timing of compaction depends on the depth of the frost line. If the entire peat layer is frozen, compaction is impeded during the frost season. In this scenario, compaction rates, as calculated in this study, may be underestimated. If only the top peat layer, or the inorganic sediment layer overlying the peat, is frozen, compaction may continue during the frost season. Because the seasonal variations in the depth of the frost line are unknown for our study sites, we were not able to quantify this process, and hence, only recognize this process to be a possible source of error in calculating compaction rates.

4.3.5 Calculation of effective stress

To determine the pressure exerted by the inorganic sediment overlying the peat layer, the effective stress (σ') imposed by the overburden was calculated from Terzaghi's formula $\sigma' = \sigma - u$ (Terzaghi 1943), in which σ is the total stress (Pa) and u is the pore water pressure (Pa). This was done for all cores in which the peat layer was sampled for ρ_{dry} and LOI. The total stress was calculated by:

$$\sigma = h\rho_s g \tag{4.3}$$

in which h is the thickness [cm], ρ_s is the saturated density of a certain texture class (g/cm^3), and g is the gravity constant. Similarly, u was calculated by:

$$u = h\rho_w g \tag{4.4}$$

in which h is the thickness of the water column and ρ_w is the density of water (= 1 g/cm^3). The thickness and texture of an inorganic sediment layer overlying the peat layer were determined in the field during logging of the cores. The saturated density of a specific texture class was calculated from the mass and dry bulk densities of the different texture classes. To determine the mass density of a texture class, the percentage of clay, silt, and sand were estimated from the American soil texture triangle (www.pedosphere.com; Table 4.1).

Table 4.1. Values for mass density, dry bulk density, pore volume, and degree of saturation used to calculate the saturated volumic mass.

	Mass density[a] (g/cm^3)	Dry bulk density[b] (g/cm^3)	Pore volume[c] (-)	Degree of saturation (%)	Saturated volumic mass[d] (g/cm^3)
clay	2.578	1.15	0.554	98	1.693
silty clay	2.590	1.22	0.529	98	1.738
sandy clay	2.606	1.32	0.493	98	1.804
silty clay loam	2.601	1.26	0.516	98	1.765
sandy clay loam	2.601	1.4	0.462	98	1.853
clay loam	2.585	1.3	0.497	98	1.787
silt loam	2.597	1.35	0.480	98	1.821
silt	2.610	1.47	0.437	99	1.903
loam	2.617	1.42	0.457	99	1.873
sandy loam	2.636	1.55	0.412	99	1.958
loamy sand	2.633	1.65	0.373	100	2.023
sand	2.629	1.7	0.353	100	2.053

[a]Mass density = $1/((f_{org}/1.47) + (f_{class}\cdot f_{clay}/2.70) + (f_{class}\cdot f_{silt+sand}/2.65))$, with f=fraction.
[b]Saxton et al. (1986); http://www.pedosphere.com/resources/bulkdensity/triangle_us.cfm?269,216.
[c]Pore volume = (1-dry bulk density/mass density).
[d]Saturated volumic mass = (dry bulk density + f_{sat}·pore volume).

4.4 Results

4.4.1 Interpretations of cross sections

North Angling Channel
The NAC cross section (Fig. 4.2) runs from the distal edge of the northern levee of the NAC northward into the Cadotte crevasse-splay complex (Fig. 4.1; Pérez-Arlucea and Smith, 1999). The NAC was active before the 1870s avulsion, and the Cadotte splay was initiated shortly after the avulsion. In the southern portion of the cross section, the substrate underlying the peat layer consists of old NAC levee deposits, which are relatively coarse-grained, mainly silt and fine sand.

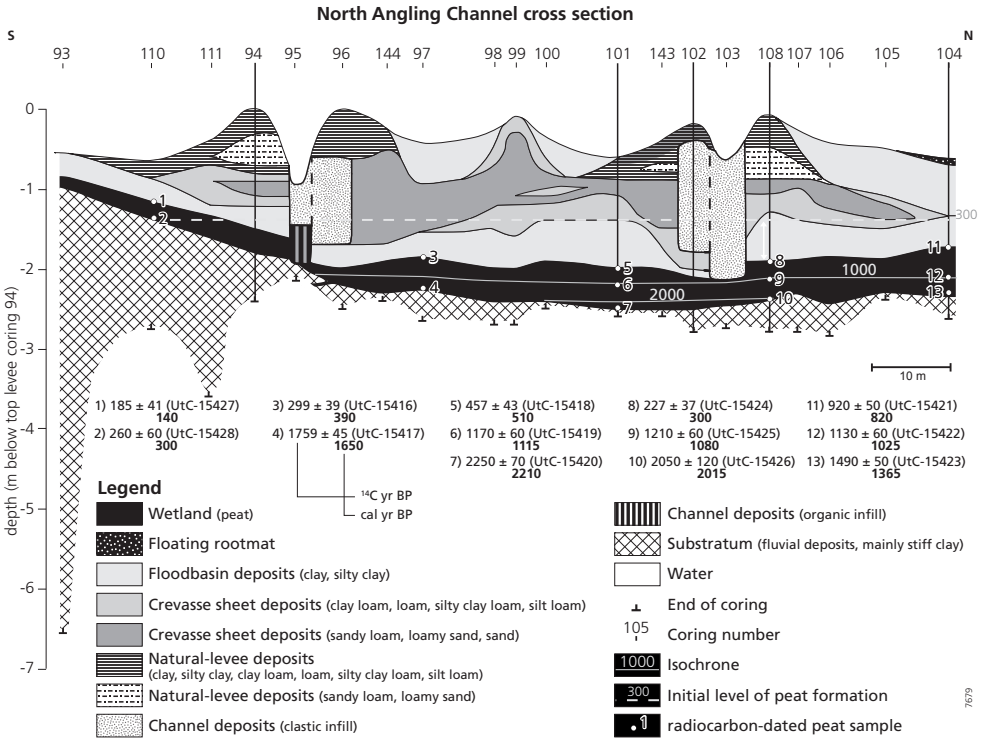

Figure 4.2. North Angling Channel cross section. For location see Fig. 4.1. Sampled cores are indicated with a thick vertical black line (94, 101, 102, 104, and 108).

In the northern portion, the substrate consists of finer floodbasin deposits, mainly stiff silty clay. The peat layer is 10 to 60 cm thick and is covered by an 1 to 2-m-thick alluvial sequence consisting of crevasse-splay sheet deposits, crevasse-channel deposits, and overbank deposits (of the crevasse channels; overbank deposits of the NAC are of minor importance). The peat layer consists mainly of brownish fen peat (Fig. 4.3a) containing predominantly woody (mainly willow) and herbaceous plant remains (mainly horsetail, sedge, and reed). At some locations at the base of the peat layer, detrital peat (Fig. 4.3c) is found containing aquatic plant remains. This indicates that shallow lakes were present, especially during the initial phase of peat formation, which started around 2000 cal yr BP at this site (Fig. 4.2; sample 7).

Pérez-Arlucea and Smith (1999) interpreted the clayey layer overlying the peat in this area as lacustrine and marsh facies deposited shortly following the 1870s avulsion, which induced flooding. Some of our dates indicate, however, that peat formation ended approximately 400 to 500 cal yr BP (Fig. 4.2; samples 3, 5). Especially the uppermost date in core NAC104 (sample 11; Fig. 4.2) was unexpectedly old (820 cal yr BP). Based on historical data and previous work (Smith et al., 1998; Pérez-Arlucea and Smith, 1999), we assume that most alluvial deposition, and hence loading of the peat layer, began approximately 135 years ago. Slightly older calibrated ages of the top of the peat layer are likely due to fluvial erosion of the top of the peat layer

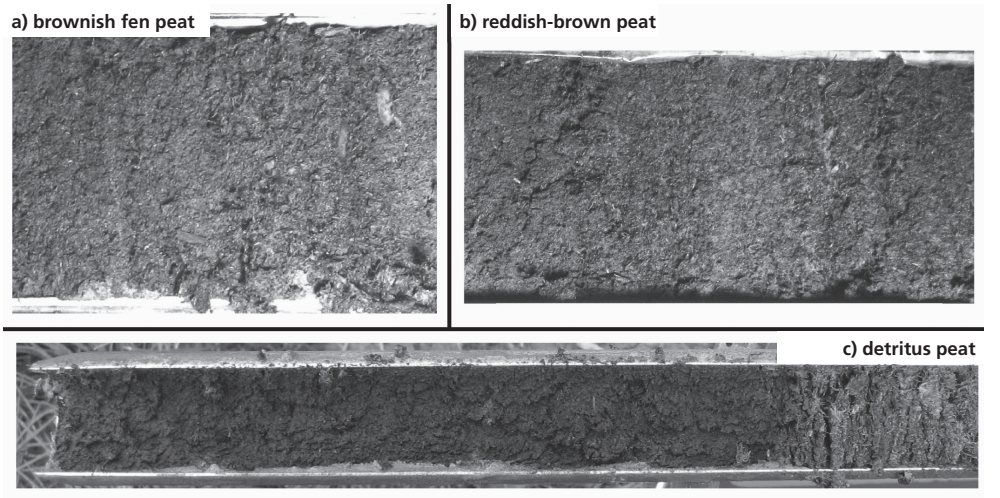

Figure 4.3. Photographs of the main peat types: a) brownish-fen peat, b) reddish-brown peat and c) detritus peat. For color version of this figure, see page 178.

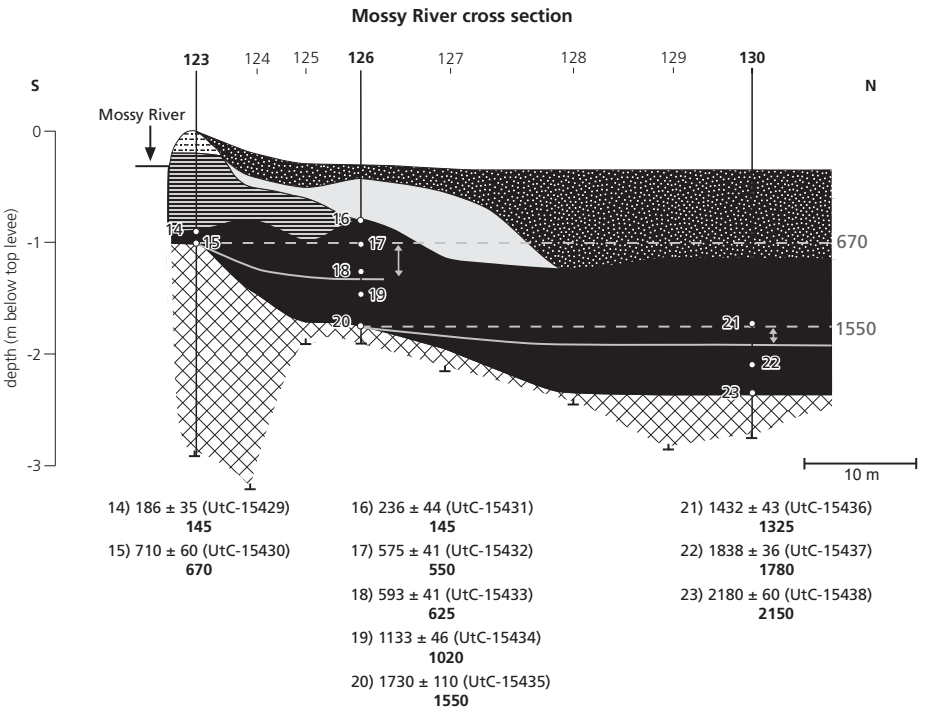

Figure 4.4. Mossy River cross section. For legend see Fig. 4.2, for location see Fig. 1.

following the 1870s avulsion. Also, calibration of samples younger than approximately 400 radiocarbon years often results in a wide range of calibrated age of up to about 300 cal years (Reimer et al., 2004), which makes it difficult to estimate the calibrated age accurately.

The coarsening-upward trend observed in the overlying alluvial deposits indicates continuous progradation of the Cadotte crevasse splay into the former peatland. This phase was followed by channelization and development of small levees. The succession observed in our cross section reflects the attainment of stage II splay development of Smith et al. (1989; see also Pérez-Arlucea and Smith, 1999).

Mossy River

The Mossy River (MR) was an independent and active tributary channel prior to the 1870s avulsion. The MR cross section extends from the north levee of the Mossy River to the northwest (Figs. 4.1, 4.4). The substrate underlying the peat layer consists of older levee deposits of the MR in the south and stiff fine-grained floodbasin deposits farther northward in the cross section. Peat formation started in the northern part of the transect at approximately 2150 cal yr BP (Fig. 4.4; sample 23) and progressively extended southward, thereby gradually covering the sloping levee of the MR. The peat layer varies in thickness from only 15 cm close to the MR channel to about 2 m in the floodbasin, where peat is still actively forming. Here, the upper first meter consists of floating root and peat mats. During floods, fine suspended sediment is trapped in these floating mats. Mainly reddish-brown fen peat is found (Fig. 4.3b), containing predominantly mosses and herbaceous plant remains (sedge, horsetail, reed), and occasionally woody remains. This peat is characterized by a dense network of fine roots. In contrast, the thin peat layer found within the MR levee has a loose structure, is more decomposed, and contains tree and sedge remains. It is interpreted as a forest litter layer and indicates a period of low fluvial activity of the Mossy River during which litter from plants and trees accumulated on the levee surface.

The top of this peat layer yielded a radiocarbon age of 186±35 yr BP (sample 14). Calibration of this age, using Oxcal Version 4.1, results in two ranges (at 68.2% probability): 291-265 cal yr BP (22%) and 217-146 cal yr BP (46.2%). We assume that the youngest range is correct: renewed levee formation started after the Mossy River was annexed by the 1870s avulsion, which caused an increase in channel size, discharge, and input of clastic sediments.

James Bond River

The James Bond River (JBR) is a small distributary of the Centre Angling Channel (Fig. 4.1). The 1870s avulsion invaded the area south of the NAC in the 1920s and 1930s (Pérez-Arlucea and Smith 1999). Before that time, most flow was directed from the New Channel to the area north of the NAC, while the area south of the NAC consisted mostly of peatland and shallow lakes. The JBR cross section runs from the JBR south levee in a southwestern direction (Figs. 4.1, 4.5). The substrate in this area consists entirely of stiff, sometimes silty, clay; a floodbasin deposit probably of the Ancestral South Angling Channel (Morozova and Smith 1999). In this area, peat formation started at approximately 2800 cal yr BP (Fig. 4.5; samples 28, 33). In general, detrital peat averaging 20 cm in thickness occurs at the base of the peat layer, indicating accumulation in a shallow lake. The detrital peat grades rapidly upwards into thicker peat consisting of herbaceous, moss, and wood remains, suggesting that the lake evolved into a fen. Throughout the peat layer of 90 to 140 cm thick, clastic input varies considerably with depth, indicating periods of peatland flooding. The peat layer is overlain by silty clay that

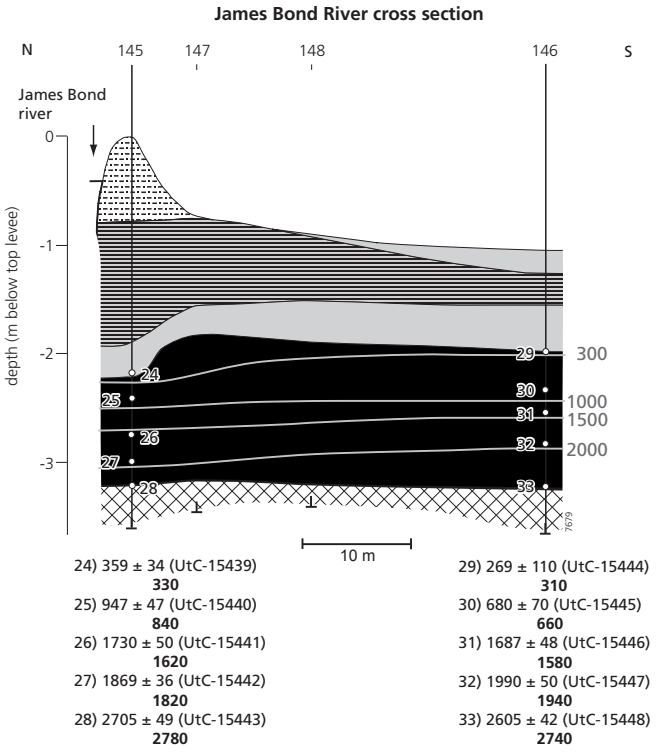

Figure 4.5. James Bond River cross section. For legend see Fig. 4.2, for location see Fig. 1.

contains shell fragments and plant remains. Two radiocarbon dates from the top of the peat layer indicate that sediment deposition started around 300 cal yr BP, before the 1870s avulsion. This is most unlikely, inasmuch as aerial photographs and historical maps (unpublished) suggest that this area was invaded no sooner than early twentieth century. Furthermore, the calibrated range calculated for the uppermost date of core JBR146 yielded 500-270 and 169-154 cal yr BP at 68% probability and 517-0 cal yr BP at 95% probability, so the 300 cal yr BP presented in Fig. 4.5 (sample 29) is uncertain. For these reasons, we assume that most loading due to alluvial deposition has occurred during the last 80 years.

The coarsening-upward trend observed in the overlying sediment profile indicates increased fluvial activity of the JBR, which probably started as a crevasse of the Centre Angling Channel. Overbank deposits of the JBR range in thickness from 230 cm (maximum levee thickness) to 90 cm (floodbasin, Fig. 4.5).

4.4.2 Amount and rate of peat compaction

North Angling Channel

The brownish forest-sedge peat occurring at the NAC site has LOI values mostly around 85%, with lower values at the transitions to overlying and underlying floodbasin deposits (Appendix 1). Peat in core NAC94, which lies closest to the NAC, has a relatively low LOI, which indicates

Table 4.2. Mean dry bulk densities for different LOI ranges of sampled cores derived from the North Angling Channel (NAC), Mossy River (MR), and James Bond River (JBR) study sites (core numbers are given). Standard deviation/number of samples are indicated in italics in parentheses below mean value.

LOI (%)	Mean dry bulk density (g/cm^3)									
	NAC					MR			JBR	
	94	101	102	104	108	123	126	130	145	146
90-100	-	-	-	-	-	-	0.16 *(0.01/5)*	0.10 *(0.01/7)*	0.15 *(0.01/5)*	0.14 *(0.01/2)*
80-90	-	0.21 *(0.02/8)*	0.21 *(0.01/6)*	0.24 *(0.02/7)*	0.25 *(0.02/5)*	-	0.17 *(0.01/3)*	0.10 *(0.01/7)*	-	0.16 *(0.03/5)*
70-80	0.24 *(0.03/2)*	0.24 *(0.02/2)*	0.26 *(0.05/4)*	0.26 *(-/1)*	0.27 *(0.06/2)*	-	0.18 *(0.01/2)*	0.11 *(-/1)*	0.22 *(-/1)*	0.19 *(0.05/2)*
60-70	0.31 *(0.04/2)*	0.39 *(-/1)*	-	0.26 *(-/1)*	0.27 *(-/1)*	-	0.21 *(-/1)*	-	0.28 *(0.01/4)*	0.23 *(0.01/7)*
50-60	0.40 *(-/1)*	-	-	0.66 *(-/1)*	-	0.26 *(0.04/2)*	0.25 *(-/1)*	0.13 *(-/1)*	0.31 *(0.01/5)*	-
40-50	-	-	-	-	-	-	0.28 *(0.02/2)*	-	0.37 *(0.04/3)*	0.33 *(0.06/5)*
30-40	0.74 *(-/1)*	-	-	0.47 *(0.03/2)*	-	-	-	0.32 *(-/1)*	0.51 *(0.07/3)*	0.35 *(-/1)*
20-30	0.91 *(-/1)*	-	-	-	0.75 *(-/1)*	0.56 *(-/1)*	0.54 *(0.12/3)*	-	0.62 *(-/1)*	0.44 *(-/1)*

a higher input of inorganic sediment at this location. Davies-Vollum and Smith (2008) also found that peat formed close to active channels tends to have low organic contents. In general, peat with a low LOI has a relatively high ρ_{dry} (Table 4.2; Fig 4.6a).

Uncompacted peat samples were obtained from the nearby fen enclosed on three sides by a large bend of the NAC west of the study site (locally called the "Horseshoe", Fig. 4.1). Here, the young peat is composed mainly of sedge and woody remains, and thus is similar to the peat found in the NAC cross section. Fitting values of LOI versus ρ_{dry} for the uncompacted peat samples yielded the following equation (R^2 = 0.99; Fig. 4.6a):

$$\rho_{dry,uncomp} = 0.7703\exp^{-0.0202LOI} \quad (4.5)$$

For most 5 cm^3 samples, the calculated compaction percentage lies between 30 and 50% (Appendix 1). Because uncompacted detrital peat was not found, Equation 4.5 was also used to calculate compaction of detrital peat. This did not introduce a large error in calculating the total compaction of the peat layer because the detrital peat material, occurring at the base of the peat layer, is only 0 to 10 cm thick. In two cases, however, the compaction calculated for a detrital peat sample is unusually high (Appendix 1: 50% at the base of NAC101 and 63% at the base of NAC104). The initial ρ_{dry} of the detrital peat is likely to be higher than the ρ_{dry} of the forest peat, due to the finer and denser structure of detrital peat. Using a higher initial ρ_{dry} would lead to lower calculated compaction percentages.

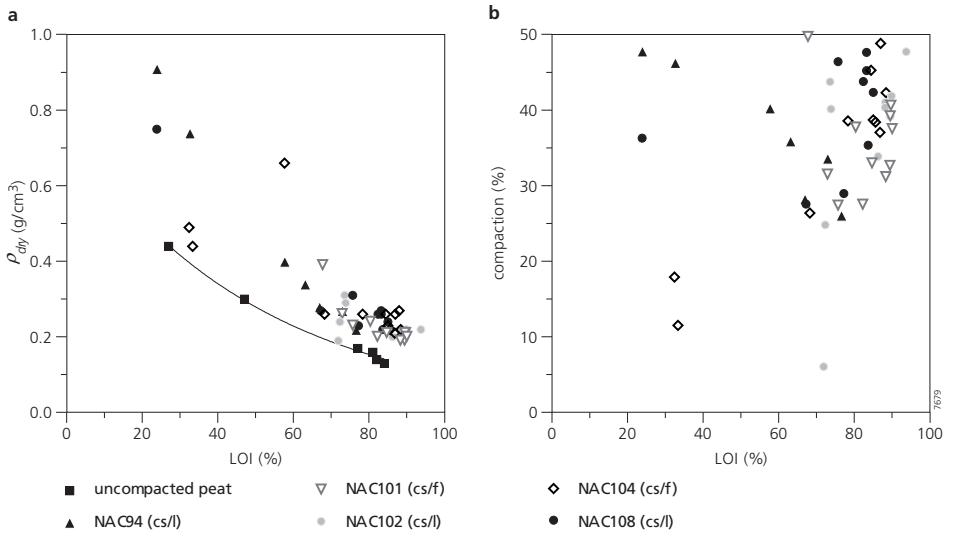

Figure 4.6. a) Plot of LOI vs. dry bulk density (ρ_{dry}), and b) plot of LOI vs. compaction for sampled cores of the NAC cross section (94, 101, 102, 104, and 108; Fig. 4.2; cs = crevasse splay deposits, f = floodbasin deposits, l = natural-levee deposits).

The amount of compaction does not show a clear relationship with LOI. Only in cores NAC102 and NAC104 does compaction seem to increase with increasing LOI (Fig. 4.6b). The calculated compaction for each core varies between 34% and 39% (Table 4.3). Assuming an uncertainty of 10% in the determination of the ρ_{dry} (section 4.3.3), all compaction values presented in this paper appeared to have an uncertainty of ±6-7% except for the MR130 core, where exceptionally low ρ_{dry} were measured and compaction percentages have an uncertainty of ±10%. Our data suggest that the peat layer has been uniformly compacted under the load of the crevasse-splay deposits.

For core NAC108, the amount of compaction was also estimated by using the isochrone method. The elevation of sample 2 (Fig. 4.2) was used to reconstruct the level of peat formation 300 cal yr BP. By comparing the elevation of this level to that of sample 8, compaction of 45% was calculated, which is reasonably similar to the compaction values calculated from ρ_{dry} measurements.

Mossy River

Three cores of the MR cross section were analyzed for ρ_{dry} and LOI (Fig. 4.4; Appendix 2). The forest-litter peat formed on the natural levee close to the channel (MR123) has a lower organic-matter content than peat formed farther into the floodbasin (MR126 and MR130), reflecting a higher input of inorganic sediment close to the channel (see also Davies-Vollum and Smith, 2008). In cores MR126 and MR130, a decrease in LOI is observed at 1.5 m and 1.7 m below the top level of the levee. This is likely caused by an episodic increase in river sediment due to flooding and/or to local trapping of fine suspended sediment by vegetation. In general, peat with a relatively high LOI has a relatively low ρ_{dry} (Fig. 4.7a; Table 4.2).

Table 4.3. Amount and rate of compaction, effective stress imposed by sediment overburden, and accumulation rates for each sampled peat core. The accumulation rate is calculated based on the current compacted thickness of the peat layer (column "comp") and based on the calculated decompacted thickness of the peat layer (column "decomp").

Core	Compaction (%)	Compaction rate (mm/yr)	Effective stress (kPa)	Accumulation rate (mm/yr)	
				comp	decomp
NAC94	38	1.58	12.48	no dates	
NAC101	34	2.06	10.77	0.26	0.41
NAC102	38	2.22	16.15	0.24	0.38
NAC104	37	2.63	8.25	0.49	0.83
NAC108	39	2.16	14.84	0.24	0.40
MR126	30	2.56	3.40	0.49	0.72
MR130	-4	0	0	0.41	0.39
JBR145	30	5.89	18.38	0.41	0.59
JBR146	17	3.09	6.42	0.45	0.55
MLS16*	43	6.08	23.24	0.31	0.54
MLS20*	32	5.87	11.61	0.48	0.71
MLS22*	37	4.14	14.04	0.27	0.43
MLS79*	42	4.29	13.57	0.23	0.40
MLS82*	41	5.18	5.31	0.29	0.49

*Peat accumulation started ~2700 cal yr BP (based on dated peat sample from the base of the peat layer at MSL1 site, ^{14}C age 2590±60).

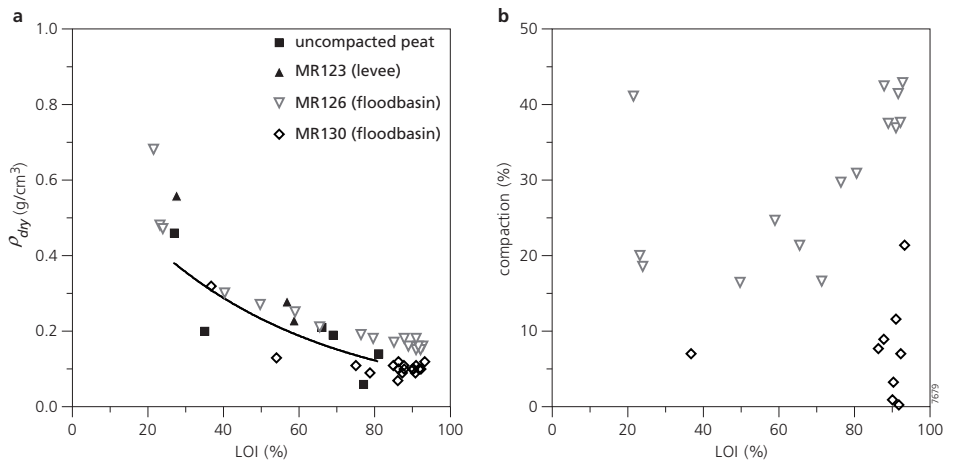

Figure 4.7. a) Plot of LOI vs. dry bulk density (ρ_{dry}), and b) plot of LOI vs. compaction for core 123, 126, and 130 of the Mossy River cross section (Fig. 4.4). Negative compaction percentages for MR130 are not shown.

Uncompacted peat samples were obtained from the uppermost meter near core M130 and in the peatland farther northward. LOI and ρ_{dry} measurements of these samples were used to construct the following equation to calculate $\rho_{dry,uncomp}$ for compacted peat (R^2=0.58; Fig. 4.7a):

$$\rho_{dry,uncomp} = 0.6212\exp^{-0.0204LOI} \quad (4.6)$$

Compaction of core MR123 was not calculated, because uncompacted forest-litter peat was not found. Calculated compaction was 30% for core MR126 and -4% for core MR130 (Table 4.3). The value -4% suggests expansion of the peat layer, which could be caused by high saturation at this site, inducing floating and expansion. Alternatively, the negative value may be caused by errors introduced during sampling (section 4.3.3). Still, our data strongly suggest that little if any compaction occurred in core MR130 except for some compaction due to its own weight at the base of the peat layer, where compaction, calculated for each 5 cm^3 sample, slightly increases (Appendix 2). Except for samples with a very low LOI (<40%), compaction increases with increasing LOI (Fig. 4.7b).

In this cross section, compaction was calculated from isochrone reconstructions. These indicate compaction of about 15% of the base of the peat layer at core MR130 (Fig. 4.4). Calculating compaction of the lowermost 50 cm from Equation 4.6 yields 5±10% compaction, so the 15% compaction estimated from isochrones falls within the range. Based on the 670 yr peat-formation level, compaction of 40% at core MR126 was calculated, which is not greatly different from that calculated from Equation 4.6 (31% for this part of the peat layer).

James Bond River

Both sampled cores (JBR145 and JBR146) show a high variation in LOI with depth and an associated variation in ρ_{dry} (Appendix 3). Peat with a relatively high LOI has a relatively low

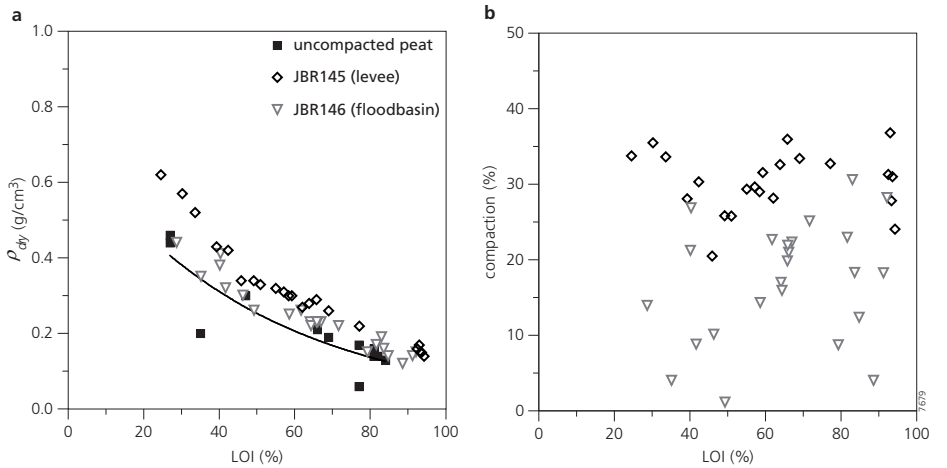

Figure 4.8. a) Plot of LOI vs. dry bulk density (ρ_{dry}), and b) plot of LOI vs. compaction for sampled cores of the James Bond River cross section (JBR145 and JBR146; Fig. 4.5).

ρ_{dry} (Fig. 4.8a; Table 4.2). Because the peat has characteristics similar to peat at both NAC and the MR, parameter values for the equation to calculate uncompacted ρ_{dry} were determined from fresh peat samples obtained from both the Horseshoe and the Mossy River wetlands. This resulted in the following equation (R^2=0.67):

$$\rho_{dry,uncomp} = 0.6641\exp^{-0.0196LOI} \quad (4.7)$$

Calculated compaction percentages for the 5 cm^3 samples were highest for peat underlying the thick levee (Fig. 4.8b). No clear trend exists between LOI and compaction percentage (Fig. 4.8b). Average compaction values of 30% and 17% for core JBR145 and JBR146 respectively were calculated (Table 4.3).

4.4.3 Compaction rates

The compaction rate is expressed as the amount of subsidence due to compaction that occurred since loading of the peat layer (mm/yr). Most peat compaction at the NAC and MR sites is likely induced by the overburden deposited after the 1870s avulsion, so most compaction has occurred within approximately 135 years. Based on aerial photographs and historical maps, we estimate a loading duration of 100 years in the Muskeg Lake Splay and 80 years in the James Bond River sites. The highest calculated compaction rate is 6.08 mm/yr (Table 4.3). Average peat accumulation rates are 0.35 mm/yr (range 0.23-0.49, standard deviation = 0.10) and 0.53 mm/yr (range 0.38-0.83, standard deviation = 0.15) for presently compacted and calculated decompacted thicknesses, respectively.

4.4.4 Overburden

Peat layers in five additional cores were analyzed for ρ_{dry} and LOI in the Muskeg Lake Splay (Fig. 4.1). In the Muskeg Lake Splay site, an approximately 1-m-thick layer of predominantly reddish-brown moss-sedge peat is overlain by crevasse-splay deposits up to 4 m thick. For each

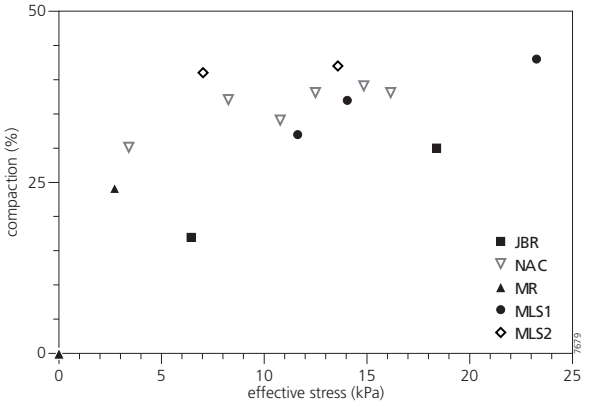

Figure 4.9. Effective stress versus percentage of compaction of 14 analyzed cores obtained from four different sites (see Fig. 4.1).

of the 14 cores examined for ρ_{dry} and LOI, the effective stress imposed on the peat layer was calculated and plotted against the amount of compaction. In the MR, JBR, and MLS1 sites, compaction increases with increasing effective stress imposed on the peat layer (Fig. 4.9). Cores obtained from the NAC and the MLS2 sites show no significant trends in the amount of compaction with the effective stress.

4.5 Discussion

4.5.1 Methods

Our data show that the dry bulk density of low-organic peat (LOI ≈ <40%) is more variable than that of high-organic peat (Table 4.2; Figs. 4.6a, 4.7a, 4.8a). Mixtures of (partly decomposed) plants and inorganic sediments apparently result in heterogeneous soil structures. The initial porosity of low-organic peat, and hence dry bulk density, is increasingly influenced by the greater content of inorganic sediments, and more specifically, by the variable grain-size distributions of those sediments. In general, a heterogeneous texture results in a denser soil matrix, because pore spaces between larger grains are easily filled by smaller grains, which leads to a higher dry bulk density. Consequently, the method for calculating compaction based on ρ_{dry} as used in this study is less reliable when used for low-organic peat, because variations in dry bulk density may be caused by variations in the sorting and mineral density of the inorganic components rather than by different degrees of compaction. This is likely to be the case for several of our analyzed cores (Figs. 4.6, 4.7, 4.8; NAC94, NAC108, MR126 and JBR145). Here, unexpected and probably erroneously high compaction percentages are calculated for low-organic peat samples.

The two methods used for calculating compaction give similar results, although the ρ_{dry} method yields slightly lower values. This might be caused by consistent small errors introduced during extraction of peat samples for measuring bulk density.

Equation 4.7 can be regarded as a combined version of Equations 4.5 and 4.6, inasmuch as parameters *a* and *b* are derived from fresh peat samples from both the NAC and MR sites. Hence, Equation 4.7 is considered as the most generalized equation, which can be used to calculate the uncompacted dry bulk density of fen peat composed of predominantly herbaceous and woody material in cold-temperate settings.

4.5.2 Factors controlling peat compaction

Our data suggest peat compaction of up to 43% occurring over approximately 135 years. Calculated compaction rates are up to 6.08 mm/yr. The amount of compaction in alluvial settings is highly variable, as shown by our results as well as those of others (e.g., Bloom, 1964; Haslett et al., 1998; Törnqvist et al., 2008). These studies calculated compaction of 13-47% and compaction rates of up to 5 mm/yr, which are of the same order of magnitude as our results but calculated over millennial timescales. Thus, our data imply that much compaction occurs relatively shortly after loading.

The following factors controlling the amount and rate of peat compaction were identified in this study:

(1) *Organic-matter content.* For similar peat types, a high organic-matter content has a higher compaction potential, as is indicated by the generally positive relation between LOI and compaction percentage (Figs. 4.6b, 4.7b, 4.8b). Still, a positive relation was observed in not all analyzed cores, which may be due to variations in plant species and textures influencing initial porosity.
(2) *Overburden.* The amount of compaction depends on the effective stress imposed on the peat layer, determined predominantly by the thickness of sediment overburden (Fig. 4.9; see also Törnqvist et al., 2008). Indeed, at the JBR site, the amount of compaction is higher under the natural levee than under contiguous but thinner floodbasin deposits (Fig. 4.5). At the NAC site, however, no significant differential compaction is observed, despite variations in thickness of the overlying alluvium. Most compaction probably occurred during burial by sheet-like splay deposits and before well-defined splay channels and their levees had formed. Such sheet-like splay deposits have a relatively uniform thickness and therefore compact the underlying peat layer evenly. It is likely that the time since the development of stable levees is too short to have caused any differential compaction at the NAC site.
(3) *Peat type.* The main peat types encountered in this study are (1) brownish fen peat containing mainly herbaceous and woody remains and (2) reddish-brown sedge-moss peat characterized by a dense network of fine roots, which creates a high initial porosity. Consequently, for a specific LOI, the uncompacted dry bulk density of the reddish-brown fen peat is on average slightly lower than that of brownish fen peat and thus has a higher compaction potential than the brownish peat. Furthermore, compaction rates at the Muskeg Lake Splay site (sedge-moss peat) are generally higher than compaction rates at the NAC site (brownish fen peat), while in both areas the effective stress imposed on the peat layer are similar (Table 4.3). Moreover, the peat layer at the Muskeg Lake Splay site has been loaded for a shorter time period, implying that the reddish-brown sedge-moss peat is more compressible. Based on laboratory compression tests, Den Haan (1994) also found that peat containing woody remains is less compressible than sedge peat. Still, based on our data, differences in the amount of compaction seem to be controlled mainly by loading conditions and organic-matter content, and less by plant species composition.

Subsidence due to peat compaction beneath overbank deposits, especially crevasse splays and natural levees, creates additional accommodation space for alluvial deposition. This implies that peat compaction increases floodplain sedimentation rates, provided that the sediment load of the river is sufficiently high. Locally increased sedimentation rates due to peat compaction have been demonstrated by both field studies (Haslett et al., 1998) and modeling studies (Allen, 1999). In this study, the effect of spatially variable factors within a delta (i.e. loading conditions and organic-matter content and type of peat) on the amount of accommodation space created by peat compaction has been quantified.

4.6 Conclusions

A relatively high amount of peat compaction occurs shortly after loading. In this study, up to 43% compaction occurred within approximately 135 years, with maximum compaction rates of 6.08 mm/yr. The most important factors controlling the amount and rate of peat compaction

are organic-matter content and weight of sediment overburden. To a lesser extent, plant species composition influences the compressibility of peat. High-organic peat containing mainly roots and small fibers is most susceptible to compaction. Thus, sites where high-organic peat underlies thick crevasse splays or natural levees are most susceptible to subsidence due to compaction. Shortly (decades) after deposition of crevasse sheet deposits, relatively uniform peat compaction occurs. Differential compaction results when stable natural levees develop; a higher amount of compaction occurs under levees than in the adjoining floodbasins. Subsidence due to compaction at such sites creates additional accommodation space for alluvial deposition, which enhances floodplain sedimentation rates.

Acknowledgements

Chris Roosendaal, Ingwer Bos, Willem Toonen, and our local guide Gary Carriere are thanked for their assistance during the fieldwork in the Cumberland Marshes. We thank Nelleke van Asch for selecting macrofossils of terrestrial vegetation suitable for radiocarbon dating, which was performed at the R.J. van de Graaff laboratory, Utrecht University. This research was funded by the Netherlands Organization for Scientific Research – Earth and Life Sciences (NWO-ALW, project 814.01.014) and Utrecht University, Faculty of Geosciences. This paper benefited greatly from reviews by Jackie Huntoon, Greg Nadon, and an anonymous reviewer.

5 The contribution of peat compaction to total basin subsidence: implications for the provision of accommodation space in organic-rich deltas

Van Asselen, S.
Accepted for publication in Basin Research.

Abstract

Provision of accommodation space for aggradation in Holocene deltaic basins is usually ascribed to eustatic sea-level rise and/or land subsidence due to isostasy, tectonics or sediment compaction. Whereas many Holocene deltas contain peat, the relative contribution of peat compaction to total subsidence has not yet been quantified from field data covering an entire delta. Subsidence due to peat compaction potentially influences temporal and spatial sedimentation patterns, and therewith, alluvial architecture. Quantification of the amount and rate of peat compaction was done based on (1) estimates of the initial dry bulk density of peat, derived from a relation between dry bulk density and organic-matter content of uncompacted peat samples, and (2) radiocarbon-dated basal peat used to reconstruct initial levels of peat formation of currently subsided peat samples.

In the Rhine-Meuse delta, peat compaction has contributed considerably to total basin subsidence. Depending on the thickness of the compressible sequence, weight of the overburden and organic-matter content of peat, subsidence of up to approximately 3 m in a 10-m-thick Holocene sequence has been calculated. Calculated local subsidence rates of peat levels are up to 0.6 mm/yr, averaged over millennia, which are twice the estimated Holocene-averaged basin subsidence rates of 0.1-0.3 mm/yr in the study area. Higher rates of subsidence due to compaction, on the order of a few mm/yr, occur over decades to centuries, following a substantial increase in effective stress caused by sediment loading. Without such an increase in effective stress, peat layers may accumulate for thousands of years with little compaction. Thus, the contribution of peat compaction to total delta subsidence is variable in time. Locally, up to 40% of total Holocene accommodation space has been provided by peat compaction. Implications of the large amount of accommodation space created by peat compaction in deltaic basins are: (1) increased sediment trap efficiency in deltas, which decelerates delta progradation and enhances the formation of relatively thick clastic sequences, and (2) enhanced local formation of thick natural levees by renewing existing accommodation space.

Keywords: peat compaction, subsidence, accommodation space, Rhine-Meuse delta.

5.1 Introduction

In Holocene deltas, accommodation space for sediment accumulation or peat formation is usually provided by a combined effect of base-level rise (e.g., forced by eustatic sea-level rise) and/or land subsidence due to isostasy, tectonics, or natural sediment compaction. The same processes make deltas, presently inhabited by about half a billion people, highly susceptible to flooding (Ericson et al., 2006; Day and Giosan, 2008; Syvitski, 2008; Syvitski et al., 2009). In modern times, anthropogenic influences such as groundwater withdrawal, hydrocarbon extraction, and land reclamation accelerate subsidence rates, thereby increasing the risks associated with delta subsidence (Ingebritsen et al, 2000; Ericson et al., 2006).

Comparing world population density maps (NCGIA, 1999) with peatland distribution maps (Charman, 2002) reveals that many deltas contain large peatlands. Peat compaction is an apparently underestimated component of land subsidence in many deltaic environments (Day and Giosan, 2008; Törnqvist et al., 2008). An alluvial sequence containing peat is susceptible to increased rates of subsidence due to compaction because peat is most compressible of all natural soils. Furthermore, peat compaction creates accommodation space for additional clastic sedimentation or peat accumulation (Haslett et al., 1998; Allen, 1999; Törnqvist et al., 2008). By

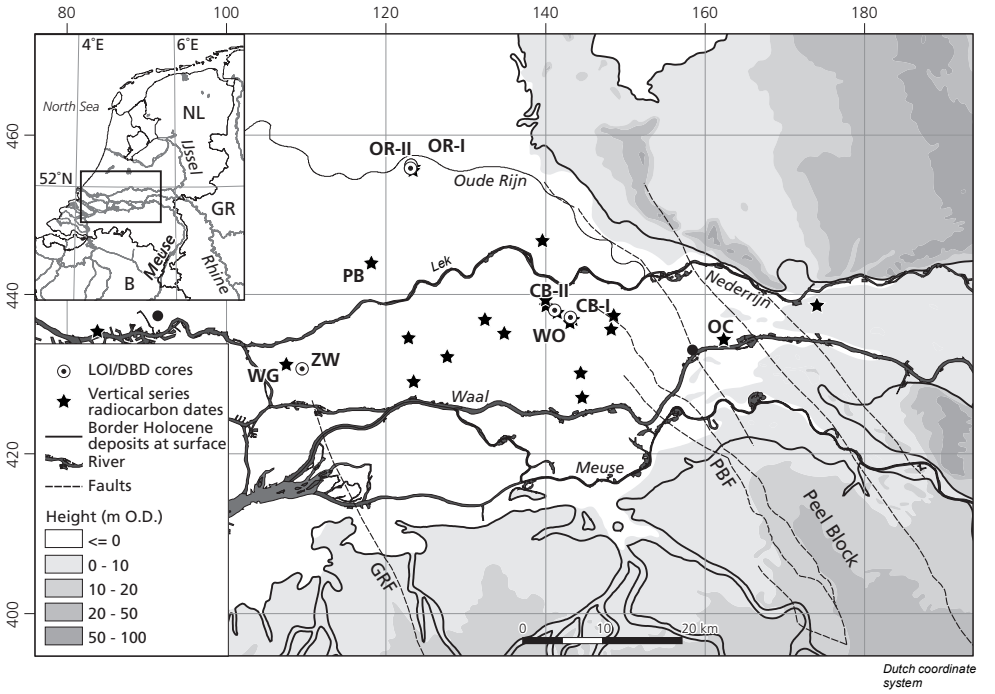

Figure 5.1. Location of the Rhine-Meuse delta in The Netherlands (inset), and of the 20 study sites (core locations) used in this research. 'LOI/DBD cores' indicate the location of sites where the Loss On Ignition (LOI) and dry bulk density (DBD) were measured at 5-cm-intervals. Black stars ('vertical series radiocarbon dates') indicate locations of cores from which radiocarbon-dated samples were used for analyses. O.D.=Dutch Ordnance Datum, GRF=Gilze Rijen Fault zone, PBF=Peel Boundary Fault zone.

local addition of accommodation space, differential compaction may even influence spatial and temporal fluvial sedimentation patterns, as was suggested by Michaelsen et al. (2000) and Rajchl and Uličný (2005), based on ancient coal-bearing sediment sequences.

Although peat compaction has been recognized as an important process creating accommodation space in deltas, the relative contribution of peat compaction to total land subsidence in Holocene deltaic basins has not been empirically quantified from field data across large deltas (spatial scale: on the order of tens of kilometers). So far, peat compaction has mainly been quantified using empirical and geotechnical models (for an overview see Van Asselen et al., 2009), resulting in estimated compaction rates in Holocene alluvial sequences of generally <2 mm/yr (e.g., Pizzuto and Schwendt, 1997; Meckel et al., 2007). The results of such modeling studies should be verified with field data; however, only a few field studies, most of which were carried out at point locations in Holocene coastal settings, have attempted to quantify the amount and rate of peat compaction. Basically two methods have been used in these studies: (1) compaction is calculated from estimates of the initial dry bulk density, derived from relations between the dry bulk density of uncompacted peat samples and physical characteristics such as organic-matter content (Bird et al., 2004), and (2) subsidence due to compaction is estimated using radiocarbon-dated basal peat samples to reconstruct initial levels of peat formation of currently subsided peat samples (Bloom, 1964; Haslett et al., 1998; Törnqvist et al., 2008). These latter studies calculated up to 80% compaction (= subsidence/original thickness of peat layer) in Holocene sequences, corresponding with subsidence on the order of a few meters. Millennia-averaged compaction rates of up to 5 mm/yr were calculated in mentioned field studies (Törnqvist et al., 2008).

In this study, both methods were applied in the fluvial dominated part of the Holocene Rhine-Meuse delta, The Netherlands (Fig. 5.1). The main objectives were to (1) quantify the amount and rate of natural peat compaction in different fluvial settings and (2) evaluate the relative contribution of peat compaction to total basin subsidence and its influence on spatial and temporal sedimentation patterns.

5.2 Evolution and setting of the Rhine-Meuse delta

Tectonic setting

The Rhine-Meuse delta is situated in the southern part of the subsiding North Sea Basin. The highest tectonic subsidence rates occur in the Roer Valley Graben between Tiel (Peel Boundary Fault zone) and Rotterdam (Gilze Rijen Fault zone; Fig. 5.1). The Peel Block, situated in the upstream part of the delta, has been relatively stable during the Holocene and may be considered as the hinge zone of the North Sea Basin (Kooi et al., 1998; Cohen, 2003). Cohen (2005) estimated that 34% of the accumulated Holocene sequence (D) can be attributed to basin subsidence due to tectonics, isostasy and compaction. Holocene subsidence rate (R), averaged over 11000 years, can therefore be calculated from R=0.34D/11000 (mm/yr). Assumed sequence thicknesses of D=3 m and D=10 m results in subsidence rates of 0.09 and 0.31 mm/yr for the upstream and downstream parts of the delta, respectively. Kiden et al. (2002) calculated tectonic subsidence rates of 0.06-0.16 mm/yr over the last 125000 years, based on the elevation difference of high-stand Eemian shorelines in Belgium (hinge zone) and the northern shoulder of the Roer Valley Graben in the central Netherlands.

Holocene natural evolution

The Holocene evolution and stratigraphy of the Rhine-Meuse delta have been studied extensively (e.g., Berendsen, 1982; Törnqvist, 1993a; Berendsen and Stouthamer, 2001; Gouw and Erkens, 2007; Fig. 5.1). The Holocene delta deposits are underlain by Late Weichselian fluvial gravely sands. To the north and south, the delta is bounded by Weichselian aeolian cover sands and ice-pushed ridges. Since approximately 9000 cal yr BP fluvial aggradation, controlled by relative sea-level rise, started in the western part of the present delta (Berendsen and Stouthamer, 2001; Gouw and Erkens, 2007; Hijma et al., 2009). Continued relative sea-level rise resulted in back-filling of the Weichselian valley. This ultimately led to the formation of a Holocene fluvial deltaic wedge which is at present approximately 20 m thick near the current coastline and thins eastward towards the apex of the delta near the Dutch-German border. Until ~5000 cal yr BP, rapid eustatic sea-level rise was the main factor controlling aggradation in the delta (Van Dijk et al., 1991; Törnqvist, 1993a; Gouw and Erkens, 2007). In the successive period, eustatic sea-level rise ceased, and accommodation space for fluvial sedimentation and peat accumulation was mainly provided by land subsidence. Most extensive peat formation in the Rhine-Meuse delta occurred between ~6000 and ~3000 cal yr BP (Gouw and Erkens, 2007). In this period, available accommodation space could not be filled by alluvial sediments from the Rhine and Meuse, which at that time were located along the northern and southern rim of the delta, respectively (Berendsen and Stouthamer, 2001). From ~3000 cal yr BP onwards, an increase in sediment supply resulted in widespread (in both upstream and downstream directions) deposition of fluvial sediments (Gouw and Erkens, 2007).

Human influence

The Rhine-Meuse delta has a long history of land reclamation. Large scale embankment of channels began approximately 1100 AD (Berendsen and Stouthamer, 2001). Artificial lowering of groundwater tables in floodbasins has resulted in increased land subsidence due to oxidation of organic matter in aerated top soil layers. In addition, lowered groundwater tables reduce hydrostatic pore pressures, which increases the effective stress and therewith enhances peat compaction. Field studies in the Rhine-Meuse delta have demonstrated that groundwater table lowering causes subsidence rates of up to 16.7 mm/yr, occurring over a few decades (Schothorst, 1977; Beuving and Van den Akker, 1996). In other cultivated deltas like the Sacramento-San Joaquin, USA (Deverel and Rojstaczer, 1996; Drexler et al., 2009), and the Venice Lagoon, Italy (Gambolati et al., 2003), even higher land subsidence rates of a few cm per year are attributed to lowered groundwater tables. A literature review by Turner (2004) reports subsidence rates of 0.17 to 55 cm/yr, with highest rates occurring shortly after initiation of artificial drainage of wetlands. All of these studies found a significant relationship between land subsidence and elevation of the groundwater table, and emphasized that oxidation and reduced hydrostatic pressures caused a significant portion of total land subsidence. In floodbasins isolated from channels by embankments, sedimentation and/or peat accumulation is impeded, and hence, cannot compensate for land subsidence.

5.3 Methods to quantify peat compaction

5.3.1 Study site description

Two field-based methods were used to quantify peat compaction at different sites within the fluvial-dominated, central part of the Rhine-Meuse delta (Fig. 5.1). A large database consisting of lithological borehole data and radiocarbon dates was already available for this area. The Holocene sequence is approximately 3 to 10 m thick and consists of sandy single-channel-belt and crevasse-splay deposits, organic-rich clayey floodbasin deposits, and peat (e.g., Gouw and Erkens, 2007). Study sites differ in stratigraphy and thickness, which allows assessment of peat-induced subsidence at various settings in the delta. Typical vertical stratigraphies consist of (1) a peat layer covered by a thin layer of floodbasin deposits, (2) peat layers intercalated by floodbasin and/or crevasse-splay deposits, and (3) a peat layer covered by natural levee deposits. Furthermore, peat layers differ in composition of plant species and in organic-matter content.

The selected study sites have not been disturbed by peat exploitation, nor have they been much affected by groundwater table lowering. Sites *Wijngaarden* (*WG*) and *Polsbroek* (*PB*) (Fig. 5.1) are most affected; here the present surface altitude is ~1.7 m below O.D. (mean sea level), presumably due to subsidence caused by lowered groundwater tables. This indicates minimum surface subsidence of 1.7 m, because the original surfaces were probably elevated slightly above O.D., considering the landward positions of these sites with associated groundwater tables that are higher relative to O.D. Surface elevations of other sites are all near or above O.D., except for five sites in the central part of the delta (roughly between X=120 and X=135), where the surface is elevated approximately ~1 m below O.D., indicating minimum surface subsidence of 1 m.

5.3.2 Quantifying peat compaction based on groundwater table reconstructions

The first method estimates subsidence of present-day peat levels based on the reconstruction of palaeogroundwater tables, which are indicative of former levels of fen peat formation. Fens are defined as minerotrophic mires, which receive water and nutrients from groundwater or surface runoff (Birks and Birks, 1980; Charman, 2002). The vertical distance between the present-day level of a radiocarbon-dated (subsided) peat sample and its reconstructed initial level of formation, is a measure of the amount of subsidence due to compaction of deposits underlying the sample and overlying an incompressible subsurface (Fig. 5.2a). Subsidence rates are determined by dividing the amount of subsidence by the age of the peat sample, representing the time since formation.

In a homogenous peat sequence, maximum subsidence due to compaction theoretically occurs in the middle of the sequence (Fig. 5.2b). At this point, optimal conditions exist for the amount of compressible sediment below this point and the load above this point. Geotechnical compaction models have predicted similar subsidence profiles (Pizzuto and Schwendt, 1997; Paul and Barras, 1998; Massey et al., 2006).

In the Rhine-Meuse delta, Holocene groundwater tables were reconstructed by Cohen (2005) based on a 3D kriging interpolation of ~350 radiocarbon-dated *Alnus* peat samples that directly overlie an incompressible subsurface, and hence have not experienced any subsidence due to compaction (referred to as basal peat; Fig. 2.13). The accuracy of the reconstructed groundwater tables varies spatially, depending on the distance to basal peat samples. In this interpolation, the standard deviation of reconstructed groundwater tables is 0.3 m close to a basal peat sample

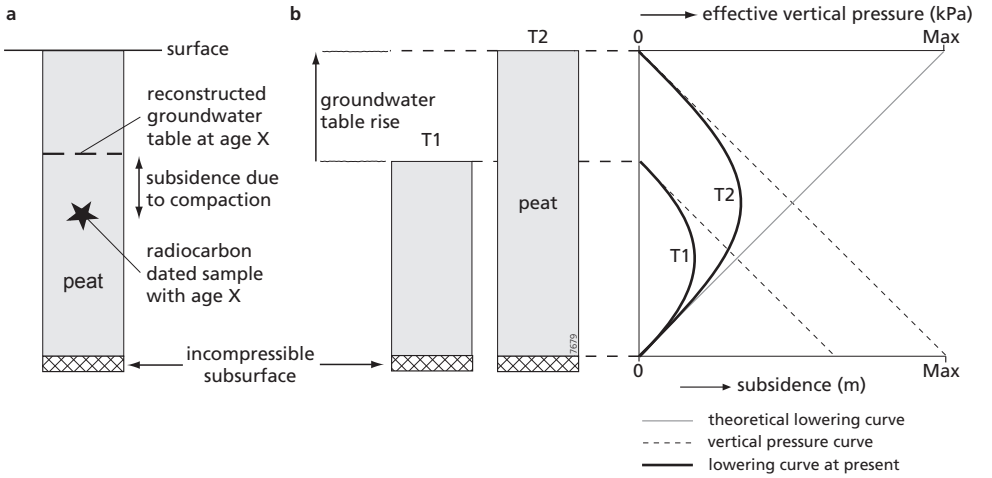

Figure 5.2. a) The amount of subsidence due to compaction is calculated based on the elevation difference between reconstructed groundwater tables and the present-day level of radiocarbon-dated peat samples. b) Theoretical subsidence profile in a homogeneous peat layer. It is assumed that peat accumulation keeps up with groundwater table rise (from Van Asselen et al., 2009).

(see semi-variograms in Fig. 6 in Cohen (2005)). Because most of the basal peat samples were obtained from the Early and Mid-Holocene sequence in the central part of the delta, the standard deviations are lowest in this area (Fig. 7b in Cohen (2005)). At the edges of the delta and in the Late Holocene part of the sequence, where the number of basal peat samples is low and the distance to basal peat samples is large, standard deviations are up to ~0.9 m.

Based on these reconstructed groundwater tables, the amount of subsidence was calculated for 93 dated peat samples (Appendix 4, paper codes 1-93, collected over the past three decades). The samples, typically 1-3 cm thick, were extracted at various depths from 20 cores, obtained from different settings in the central part of the Rhine-Meuse delta (Fig. 5.1). AMS ^{14}C methods were used for 77 samples. These were treated with a 5% KOH solution, then washed and wet-sieved over a 150 µm mesh. Next, macrofossils of terrestrial vegetation were selected from the residue. For 16 samples conventional dating of larger bulk peat samples was used. Radiocarbon dates were calibrated using Oxcal 4.1 (Bronk Ramsey, 2001) with the INTCAL04 calibration curve (Reimer et al., 2004). The *Sequence* deposition model was used for calibration of multiple samples within a single core. This model assumes that deposition occurs in a specific order, i.e. age increases with depth (Bronk Ramsey, 2008).

It is assumed that wood and sedge peat samples originally formed at 0±0.2 m relative to the former groundwater table (in agreement with Törnqvist et al. (1998), Cohen (2005) and Berendsen et al. (2007)). Because reed (*Phragmites Australis*) preferably grows in shallow waters, a correction of +0.3±0.2 m, which is the optimal water depth for reed growth (Den Held et al., 1992) was made to calculate subsidence of reed peat samples. It is acknowledged that reeds tolerate more variable water depths, which potentially leads to more uncertain subsidence calculations. But because most (reed) peat samples were dated from associated terrestrial plant

seeds, assumed to have grown in close proximity to the sampling site, conditions could never have been extremely wet or the terrestrial plants would not have survived.

Each of the 20 cores was logged at 10-cm intervals for sediment texture, color, organic-matter content, plant remains, and other noteworthy soil characteristics (cf. Berendsen and Stouthamer, 2001). To relate peat compaction to loading conditions, the effective stress (σ') imposed on a sample point was calculated using Terzaghi's formula $\sigma' = \sigma - u$ (Terzaghi, 1943), in which σ is the total stress (kPa) and u is the pore water pressure (kPa). The total stress is calculated by:

$$\sigma = h\rho_s g \tag{5.1}$$

in which h (m) is the thickness of the overlying sediment layer, ρ_s (kg/m^3) is the saturated density of the overlying sediment, and g is the gravity constant (=9.81 m/s^2). The thickness and texture of all sediment layers were recorded at 10-cm-intervals in the field. Similarly, u is calculated by:

$$u = h\rho_w g \tag{5.2}$$

in which h is the thickness of the overlying water column (m) and ρ_w is the density of water (=1000 kg/m^3).

The saturated density of a texture class is calculated from the mass and dry bulk densities of that texture class (Table 5.1; Poelman, 1975; Erkens, 2009). To calculate the mass density,

Table 5.1. Organic-matter content (assumed average value for texture class), mass density ($\rho_{particle}$), dry bulk density, porosity, estimated degree of saturation (f_{sat}) and saturated density for texture classes occurring in analyzed cores.

Texture class	Organic matter content (%)	Mass density[a] (g/cm^3)	Dry bulk density (g/cm^3)	Porosity[b] (-)	Degree of saturation (-)	Saturated density[c] (g/cm^3)
peat_org1	75	1.657	0.12[d]	0.928	98	1.029
peat_org2	50	1.900	0.22[d]	0.884	98	1.087
peat_org3	30	2.151	0.35[d]	0.837	98	1.171
humic clay	20	2.298	0.45[d]	0.804	98	1.238
slighly humic clay	6	2.549	0.8[d]	0.686	98	1.472
(silty) clay	2	2.632	1.15[d]	0.563	98	1.702
sandy clay	2	2.632	1.28[e]	0.514	98	1.783
silty clay loam	2	2.622	1.31[e]	0.500	98	1.800
loam	1	2.638	1.44[e]	0.454	98	1.885
sandy loam	1	2.634	1.55[e]	0.411	99	1.957
sand	0	2.652	1.7[e]	0.359	100	2.059

[a]Mass density = $1/((f_{org}/1.47) + (f_{class}\cdot f_{clay}/2.7) + (f_{class}\cdot f_{silt+sand}/2.65))$, with f=fraction (Poelman, 1975; Erkens, 2009).
[b]Porosity = (1-dry bulk density/mass density).
[c]Saturated density = (dry bulk density + f_{sat}·pore volume).
[d]Dry bulk density estimated based on field measurements (section 3.3; Chapter 3).
[e]Dry bulk density estimated using $\rho_{dry} = (1\text{-}porosity)\cdot \rho_{particle}$ (Saxton et al., 1986).

the percentage of organic matter, clay, silt and sand, representative for a specific texture class, was derived from a soil texture triangle based on a Dutch classification system (De Bakker and Schelling, 1966). The dry bulk density (ρ_{dry}) was either estimated from measurements at various study sites (section 5.3.3) or derived from soil porosity and soil particle density ($\rho_{particle}$) estimates using the equation $\rho_{dry} = (1\text{-}porosity) \cdot \rho_{particle}$ (Saxton et al., 1986).

5.3.3 Quantifying peat compaction based on dry bulk density measurements

The second method used in this study estimated the amount of compaction by comparing the dry bulk density of compacted and uncompacted peat (Bird et al., 2004; Van Asselen et al., 2009, 2010). Besides compaction, the dry bulk density of peat is influenced by the organic-matter content, texture of inorganic sediment and plant species composition. Therefore, a precondition for using this method is that these properties are similar for compacted and uncompacted peat. In the Holocene Rhine-Meuse delta, clastic inputs to floodbasin peat consisted predominantly of clay deposited during floods. Locally, sand and silt may occur, depending on the hydrogeomorphic position of the peatland. Hence, the texture of the inorganic material was assumed to be similar in all peat samples. The organic-matter content was estimated by loss on ignition (LOI), and the plant species composition was determined during logging in the field and in the laboratory (see next sections).

Sampling compacted peat

The ρ_{dry} and LOI of peat were measured at 5-cm intervals in four cores obtained from different fluvial settings (*Oude Rijn* (*OR-I*, *OR-II*) and *Culemborg* (*CB-I*, *CB-II*) in Fig. 5.1), using a 1 cm x 1 cm x 5 cm sampler. The sediment sequence of cores *OR-II* and *CB-II* consist of mainly peat. In core *OR-I*, natural levee deposits overlie a peat layer. Core *CB-I* is characterized by an alternation of organic and clastic sediment layers (see lithological columns in Fig. 5.6).

The cores, each 5 to 6 m in length, were extracted with a 100 cm x 6 cm wide gouge auger and logged as described in section 5.3.2. To allow sampling of the inner, least disturbed part of the core, it was first cut in half lengthways using a thin stretched wire. Each 5-cm^3 peat sample was dried at 105°C and weighed on an electronic scale (precision of 0.001 g) to determine the dry bulk density (=dried weight in g/5 cm^3). The samples were subsequently heated at 550°C for 4 hours to determine loss on ignition (= ((dried weight – ashed weight)/dried weight) · 100%; cf. Heiri et al., 2001). During the procedure to determine ρ_{dry}, the greatest error is introduced by the 5 cm^3 field sampler. It is estimated that the error in sampling volume may be up to 10% (5±0.5 cm^3). Because the uncertainty in measuring the weight of a sample is low, the propagated error in the calculated dry bulk density is assumed to be also 10%.

Sampling uncompacted peat

Uncompacted peat samples were obtained from the Biebrza National Park (BNP, Poland) and the Rhine-Meuse (RM) delta. The BNP is a wetland that has experienced minimal human disturbance (e.g., Oświt, 1993) and displays the same peat types as those in the subsurface of the Rhine-Meuse delta (mainly fen peat composed of reed, sedge or wood peat). The heterogeneous and fragile structure of surficial peat requires a special device to sample an undisturbed relatively large volume of peat, for which a new peat sampler was devised (Van Asselen and Roosendaal, 2009). For all uncompacted peat samples, ρ_{dry} and LOI were determined using a similar procedure as for compacted peat samples (see also Van Asselen and Roosendaal, 2009).

Peat in the BNP generally has a high organic-matter content (LOI >80%). For ρ_{dry} data on low-organic uncompacted peat, additional samples were obtained from the Rhine-Meuse delta. Modern peat is rare in this cultivated area, and surficial peat layers are often influenced by lowered groundwater tables and/or soil tillage. Therefore, near-surface peat (approximately 1-3 m below surface) with little or no inorganic overburden was sampled (at sites *OR-II* and *Zijdeweg* (*ZW*) in Fig. 5.1), acknowledging that this peat might have experienced some compaction due to self-weight and/or increased pressure following artificial drainage of the top layer. Nevertheless, these samples at least give maximum values of the ρ_{dry} of uncompacted peat. Moreover, field observations indicated that the sampled peat had not experienced significant compaction. Peat cores were obtained from floodbasins where peat had accumulated until the floodbasins were embanked (~800 years ago). The newly designed peat sampler was used to sample surficial peat, whereas the 1000 x 60 mm gouge auger and the 5 cm^3 sampler were used for sampling the deeper buried peat at sites *OR-II* and *ZW*. Hence, relatively small uncompacted samples were extracted from these cores, compared to the samples extracted with the new device (708 cm^3). These smaller samples are less representative for larger volumes of heterogeneous peat and consequently yield less accurate values of ρ_{dry}. Nevertheless, the large number of analyzed samples (~220) allowed a reliable approximation of the ρ_{dry} of uncompacted peat with different LOI values.

Calculating compaction

Since the uncompacted peat samples from the Rhine-Meuse delta most likely had experienced some compaction, only the lowest ρ_{dry} values for a specific LOI were used for constructing the equation for calculating uncompacted dry bulk density, resulting in (Fig. 5.5):

$$\rho_{dry,uncomp} = a - c\, e^{-(b/LOI)} \tag{5.3}$$

in which *a, b* and *c* are fitted parameters. The $\rho_{dry,uncomp}$ was subsequently used to calculate the decompacted thickness of each 5 cm^3 compacted sample, ignoring lateral strain (h_{decomp}=($\rho_{dry,comp}$/ $\rho_{dry,uncomp}$)·5). The percentage of compaction is expressed as the ratio of volume reduction (v_{red} =1·1· (h_{decomp}) – 1·1·5) to the calculated decompacted volume in a 5 cm^3 peat sample (v_{decomp} =1·1· h_{decomp}):

$$comp\,action = \frac{v_{red}}{v_{decomp}} \cdot 100\% \tag{5.4}$$

It is difficult to assess the uncertainty of a predicted $\rho_{dry,uncomp}$ value using Eq. 5.3, and therewith, of the calculated compaction. Based on observed variations in field measurements of uncompacted peat (Van Asselen and Roosendaal, 2009; Van Asselen et al., 2010), the uncertainty is assumed to be 20%. The propagated error (combined effect of uncertainties in predicting $\rho_{dry,uncomp}$ and $\rho_{dry,uncomp}$) in the calculated compaction is on the order of 15%.

5.4 Peat compaction and subsidence

5.4.1 Estimates based on groundwater table reconstructions

Results of Holocene groundwater table analyses in six cores, obtained from different fluvial settings, are presented (Figs. 5.1 and 5.3; Table 5.2; Appendix 5). Sites *CB-II* and *Woerden* (*WO*) are both situated in a floodbasin where peat accumulated throughout the Holocene (Figs. 5.3a and 5.3b) except for a short period of clay deposition at site *WO*. In both cores, the maximum amount of subsidence due to compaction occurs in the middle part, as was expected (section 5.3.2). Maximum subsidence is highest in core *CB-II*, which is most likely due to the thicker peat layer at this site.

Alternating clay and peat layers occur in the lower half of the *WG* core (Fig. 5.3c), indicating that until approximately 6050 cal yrs BP (sample 25 in Fig. 5.3c; Table 5.2), peat accumulation was periodically interrupted by deposition of (sandy) clay following flooding or crevassing of nearby river channels. These clay layers have imposed a relatively high stress on the wood peat layer at the base of the sequence, resulting in subsidence of up to ~3 m.

At the site of core *PB*, a thick natural levee formed until 6610 cal yrs BP (sample 31 in Fig. 5.3d; Table 5.2). After that period, the river channel belt apparently was abandoned and peat formation started. Maximum subsidence occurs in the middle part of the overlying peat layer.

The lowest part of core *CB-I* consists of wood peat (Fig. 5.3e). Peat formation ended by deposition of (sandy) clay following crevassing of a nearby natural levee. After approximately 200 years (time interval between formation of peat samples 35 and 36; Fig. 5.3e; Table 5.2), peat accumulation resumed. Two peaks in the amount of subsidence are observed; peat levels directly below a clayey interval and overlying a peat layer experienced most subsidence due to compaction. The low amount of subsidence of the peat level where sample 35 was taken (Figure 5.3e) indicates that much compaction of the wood peat layer occurred before peat started to accumulate on top of the crevasse splay deposits.

Core *Ochten* (*OC*) is characterized by a thick layer of mainly natural levee deposits overlying a peat layer (Fig. 5.3f). Even though the peat layer (and Holocene sequence) has a compacted thickness of only ~1 m, the high effective stress induced by the natural levee deposits has caused a relatively high amount of maximum subsidence (1.92 m; sample 41 in Fig. 5.3f; Table 5.2).

Additionally, isochrones were reconstructed in a cross section perpendicular to the *Oude Rijn* river, based on two vertical series of radiocarbon-dated peat samples in cores *OR-I* and *OR-II* respectively (Fig. 5.4). The isochrones significantly drop below the natural levee, due to greater compaction of the peat layer at this site (see also section 5.4.2; Figs. 5.6c and 5.6d).

⇨ *Figure* 5.3. The amount of subsidence (m) and effective stress (kPa) of radiocarbon-dated peat samples obtained from cores *CB-I, WO, WG, PB, CB-I* and *OC* (a to f resp.), plotted against the relative depth in the Holocene sequence (for core locations see Fig. 5.1). Subsidence is derived from the elevation difference between the present-day position of a sample and a reconstructed groundwater table that is indicative of the initial level of formation of the sample. The thickness and lithology of each core are indicated next to each graph. The ages of the samples are given in Table 5.2. The standard deviation, indicated by the grey area, results from uncertainties in the reconstruction of palaeogroundwater tables, and in the vertical distance to the groundwater table at the time of formation of the peat sample (see text for further explanation). For age-depth plots of analyzed cores see Appendix 5.

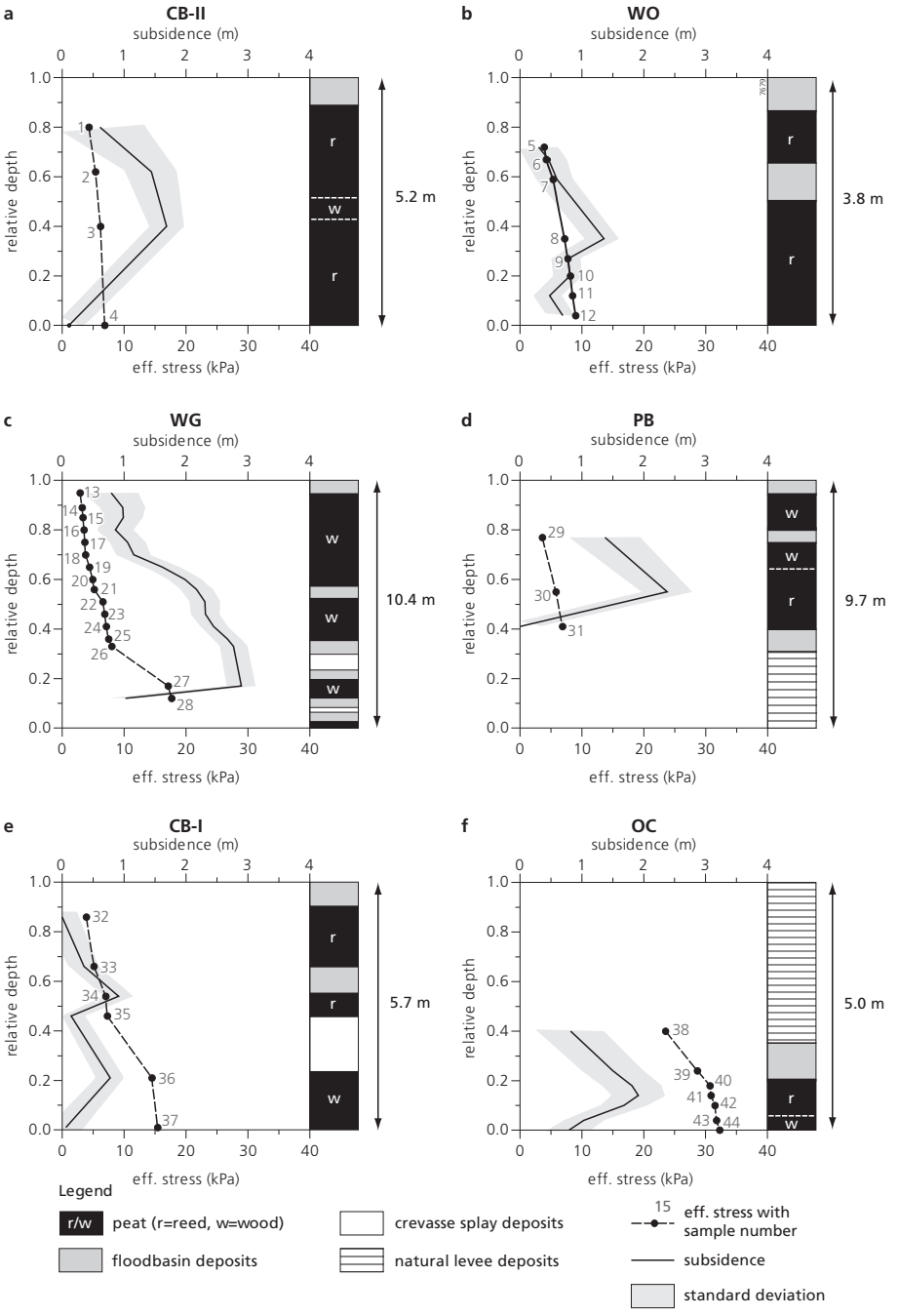
a
CB-II
subsidence (m)
relative depth
eff. stress (kPa)
5.2 m
b
WO
3.8 m
c
WG
10.4 m
d
PB
9.7 m
e
CB-I
5.7 m
f
OC
5.0 m
Legend
r/w peat (r=reed, w=wood)
floodbasin deposits
crevasse splay deposits
natural levee deposits
15 eff. stress with sample number
subsidence
standard deviation

Table 5.2. Calibrated radiocarbon dates, amount of subsidence and subsidence rate of peat samples obtained from cores presented in Figure 5.3 (see also Appendix 4).

Core	Nr	Lab. nr.	Cal age (yrs BP)	Sub (m)	Sub rate (mm/yr)
CB-II	1	UtC-14349	2735	0.61	0.22
	2	UtC-14275	4470	1.44	0.32
	3	UtC-14276	5740	1.69	0.29
	4	UtC-14350	7820	0.11	0.01
WO	5	UtC-13504	4835	0.30	0.06
	6	UtC-13505	5000	0.46	0.09
	7	UtC-13506	5390	0.60	0.11
	8	UtC-13507	5620	1.36	0.24
	9	UtC-13508	6245	0.78	0.12
	10	UtC-13509	6380	0.81	0.13
	11	UtC-13510	6670	0.48	0.07
	12	UtC-13511	6710	0.69	0.10
WG	13	UtC-13762	2760	0.79	0.29
	14	UtC-13763	3175	0.98	0.31
	15	UtC-13764	3620	0.99	0.27
	16	UtC-13765	4240	0.86	0.20
	17	UtC-13766	4550	1.06	0.23
	18	UtC-13767	4890	1.16	0.24
	19	UtC-13768	4935	1.62	0.33
	20	UtC-13799	5020	1.99	0.40
	21	UtC-13800	5210	2.17	0.42
	22	UtC-13801	5415	2.31	0.43
	23	UtC-13802	5675	2.32	0.41
	24	UtC-13803	5885	2.45	0.42
	25	UtC-13804	6050	2.67	0.44
	26	UtC-13805	6220	2.77	0.45
	27	UtC-13808	6940	2.90	0.42
	28	UtC-13809	7530	1.02	0.14
PB	29	GrN-9403	4493	1.37	0.30
	30	GrN-9404	5415	2.38	0.44
	31	GrN-9405	6610	-0.02	0.00
CB-I	32	UtC-14351	4835	-0.08	-0.02
	33	UtC-14532	5925	0.35	0.06
	34	UtC-14353	5975	0.91	0.15
	35	UtC-14277	6650	0.15	0.02
	36	UtC-14278	6860	0.78	0.11
	37	UtC-14354	8410	0.06	0.01
OC	38	UtC-01187	4000	0.82	0.21
	39	UtC-01188	5080	1.50	0.30
	40	UtC-01189	5210	1.81	0.35
	41	UtC-01190	5640	1.92	0.34
	42	UtC-01191	6060	1.68	0.28
	43	UtC-01192	6600	1.03	0.16
	44	UtC-01235	6900	0.79	0.11

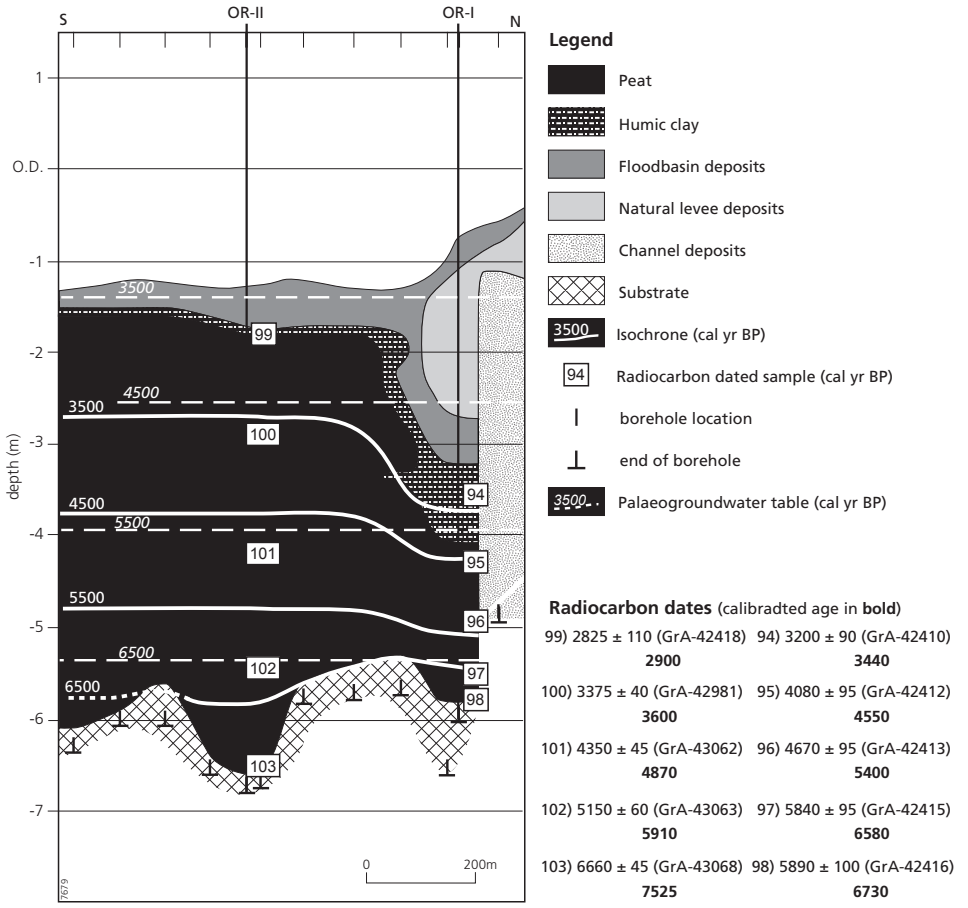

Figure 5.4. Cross section of the *Oude Rijn* study site, with isochrones and reconstructed groundwater tables shown (for position in the Rhine-Meuse delta see Fig. 5.1). Because the uncertainty of reconstructed Mid and Late Holocene groundwater tables is large in this area, subsidence, using method 1 (section 5.4.1), has only been calculated for the oldest samples at this site (GrA-42415, GrA-42413 and GrA-43063; section 5.6; paper codes 96, 97 and 102 in Appendix 4).

5.4.2 Estimates based on dry bulk density measurements

The equation to calculate the initial ρ_{dry} of compacted peat (Eq. 5.3) is constructed from ρ_{dry} measurements of different types of uncompacted fen peat. The average ρ_{dry} of high-organic uncompacted wood peat samples (0.12 g/cm^3), obtained from the BNP, appeared to be slightly higher than the average ρ_{dry} of high-organic uncompacted reed- and sedge peat (0.10 g/cm^3). This is likely due to the composition of wood peat. A mixture of wood, twigs and leaves as well as grass, sedge, and reed remains results in a slightly lower initial pore volume because pore spaces are filled with small plant remains, and hence in a higher ρ_{dry}. Furthermore, wood fragments are relatively heavy because they contain relatively high amounts of lignin. Modern reed- and sedge

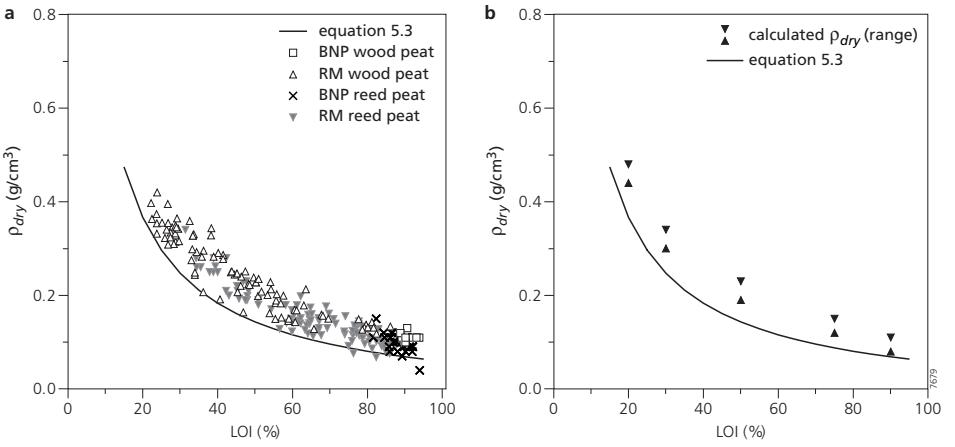

Figure 5.5. a) Equation used to calculate the uncompacted dry bulk density (ρ_{dry}) of compacted peat samples, based on ρ_{dry} and LOI measurements of uncompacted peat obtained from the Biebrza National Park (BNP; Van Asselen and Roosendaal, 2009) and the Rhine-Meuse delta (RM; this research), b) uncompacted ρ_{dry} of peat with different organic-matter contents, calculated based on mass density and porosity (see Table 5.3).

peat on the other hand mostly consist of dense networks of fine (and lighter) roots and larger hollow roots and stems, resulting in a higher initial pore volume and lower ρ_{dry}. Uncompacted peat with relatively low LOI values does not show a significant difference between the ρ_{dry} of wood and reed-/sedge peat. This suggests that the clastic content is a more important factor in ρ_{dry} of uncompacted peat than the plant species composition. Hence, considering that peat in the Rhine-Meuse delta has LOI values that rarely exceed 80%, a single equation for calculating the uncompacted dry bulk density of different types of compacted fen peat was constructed (Fig. 5.5a). Fitting Equation 5.3 to uncompacted peat data resulted in parameter values a = 1.5, b = 6 and c = 1.53. This parameter set was subsequently used to calculate peat compaction in four cores (*OR-I, OR-II, CB-I* and *CB-II*).

Table 5.3. The dry bulk density of uncompacted peat and organic clay calculated based on the mass density, which is calculated based on texture composition and porosity estimates (for used equations see Table 5.1).

Organic content (%)	Inorganic content (%)	Clay (%)	Silt (%)	Sand (%)	Mass density (kg/m³)	Porosity (-)	Dry bulk density (g/cm³)
90	10	70	29	1	1539.7	94.0±1	0.08 – 0.11
75	25	70	29	1	1657.5	92.0±1	0.12 – 0.15
50	50	70	29	1	1899.8	89.0±1	0.19 – 0.23
30	70	70	29	1	2151.4	85.0±1	0.30 – 0.34
20	80	50	45	5	2298.1	80.0±1	0.44 – 0.48

To verify the validity of Equation 5.3 with these parameter values, ρ_{dry} of surficial peat was also estimated from mass density and porosity of uncompacted peat with varying organic-matter contents (see section 5.3.2; Tables 5.1, 5.3; Fig. 5.5b). The porosity was estimated from ρ_{dry} measurements of uncompacted peat obtained from both the Rhine-Meuse delta and the Biebrza National Park (porosity = $1 - (\rho_{dry}/\rho_{particle})$). For a certain LOI, all calculated dry bulk densities are higher than the ρ_{dry} obtained from Equation 5.3, but within the range of dry bulk densities presented in Fig. 5.5a. This suggests that the uncompacted dry bulk densities derived from Equation 5.3 represent minimum values, and hence calculated compaction percentages are maximum values.

The amount of compaction, calculated for 5 cm^3 samples from peat cores, appears to be quite variable (Fig. 5.6), likely caused by the heterogeneous structure of peat, resulting in variable dry bulk densities. To obtain a more generalized view of compaction variations, compaction percentages using a 25-cm moving were calculated in addition (Fig. 5.6).

In core *CB-I*, the wood peat layer (4.25-5.5 m below surface, LOI ≈ 60%) beneath the crevasse-splay deposits is most compacted (~45%; Fig. 5.6a) and the top of this layer has subsided ~0.8 m (Fig. 5.3e). In the reed peat layers above the crevasse-splay deposits, compaction percentages are moderately high (~20-30%), with highest values occurring in the lowest layer (2.65-3.20 m below surface, LOI ≈ 60%; Fig. 5.6a). Accordingly, the top of this layer also has experienced relatively high subsidence (~0.9 m; Fig. 5.3e).

Core *CB-II*, extracted approximately 2 km from core *CB-I* (Fig. 5.1), consists of a thick reed peat layer overlain by a thin clay layer (Fig. 5.6b). Although core *OR-II* (Fig. 5.6d) has a similar profile, higher amounts of compaction are calculated at site *CB-II*. Presumably, this is due to the high variation in inorganic content in the top part of core *CB-II*, inducing a higher load on the underlying high-organic peat (LOI ≈ 80%). The decreasing compaction percentages at the base of core *CB-II* correspond with a decreasing LOI with depth. In contrast, compaction increases at the base of core *OR-II*, where the LOI remains approximately 80%. Also, at the top of the peat layer in this core, an increase in compaction is observed. This is ascribed to both oxidation of organic matter, following artificially induced groundwater fluctuations, and to compaction due to agricultural practices (e.g., soil tillage, loading by heavy machinery).

The peat layer in core *OR-I* (LOI ≈ 80%), located approximately 425 m from *OR-II*, is much more compacted than the other analyzed cores due to the weight of thick overlying natural levee deposits (Fig. 5.6c).

In two of the four cores, LOI and calculated compaction are positively correlated (core *CB-I* and *OR-I*; Figs. 5.7a and 5.7c), and a weak correlation is observed in core *CB-II* (R^2=0.38; Fig. 5.7b). In core *OR-II*, no correlation is observed (Fig. 5.7d) because the range in LOI values is small and, as explained above, the highest compaction values in this core are most likely related to human influences.

The average amount of compaction within one peat sequence (average of all 5-cm thick peat samples) is positively related to the average effective stress of that peat sequence (Fig. 5.8). The observed variability in compaction within one peat sequence derives from variations in organic-matter content and fiber structure, which is mainly determined by the plant species composition and degree of degradation.

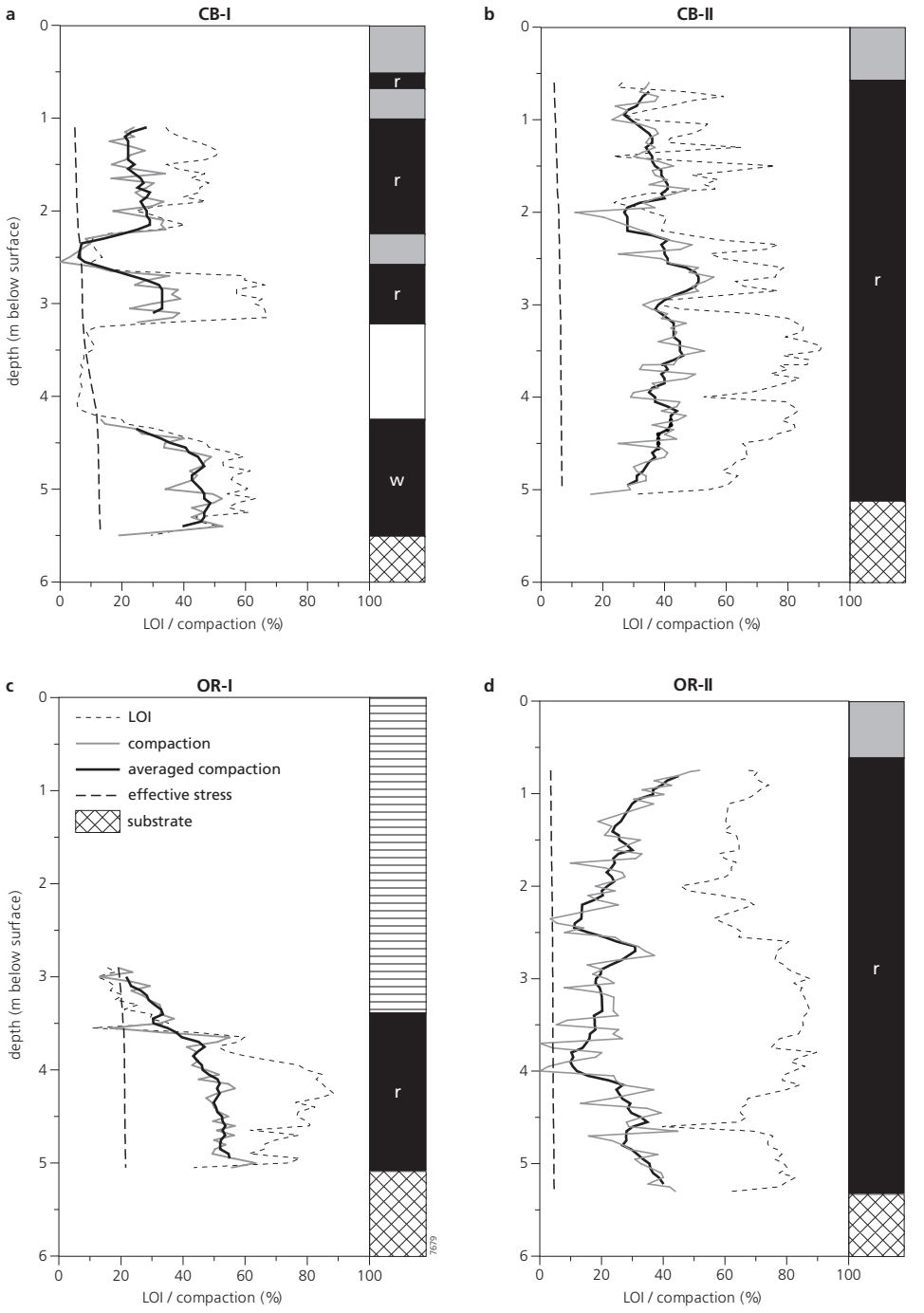
a
CB-I
b
CB-II
c
OR-I
d
OR-II
depth (m below surface)
LOI / compaction (%)
LOI
compaction
averaged compaction
effective stress
substrate
r
w
7079

Figure 5.6. Plots of the percentage of compaction and LOI vs. absolute depth below the surface for cores *CB-I, CB-II, OR-I* and *OR-II* (for locations see Fig. 5.1). The uncertainty in the calculated compaction percentages is estimated at 15% (see section 5.3.3). The effective stress is calculated assuming full saturation of all sediment and peat layers. The lithology of each core is shown next to each graph (for the legend see Fig. 5.3).

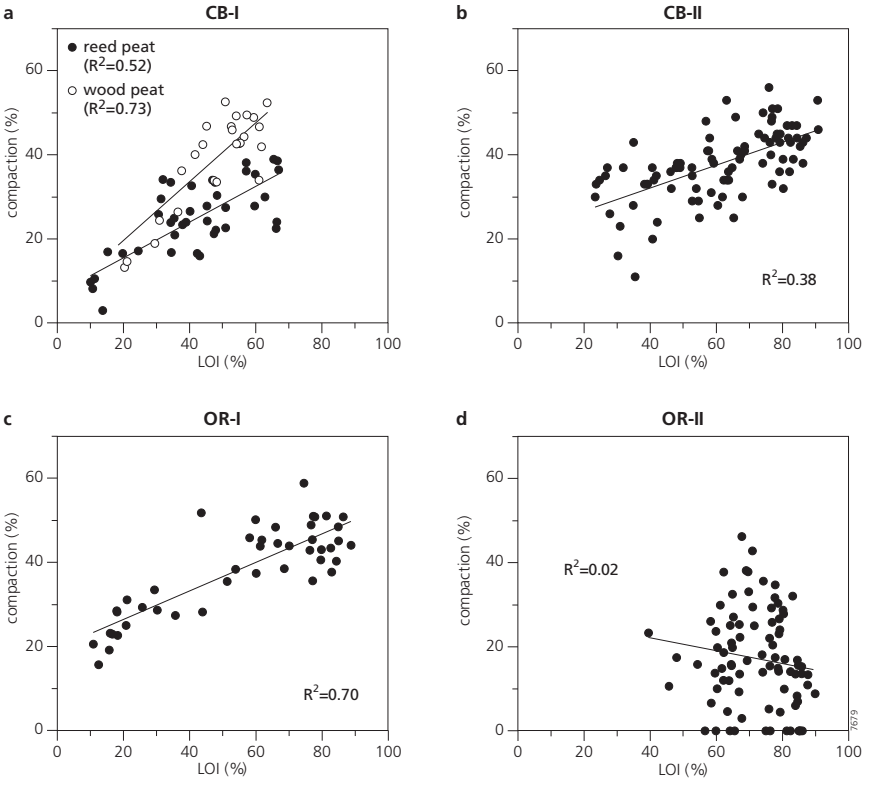

Figure 5.7. Plots of the percentage of compaction calculated for each 5 cm^3 sample vs. LOI (%). R^2 values of linear regression lines are indicated in each plot. The uncertainty in calculated compaction percentages is estimated at 15% (see section 5.3.3).

5.5 Spatial and temporal subsidence patterns in the Rhine-Meuse delta

Results from this study demonstrate that thick high-organic peat layers beneath natural levees and crevasse splay deposits are most susceptible to compaction. As expected, the highest amounts of subsidence due to peat compaction tend to occur where the Holocene sediment sequence is relatively thick and contains a substantial amount of compressible sediment such as peat and organic-rich clay (Fig. 5.9a). These conditions occur approximately between X = 100-120 and Y = 430-445 (Fig. 5.1; Van der Meulen et al., 2007). In this area, the cumulative

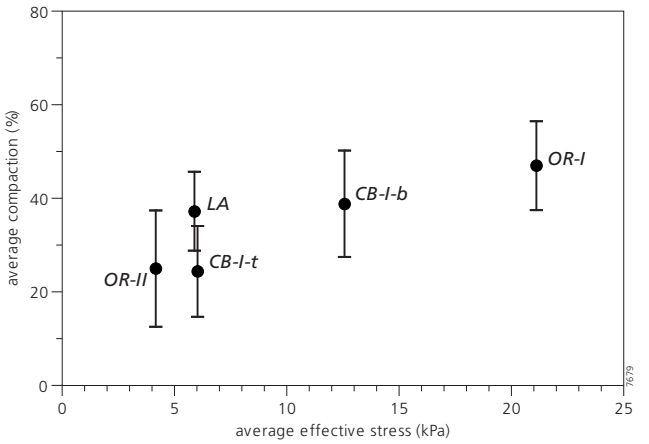

Figure 5.8. The average amount of compaction of a peat sequence (average of all 5-cm-thick peat layers; vertical lines indicate standard deviation) vs. the average effective stress within the peat sequence in cores *OR-I*, *OR-II*, *CB-I* and *CB-II* (for core location see Fig. 5.1). *CB-I-t* denotes the top reed peat layer and *CB-I-b* denotes the wood peat layer at the base in core *CB-I* (see Fig 5.6a).

thickness of peat layers reaches values of up to 8 m in a Holocene sequence of approximately 10 m thickness. Here, subsidence of up to ~3 m has been calculated (Figs. 5.9c, 5.9d). North-, south- and eastward from this area, the thickness of the Holocene sequence, and hence the potential thickness of peat layers, decreases due to the up-sloping Late Weichselian subsurface. In the distal, most western part of the delta, the Holocene sequence thickens, but the cumulative thickness of peat layers decreases (generally 3-5 m thick). The Holocene succession in this area is dominated by marine tidal sediments (Hijma et al., 2009), which are much less susceptible to compaction than peat (Mesri and Ajlouni, 2007; Locher and De Bakker, 1990). Furthermore, in some large areas the peat has been completely removed for fuel. Still, relatively thick peat layers may occur locally, leading to high amounts of subsidence (e.g., De Groot and De Gans, 1996).

Greatest subsidence was measured in the thick peat layers in the central delta, which mainly formed between ~6000 and 3000 cal yrs BP (Gouw and Erkens, 2007). Compaction of these peat layers resulted in subsidence of up to ~3 m (Fig. 5.9b), thereby creating significant accommodation space.

5.6 Timing of peat compaction

Besides quantifying the amount and rate of subsidence due to peat compaction, the data presented in this paper may be used to assess the timing of peat compaction. Two extreme situations are considered: (1) compaction of multiple thin peat layers occurs simultaneously following a substantial increase in effective stress, or (2) compaction of thin peat layers occurs successively during aggradation of a peat sequence (Fig. 5.10). *Situation 1* is illustrated in Fig. 5.10a in which 5-cm-thick peat layers accumulate at a rate equal to the rate of groundwater table

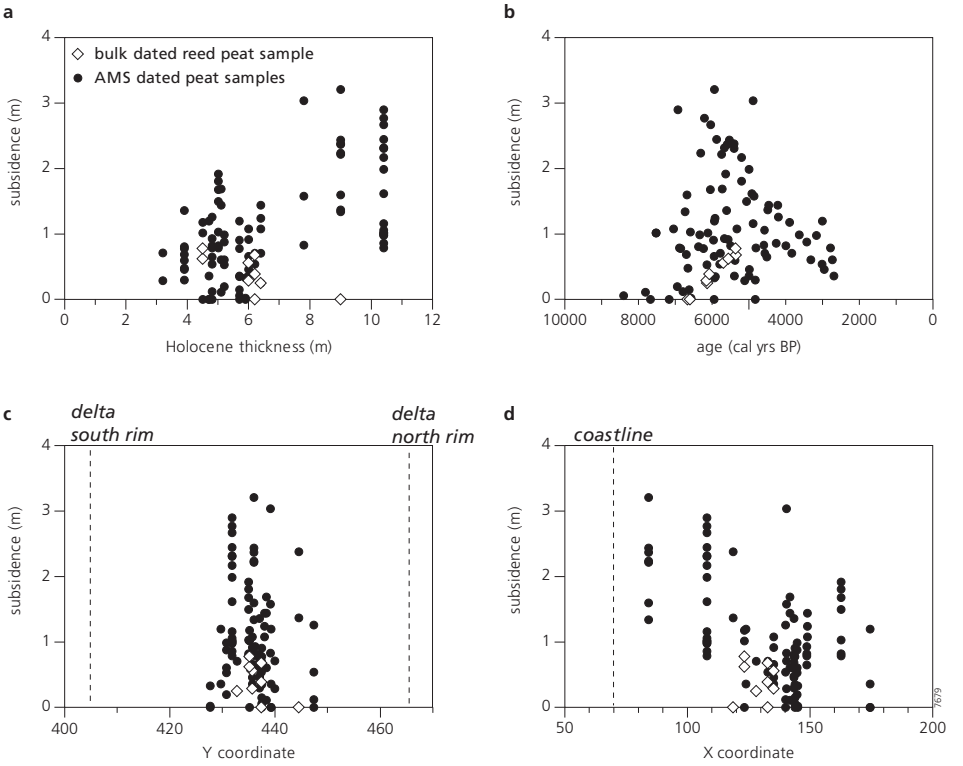

Figure 5.9. Plots of subsidence due to compaction vs. a) thickness of the Holocene sequence, b) age of subsided peat sample, c) north-south position (Y-coordinate) and d) west-east position (X-coordinate) of 93 peat samples obtained from 20 cores in the Rhine-Meuse delta (for core locations see Fig. 5.1). Subsidence values of up to ~1 m occur at all analyzed sites. The highest amounts of subsidence are calculated for Mid-Holocene peat levels in the central-western part of the delta, where the Holocene sequence is thick. No clear relation between the amount of subsidence and the vertical position within one core was found.

rise. No significant compaction occurs until time step 3, after which all layers below the peat sample compact simultaneously. In this situation, the amount of subsidence determined from groundwater table reconstruction (Δs) is equal to the sum of the amounts of subsidence of all 5-cm-thick peat layers below the peat sample ($\Delta h_1 + \Delta h_2$ in Fig. 5.10a). Alternatively, in *situation 2* each peat layer experiences most compaction before the next layer accumulates. Then, Δs is equal to the amount of subsidence of the most recently accumulated peat layer (Δh_2; Fig. 5.10b).

If the cumulative subsidence of all 5-cm-thick peat layers below a sample point ($\Delta h_1 + \Delta h_2 + \ldots + \Delta h_t$) is similar to the amount of subsidence calculated from groundwater table reconstruction (Δs), then the situation outlined in Fig. 5.10a is most likely; i.e., most subsidence due to compaction of underlying peat layers has occurred simultaneously. If, on the other hand, $\Delta h_1 + \Delta h_2 + \ldots + \Delta h_t$ is much larger than Δs, then most compaction probably occurred shortly after formation of each peat layer (Fig. 5.10b).

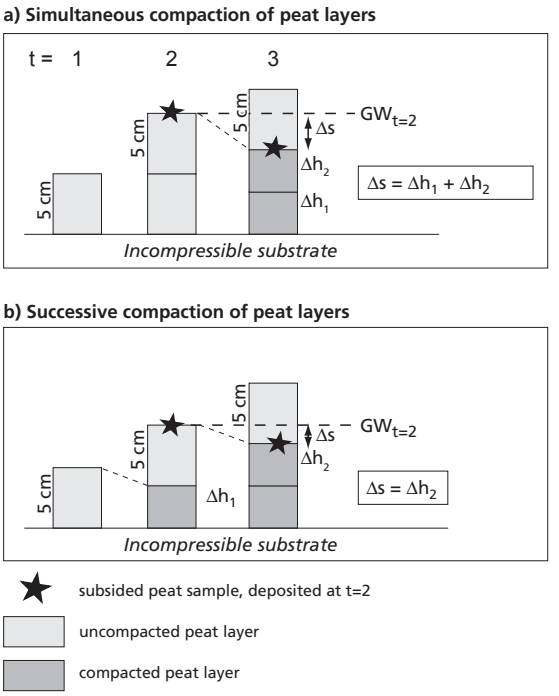

Figure 5.10. a) Compaction of all layers below a peat sample (black star) occurs simultaneously after the most recent peat layer has accumulated. b) Most compaction of a 5-cm-thick peat layer has occurred before the next peat layer accumulates. Δh = amount of subsidence of a 5-cm-thick peat layer, Δs = amount of subsidence of a peat sample.

Based on this concept, the timing of peat compaction was assessed at four sites where both methods for quantifying compaction were applied (Table 5.4). To achieve optimal accuracy, sample locations and depths were chosen for which (1) the error of reconstructed groundwater level is relatively low and (2) the depth to the Pleistocene substrate is not too great (<1.5 m). This minimizes cumulative errors in determination of the decompacted thickness of each 5-cm-thick peat layer.

Based on groundwater table reconstructions (method 1), 0.78±0.11 m subsidence of sample 36 (UtC-14278 in core *CB-I*; Fig. 5.3e; Table 5.4) was calculated. Results of dry bulk density measurements (method 2) indicate maximum subsidence of 0.89±0.22 m (=sum of Δh_{decomp} of all 5-cm peat layers below sample 36). Since the amount of subsidence calculated by the two methods is similar, a situation shown in Fig. 5.10a is most likely. This suggests that most compaction of the wood peat layer occurred rapidly following loading by the overlying crevasse-splay deposits. Also for sample 3 (UtC-14276) in core *CB-II* (Fig. 5.3a), subsidence calculated by both methods is similar (Table 5.4), which indicates that most compaction occurred after 5740 cal yr BP (Table 5.2). Since that time, the input of clastics increased progressively (Figs. 5.3a, 5.6b) and thereby increased the effective stress on underlying peat layers.

Table 5.4. Comparing results of method 1 (reconstructed groundwater tables/radiocarbon dating) and method 2 (dry bulk density measurements) used to calculate subsidence due to peat compaction. The error in method 1 calculations is mainly introduced by uncertainties in the elevation of reconstructed groundwater table and in the vertical distance between the sample and the groundwater table at the time of formation of the sample. The error in method 2 is mainly introduced by measuring the dry bulk density from field settings and estimating the initial dry bulk density of a peat sample. Sample numbers (between brackets) correspond with paper codes in Appendix 4.

Core	Sample (nr)	Method 1 (m)	Error method 1 (m)	Method 2 (m)	Error method 2 (m)
CB-I	UtC-14278 (36)	0.78	0.23	0.89	~0.22
CB-II	UtC-14276 (3)	1.69	0.28	1.65	~0.40
OR-I	GrA-42415 (97)	0.13	0.23	0.21	~0.04
OR-I	GrA-42413 (96)	0.84	0.48	0.91	~0.20
OR-II	GrA-43063 (102)	0.60	0.34	0.57	~0.20

Both methods give similar subsidence values for two sample points in core *OR-I*, indicating that most compaction was induced by loading by the natural levee deposits (samples 96 and 97; Table 5.4; Fig. 5.4). Also in the floodbasin (sample 102 in core *OR-II*; Table 5.4; Fig. 5.4), most compaction occurred after accumulation of a peat layer of at least 1 meter thick.

In general, in this aggrading Holocene sequence, high-organic peat accumulated for a few millennia without substantial natural compaction. Compaction of individual peat layers occurred simultaneously after a substantial increase in the effective stress, particularly caused by loading by fluvial sediments (*situation 1*; Fig. 5.10a). This is supported by data from the Cumberland Marshes (Van Asselen et al., 2010), where minimal compaction was measured in an unburied 2-m-thick, high-organic peat layer that started to accumulate ~2000 years ago. At Holocene timescales, *situation 2* (Fig. 5.10b) may occur during periods of lowered groundwater table, or when the accumulation rate is higher than the groundwater table rise. Furthermore, this situation likely applies to thicker sequences formed over longer time periods (>10^4 years). Such sequences, in which peat may have transformed into coal, most likely have experienced compaction during aggradation, for example during periods of burial by fluvial sediments. Hence, the amount of subsidence due to compaction in such sequences should not be calculated by summing the amount of subsidence of individual peat (coal) layers. This would lead to an overestimation of the amount of subsidence (Nadon, 1998).

Törnqvist et al. (2008) calculated subsidence rates of up to 5 mm/year in the Mississippi delta, based on a reconstructed groundwater table representing the level of a 1500-year-old isochronous peat-forming surface. They suggested that even higher rates of ~10 mm/yr might occur on timescales of decades to centuries. In this study, subsidence rates of up to 0.62 mm/yr were calculated. The higher rates calculated by Törnqvist et al. (2008) may be due to (1) the relatively short time period over which subsidence was averaged to calculate compaction rates, whereas in this paper, subsidence rates are mostly averaged over longer time periods of 4000 to 6000 years, and (2) a thicker compaction-prone Holocene sequence (up to ~40 m) at the study

site of Törnqvist et al. (2008), which potentially leads to higher amounts of subsidence due to compaction.

Subsidence rates due to peat compaction presented by Törnqvist et al. (2008) likely occur in thinner Holocene compaction-prone sequences as well, but on shorter time frames. This was demonstrated in the Cumberland Marshes by Van Asselen et al. (2010), where subsidence rates due to compaction of up to 6 mm/yr occurred over decades to a few centuries after loading of a peat layer. Furthermore, as outlined above, subsidence of sample 36 in core *CB-I* largely occurred after loading by crevasse splay deposits (section 5.4.1). The low amount of subsidence calculated for sample 35 indicates that most of the subsidence of sample 36 occurred within ~200 years at an average rate of 3.9 mm/yr.

5.7 Accommodation space provided by peat compaction

Formation of accommodation space during the Holocene in the Rhine-Meuse delta has been mainly attributed to eustatic sea-level rise and differential basin subsidence (section 5.2). Peat compaction is recognized as a process contributing to total subsidence, and this paper has attempted to quantify this process. The results of this study demonstrate that peat compaction has contributed significantly to the creation of accommodation space. In the central part of the Rhine-Meuse delta, where the Holocene sequence is approximately 5 to 10 meter thick, subsidence due to peat compaction of up to ~3 m was calculated (e.g., core *WG*; Fig. 5.3c), corresponding to 28% (= 2.9/10.4·100%) of the total Holocene accommodation space at this

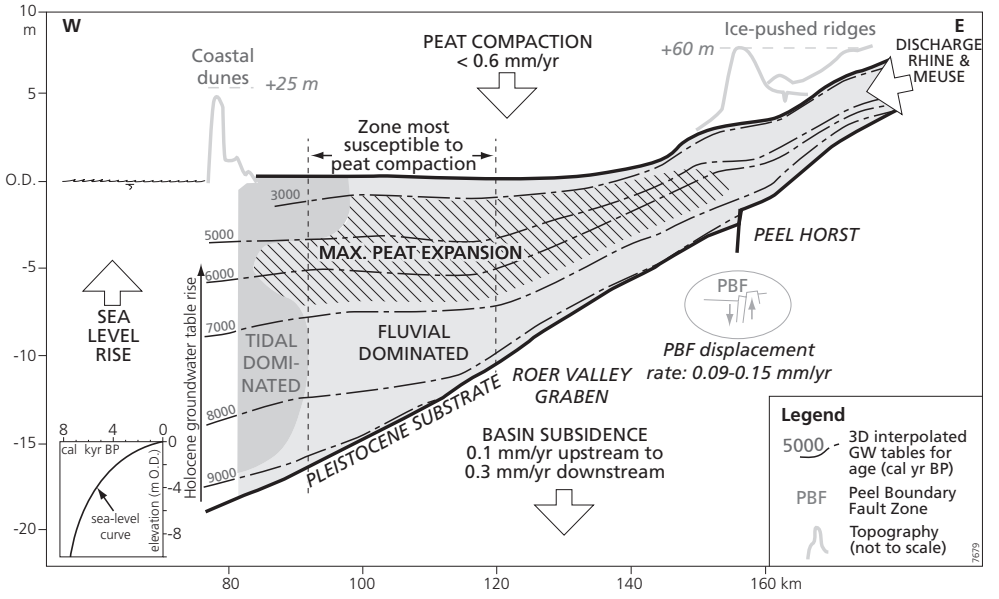

Figure 5.11. Schematic east-west oriented transect of the Holocene Rhine-Meuse delta (from apex, through central part of the delta, to the coast). The main factors driving Holocene aggradation are indicated. After Cohen (2005). Subsidence rates are millennia-averaged.

location. In other cores, subsidence due to peat compaction has created up to 40% of total available Holocene accommodation space. Furthermore, subsidence rates of up to 0.62 mm/yr, averaged over 4000-6000 years, are twice the basin subsidence rates of 0.1-0.3 mm/yr estimated previously (Kiden et al. 2002; Cohen, 2005; Fig. 5.11). On timescales of decades to centuries, even higher rates can be expected (section 5.6). Thus, the contribution of peat-induced subsidence to the creation of accommodation space is variable in time, depending on such factors as loading conditions and the thickness and organic contents of peat.

At a local scale, the geometry of overbank deposits is affected by differential peat compaction. The weight of natural levees increases subsidence rates due to compaction of underlying peat, thereby creating accommodation space for additional fluvial sedimentation, which leads to the formation of unusually thick natural levees (Stouthamer, 2005). Still, the effect of varying stratigraphic successions (e.g., proportional amounts of clay and peat) on the build-up of natural levees should be further explored. For example, the effect of differential subsidence due to peat compaction on cross-valley topographic slopes is particularly important because this is often considered to be a key factor influencing the initiation of avulsion (e.g., Mackey and Bridge, 1995).

At a regional scale, peat compaction has had significant implications for the evolution of the Rhine-Meuse delta. Between ~6000 and 3000 cal yr BP, clastic sediment supply to the delta was insufficient to fill the available accommodation space, which consequently was filled mainly by peat (section 5.2). Subsequent compaction of this peat made existing accommodation space available once again for additional peat formation and/or fluvial deposition. Most peat compaction probably started about 5000 cal yr BP, when eustatic sea-level rise ceased and accommodation space was largely created by land subsidence (Gouw and Erkens, 2007). Subsidence due to peat compaction occurred at different spatial scales, for example in areas where peat was loaded by fluvial sediments following river flooding.

Thus, in deltas containing substantial amounts of peat, peat compaction revitalizes existing accommodation space. The compaction-induced accommodation space increases the sediment trap efficiency (Erkens, 2009), by which delta progradation may be slowed down.

Field data showed that at many sites in the Rhine-Meuse delta, peat layers have not yet reached their maximum compaction potential, and hence, accommodation space may still develop from these peat layers. In this delta, however, it is unlikely that the accommodation space currently filled with peat will be aggraded with river sediment when the space once again becomes available because floodbasins are now embanked and artificially drained, such that little aggradation of any kind takes place. Based on a modeling study, Van der Meulen et al. (2007) estimated that subsidence of up to 1.5 m will occur in the upcoming decade due to peat compaction and oxidation in such artificially drained floodbasins.

5.8 Conclusions

Subsidence due to peat compaction has contributed up to 40% of the available Holocene accommodation space for aggradation in the Rhine-Meuse delta. Absolute values of up to ~3 m subsidence are calculated for a 10-m-thick Holocene succession. The amount of subsidence

due to peat compaction mainly depends on the thickness of the compressible sequence, weight of the overburden, and organic-matter content of peat. Compaction rates of up to 0.62 mm/yr, averaged over millennia, are measured. Higher rates of a few mm/yr occur over decades to centuries, shortly after loading. Thus, the contribution of peat compaction to total subsidence has been variable in time. Still, millennia-averaged compaction rates significantly add to basin subsidence rates, which are on average 0.1-0.3 mm/yr in this area. Important implications of accommodation space created by peat compaction-induced subsidence: (1) it increases sediment trap efficiency in deltas and thereby decelerates delta progradation and enhances the formation of thicker clastic sequences, and (2) at a local scale, it enhances the formation of thick natural levees by renewing existing accommodation space.

Acknowledgements

This paper greatly benefited from critical and constructive reviews by Greg Nadon, Torbjörn Törnqvist, Eugene Turner, Norm Smith and an anonymous reviewer. Esther Stouthamer and Kim Cohen are thanked for fruitful discussions and comments on earlier drafts of this paper. This research was funded by the Netherlands Organization for Scientific Research – Earth and Life Sciences (NWO-ALW, project 814.01.014) and Utrecht University, Faculty of Geosciences.

6 Holocene peat compaction in fluvial lowlands: implications to subsidence within deltas

Van Asselen, S., Karssenberg, D. and Stouthamer, E.

Abstract

Drowning and flooding of often densely populated deltas are accelerated by subsidence of Holocene deposits. Delta subsidence is caused by tectonics, isostasy, sediment compaction and/or anthropogenic processes, combined with eustatic sea-level rise. Many deltaic sedimentary successions include substantial amounts of peat, the most compressible soil type. Peat compaction, therefore, may contribute considerably to total delta subsidence. Existing studies are inadequate for quantifying peat compaction across large deltas. We present a numerical peat compaction model calibrated with an extensive field dataset. The model quantifies spatial and temporal trends in peat compaction within Holocene floodbasin sequences of different compositions. Compared to existing estimates, present subsidence rates due to peat compaction predicted by the model are much lower (<0.2 mm/yr) where peat is overlain by a substantially thick (>~1 m) clastic layer. But, much higher rates (up to 15 mm/yr) occur shortly (decades) after loading 8-m-thick peat layers. Artificial groundwater table lowering may cause additional subsidence of up to 1.5 m in 6-m-thick peat layers. Spatially, the distal portions of deltas are most susceptible to subsidence, where on decadal timescales peat compaction significantly contributes to delta drowning, thereby increasing human vulnerability to flooding

Keywords: numerial peat compaction model, subsidence, Holocene deltas.

6.1 Introduction

Subsidence is a critical control on delta formation. Many deltaic sequences include substantial amounts of peat, with peat compaction representing a fundamental control on subsidence. A limited number of field studies shows that millennia-averaged peat compaction rates in Holocene successions of up to 40 m thick, are locally up to 5 mm/yr (Bloom, 1964; Haslett et al., 1998; Törnqvist et al., 2008). Similar rates are also estimated over ~100 years in relatively thin Holocene sequences (up to ~4 m; Van Asselen et al., 2010). A major concern with estimating compaction rates based solely on field data is that these comprise local values averaged over longer time periods. Such analyses are inadequate for understanding peat compaction over finer temporal and spatial scales, which is fundamental to comprehending modern environmental problems within deltaic settings, such as flooding associated with delta drowning caused by subsidence and sea-level rise. Numerical models represent valuable tools useful for

understanding and predicting peat compaction at finer spatial and temporal resolutions. Existing peat compaction models generally predict rates of <2 mm/yr (Meckel et al., 2007; Van Asselen et al., 2010). The three main types of peat compaction models are based on (1) porosity-depth relations (Allen, 1999; Sheldon and Retallack, 2001), (2) effective stress (Terzaghi, 1943), related to changes in porosity (Paul and Barras, 1998; Massey et al., 2006; Meckel et al., 2007), and (3) soil mechanics, distinguishing primary and secondary compression (Den Haan, 1994, 2008; Kruse, 1998; Appendix 6a). These models have critical shortcomings in that they are inadequate for considering timescales associated with Holocene sequences and the spatial complexity of broad fluvial-deltaic settings. Most importantly, geotechnical peat parameters are problematic to estimate because of the heterogeneity of peat (Lefebvre et al., 1984, Price et al., 2005; Van Asselen et al., 2009, 2010), and are usually estimated based on short-duration compression tests and laboratory analysis of few peat samples in an already compressed state. Such analyses are unlikely to be applicable for accurately modeling peat compaction over Holocene timescales. Further, empirical relations (model type 1 and 2) are often derived from deeply-buried clastic sediments (Sclater and Christie, 1980) and thus likely do not apply to Holocene peat, which has very distinctive geotechnical properties (Mesri and Ajlouni, 2007). Finally, time-dependent compaction is seldom considered by these models.

We present a new one-dimensional peat compaction model that incrementally calculates deposition and compaction due to an increase in stress and time of 5 to 10-cm-thick peat layers in an aggrading sequence over Holocene timescales. The model is calibrated with an extensive field dataset (100 samples) from a Holocene deltaic succession within the Cumberland Marshes (Van Asselen et al., 2010), Canada, which has experienced minimum human influence. This dataset ensures reliable determination of model parameters.

6.2 Model description and calibration

In the new peat compaction model, peat and sediment layers are successively added to an alluvial sequence. Each layer i is characterized by an initial thickness $h_{0,i}$ (m), Loss On Ignition LOI_i (fraction), which is indicative for the organic-matter content, saturated density $\rho_{s,i}$ (g/cm^3) and time of deposition $t_{dep,i}$ (yr). The model considers peat and clay layers. Clay, which is much less compressible than peat (Mesri and Ajlouni, 2007), is assumed to be incompressible over Holocene timescales. At each timestep, a new layer is deposited, after which the thickness of all layers in the aggrading sequence is calculated using:

$$h_{i,t} = h_{0,i}\, exp\,(-\varepsilon_{i,t}) \tag{6.1}$$

in which $\varepsilon_{i,t}$ is natural strain (Appendix 6b) of layer i at time t (yr), which better describes large compressions occurring in soft soils like peat, compared to the commonly used linear strain (Den Haan, 1994). Natural strain is calculated using:

$$\varepsilon_{i,t} = a_i \ln\left(\frac{\sigma'_{i,t}}{\sigma'_0}\right) + b \ln\left(\frac{t - t_{dep,i}}{t_0}\right) \tag{6.2}$$

in which a_i and b are calibration parameters (-), $\sigma'_{i,t}$ is the effective stress (kPa), σ'_0 and t_0 are initial conditions (=1; Appendix 6c). Also, at each timestep, the total amount of subsidence (s_p

(m)=sum of subsidence of all layers) and the average subsidence rate (m/yr; s_p, divided by the accumulation time of the youngest layer) are calculated. The logarithmic relation with both stress and time in Equation 6.2, usually assumed in models based on soil mechanics theory (Den Haan, 1994, 2008; Kruse, 1998), is based on good fits with data derived from short-duration compression tests, but is not necessarily valid over longer geological timescales. Therefore, linear and power formulations were also tested (described below).

The effective stress is calculated based on Terzaghi's principle of effective stress (Terzaghi, 1943; Appendix 6d). The value of a_i is linearly related with LOI_i, as has been determined based on results from compression tests (Den Haan, 1994; Kruse, 1998):

$$a_i = cLOI_i + d \tag{6.3}$$

Parameters *b*, *c* and *d* are calibrated using field data from the Cumberland Marshes. Here, in the 1870s an avulsion of the Saskatchewan River invaded a peatland, thereby partly burying an up to ~2-m-thick Late Holocene fen peat layer by up to ~2 m thick alluvium (Smith et al., 1998; Morozova and Smith, 2003). Data from six cores obtained from this area (Van Asselen et al., 2010) were used to generate the model calibration dataset. In each core, the dry bulk density ($\rho_{d,i}$) and LOI_i of the compacted peat layer were determined at 5-cm intervals (1x1x5 cm samples; Van Asselen et al., 2010). In addition, the ρ_d and LOI of different types of uncompacted surface peat were determined using a new peat sampler (Van Asselen and Roosendaal, 2009). From these data we established exponential relations between ρ_d and LOI of different types of uncompacted fen peat (Van Asselen et al., 2010). These relations were used to calculate the decompacted height ($h_{0,i}$) of each 5-cm-thick compacted peat sample, based on its LOI_i.

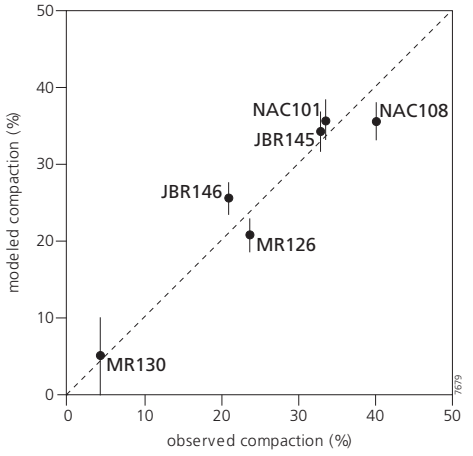

Figure 6.1. Plot of the modeled vs. observed compaction (%) of the 6 cores (labels denote core codes) used for calibration, using the parameter set *c*=0.09, *d*=0.05 and *b*=0.009. The vertical bars represent 95% confidence intervals (Appendices 6e and 6f).

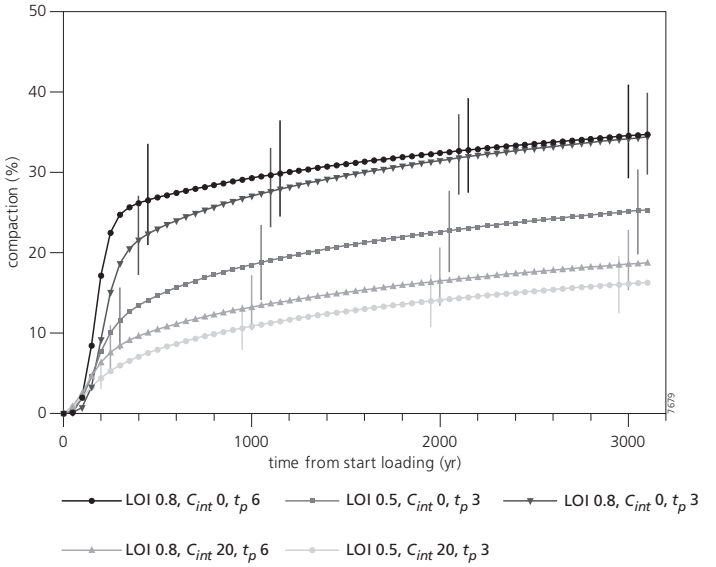

Figure 6.2. The amount of compaction (%) over time after loading of peat sequences varying in initial thickness (t_p in m), *LOI* (fraction of 1) and percentage of intercalated clay layers (C_{int}). Symbols represent data points and vertical bars represent 95% confidence intervals.

The $\sigma'_{i,t}$ of each 5-cm-thick layer in the calibration dataset was derived from the thickness and texture composition of overlying layers, determined during field logging of the cores at a 10-cm depth interval (Van Asselen et al., 2010; Appendix 6d).

The $t_{dep,i}$ was estimated based on linear interpolation between AMS radiocarbon-dated peat samples within a core (maximum vertical distance of 20 cm; Van Asselen et al., 2010). In the calibration dataset, the deposition time of one 5-cm-thick peat layer is on average ~115 years. Clastic layers of similar thickness overlying the peat layer accumulated much faster (<20 yrs).

Using the above described field data (h_0, LOI, ρ_s and t_{dep} of each 5-cm-thick layer), parameters *b*, *c* and *d* were calibrated by minimizing the objective function:

$$\Phi = \sum_{i=1}^{n} \left(h_{i,endtime} - h_{i,obs} \right)^2 \tag{6.4}$$

with, $h_{i,endtime}$ and $h_{i,obs}$, the modeled and observed final thickness of layer *i*, respectively. Calibration was done by an exhaustive search in parameter space (Appendix 6e-I), resulting in the parameter set *c*=0.09, *d*=0.05 and *b*=0.009 with the lowest value of the Φ. This parameter set results in a good fit between observed and modeled sequences (Fig. 6.1; Appendix 6f), and was used in subsequent model runs, calculating 95% confidence intervals (Seber and Wild, 2003; Doherty, 2004; Appendix 6e-II). Alternative forms of Equation 6.2 were rejected because these resulted in higher values of Φ (Appendix 6e-III).

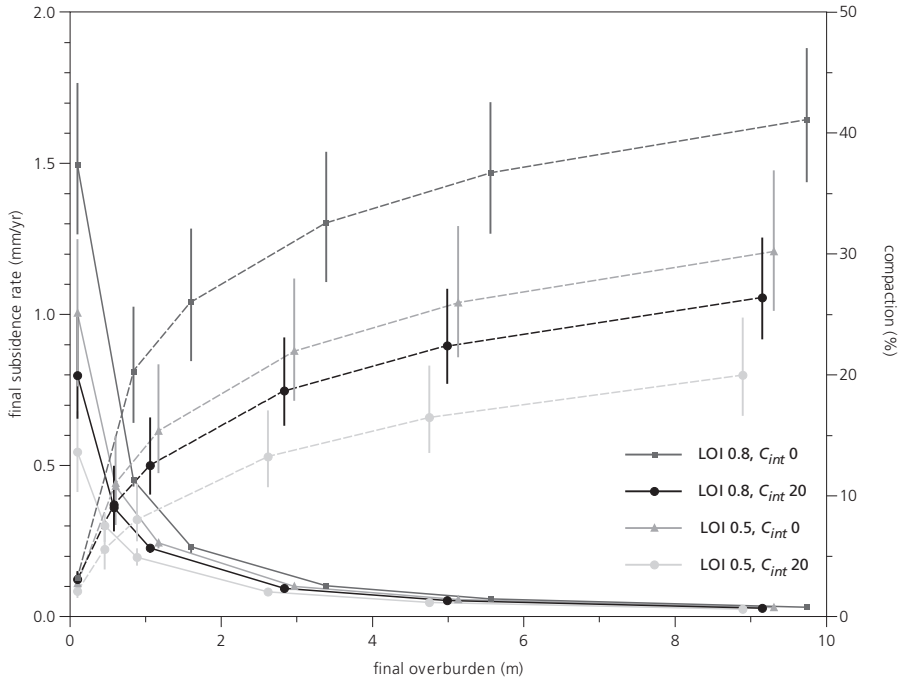

Figure 6.3. Plot of the percentage of peat compaction and final average subsidence rate vs. final overburden thickness, in a peat sequence with an uncompacted thickness (i.e., base-level rise multiplied by time of peat accumulation) of 4 m, and 100 years of constant aggradation of 0.001 m/yr starting at the end of overburden deposition (C_{int} = percentage of intercalated clay layers). The solid lines denote final subsidence rate, the dashed lines denote percentage of compaction. Vertical bars represent 95% confidence intervals.

The calibrated model was used to calculate past and present rates and amounts of subsidence due to compaction of a peat layer overlain by a clay layer (overburden), for different scenarios regarding duration of peat accumulation (t_p), duration of overburden deposition (t_c), LOI of peat and percentage of intercalated 5-cm-thick clay layers (C_{int}; percentage of t_p). Two consecutive situations are considered: constant base-level rise and constant aggradation. *Situation 1* represents the natural Holocene situation, during which a peat and overburden layer is successively formed. It is assumed that vertical accommodation space created by peat compaction after deposition of a new layer is filled by increased peat or clay deposition during the next timestep. The level to which increased sedimentation fills up accommodation space is determined by the rate of base-level rise (in this study 0.001 m/yr). *Situation 2* represents reduced aggradation rates currently observed in many deltas, caused for example by upstream damming and channel embankments (Blum and Roberts, 2009; Syvitski et al., 2009; Appendix 6g). The effect of reduced aggradation rates, resulting in the inability to infill accommodation space created by peat compaction, has been simulated by assuming 100 years of constant clay aggradation from the moment overburden deposition ceases.

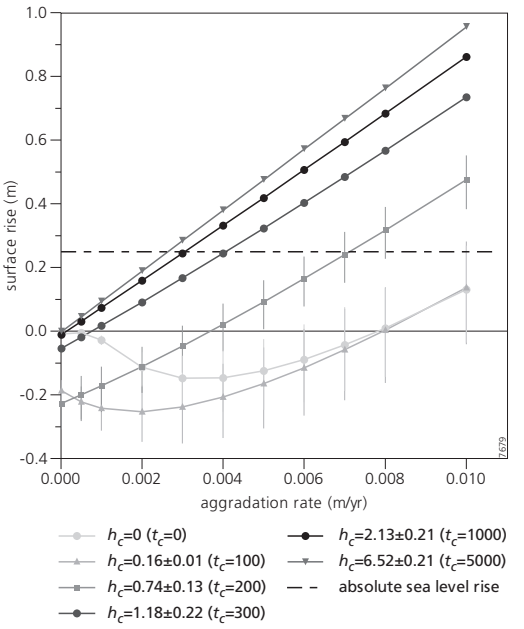

Figure 6.4. Plot of final surface elevation rise vs. aggradation rate after 100 years of constant aggradation, in a initially 4-m-thick peat layer (LOI 0.8) that was subsequently loaded by a clay layer with thickness h_c (deposited during a period of overburden deposition in *situation 1*; t_c in years). Negative values indicate subsidence. Maximum and minimum h_c are given in the figure legend and are introduced by using different calibration parameter sets. The intercalated line denotes global mean sea-level rise, based on estimated rates averaged over the period 2003-2008 (Cazenave et al., 2008). The Intergovernmental Panel on Climate Change (IPCC) predicts a global mean sea-level rise of 0.2-0.5 m in 2100 (Bindoff et al., 2007).

6.3 Modeling results

Model results show that most compaction occurs shortly after the start of overburden deposition, but continues over time at a subdued rate (Fig. 6.2). The amount of subsidence due to peat compaction at any moment in time is positively related with the thickness and LOI of the peat sequence, and negatively related with C_{int} (Fig. 6.2). The model predicts average subsidence rates of up to 15 mm/yr in 8-m-thick peat sequences with LOI=0.8.

The total amount of compaction of a peat sequence is positively related with the final overburden thickness (Fig. 6.3). However, the present rate of subsidence due to peat compaction is negatively related with the final overburden thickness; most compaction has occurred shortly after the start of overburden deposition.

Hence, in areas where a peat layer is covered by an adequately thick clastic sediment layer (h_c>~1 m), low aggradation rates (~0.001 m/yr) are sufficient to prevent subsidence due to peat compaction (Fig. 6.4). However, in areas where the clastic sediment layer is thin (few decimeters) or absent, high aggradation rates are needed to prevent subsidence due to peat compaction.

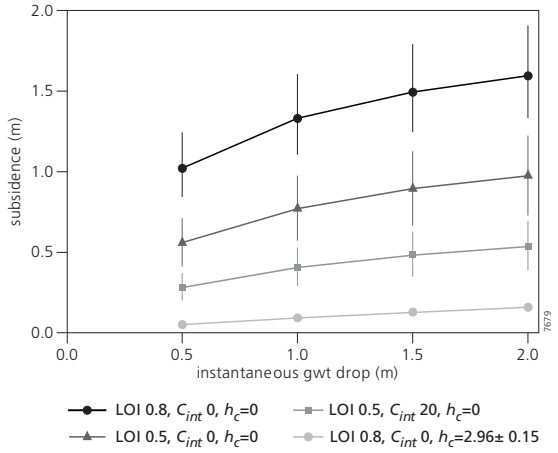

Figure 6.5. The amount of subsidence following instantaneous lowering of the groundwater table (gwt), for different peat sequences with an initial thickness of 6 m (h_c = overburden thickness in m, C_{int}=percentage of intercalated clay layers).

In scenarios h_c=0 and h_c=0.16, continued aggradation initially accelerates peat compaction. An optimal aggradation rate exists for which the amount of subsidence is maximal; lower rates do not sufficiently increase the effective stress causing compaction, higher rates increasingly fill up the amount of accommodation space provided by peat compaction. In scenario h_c=0.74, the sequence is still considerably subsiding at the start of constant aggradation; a rate of ~0.004 m/yr is needed to compensate for subsidence due to peat compaction. Even higher aggradation rates are usually needed to prevent subsidence relative to local sea-level rise. In the example given in Fig. 6.4, a rate of >~0.3 m/100yr is needed to keep up with the rate of global sea-level rise averaged over the period 2003-2008 (Cazenave et al., 2008; other scenarios in Appendix 6h).

Additional subsidence is caused by groundwater table lowering, which results in increased effective stress (higher $\sigma'_{i,t}$ in Equation 6.2) because the pore water pressure is strongly reduced. To study this effect, the groundwater table was instantaneously lowered at the end of overburden deposition. The amount of subsidence following groundwater table lowering is positively related with peat thickness and LOI, and is negatively related with overburden thickness; if a peat layer has already experienced much compaction due to loading, the additional amount of subsidence caused by groundwater table lowering will be less than in an area where the peat layer still is in a relatively uncompacted state (Fig. 6.5).

6.4 Discussion and conclusions

Rates of subsidence due to compaction predicted by recent field studies are often averaged over millennia (Bloom, 1964; Haslett et al., 1998; Törnqvist et al., 2008). Our model results demonstrate that actual present rates in deltas are much lower (<0.2 mm/yr; Fig. 6.3) if the peat layer has already experienced compaction by loading, whereas much higher rates (up to ~15 mm/

yr) occur within decades to a few centuries after loading. The amount and rate of subsidence due to peat compaction in deltas is highly variable in space and time, depending on e.g. peat thickness, overburden thickness, percentage of intercalated clay layers and organic-matter content of peat (Bloom, 1964; Haslett et al., 1998; Meckel et al., 2007; Törnqvist et al., 2008; Van Asselen et al., 2009, 2010). Hence, current estimated rates should be revisited. This study reveals that especially distal parts of deltas, where thickest peat layers occur and an overburden is often absent, are most vulnerable for high amounts of subsidence due to peat compaction. Human interventions causing reduced aggradation rates and groundwater table lowering in such areas enhances subsidence and thereby increases the risk of drowning (Ericson et al., 2006; Day and Giosan, 2008; Blum and Roberts, 2009; Syvitski et al., 2009). Thus, the threat of drowning caused by subsidence due to peat compaction varies both temporally and spatially in a delta, which is vital knowledge for sustainable management of deltaic environments in the context of forecasted rates of global sea-level rise.

Acknowledgements

This paper greatly benefited from comments on earlier drafts by Paul Hudson (University of Texas at Austin, USA) and Meindert Van (Deltares, The Netherlands). Theo van Asch (Utrecht University, The Netherlands), Gerard Kruse and Henk Kruse (both employed at Deltares, The Netherlands) are thanked for their contributions to developing the compaction model. This research was funded by the Netherlands Organization for Scientific Research – Earth and Life Sciences (NWO-ALW, project 814.01.014) and Utrecht University, Faculty of Geosciences.

7 Synthesis

The main objectives of this research were to (1) quantify the amount and rate of subsidence due to peat compaction in Holocene alluvial sequences based on field data, (2) develop a numerical peat compaction model, calibrated with field data, to predict temporal and spatial variations in subsidence due to peat compaction within deltas, and (3) evaluate the effect of subsidence due to peat compaction on spatial and temporal sedimentation patterns in deltaic settings, and therewith on delta evolution. This chapter synthesizes the main results of this research, and gives directions for future research.

7.1 Using field data and models to quantify subsidence due to peat compaction

Methods to quantify peat compaction

Subsidence due to peat compaction has been quantified using two field methods (chapter 4 and 5) and a new numerical peat compaction model (chapter 6). The first field method relies on the reconstruction of palaeogroundwater tables, which are indicative of former levels of fen peat formation, based on radiocarbon-dating of basal peat samples (chapter 2). In a peat sequence, the vertical distance between the present-day level of a radiocarbon-dated peat sample and its reconstructed initial level of formation is a measure for the amount of subsidence of the sampled level, caused by compaction of deposits situated in between the sampled peat level and an underlying incompressible subsurface. Thus, this method provides information regarding the total amount of subsidence of peat samples, experienced since a sample was formed.

The second field method estimates the amount of compaction experienced since the time of peat formation, based on dry bulk density measurements of the compacted peat, and of uncompacted peat with similar LOI and plant species composition (chapter 4 and 5). So, this method provides information regarding the degree of peat compaction, and not directly on the amount of subsidence. By sampling an alluvial succession containing one or more peat sequences of various compositions, a detailed record of variations in the amount of compaction is obtained, which can be related to for example variations in LOI, plant species compositions and effective stress (chapter 4 and 5). The amount of subsidence, caused by peat compaction, can be assessed by assuming that compaction of a peat sequence occurs at once following a substantial increase in effective stress (chapter 5). In general, this will overestimate the amount of subsidence, because compaction may have occurred during the time of formation of a peat sequence. For example, groundwater table lowering and/or deposition of sediment associated with peatland flooding increase the effective stress in the peat layer and thereby induce compaction. In areas receiving no, or very small amounts of sediment, high-organic peat may accumulate for thousands of years without significant compaction occurring. In this case, most compaction is indeed induced after loading a peat sequence. In this method, it is essential to accurately determine the dry bulk density of uncompacted surface peat from field settings, which is difficult because of the commonly loose and heterogeneous character of peat (Lefebvre et al., 1984). The new peat sampler devised for this purpose proved to be successful to extract sufficiently large samples of different types of fen peat while introducing minimum disturbance (chapter 3).

Field trials proved that the device can also be used to sample less saturated surface peat. In this research, the extracted samples were analyzed for the bulk density and LOI of peat, but, the sampler may also be used to determine other peat characteristics such as nutrient concentrations and fiber structure.

The two field methods provide information regarding the amount of subsidence and the degree of compaction of peat within a peat sequence, experienced since it was formed. However, from these field data it cannot be directly derived when most compaction occurred, although field data obtained from the Cumberland Marshes (CM) and the Rhine-Meuse (RM) delta strongly indicated that much compaction occurs shortly (decades to a few centuries) after loading a peat sequence (chapter 4 and 5). To estimate the amount and rate of peat compaction occurring in Holocene alluvial sequences of different composition over fine temporal scales more accurately, a new numerical peat compaction model was developed (chapter 6). The most important advantages of this model compared to existing peat compaction models are that (1) it is calibrated with an extensive field dataset obtained from a natural Holocene deltaic setting, (2) it numerically calculates peat compaction on Holocene timescales, and (3) it uses natural strain, which is logarithmically related to both stress and time. Calibration with the CM field dataset ensures reliable fitting of parameters that are valid on Holocene timescales. In existing compaction models, geotechnical parameters are mostly estimated from results from short-duration compression tests and laboratory tests on small peat samples in an already compressed state, and hence, such analyses are unlikely to be applicable to Holocene deltaic successions. Other compaction models use empirical relations derived from deeply-buried sediments (Sclater and Christie, 1980). Such relations also are likely not applicable to calculate compaction of Holocene peat, which occurs at much shallower depths and has very distinctive geotechnical properties, for example regarding the permeability and compressibility, compared to clastic sediments (Mesri and Ajlouni, 2007). Regarding the use of natural strain, this better describes large strains as occur in soft soils like peat compared to the more commonly used linear strain (Den Haan, 1994). Including time-dependent compaction is important because it may cause substantial amounts of peat compaction additional to stress-induced compaction (Den Haan, 1994). Current models that do take into account time-dependent peat compaction are isotach models, which are increasingly considered to be most reliable for modeling compression of peat soils (chapter 2). However, such models have mostly been applied for engineering purposes, which generally require subsidence calculations over very short timescales of days to months. To predict effects of subsidence due to peat compaction on delta evolution, longer timescales should be considered, as is done in the new model.

The new peat compaction model provides estimates of peat compaction rates, generally averaged over 50 years, in deltaic settings that differ in sequence composition, for example regarding the thickness and LOI of the peat succession, occurrence of intercalated clay layers, and overburden thickness. By changing initial model settings, the model can be used to explore and understand temporal and spatial subsidence patterns in a delta containing peat, and the inherent sedimentation patterns. In addition, the model can be used to predict present and near-future subsidence rates, caused by peat compaction, in different deltaic settings under specific conditions of base-level rise and aggradation rate (chapter 6). This is of utmost importance because many densely populated deltas are increasingly threatened by for example eustatic sea-level rise and sediment starvation, and therefore need sustainable delta management plans that

require reliable subsidence estimates (chapter 6). This research demonstrated that stratigraphic data is essential for developing such plans.

The amount and rate of peat compaction in deltas

Subsidence due to peat compaction in deltas is highly variable in time and space. Field data obtained from both the CM and the RM delta showed that peat layers may accumulate over thousands of years without experiencing significant compaction, whereas considerable compaction was measured in peat layers that are loaded by fluvial sediment. In the CM, peat has experienced up to ~50% compaction, most of which appeared to have occurred shortly after the start of deposition of an alluvial wedge on top of the peat layer, approximately 135 years ago (chapter 4). Measured subsidence rates of peat levels, averaged over this time period, are up to ~6 mm/yr. In the RM delta similar maximum peat compaction percentages were obtained, but millennia-averaged rates measured in the RM delta are an order of magnitude lower; up to ~0.6 mm/yr. Here, the highest percentages (up to ~60%) were measured at sites where the peat sequence is overlain by a thick natural levee and where overburden deposition started several thousands of years ago (chapter 5). Comparing results of the CM and RM delta indicates that most peat compaction occurs decades to centuries after loading. The highest amounts of subsidence caused by peat compaction have been measured in the RM delta (up to 3 m in a 10-m-thick Holocene sequence), which is mainly attributed to the thicker peat sequences occurring in this delta.

Results of the modeling study showed that subsidence rates, due to peat compaction, in Holocene sequences containing thick (8 m) homogenous high-organic (LOI=0.8) peat sequences may be as high as 15 mm/yr, occurring shortly (decades) after loading (chapter 6). In the model scenarios, the timestep (accumulation time of one layer) is 50 years, and hence, even higher rates may occur over shorter time periods. With continued overburden deposition, the subsidence rate, caused by peat compaction, usually drops to values <0.2 mm/yr within a few centuries, depending mainly on the thickness and inorganic content of the peat sequence. Hence, present subsidence rates at sites where the peat layer is presently loaded by a substantially thick (>~1 m) clastic sediment layer that is deposited during a few centuries, is low, especially compared to millennia-averaged rates estimated from other field studies (up to 5 mm/yr; Bloom, 1964; Haslett et al., 1998; Törnqvist et al., 2008). However, higher subsidence rates (i.e. ~15 mm/yr) are expected to occur at sites where the peat sequence is still relatively uncompacted. Under conditions of base-level rise and/or low aggradation rates, caused by e.g. upstream damming and river embankments, subsidence due to peat compaction will significantly increase the risk of flooding of such areas.

Factors influencing peat compaction

Results of the different methods used to quantify peat compaction reveal that the effective stress is the most important factor inducing peat compaction. Another factor influencing the amount of peat compaction is the organic-matter content of peat; high-organic peat is more compressible compared to low-organic peat. These two factors seem to be much more important than the effect of plant species composition of peat, although this must have some effect (chapter 3; also discussed in section 7.4). For example, the initial porosity of peat, and therewith the maximum compaction potential, is partly determined by the fiber structure. Furthermore, the arrangement, size and strength of fibers also likely influence peat compressibility; peat comprising small fibers

like roots of herbaceous plants is more easily compressed than peat comprising thick reed stems or large and stiff wood fragments. Still, from the results of this research, it may be concluded that the amount and rate of subsidence due to peat compaction is mainly influenced by the thickness of the peat layer, changes in effective stress and organic-matter content of peat (chapter 4-6). Furthermore, model results indicate that changes in effective stress (stress-induced strain) cause relatively more peat compaction than changes in the time since formation of a peat layer (time-induced strain). In high-organic peat layers without any overburden (effective stress is very low), only some time-dependent compaction occurs. Once the effective stress in the peat layer significantly increases, for example due to sediment deposition or groundwater table lowering, most compaction is induced by this increase in effective stress. But, although time-dependent compaction is relatively small, it continues through time, and hence, may induce substantial amounts of peat compaction over long time periods.

7.2 Peat formation and compaction in deltas; causes and consequences

Effect of peat compaction on fluvial sedimentation patterns in deltas

On a local scale, subsidence due to peat compaction results in locally increased sedimentation rates, provided that the rate of sediment supply is sufficiently high. This enhances the formation of relatively thick natural levees (Stouthamer, 2005). Moreover, subsidence due to peat compaction beneath natural levees, or in floodbasins, possibly influences the occurrence of avulsion, which is one of the most important processes for delta building (chapter 2). In this context, the main question is whether subsidence due to peat compaction creates changes in cross-valley slopes, which is considered to be one of the main driving forces of avulsion (e.g., Mackey and Bridge, 1995), although it is also influenced by many other factors such as substrate erodibility and log-, ice and beaver dams (Aslan et al., 2007; Stouthamer and Berendsen, 2007). Observations and results from this study imply that peat compaction initially will not stimulate the occurrence of avulsion. Subsidence due to peat compaction beneath natural levees will reduce rather than increase cross-valley topographic slopes, and created accommodation space is generally easily filled by increased sedimentation or peat formation. Furthermore, raised bogs formed in floodbasins, as for example occurred during the Mid-Holocene in the Rhine-Meuse delta, will not favor increased cross-valley topographic slopes.

In general, topographic slopes in peatlands are low, which reduces stream power, and bank stability is high because peat is highly resistant to erosion. The high permeability of river banks consisting of peat might further decrease stream power by water leaking from the channels (Tooth and McCarthy, 2004). These factors stimulate rivers in peatlands to evolve into anastomosing rivers with low width/depth ratios (Gouw and Berendsen, 2007; Watters and Stanley, 2007). The low transport capacity of such rivers stimulates frequent crevassing, as is for example observed in the Mid-Holocene central part of the Rhine-Meuse delta. Crevasse splays are features prone to evolve into avulsions (Smith et al., 1998), but, in case of rivers in peatlands, low regional topographic slopes and efficient trapping of fluvial sediments by subsidence due to peat compaction likely prevent or at least slow down full evolution of a crevasse splay into an avulsion.

Still, in some situations, the occurrence of avulsion may be stimulated by subsidence due to peat compaction. For example, if the maximum peat compaction potential is approached in some

parts of a floodplain, while in adjacent parts of the floodplain relatively high rates of subsidence due to peat compaction still prevail, gradient advantages might be created which increases the chance of avulsion (Michaelsen et al., 2000; Rajchl and Uličný, 2005). Also, subsidence in floodbasins due to natural or artificial groundwater table lowering might lead to amplification of the relief of sandy channel belts (chapter 2), which potentially leads to increased cross-valley slopes.

Subsidence due to peat compaction also has regional-scale effects on delta evolution. Because peat has a very low mass density, compaction by self-weight is minimal. Hence, extensive high-organic peat layers of meters thick may accumulate in wetlands with low sediment input, without any significant compaction occurring. Groundwater table lowering or enhanced deposition of fluvial sediment on top of a peat layer increases the effective stress in the peat sequence. This causes substantial amounts of subsidence due to compaction, thereby revitalizing existing accommodation space for increased fluvial deposition. In this situation, accommodation space is first temporary filled with peat, and is later 'refilled' by fluvial deposits. Such a situation has occurred in the Rhine-Meuse delta, where extensive peat formation occurred between 6000 and 3000 cal yr BP, when sediment delivery to the delta was insufficient to fill up accommodation space created during that time period. Compaction of these thick Mid-Holocene peat layers probably started at a local scale approximately 5000 cal years ago, when eustatic sea-level rise ceased and accommodation space was mainly created by land subsidence (Gouw and Erkens, 2007). Peat was compacted for example as a result of sediment deposition in floodbasins subject to river flooding. Associated created accommodation space was filled by continued peat formation or by fluvial sedimentation.

Field data from the RM delta showed that locally up to 40% of Holocene accommodation space has been created by subsidence due to peat compaction (chapter 5). Also in the Cumberland Marshes, accommodation space initially filled by peat was later refilled by fluvial sediments that were deposited following the 1870s avulsion of the Saskatchewan River. This process of revitalizing existing accommodation space has likely occurred in many other deltas containing peat. The compaction-induced accommodation space increases the sediment trap efficiency, by which thick alluvial sequences are expected to develop if they overly meters-thick peat layers. Furthermore, delta progradation may be slowed down.

Alluvial architecture

The effect of peat compaction on local and regional sedimentation patterns obviously affects alluvial architecture, which is important information for the exploration of natural resources. Especially in lithologically diverse sequences, i.e. with a high alternation of sandy channel belt deposits and organic-rich floodbasin deposits, compaction of intercalated peat layers may lead to considerable distortion of the original stratigraphy (De Groot and De Gans, 1996; Allen, 1999). Subsidence due to peat compaction may also affect the geometry of channel belts. Observations of ancient strata suggest that channel belts directly overlying peat tend to aggrade vertically due to compaction of underlying peat, which initially leads to channel belts with a low width/depth ratio (Michaelsen et al., 2000; Rajchl and Uličný, 2005). Lateral migration, leading to higher width/depth ratios, is promoted when the maximum compaction potential beneath the channel is approached. Also, if an incising channel encounters a relatively thin peat layer intercalated between clastic sediment layers, the erosion resistant peat will initially prevent further down-

cutting, which stimulates the development of channels with high width/depth ratios, until the peat layer is completely eroded (Smith and Pérez-Arlucea, 2004; chapter 2).

Peat-to-coal

In the study areas used in this research peat has not yet transformed into coal, and hence, this research does not provide direct evidence regarding how alluvial systems containing peat evolve on longer geological timescales (>10^4 years). This research does show that much compaction, up to ~50%, occurs shortly after loading, nearby the surface, as has also been concluded in studies on coal-bearing strata (Nadon, 1998; Rajchl and Uličný, 2005). These studies demonstrated, based on sandstone-channel geometries and dinosaur tracks, that the amount of compaction associated with the transition of peat into coal is minimal. This is relevant information for the interpretation of ancient sequences containing coal seams, for example regarding estimations of the amount of accommodation space that was available during the time of formation; coal seams are generally associated with periods of high-accommodation (Diessel et al., 2000; Gibling et al., 2004; Davies et al., 2005). Minimum compaction associated with the peat-to-coal transition implies that the thickness of peat layers in the Cumberland Marshes and Rhine-Meuse delta that have already experienced much compaction due to loading will approximately be similar to the thickness of their future coal seam equivalents. However, there are still large areas in these deltas with no or only a thin overburden, which hence are still highly susceptible for high amounts of subsidence due to peat compaction.

Accelerated subsidence due to human-induced peat compaction and oxidation

Many deltas are densely populated (Ericson et al., 2006; Syvitski et al., 2009), and often contain extensive peatlands (chapter 5, 6; Charman, 2002). Besides subsidence due to natural compaction of peat, as thoroughly described in this thesis, accelerated subsidence due to human interventions seriously increases the risk of delta drowning and floods, thereby threatening hundreds of millions of people currently living in deltas. The main causes of human-induced subsidence are artificial groundwater table lowering for land reclamation and exploration of hydrocarbons and groundwater.

Although this research focused on natural peat compaction, data obtained from the Rhine-Meuse delta did demonstrate the impact of groundwater table lowering; relatively high dry bulk densities were sometimes measured in the top meters of peat sequences, which was attributed to peat oxidation, and additional compaction due to groundwater table lowering and soil tillage (chapter 5). Other studies in the Rhine-Meuse delta measured land subsidence following groundwater table lowering of up to 1.67 cm/yr, averaged over 6 years (Schothorst, 1977; Beuving and Van den Akker, 1996). Similarly, in the reclaimed San Joaquin Delta in California, relatively high land subsidence rates have occurred during the past decades, mainly caused by oxidation and reduction of the hydrostatic pressure following groundwater table lowering (Drexler et al., 2009). In this area, subsidence rates decreased from 2.8-11.7 cm/yr in the mid-twentieth century to 0.5-4 cm/yr in the 1980s and 1990s, to current rates of 0.5-3 cm/yr (Drexler et al. 2009 and references therein). Gambolati et al. (2003) measured subsidence rates of up to 5 cm/yr in artificially drained areas in the Venice Lagoon. The peat compaction model developed for this research also demonstrated the significant effect of groundwater table lowering; the model predicted up to 1.5 m subsidence following an instantaneous 2-m-drop of the groundwater table in a 6-m-thick high-organic peat layer (chapter 6). Areas

where the sediment layer overlying peat is thin or absent, and hence, minimum compaction has yet occurred, are especially susceptible to high amounts of subsidence following artificial groundwater table lowering.

In comparison, deep and shallow groundwater extraction may lead to extremely high subsidence rates of up to ~27 cm/yr, averaged over six years (Abidin et al., 2001). Subsidence rates of up to ~2 cm/yr occurred between 1982 and 1993 in the Gulf Coast region, an area subjected to exploration of oil and gas (Morton et al., 2006). More examples of studies on subsidence due to groundwater and hydrocarbon extraction are given in Syvitski (2008).

Other anthropogenic threats potentially increasing the risk of delta flooding are decreasing sediment supply to a delta due to upstream river damming, and sediment routing by reducing the number of active channels and constructing of river dykes, which results in sediment deficits in floodbasins (Van der Meulen et al., 2007; Syvitski., 2008; Syvitski et al., 2009). Deltaic environments experiencing a sediment deficit are unable to fill up accommodation space for example created by peat compaction, which consequently leads to land subsidence.

Concluding, on short timescales (decades) human-induced subsidence rates in deltas reach values on the order of a few cm/yr, which generally is one to two orders of magnitude higher than natural compaction rates, although the model did predict similar natural subsidence rates occurring shortly after loading of a thick high-organic peat layer. Hence, human impact seriously increases the risk of delta drowning, and therefore should be taken into account in delta-managements plans, besides important factors such as the composition of the sediment succession.

7.3 Future research

This thesis presents detailed quantitative data regarding spatial and temporal variations in peat compaction in deltas, at an extent as was not done before. In this way, it may be seen as a pilot study in the research field of subsidence due to peat compaction, which has increasingly been recognized as an important process contributing to total subsidence in Holocene deltas. Obviously, there are still topics that need to be investigated, several of which are outlined below.

(1) The *compressibility of different peat types* should be further explored. Both data obtained from the Cumberland Marshes and the Biebrza National Park showed that high-organic moss and sedge peat generally has a slightly lower initial dry bulk density, and higher initial porosity, than peat including wood fragments (chapter 3 and 4). This suggests that moss and sedge peat is more compressible than wood peat, as has also been predicted based on results of compression tests (Den Haan, 1994). Also, the degree of decomposition seems to be negatively related with the compressibility (Price et al., 2005). To investigate the effect of the plant species composition on compressibility, more measurements on different peat types in different alluvial settings (especially compacted wood peat was insufficiently sampled in this research) are needed. Related to this, it is of interest to evaluate *the spatial and temporal distribution of different peat types within a delta*, which likely is dependent on for example the distance to a river, the nutrient status of groundwater and the rate of base level rise. Such information also provides valuable information regarding the quality of coal seams in ancient strata.

(2) Evaluate *the effect of natural and artificial groundwater table fluctuations on peat formation and subsidence due to peat compaction*. Local natural groundwater table fluctuations may for example be caused by avulsion; water tables may be temporarily raised in an area that is invaded by an avulsion (Berendsen et al., 2007). Groundwater table fluctuations associated with avulsions have never been quantified however, and their effect on peat compaction is unknown. Artificial groundwater table lowering for land reclamation may significantly increase land subsidence (section 7.2), but it is of interest to further unravel the main factors determining the amount of subsidence associated with groundwater table lowering. Modeling results (chapter 6) indicate that peat thickness, LOI, occurrence of intercalated clay and present overburden thickness all influence the amount of subsidence following a sudden increase in effective stress caused by a drop in hydrostatic pressure. The new compaction model provides a valuable tool to estimate the amount of subsidence following groundwater table lowering, given the stratigraphy of the compressible sequence. Still, a more refined verification of modeling results with field studies on groundwater table lowering is needed.

(3) *Extend the peat compaction model.* For example, land subsidence due to peat oxidation is not included in the model yet. This could be done by estimating the amount of organic matter that has vanished, based on the LOI, and the associated loss of volume. The model has been designed for fen peat environments, and has been calibrated with fen peat data. Applying the model to bog environments would require calibration with field data obtained from bogs. For this, the model should be extended to include peat growth above the groundwater table, which also requires to model peat decomposition. Another model extension could be to include erosion processes. For example, when a river enters a peatland, erosion of the top of the peat layer may take place, depending on the stream power of the river. Furthermore, in the modeling study presented in chapter 6 only peat and clay layers are considered. The effect of loading by other types of sediments, such as sand and silt, may easily be assessed by changing the saturated density of the clastic sediment layers. Similarly, compaction of peat with different organic-matter contents can be estimated by changing the LOI of peat layers.

(4) *The effect of peat compaction on topographic slopes*, which potentially influences the occurrence of avulsion, should be further investigated. In general, peat compaction is thought to slow down the occurrence of avulsion, except in some situations (section 7.2). Still, this statement should be tested based on field evidence, for example by relating sites of avulsion with the amount of peat compaction occurring during the time of avulsion. Once the effect of peat compaction on topographic slopes has better been investigated, *a peat compaction module as developed in this research (chapter 6) should be incorporated into alluvial architecture models* (e.g., Mackey and Bridge, 1995; Karssenberg and Bridge, 2008). This will improve predictions of reservoir architecture, which is important information for the e.g. exploration of natural resources.

Summary

Peat compaction in deltas
Implications for Holocene delta evolution

Rationale

The formation and evolution of deltas is basically controlled by sediment supply and the provision of accommodation space. Sediment supply is affected by processes influencing river discharge and sediment yield, such as climate, human impact and erodibility of sediments and rocks in the upstream drainage basin of a river. The provision of accommodation space is controlled by the rate of eustatic sea-level rise and land subsidence due to tectonics, isostasy and sediment compaction. This research focuses on subsidence due to natural compaction of peat in Holocene fluvial-deltaic settings. Because peat is the most compressible soil type, peat compaction potentially leads to high amounts of subsidence in deltas, thereby creating accommodation space and influencing sedimentation patterns in deltas. Also, subsidence due to peat compaction potentially increases the risk of flooding of deltaic environments, which often are densely populated (close to half a billion people currently live on or near deltas). Furthermore, through its control on sedimentation patterns and by post-depositional distortion of the original stratigraphy, peat compaction likely influences the alluvial architecture of ancient deltaic successions. This is important information for the exploration of natural resources, and for the interpretation of sedimentary archives regarding past changes in the amount of accommodation space.

Despite the potentially large effects of subsidence due to peat compaction on Holocene delta evolution and alluvial architecture, they have never been studied in detail. Therefore, the main objective of this research was to quantify subsidence due to peat compaction in different Holocene fluvial-deltaic settings and to evaluate effects of peat compaction on delta evolution. For this purpose, field research has been carried out in the Cumberland Marshes (CM; Canada), the Rhine-Meuse delta (RM delta; The Netherlands) and the Biebrza National Park (BNP; Poland). Additionally, a new numerical peat compaction model calibrated with an extensive field dataset has been developed.

Methods to quantify peat compaction

Field methods

Two field methods have been used to quantify peat compaction from field settings. The first field method (method 1) relies on the reconstruction of palaeogroundwater tables, which are indicative of former levels of fen peat formation, based on radiocarbon dating of basal peat samples (chapters 2, 4 and 5). The vertical distance between the present-day level of a radiocarbon-dated fen peat sample and its reconstructed initial level of formation is a measure for the amount of subsidence of the peat sample since it was formed. Calculated subsidence is assumed to be caused by compaction of deposits underlying the sampled level and overlying

an incompressible subsurface. This method was used in both the CM and the RM delta. Peat compaction occurring on relatively short timescales of decades to centuries was studied in the CM. This area has experienced minimum human influence, and was recently (~135 years ago) invaded by an avulsion of the Saskatchewan River, which partly covered a Late Holocene fen peat layer with an alluvial sediment layer of up to ~3 m thick. Peat compaction occurring over millennia timescales was studied in the RM delta, for which an extensive field dataset was already available.

The second method is based on measurements of the dry bulk density (ρ_{dry}) and Loss On Ignition (LOI), which is indicative of the organic-matter content, of compacted and uncompacted peat samples (method 2; chapters 2-5). By plotting the LOI versus the dry bulk density of uncompacted samples of a specific type of fen peat, and fitting an exponential regression equation on these data, the initial dry bulk density of a compacted peat sample was estimated based on its LOI. This information was subsequently used to determine the uncompacted thickness of a compacted peat sample, and therewith, the percentage of compaction a sample has experienced since formation (compaction=reduction in thickness/initial thickness·100%). Compacted peat was sampled directly from a 3-cm-wide gouge auger using a 1 cm x 1 cm x 5 cm sampler. Sampling uncompacted surface peat is more difficult, mainly because of the loose and heterogenic character of surface peat, which partly may consist of a living root mat. Therefore, relatively large peat samples should be extracted from field settings while introducing minimum disturbance, which was successfully done by using the new peat sampler that was devised for this purpose (chapter 3).

The second method was also used in both the CM and the RM delta. Because uncompacted surface peat is rare in the largely cultivated RM delta, these samples were partly obtained from the BNP, where peat of the same type as occurs in the subsurface of the RM delta is presently forming. Field data demonstrated that the dry bulk density of surface peat is variable, which is mainly due to variations in plant species composition (e.g., inclusion of wood fragments) and inorganic content. The lowest dry bulk densities occurred at shallowest depths. High-organic uncompacted wood peat obtained from the Biebrza National Park has on average a slightly higher dry bulk density (0.12 g/cm^3) compared to high-organic uncompacted sedge- and reed peat (0.10 g/cm^3) obtained from the same area. This is attributed to the inclusion of relatively large and heavy wood fragments and to the plant species composition of wood peat; a mixture of wood, twigs, leaves, as well as of grass, sedge-, and reed remains results in a slightly lower initial pore volume, because pore spaces are filled with small plant remains, and hence, a higher initial ρ_{dry}. For low-organic fen peat, the inorganic content seems to be a more important factor determining the dry bulk density than the plant species composition.

Peat compaction model

A new numerical peat compaction model has been developed because current compaction models have several shortcomings in that they are inadequate for considering Holocene timescales and the spatial complexity of fluvial-deltaic settings (chapter 6). Most importantly, (1) geotechnical peat parameters are often estimated based on short-duration compression tests and laboratory analysis, and hence, are unreliable at Holocene timescales, (2) the often-used empirical relations are derived from deeply-buried clastic sediments and are therefore likely not applicable to Holocene peat, which occurs at much shallower depths and has significantly

different geotechnical characteristics compared to clastics, and (3) time-dependent compaction is seldom included whereas this is considered to cause substantial amounts of peat compaction.

In the new numerical peat compaction model is the natural strain of peat layers with an initial thickness of 5-10 cm logarithmically related to both the effective stress and time since formation (chapter 6). Natural strain is used because it better describes large compressions as occur in soft soils like peat compared to the more commonly used linear strain. Model parameters were calibrated with an extensive field dataset (100 peat samples) obtained from the CM, and were subsequently used in numerous model analyses. In each model run, two successive situations were considered: (1) a constant rate of base-level rise, where accommodation space created by base-level rise and subsidence due to peat compaction during each timestep, is filled up by increased peat formation or clay deposition, and (2) a constant aggradation rate, in which created accommodation space might not be filled up due to a sediment deficit. During situation 1, a peat and overburden layer is successively formed, after which situation 2 starts for a fixed time period (100 years in this study). The model can be used to estimate past, present and near-future amounts and rates of subsidence due to peat compaction in Holocene deltaic sequences that differ in thickness (in the model determined by the duration of formation) of the peat layer and the overburden (clay), LOI of peat and/or the occurrence of intercalated clay layers.

The amount and rate of peat compaction in deltas

The amount and rate of subsidence due to peat compaction in deltas are highly variable in space and time, mainly depending on the effective stress, thickness of the peat layer, organic-matter content of peat, occurrence of intercalated clay layers, and, to a lesser extent, plant species composition. Peat sequences may accumulate for thousands of years without any significant compaction occurring. Most compaction occurs within decades to a few centuries after a substantial increase of the effective stress, for example caused by deposition of fluvial sediment on top of the peat layer or by groundwater table lowering. In this research, the highest *amounts of subsidence* were measured in the RM delta, which is attributed to the thicker compressible sequences occurring in this delta (up to 3 m subsidence was measured in a 10-m-thick Holocene succession largely composed of peat; chapter 5). In the CM, subsidence due to peat compaction of up to ~0.5 m was measured in ~2 to 3 m thick Holocene successions. Here, 5-cm-thick peat samples have been compacted up to ~50% since the start of overburden deposition that was initiated by the avulsion of the Saskatchewan River approximately 135 years ago. Measured subsidence rates of peat levels, averaged over the same time period, are up to ~6 mm/yr in this area. Slightly higher *compaction percentages* of up to ~60% have been measured in the RM delta, where thicker overburden layers occur and where loading started millennia ago. Millennia-averaged rates measured in the RM delta are an order of magnitude lower compared to those measured in the CM; up to ~0.6 mm/yr. Such rates significantly contribute to long-term basin subsidence rates of up to ~0.3 mm/yr estimated for the Rhine-Meuse delta (chapter 5). The higher rates measured in the CM show that the contribution to basin subsidence rates may temporarily be even higher.

Results of the modeling study showed that subsidence rates, due to peat compaction, in Holocene sequences comprising thick high-organic peat sequences (8 m thick, LOI=0.8) may be as high as 15 mm/yr, occurring within decades to a few centuries after the start of sediment

deposition, or following groundwater table lowering (chapter 6). In the model scenarios, the timestep (accumulation time of one layer) is 50 years, and hence, even higher rates may occur over shorter time periods. In areas where the peat layer is presently loaded by a substantially thick (>~1 m) sediment layer, subsidence rates are low (<~0.2 mm/yr), when compared to current millennia-averaged estimates (up to 5 mm/yr). Sites where the overburden is thin or absent, and the peat sequence is still relatively uncompacted, are however highly susceptible to high amounts of subsidence due to peat compaction. In such areas, peat compaction may significantly enhance the risk of flooding, thereby threatening people living in those areas.

Effect of peat compaction on delta evolution

Local scale effects

The formation of natural levees or crevasse splays on top of a peat layer causes locally high peat compaction rates. If the sediment supply of the river is sufficiently high, accommodation space created by peat compaction enhances the formation of thick natural levees (or crevasse splays). An important question related to the formation of natural levees, is whether differential peat compaction in a floodplain influences cross-valley gradients. Besides factors such as substrate erodibility, log-, ice- and beaver dams, cross-valley gradient is considered to be one of the main driving factors of avulsion, which is one of the most important processes influencing delta evolution. This research demonstrates that peat compaction initially does not stimulate the occurrence of avulsion. Subsidence due to peat compaction beneath natural levees reduces rather than increases cross-valley gradients. Also, in most situations accommodation space created by peat compaction in floodbasins will be filled by increased sediment deposition or peat formation, which impedes the development of increased cross-valley gradients. Furthermore, in general, regional gradients are low in peatlands, which inhibits a crevasse splay to evolve into an avulsion, as is usually the mechanism of avulsion initiation. Only if the maximum peat compaction potential at a certain location has been reached, while at a nearby location on the floodplain rates of subsidence due to peat compaction are still relatively high, differential peat compaction may lead to gradient advantages. This may subsequently affect spatial sedimentation patterns on a floodplain.

Regional scale effects

Accommodation space in deltaic environments with low sediment input may be temporarily filled with peat, provided that peat formation can keep up with the rate of creation of accommodation space. Groundwater table lowering or deposition of fluvial sediments on top of the peat layer, for example following an upstream avulsion, impedes peat formation and induces subsidence due to peat compaction, thereby revitalizing existing accommodation space for increased fluvial deposition and/or peat formation. In this way, compaction-induced accommodation space increases the sediment trap efficiency, by which thick fluvial sediment layers may develop and delta propagation may be slowed down (chapter 5). In the RM delta, this mechanism of filling and refilling of accommodation space on regional scales occurred when thick peat layers, mainly formed between 6000 and 3000 cal years ago, were subsequently compacted which made existing accommodation space available once again for continued peat formation and/or fluvial sedimentation. Field data from this area demonstrated that locally up

to 40% of total Holocene accommodation space has been (re)created by subsidence due to peat compaction. Similarly, in the CM accommodation space initially filled by peat was later refilled by alluvial sediments that were deposited following the 1870s avulsion of the Saskatchewan River.

Alluvial architecture
Differential peat compaction may significantly distort the original stratigraphy, and therewith influences the ultimate alluvial architecture of deltaic sequences containing peat. For example, peat compaction beneath channels stimulates vertical aggradation, which leads to the formation of channel belts with a low width/depth ratio. On the other hand, if an incising channel encounters a relatively thin peat layer intercalated between clastic sediment layers, the erosion resistant peat will initially prevent further down-cutting, which stimulates the development of channels with high width/depth ratios. Based on both this research and studies on ancient coal-bearing strata, it was concluded that most peat compaction occurs shortly after loading nearby the surface, and hence, that compaction involved with the transformation of peat into coal is minimal.

Human-induced peat compaction
Many deltas are densely populated, and consequently suffer from human pressures that increase the risk of delta flooding. In this context, important human influences are subsidence due to exploration of natural resources, reduced sediment supply by upstream damming and river embankments, and subsidence due to peat compaction and oxidation following artificial groundwater table lowering for land reclamation. Last-mentioned aspect may cause subsidence rates on the order of a few cm/yr. Modeling results demonstrated that especially thick high-organic peat layers that have experienced little compaction are susceptible to high amounts of subsidence following a groundwater table drop (chapter 6). Such areas especially occur in distal parts of deltas.

Future research

Most important future research topics arising from the results of this research are: (1) the compressibility of different peat types, (2) the effect of natural and artificial groundwater table fluctuations on peat formation and compaction, (3) extension of the peat compaction model to include e.g., peat oxidation, bog formation and peat erosion, (4) the effect of peat compaction on topographic slopes regarding its effect on avulsion, and (5) incorporation of the new peat compaction model into alluvial architecture models.

Samenvatting

Veencompactie in delta's
Implicaties voor holocene delta-ontwikkeling

Kader

De vorming en ontwikkeling van delta's wordt grotendeels bepaald door sedimentaanvoer en het creëren van accommodatieruimte. De sedimentaanvoer wordt bepaald door processen die het debiet en de sedimentlast van een rivier beïnvloeden, zoals het klimaat, menselijk ingrijpen en de erodibiliteit van sedimenten en gesteenten in het bovenstroomse deel van het stroomgebied van een rivier. Het creëren van accommodatieruimte wordt bepaald door de snelheid van eustatische zeespiegelstijging en bodemdaling door tektoniek, isostasie en compactie van sedimenten. Dit onderzoek richt zich op bodemdaling als gevolg van de natuurlijke compactie van veen in het fluviatiele deel van holocene deltagebieden. Omdat veen vergeleken met sedimenten zoals klei, silt en zand zeer compacteerbaar is, kan veencompactie potentieel tot grote bodemdalingen leiden. Daarnaast creëert veencompactie accommodatieruimte voor sedimentatie, waardoor het sedimentatiepatronen in delta's kan beïnvloeden. Tevens kan bodemdaling door veencompactie leiden tot verhoogde overstromingsrisico's in deltagebieden, welke vaak dichtbevolkt zijn. Wereldwijd leven bijna een half biljoen mensen in deltagebieden. Doordat veencompactie sedimentatiepatronen beïnvloedt, en de oorspronkelijke stratigrafie verstoort, heeft veencompactie ook invloed op de alluviale architectuur van deltasequenties. Hoe veencompactie de opbouw van deltasequenties beïnvloedt is belangrijke informatie voor het winnen van natuurlijke hulpbronnen, en voor het interpreteren van deltasequenties met betrekking tot vroegere veranderingen in de hoeveelheid beschikbare accommodatieruimte.

Ondanks dat bodemdaling door veencompactie potentieel veel invloed heeft op holocene delta-ontwikkeling en de alluviale architectuur, is het nog nooit in detail onderzocht. Daarom is het hoofddoel van dit promotieonderzoek het kwantificeren van bodemdaling door veencompactie in het fluviatiele deel van holocene deltagebieden, en het evalueren van effecten van veencompactie op de ruimtelijke en temporele ontwikkeling van delta's. Om dit doel te bereiken is veldonderzoek gedaan in de Cumberland Marshes (CM; Canada), de Rijn-Maas delta (RM delta; Nederland) en in het Biebrza National Park (BNP; Polen). Tevens is er een numeriek veencompactiemodel ontwikkeld, welke is gekalibreerd met velddata.

Methoden om veencompactie te kwantificeren

Veldmethoden
Er zijn twee veldmethoden gebruikt om veencompactie te kwantificeren. De eerste methode (methode 1) is gebaseerd op het reconstrueren van vroegere grondwaterspiegels. Aangezien laagveen ongeveer op hetzelfde niveau als de gemiddelde grondwaterspiegel vormt, kunnen gereconstrueerde holocene grondwaterspiegels gebruikt worden als indicatie voor oude niveaus van laagveenvorming. De vroegere grondwaterspiegels zijn gereconstrueerd op basis

van koolstofdateringen van basisveenmonsters, welke direct boven een niet-compacteerbaar oppervlak zijn genomen en dus minimale zakking door compactie hebben ondervonden (hoofdstukken 2, 4 en 5). De verticale afstand tussen het huidige niveau van een gedateerd veenmonster, en het bijbehorende gereconstrueerde initiële niveau waarop het veenmonster gevormd is, wordt gebruikt als maat voor de hoeveelheid zakking van het veenmonster sinds het gevormd is. Hierbij is aangenomen dat de berekende hoeveelheid zakking is veroorzaakt door compactie van afzettingen die tussen het veenmonster en een dieper liggend niet-compacteerbaar oppervlak liggen. Deze methode is in zowel de CM als in de RM delta gebruikt. Veencompactie op tijdschalen van decennia tot eeuwen is bestudeerd in de CM. Dit gebied is nauwelijks door menselijk ingrijpen beïnvloed. Een recente avulsie, een rivierverlegging waarbij een nieuwe loop ontstaat, van de Saskatchewan Rivier (~135 jaar geleden) heeft ervoor gezorgd dat deze rivier het studiegebied is binnengedrongen, waardoor een laat-holocene veenlaag bedekt is geraakt met een alluviale sedimentlaag met een maximale dikte van ~3 m. Veencompactie op tijdschalen van millennia is bestudeerd in de RM delta, waarvoor een uitgebreide dataset met veldgegevens al beschikbaar was bij aanvang van dit onderzoek.

De tweede methode is gebaseerd op metingen van de droge dichtheid (ρ_{droog}) en het organische stofgehalte (LOI; Loss On Ignition) van gecompacteerd en ongecompacteerd veen (methode 2; hoofdstukken 2-5). Door de LOI en de droge dichtheid van ongecompacteerd veen tegen elkaar uit te zetten, en deze data te fitten met een exponentiële regressievergelijking, kan de initiële droge dichtheid van gecompacteerd veen worden geschat op basis van de LOI. Hiermee kan vervolgens de initiële dikte van een gecompacteerd veenmonster worden berekend, en daarmee, het percentage compactie van het veenmonster sinds het is gevormd (compactie=afname van de dikte/initiële dikte·100%). Gecompacteerd veen is in het veld bemonsterd met behulp van een bemonsteringsapparaat met afmetingen van 1 x 1 x 5 cm, direct vanuit een veenkern die is gestoken met een guts (diameter van 3 cm). Het bemonsteren van ongecompacteerd veen is lastiger, vooral omdat het zeer los is en een heterogene structuur heeft. Om een representatieve waarde voor de droge dichtheid van zulk veen te verkrijgen, is het noodzakelijk om veenmonsters met een relatief groot volume te nemen waarbij de structuur van het monster minimaal wordt verstoord. Dit is gedaan met behulp van een veenbemonsteringsapparaat dat speciaal voor dit onderzoek is ontwikkeld (hoofdstuk 3).

De tweede methode is ook in zowel de CM als in de RM delta toegepast. Omdat ongecompacteerd veen zeldzaam is in de RM delta, is dit deels in het BNP bemonsterd. In dit gebied worden momenteel dezelfde veensoorten gevormd als die voorkomen in de holocene sequentie van de RM delta. Veldgegevens laten zien dat de droge dichtheid van ongecompacteerd veen variabel is, wat met name veroorzaakt wordt door variaties in de plantensamenstelling en de klastische component. De laagste droge dichtheden zijn gemeten in de meest ondiep gelegen veenlagen. In het BNP heeft hoogorganisch ongecompacteerd bosveen gemiddeld genomen een hogere droge dichtheid (0.12 g/cm^3) dan hoogorganisch ongecompacteerd zegge- en rietveen (0.10 g/cm^3). Dit is verklaard door het voorkomen van relatief grote en zware houtfragmenten en door de plantensamenstelling van bosveen. Deze veensoort bestaat uit een mengsel van hout, takken, bladeren, wortels, maar ook gras-, zegge- en rietrestanten. Deze heterogene samenstelling zorgt ervoor dat relatief grote poriën worden opgevuld met kleinere plantenresten, waardoor het initiële poriënvolume relatief laag, en de ρ_{dry} wat hoger is. Voor laagorganisch laagveen lijkt het klastische sedimentgehalte belangrijker te zijn bij de bepaling van de droge dichtheid dan de plantensamenstelling.

Veencompactiemodel

Een nieuw numeriek veencompactiemodel is ontwikkeld omdat bestaande compactiemodellen niet geschikt zijn voor het modelleren van veencompactie op holocene tijdschaal in ruimtelijk complexe deltasequenties (hoofdstuk 6). De meest belangrijke tekortkomingen van bestaande modellen zijn: (1) geotechnische parameters van veen worden vaak geschat op basis van kortdurende samendrukkingproeven en andere laboratoriumtesten, en zijn daarom onbetrouwbaar op holocene tijdschaal, (2) veel gebruikte empirische relaties zijn gebaseerd op data van diep begraven klastische sedimenten en zijn daarom waarschijnlijk niet toepasbaar op holoceen veen, dat op veel minder grote diepte voorkomt en duidelijk andere geotechnische eigenschappen heeft dan klastische sedimenten, en (3) tijdsafhankelijke veencompactie wordt zelden meegenomen terwijl wordt aangenomen dat dit een substantieel deel van de totale hoeveelheid veencompactie veroorzaakt.

In het nieuwe veencompactiemodel is de natuurlijke rek (vervorming) van veenlagen, met een initiële dikte van 5 tot 10 cm, logaritmisch gerelateerd met de effectieve spanning en de tijd sinds veenvorming (hoofdstuk 6). Er is gebruik gemaakt van natuurlijk rek omdat dit beter grote samendrukkingen beschrijft, zoals die voorkomen in slappe gronden als veen, dan lineaire rek. Dit laatste is tot nog toe meestal gebruikt in compactiemodellen. Modelparameters zijn gekalibreerd met een grote dataset (100 veenmonsters) bestaande uit veldgegevens die verzameld zijn in de CM, en zijn vervolgens gebruikt in modelanalyses. In elke modelrun zijn twee opeenvolgende situaties aangenomen: (1) een constante stijging van de erosiebasis, waarbij accommodatieruimte, dat tijdens elke tijdstap gecreëerd wordt door de stijging van de erosiebasis en bodemdaling door veencompactie, opgevuld wordt door veenvorming of kleisedimentatie, en (2) een constante aggradatiesnelheid, waarbij gecreëerde accommodatieruimte mogelijk niet helemaal wordt opgevuld, bijvoorbeeld indien er een sedimenttekort is. Gedurende situatie 1 wordt er opeenvolgend een veenlaag en een overliggend kleipakket gevormd. Hierna start situatie 2 voor een bepaalde tijd (100 jaar in dit onderzoek). Het model kan worden gebruikt om vroegere, huidige en toekomstige hoeveelheden en snelheden van bodemdaling door veencompactie in holocene deltasequenties te schatten. Deze sequenties kunnen verschillen in dikte (in het model bepaald door de duur van opbouw) van zowel het veen- als het bovenliggende kleipakket, de LOI van het veen en/of het voorkomen van dunne kleilaagjes binnen het veenpakket.

De hoeveelheid en snelheid van veencompactie in delta's

De hoeveelheid en snelheid van bodemdaling door veencompactie in delta's is zeer variabel in ruimte en tijd. Het is vooral afhankelijk van de effectieve spanning, de dikte van de veenlaag, het organische stofgehalte van het veen, het voorkomen van dunne veenlaagjes binnen het veenpakket, en, in mindere mate, de plantensamenstelling. Veenpakketten kunnen gedurende duizenden jaren accumuleren terwijl er minimale compactie optreedt. De meeste compactie treedt op binnen decennia tot enkele eeuwen na een substantiële verhoging van de effectieve spanning. Dit kan bijvoorbeeld worden veroorzaakt door sedimentatie van fluviatiele sedimenten bovenop de veenlaag, of door grondwaterstandverlaging. In dit onderzoek zijn de grootste bodemdalingen door veencompactie in de RM delta gemeten: tot ~3 m zakking in een 10 m dikke holocene sequentie die hoofdzakelijk uit veen bestaat. In de CM is bodemdaling

door veencompactie van maximaal ~0.5 m gemeten in 2 tot 3 m dikke holocene sequenties. De grotere zakkingen die zijn gemeten in de RM delta kunnen worden verklaard door de relatief dikke holocene sequentie, en veenlagen, in dit gebied. In de CM zijn de 5 cm dikke veenmonsters tot ~50% gecompacteerd sinds belasting van het veenpakket als gevolg van een toename van fluviatiele sedimentatie door de avulsie van Saskatchewan Rivier 135 jaar geleden. Dalingssnelheden (gemiddeld over 135 jaar) van niveaus binnen het veenpakket van maximaal ~6 mm/j zijn gemeten. In de RM delta zijn iets hogere compactiepercentages gemeten, van maximaal ~60%. Dit kan worden verklaard door het voorkomen van dikkere klastische pakketten op veenlagen, en doordat belasting van veenlagen soms al duizenden jaren geleden begon. Gemeten dalingssnelheden, gemiddeld over millennia, zijn in de RM delta een orde grootte lager dan in de CM: tot ~0.6 mm/j. Deze waarden dragen significant bij aan de dalingssnelheid van het Noordzeebekken (geschatte waarde van tot ~0.3 mm/j in de RM delta; hoofdstuk 5). De hogere snelheden die zijn gemeten in de CM laten zien dat de relatieve bijdrage van daling door veencompactie ten opzichte van daling van een bekken tijdelijk nog hoger kan zijn.

Resultaten van de modelstudie laten zien dat de snelheid van bodemdaling door veencompactie tot 15 mm/j kan zijn. Zulke waarden komen voor in dikke hoogorganische veenpakketten (8 m dik, LOI=0.8), decennia tot enkele eeuwen na het begin van klastische sedimentatie bovenop het veenpakket, of na grondwaterstandverlaging (hoofdstuk 6). Aangezien in de modelruns de tijdstap (accumulatietijd van een laagje) 50 jaar is, kunnen er nog hogere snelheden in kortere tijdsperioden voorkomen. Het model voorspelt dat in gebieden waar de veenlaag momenteel belast is door een voldoende dik klastisch pakket (>~1 m) dat er tenminste al enkele eeuwen op ligt, de bodemdalingsnelheid laag is (<~0.2 mm/j) vergeleken met huidige schattingen (tot 5 mm/j; gemiddeld over millennia). Gebieden waar het bovenliggende klastische pakket dun of afwezig is, en dus het veen nog relatief ongecompacteerd is, zijn echter nog zeer gevoelig voor grote bodemdalingen als gevolg van veencompactie. In deze gebieden kan veencompactie het overstromingsrisico significant verhogen, en vormt daarbij een bedreiging voor mensen die in deze gebieden leven.

Effecten van veencompactie op delta-ontwikkeling

Lokale effecten

De vorming van oeverwallen of crevasses bovenop een veenlaag veroorzaakt lokaal hoge veencompactiesnelheden. Indien de sedimentaanvoer van de rivier voldoende hoog is, wordt de accommodatieruimte die gecreëerd is door veencompactie opgevuld met sediment, waardoor er dikke oeverwallen (of crevasses) ontstaan. Een belangrijke vraag gerelateerd aan de vorming van oeverwallen, is of differentiële veencompactie gradiënten dwars op de riviergradiënt beïnvloedt. Naast factoren zoals de erodibiliteit van de ondergrond en boomstam-, ijs- en beverdammen, wordt deze gradiënt gezien als één van de belangrijkste factoren die avulsies veroorzaken. Avulsie is een van de meest belangrijke processen die de opbouw van een delta bepalen. Dit onderzoek laat zien dat veencompactie in eerste instantie het optreden van avulsies niet stimuleert. Bodemdaling door compactie van veen onder een oeverwal zal de gradiënt dwars op de riviergradiënt eerder kleiner dan groter maken. Bovendien zal in de meeste situaties de accommodatieruimte, gecreëerd door veencompactie, worden opgevuld door fluviatiele sedimentatie of veenvorming. Verder zijn in veengebieden regionale terreingradiënten meestal

laag. Hierdoor zullen crevasses minder snel uitgroeien tot een avulsie, wat normaal gesproken juist vaak voor komt. Alleen als het maximale veencompactiepotentiaal is bereikt in een gebied, terwijl in een nabijgelegen gebied in de delta bodemdaling door veencompactie nog relatief hoog is, kan differentiële veencompactie tot een gradiëntvoordeel leiden. Dit kan vervolgens het ruimtelijke sedimentatiepatroon in een delta beïnvloeden.

Regionale effecten
Accommodatieruimte in deltagebieden met een lage sedimentaanvoer kan tijdelijk door veen worden opgevuld, mits veenvorming de snelheid waarmee accommodatieruimte wordt gecreëerd kan bijhouden. Grondwaterstandverlaging of fluviatiele sedimentatie bovenop een veenpakket, bijvoorbeeld als gevolg van een bovenstroomse avulsie, zal veenvorming tegengaan en veencompactie veroorzaken, waardoor hernieuwde accommodatieruimte voor fluviatiele sedimentatie wordt gecreëerd. Op deze manier wordt fluviatiel sediment effectief ingevangen in delta's met veel veen, waardoor er dikke fluviatiele sedimentlagen kunnen ontstaan, en delta-uitbouw kan worden afgeremd (hoofdstuk 5). Dit mechanisme van het opvullen van accommodatieruimte door veen, en het hernieuwd opvullen van accommodatieruimte door veen en/of fluviatiele sedimenten is ook in de RM delta opgetreden. Dikke veenlagen, welke voornamelijk tussen 6000 en 3000 jaar geleden gevormd zijn, zijn na vorming gecompacteerd waardoor accommodatieruimte opnieuw beschikbaar werd gesteld voor veenvorming en/of fluviatiele sedimentatie. Veldgegevens laten zien dat lokaal tot 40% van de totale holocene accommodatieruimte door veencompactie is gecreëerd. Op gelijke wijze is accommodatieruimte in de CM in eerste instantie door veenvorming opgevuld, en na de avulsie van de Saskatchewan Rivier door fluviatiele sedimenten.

Alluviale architectuur
Differentiële veencompactie kan de initiële stratigrafie aanzienlijk verstoren, en daarmee de uiteindelijke alluviale architectuur van deltasequenties sterk beïnvloeden. Veencompactie onder beddingafzettingen kan bijvoorbeeld verticale aggradatie stimuleren, wat resulteert in de vorming van rivierbeddingen met een lage breedte/diepte verhouding. Echter, wanneer een insnijdende rivier een veenlaag tussen klastische sedimentlagen tegenkomt, zal de veenlaag, die relatief resistent is tegen erosie, verdere insnijding in eerste instantie tegengaan, en zal de laterale accretie toenemen waardoor rivierbeddingen met een relatief hoge breedte/diepte verhouding ontstaan. Gebaseerd op resultaten van dit onderzoek en op studies gericht op oude deltasequenties met steenkool, is er geconcludeerd dat de meeste veencompactie relatief kort na belasting van de veenlaag optreedt, relatief dicht onder het oppervlak, en dat de compactie tijdens de omzetting van veen naar steenkool minimaal is.

Veencompactie als gevolg van menselijk ingrijpen
Veel delta's zijn dichtbevolkt, waardoor deze gebieden onderhevig zijn aan menselijke invloeden die het overstromingsrisico vergroten. Voorbeelden van menselijke invloeden zijn winning van natuurlijke hulpbronnen, verminderde sedimentaanvoer door het bouwen van stuwdammen en dijken, en bodemdaling door veencompactie en -oxidatie als gevolg van grondwaterstandverlaging in polders. Dit laatste kan bodemdaling in de orde grootte van een aantal cm/j veroorzaken. Modelresultaten laten zien dat met name dikke hoogorganische veenpakketten, welke nog weinig gecompacteerd zijn, het meest gevoelig zijn voor bodemdaling

als gevolg van grondwaterstandverlaging (hoofdstuk 6). Dit soort gebieden komt vooral voor in het distale deel van delta's.

Toekomstig onderzoek

De belangrijkste onderwerpen voor toekomstig onderzoek die voortkomen uit dit promotieonderzoek zijn: (1) de compressibiliteit van verschillende veensoorten, (2) het effect van natuurlijke en artificiële grondwaterstandfluctuaties op veenvorming en -compactie, bijvoorbeeld als gevolg van avulsies of klimaatverandering (3) uitbreiding van het veencompactiemodel zodat het onder andere veenoxidatie, hoogveenvorming en veenerosie meeneemt, (4) het effect van veencompactie op terreingradiënten met betrekking tot de invloed op avulsies, en (5) het opnemen van het veencompactiemodel in 3D alluviale architectuurmodellen.

About the author

Sanneke van Asselen was born on the 1st of November 1979 in Vinkeveen, The Netherlands. She attended primary school in Vinkeveen (*Sint Jozefschool*) and secondary school in Uithoorn (*Alkwin Kollege*). After studying Physical Geography at the University of Amsterdam (1998-2003), she worked two years for a European project on soil conservation and protection. After that, she started with the PhD research described in this thesis.

More interesting is to talk about on her hometown Vinkeveen. Maybe it was destiny for her to start this research on peat compaction in deltas; for non-Dutch-speaking people, '*veen*' is the Dutch word for peat. Many jokes have been made about the fact she was born in this village in the distal part of the Rhine-Meuse delta, 25 km south of Amsterdam, and about the Vinkeveen dialect she apparently speaks now and then. In response to that a small tribute to this lovely village seems in place.

Since approximately 5000 years ago, extensive peat formation occurred in his part of the Rhine-Meuse delta, resulting in thick peat layers. Vinkeveen is presently part of the council '*De Ronde Venen*', which translates into 'The Round Peatlands'. Around 1000 A.D., a large raised bog existed in this area, which was bordered by peatland forests. Small rivers flowed in a circular around the peatland, which explains the present name of the council. From about that time, land reclamation started. People dug drainage canals perpendicular to the peatland rivers, using the clayey natural levees as a solid basis. About 3 to 4 kilometers from these levees, a dike was constructed that enclosed the most inner part of the peatland. Villages were built on this dike, which is now called the 'inner ring' ('*binnenring*' in Dutch).

Local inhabitants have always used peat for fuel, and initially used reclaimed peatland for agriculture. In the 14th and 15th centuries, the most important crops (for trade) were flax (*Linum usitatisimum*; '*vlas*' in Dutch), hemp (*Cannabis sativa*; '*hennep*' in Dutch; used for rope and sails) and rapeseed (*Brassica napus*; '*koolzaad*' in Dutch). Because subsidence due to peat compaction and oxidation resulted in too wet conditions, farmers shifted to cattle-breeding (grassland). In 1413, a canal ('*Bijleveld*') was dug straight across the reclaimed peatland area. This canal was originally dug to drain excess water, but was also very important for shipping traffic going from the Rhine to Amsterdam.

Large-scale peat exploitation started in the 17th century, when the demand from Amsterdam and Utrecht increased enormously. Peat was extracted from below the groundwater table and was spread out and tamped down on small elongated field in between the canals. Here, the peat could dry, after which it was cut in blocks ('*turf*'). Because the fields used for drying were often too small (people ignored regulations), they were easily destroyed by waves. Consequently, the agricultural landscape was replaced by lakes. Because valuable agricultural land was destroyed and the water threatened areas where the people lived, artificial drainage started in the 18th century. Windmills and steam pumping-stations were used to reclaim the lakes. Five former lakes were successively drained, which was not an easy task. It took almost 60 years to drain the first lake!

At present, the deepest (central) part of '*De Ronde Venen*' (~1 km west of Vinkeveen) is elevated ~6 m below mean sea level (msl). The surface of the raised bog that existed before people invaded the area was elevated ~4 m above msl. Thus, at this location the surface has been lowered with ~10 m! Peatlands that were reclaimed for agriculture, but where lakes did not develop, are presently elevated ~1.5 m below msl; the surface has been lowered due to peat compaction and oxidation. At present, these areas are mainly used as grassland and are called, ironically, 'upper land' ('*bovenland*'). Northwest of Vinkeveen large lakes still exist ('*Vinkeveense Plassen*'). Because sand has been extracted from the bottom of these lakes they are at present locally ~50 m deep. The lakes offer great opportunities for sailing, surfing and swimming in summer, and skating in winter. Rare flora and fauna are found in the swampy nature reserve the '*Botshol*', located north of the lakes.

There is a lot more is to tell about Vinkeveen and surroundings, but then this section will get too long. Therefore, the story will end here, but not without showing an old photograph of the 'main' street of Vinkeveen, with the grocery shop that was set up by the great-grandfather of Sanneke at the right side of the street, left of the white house with the lady standing in front of. The picture was taken in ~1910, and is signed by L. van Asselen; the great-grandfather of Sanneke.

References

Abidin, H.Z., Djaja, R., Darmawan, D., Hadi, S., Akbar, A., Rajiyowiryono, H., Sudibyo, Y., Meilano, I., Kasuma, M.A., Kahar, J. and Subarya, C., 2001. Land subsidence of Jakarta (Indonesia) and its geodetic monitoring system. Natural Hazards 23, 365-387.

Allen, J.R.L., 1978. Studies in fluviatile sedimentation: an exploratory quantitative model for the architecture of avulsion-controlled alluvial suites. Sedimentary Geology 21, 129-147.

Allen, J.R.L., 1999. Geological impacts on coastal wetland landscapes: some general effects of sediment autocompaction in the Holocene of northwest Europe. The Holocene 9, 1-12.

Allen, J.R.L., 2000. Holocene coastal lowlands in NW Europe: autocompaction and the uncertain ground. In: Pye, K, Allen, J.R. (eds.) Coastal and Estuarine Environments: sedimentology, geomorphology and geoarchaeology. Geological Society of London, Special Publications, 175, 239-252.

Amorosi, A. and Milli, S., 2001. Late Quaternary depositional architecture of Po and Tevere river deltas (Italy) and worldwide comparison with coeval deltaic successions. Sedimentary Geology 144, 357-375.

Anderson, S., 1991. Differential compaction in alluvial sediments. Unpublished PhD thesis, University of Wales, Cardiff, Wales.

Aslan, A., Autin, W.J. and Blum, M.D., 2005. Causes of river avulsion: insights from the Late Holocene avulsion history of the Mississippi River, U.S.A., Journal of Sedimentary Research 75, 648-662.

Audet, D.M., 1996. Compaction and overpressuring in Pleistocene sediments on the Louisiana Shelf, Gulf of Mexico. Marine and Petroleum Geology 13, 467-474.

Baldwin, B., 1971. Ways of deciphering compacted sediments. Journal of Sedimentary Petrology 41, 293-301.

Baldwin, B. and Butler, C.O., 1985. Compaction curves: American Association of Petroleum Geologists Bulletin 69, 622-626.

Berendsen, H.J.A., 1982 (in Dutch). De genese van het landschap in het zuiden van de provincie Utrecht: een fysisch-geografische studie. Ph.D. Thesis, Utrecht University, Utrecht, The Netherlands, Utrechtse Geografische Studies 10, p. 256.

Berendsen, H.J.A. and Stouthamer, E., 2001. Palaeogeographic Development of the Rhine-Meuse Delta, The Netherlands. Koninklijke Van Gorcum, Assen, The Netherlands.

Berendsen, H.J.A., 2000 (in Dutch). Landschap in delen. Overzicht van de geofactoren. Fysische geografie van Nederland, 2nd edition. Van Gorcum, Assen, The Netherlands.

Berendsen, H.J.A., 2005 (in Dutch). Landschappelijk Nederland. De fysisch-geografische regio's. Fysische Geografie van Nederland. 3rd edition. Van Gorcum, Assen, The Netherlands.

Berendsen, H.J.A. and Vollenberg, K.P., 2007. New prospects in geomorphological and geological mapping of the Rhine-Meuse Delta – Application of detailed digital elevation maps based on laser altimetry. Netherlands Journal of Geosciences 86, 15-22.

Berendsen, H.J.A., Makaske, B., Van de Plassche, O., Van Ree, M.H.M., Das, S., Van Dongen, M., Ploumen, S. and Schoenmakers, W., 2007. New groundwater-level rise data from the Rhine-Meuse delta – implications for the reconstruction of Holocene relative mean sea-level rise and differential land-level movements. Netherlands Journal of Geosciences 86, 333-354.

Beuving, J. and van den Akker, J.J.H., 1996 (in Dutch). Maaiveldsdaling van veengrasland bij twee slootpeilen in de polder Zegvelderbroek. Vijfentwintig jaar zakkingsmetingen op het ROC Zegveld. DLO-Staring Centrum, Wageningen, Rapport 377.

Bindoff, N.L., Willebrand, J., Artale, V., Cazenave, A., Gregory, J., Gulev, S., Hanawa, K., Le Quéré, C., Levitus, S., Nojiri, Y., Shum, C.K., Talley L.D. and Unnikrishnan, A., 2007. Observations: Oceanic Climate Change and Sea Level. In: Solomon, S., Qin, D., Manning, M., Chen, Z., Marquis, M., Averyt, K.B., Tignor, M. and Miller, H.L. (eds.) Climate Change 2007: The Physical Science Basis. Contribution of Working Group I to the Fourth Assessment Report of the Intergovernmental Panel on Climate Change. Cambridge University Press, Cambridge, United Kingdom and New York, NY, USA.

Bird, M.I., Fifield, L.K., Chua, S. and Goh, B., 2004. Calculating sediment compaction for radiocarbon dating of intertidal sediments. Radiocarbon 46, 421-435.

Birks, H.J.B. and Birks, H.H., 1980. Quaternary Palaeoecology. The Blackburn Press, Caldwell, New Jersey.

Bjerrum, L., 1967. Engineering geology of Norwegian normally-consolidated marine clays as related to settlements of buildings. Geotechnique 17, 81-118.

Bloom, A.L., 1964. Peat accumulation and compaction in a Connecticut coastal marsh. Journal of Sedimentary Petrology 34, 599 – 603.

Blum, M.D. and Roberts, H.H., 2009. Drowning of the Mississippi Delta due to insufficient sediment supply and global sea-level rise. Nature Geoscience 2, 488-491.

Boussinesq, J., 1885. Application des potentiels à l'étude de l'e´quilibre et du mouvement des solides élastiques. Gauthier-Villars, Paris, 30 pp.

Boumans, R. and Day, J.W. Jr., 1993. High precision measurements of sediment elevation in shallow coastal areas using a sedimentation-erosion table. Estuaries 16, 375-380.

Bosch, J.H.A. and Kok, H., 1994. Toelichtingen bij de geologische kaart van Nederland 1: 50.000. Blad Gorinchem (Gorkum) West (38W). Haarlem: Rijks Geologische Dienst.

Brandyk, T., Szatylowicz, J., Oleszczuk, R. and Gnatowski, T., 2002. Water-related physical attributes of organic soils. In: Parent, L.E. and Ilnicki, P. (eds.) Organic soils and peat materials for sustainable agriculture. CRC Press LLC, US.

Bridge, J.S. and Leeder, M.R., 1979. A simulation model of alluvial stratigraphy. Sedimentology 26, 617-644.

Bronk Ramsey, C., 2001. Development of the radiocarbon calibration program OxCal. Radiocarbon 43, 355-363.

Bronk Ramsey, C., 2008. Deposition models for chronological records. Quaternary Science Reviews 27, 42-60.

Buisman, A.S.K., 1940. Grondmechanica. 294 p. Reprinted by Balkema, 1996.

Buttler, A., Grosvernier, P. and Matthey, Y., 1998. A new sampler for extracting undisturbed surface peat cores for growth pot experiments. New Phytologist 140, 155-160.

Cahoon, D.R., Reed, D.J. and Day, J.J.W., 1995. Estimating shallow subsidence in microtidal salt marshes of the southeastern United States: Kaye and Barghoon revisited. Marine Geology 128, 1-9.

Cahoon, D.R., Marin, P.E., Black, B.K. and Lynch, J.C., 2000. A method for measuring vertical accretion, elevation, and compaction of soft, shallow-water sediments. Journal of Sedimentary Research 70, 1250-1253.

Cazenave, A., Lombard, A. and Llovel, W., 2008. Present-day sea level rise: A synthesis. CR Geoscience. 340, 761-770.

Charman, D.J., 2002. Peatland systems and environmental change. John Wiley & Sons, Chichester, p. 301.

Chen, C., Pei, S. and Jiao, J.J., 2003. Land subsidence caused by groundwater exploitation in Suzhou City, China. Hydrogeology Journal 11, 275-287.

Clari, P.A. and Martire, L., 1996. Interplay of cementation, mechanical compaction, and chemical compaction in nodular limestones of the Rosso Ammonitico Veronese (Middle-upper Jurassic, northeastern Italy). Journal of Sedimentary Research 66, 447-458.

Clymo, R.S., 1988. A high-resolution sampler of surface peat. Functional Ecology 2, 425-431.

Cohen, K.M., 2003. Differential subsidence within a coastal prism: late-Glacial – Holocene tectonics in The Rhine-Meuse delta, The Netherlands. PhD Thesis, Utrecht University. Netherlands Geographical Studies 316.

Cohen, K.M., 2005. 3D Geostatistical interpolation and geological interpretation of paleo-groundwater rise in the Holocene coastal prism in the Netherlands. In: Giosan, L. and Battacharya, J.P. (eds.) River Deltas – Concepts, models, and examples, SEPM Special Publication 83, 341-364.

Craig, R.F., 1987. Soil Mechanics. Fourth Edition. Van Nostrand Reinhold (International).

Cuttle, S.P. and Malcolm, C., 1979. A corer for taking undisturbed peat samples. Plant and Soil, 51, 297-300.

Davies, R., Diessel, C., Howell, J., Flint, S. and Boyd, R., 2005. Vertical and lateral variation in the petrography of the Upper Cretaceous Sunnyside coal of eastern Utah, USA – implications for the recognition of high-resolution accommodation changes in paralic coal seams. International Journal of coal Geology 61, 13-33.

Davies-Vollum, K.S. and Smith, N.D., 2008. Factors affecting the accumulation of organic-rich deposits in a modern avulsive floodplain: examples from the Cumberland Marshes, Saskatchewan, Canada. Journal of Sedimentary Research 78, 683-692.

Day, J.W. and Giosan, L., 2008. Survive or subside? Nature Geoscience 1, 156-157.

De Bakker, H. and Schelling, J., 1966 (in Dutch). Systeem van Bodemclassificatie voor Nederland. Wageningen, The Netherlands, Pudoc, p. 217.

De Groot, T.A.M. and De Gans, W., 1996. Facies variations and sea-level-rise response in the lowermost Rhine-Meuse area during the last 15000 years (The Netherlands) Mededelingen Rijks Geologische Dienst 57, 229-250.

Den Haan, E.J., 1994. Vertical compression of soils. Delft University, PhD Thesis, Delft, The Netherlands.

Den Haan, E.J., 2003 (in Dutch). Het a,b,c-isotachenmodel: Hoeksteen van een nieuwe aanpak van zettingsberekeningen. Geotechniek, oktober 2003, 28-35.

Den Haan, E.J., 2008 (in Dutch). De intrinsieke tijd in het Isotachenmodel. Geotechniek jan, 32-36.

Den Haan, E.J. and Edil, T.B., 1993. Secondary and tertiary compression of peat. In: International workshop "Advances in understanding and modelling the mechanical behaviour of peat", June 16-18, 1993, Delft, The Netherlands.

Den Haan, E.J. and El Amir, L.S.F., 1994. A simple formula for final settlement of surface loads on peat. In: International workshop "Advances in understanding and modelling the mechanical behaviour of peat", June 16-18, 1993, Delft, The Netherlands.

Den Held, A.J., Schmitz, M. and Van Wirdum, G., 1992. Types of terrestrializing fen vegetation in the Netherlands. In: Verhoeven, J.T.A. (eds.) Fens and Bogs in the Netherlands: Vegetation, History, Nutrient Dynamics and Conservation, 237- 321, Dordrecht, The Netherlands.

Deverel, S.J. and Rojstaczer, S., 1996. Subsidence of agricultural lands in the Sacramento-San Joaquin Delta, California: role of aqueous and gaseous carbon fluxes. Water Resources Research 32, 2359-2367.

Diessel, C., Boyd, R., Wadsworth, J., Leckie, D. and Chalmers, G., 2000. On balanced and unbalanced accommodation/peat accumulation ratios in the Cretaceous coals from Gates Formation, Western Canada, and their sequence-stratigraphic significance. International Journal of Coal Geology 43, 143-186.

Digerfeldt, G., 1966, A new type of large-capacity sampler. Geologiska Föreningens i Stockholm Förhandlingar, 87, 425-430.

Dirschl, H.J., 1972. Geobotanical processes in the Saskatchewan River Delta. Canadian Journal of Earth Sciences 9, 1529-1549.

Dirschl, H.J. and Coupland, R.T., 1972. Vegetation patterns and site relationships in the Saskatchewan River delta. Canadian Journal of Botany 50, 647-675.

Doherty, J., 2004. PEST, Model-Independent Parameter Estimation, User Manual 5th Edition. Watermark Numerical Computing, Brisbane.

Drexler, J.Z., Defontaine, C.S. and Deverel, S.J., 2009. The legacy of the wetland drainage on the remaining peat in the Sacramento – San Joaquin Delta, California, USA. Wetlands 29, 372-386.

Ericson, J. P., Vörösmarty, C. J., Dingman, S. L., Ward, L. G. and Meybeck, M., 2006. Effective sea-level rise and deltas: Causes of change and human dimension implications. Global and Planetary Change 50, 63-82.

Erkens, G., 2009. Sediment dynamics in the Rhine catchment: Quantification of fluvial response to climate change and human impact. Ph.D. thesis, Utrecht University, Netherlands Geographical Studies 388.

Fenton, J.H., 1980. The rate of peat accumulation in Antarctic moss banks. Journal of Ecology 68, 211-228.

Fokkens, B., 1970 (in Dutch). Berekening van de samendrukking van veenlagen uit het gehalte aan organische stof en water. De ingenieur, Bouw- en waterbouwkunde 3, 1-20.

Galloway, D.L., Hudnut, K.W., Ingebritsen, S.E., Phillips, S.P., Peltzer, G., Rogez, F. and Rosen, P.A., 1998. Detection of aquifer system compaction and land subsidence using interferometric synthetic aperture radar, Antelope Valley, Mojave Desert, California. Water Resources Research 34, 2573-2585.

Gambolati, G., Putti, M., Teatini, P. and Gasparetto Stori, G., 2003. Subsidence due to peat oxidation and impact on drainage infrastructures in a farmland catchment south of the Venice Lagoon. Environment Geology 49, 814-820.

GeoDelft, 2003. Geotechnics, working lectures practical work visit. Brinkman, J., Kruse, G.A.M., Dillingh, D.A., Kruse, H.M.G. (eds.) project number 450050. GeoDelft, March 2003.

Gibling, M.R., Sounders, K.I., Tibert, N.E. and White, J.A., 2004. Sequence sets, high-accommodation events, and the coal window in the Carboniferous Sydney coalfield, Atlantic Canada. In: Pashin, J.C. and Gastaldo, R.A. (eds.) Sequence stratigraphy, paleoclimate, and tectonics of coal-bearing strata. AAPG Studies in Geology 51, 169-197.

Givelet, N., Le Roux, G., Cheburkin, A., Chen, B., Frank, J., Goodsite, M.E., Kempter, H., Krachler, M., Noernberg, T., Rausch, N., Rhuinberger, S., Roos-Barraclough, F., Sapkota, A., Scholz, C. and Shotyk, W., 2004. Suggested protocol for collecting, handling and preparing peat cores and peat samples for physical, chemical, mineralogical and isotopic analyses. Journal of Environmental Monitoring 6, 481-492.

Glew, J.R., Smol, J.P., and Last, W.M., 2001. Sediment core collection and extrusion., In: Last, W.M., and Smol, J.P. (eds.) Tracking Environmental Change Using Lake Sediments. Volume 1: Basin Analysis, Coring, and Chronological Techniques: Dordrecht, The Netherlands, Kluwer Academic Publishers, p. 73-105.

Gouw, M.J.P., 2007. Alluvial architecture of the Holocene Rhine-Meuse delta (The Netherlands) and the Lower Mississippi Valley (U.S.A). PhD Thesis, Utrecht University. Netherlands Geographical Studies 364.

Gouw, M.J.P. and Berendsen, H.J.A., 2007. Variability of channel-belt dimensions and the consequences for alluvial architecture: observations from the Holocene Rhine-Meuse delta (The Netherlands and Lower Mississippi valley (U.S.A). Journal of Sedimentary Research 77, 124-138.

Gouw, M.J.P. and Erkens, G., 2007. Architecture of the Holocene Rhine-Meuse delta (The Netherlands) – A result of changing external controls. In: Stouthamer, E. and Ten Brinke, W. (eds.) Fluvial Sedimentology, Netherlands Journal of Geosciences/Geologie en Mijnbouw 86, 23 – 54.

Guenet, P. and Reille, M., 1988. Analyse pollinique du lac-tourbière de Chambedaze (Massif Central, France) et datation de l´exposion des plus jeunes volcans d´Auvergne. Bulletin de l´Association Française d´Etude du Quaternaire 4, 175-194.

Gutierrez, M. and Wangen, M., 2005. Modeling of compaction and overpressuring in sedimentary basins. Marine and Petroleum Geology 22, 351-363.

Hargis, T.G., and Twilley, R.R., 1994. A multi-depth probe for measuring oxidation-reduction (redox) potential in wetland soils. Journal of Sedimentary Research 64, 684-685.

Haslett, S.K., Davies, P., Curr, R.H.F., Davies, C.F.C., Kennington, K., King, C.P. and Margetts, A.J., 1998. Evaluating late-Holocene relative sea-level change in the Somerset Levels, southwest Britain. The Holocene 8, 197-207.

Heiri, O., Lotter, A.F. and Lemcke, G., 2001. Loss on ignition as a method for estimating organic and carbonate content in sediments: reproducibility and comparability of results. Journal of Paleolimnology 25, 101-110.

Heller, P.L. and Paola, C., 1996. Downstream changes in alluvial architecture: an exploration of controls on channel-stacking patterns. Journal of Sedimentary Research 66, 297-306.

Hijma, M.P., Cohen, K.M., Hoffmann, G., Van Der Spek, A. J. F. and Stouthamer, E., 2009. From river valley to estuary: the evolution of the Rhine mouth in the early to middle Holocene (western Netherlands, Rhine-Meuse delta). Netherlands Journal of Geosciences 88, 13-53.

Ingebritsen, S.E., Ikehara, M.E., Galloway, D.L.and Jones, D.R., 2000. Delta subsidence in California. U.S. Department of the Interior, U.S. Geological Survey, Reston, VA, USA. Fact Sheet FS-005-00, 4 p.

Jowsey, P.C., 1965. An improved peat sampler. New Phytologist 65, 245-248.

Karssenberg, D. and Bridge, J.S., 2008. A three-dimensional model of sediment transport, erosion and deposition within a network of channel belts, floodplain and hillslope: extrinsic and intrinsic controls on floodplain dynamics and alluvial architecture. Sedimentology 55, 1717-1745.

Kaye, C.A. and Barghoon, E.S., 1964. Late Quaternary sea level change and crustal rise at Bostion, Massachusetts, with notes on autocompaction of peat. Geological Society of America Bulletin 75, 63-80.

Kiden, P., Denys, L. and Johnston, P., 2002. Late Quaternary sea-level change and isostatic and tectonic land movements along the Belgian – Dutch North Sea coast: geological data and model results. Journal of Quaternary Science 17, 535 – 546.

Kooi, H., 1997. Insufficiency of compaction disequilibrium as the sole cause of high pore fluid pressures in pre-Cenozoic sediments. Basin Research 9, 227-241.

Kooi, H. and De Vries, J.J., 1998. Land subsidence and hydrodynamic compaction of sedimentary basins. Hydrology and Earth System Sciences 2, 159-171.

Kooi, H., Johnston, P., Lambeck, K., Smither, C. and Molendijk, R., 1998. Geological causes of recent (~100 yr) vertical land movement in the Netherlands. Tectonophysics 299, 297-316.

Kool, D.M., Buurman, P. and Hoekman, D.H. 2006. Oxidation and compaction of a collapsed peat dome in Central Kalimantan. Geoderma 137, 217-225.

Kruse, H.M.G., 1998. Deformation of a river dyke on soft soil. PhD Thesis, Utrecht University, The Netherlands.

Kruse, H.M.G., 2004 (in Dutch). Bouwrijp maken Delft Technopolis. Rapportnummer CO-410031-0008 v03. GeoDelft, Delft, The Netherlands.

Latter, P.M., Howson, G., Howard, D.M. and Scott, W.A., 1998. Long-term study of litter decomposition on a Pennine peat bog: which regression? Oecologia 113, 94-103.

Leeder, M.R., 1978. A quantitative stratigraphic model for alluvium, with special reference to channel deposit density and interconnectedness. In: Miall, A.D. (eds.) Fluvial Sedimentology. Canadian Society of Petroleum Geologists Memoir 5, 587-596.

Lefebvre, G., Langlois, P., and Lupien, C., 1984. Laboratory testing and in situ behaviour of peat as embankment foundation: Canadian Geotechnical Journal 21, 322-337.

Locher, W.P. and De Bakker, H., 1990 (in Dutch). Bodemkunde van Nederland, Deel 1, Algemene bodemkunde. Malmberg, Den Bosch.

Long, A.J., Waller, M.P., and Stupples, P., 2006. Driving mechanisms of coastal change: Peat compaction and the destruction of late Holocene coastal wetlands: Marine Geology 225, 63-84.

Mackey, S.D. and Bridge, J.S., 1995. Three-dimensional model of alluvial stratigraphy: theory and application. Journal of Sedimentary Research B65, 7-31.

Magnan, J.P., 1993. Construction on peat: state of the art in France. In: Proceedings of International Workshop on Advances in understanding and modelling the mechanical behaviour of peat, April 1993.

Makaske, B., 1998. Anastomosing rivers. Forms, processes and sediments. PhD Thesis. Utrecht University, The Netherlands.

Makaske, B., 2001. Anastomosing rivers: a review of their classification, origin and sedimentary products. Earth-Science Reviews 53, 149-196.

Massey, A.C., Paul, M.A., Gehrels, W.R. and Charman, D. J., 2006. Autocompaction in Holocene coastal back-barrier sediments from south Devon, southwest England, UK. Marine Geology 226, 225-241.

Meckel, T.A., Ten Brink, U.S. and Williams, S.J., 2007. Sediment compaction rates and subsidence in deltaic plains: numerical constraints and stratigraphic influences. Basin Research 19, 19-31.

Mesri, G. and Ajlouni, M., 2007. Engineering properties of fibrous peats: Journal of Geotechnical and Geoenvironmental Engineering 133, 850-866.

Michaelsen, P., Henderson, R.A, Crosdale, P.J. and Mikkelsen, S.O., 2000. Facies architecture and depositional dynamics of the Upper Permian Rangal Coal Measures, Bowen Basin, Australia. Journal of Sedimentary Research 70, 879-895.

Morozova, G.S. and Smith, N.D., 1999. Holocene avulsion history of the lower Saskatchewan fluvial system, Cumberland Marshes, Saskatchewan-Manitoba, Canada. In: Smith, N.D., and Rogers, J. (eds.) Fluvial Sedimentology VI. International Association of Sedimentologists Special Publication 28, Blackwell Science, Oxford, p. 231-249.

Morozova, G.S. and Smith, N.D., 2000. Holocene avulsion styles and sedimentation patterns of the Saskatchewan River, Cumberland marshes, Canada, Sedimentary Geology 130, 81-105.

Morozova, G.S. and Smith, N.D., 2003. Organic matter deposition in the Saskatchewan River floodplain (Cumberland Marshes, Canada): effect of progradational avulsions: Sedimentary Geology 157, 15-29.

Morton, R.A., Bernier, J.C. and Barras, J.A., 2006. Evidence of regional subsidence and associated interior wetland loss induced by hydrocarbon production, Gulf Coast region, USA. Environmental Geology 50, 1432-0495.

Nadon, G.C., 1998. Magnitude and timing of peat-to-coal compaction. Geology 26, 727-730.

NCGIA, (NASA) National Center for Geographic Information and Analysis, 1999. http://visibleearth.nasa.gov/view_rec.php?id=116.

Oświt, J., 1993. The development of the Lower Biebrza Valley peatlands against the background of the water conditions. In: Okruszko, H., and Wassen, M.J. (eds.) Towards Protection and Sustainable Use of the Biebrza Wetlands: Exchange and Integration of Research results for the Benefit of a Polish – Dutch Joint Research Plan, Report 3, Volume B., Department of Environmental Studies, Utrecht University, Utrecht, The Netherlands, p. 75-135.

Paul, M.A. and Barras, B.F., 1998. A geotechnical correction for post-depositional sediment compression: examples from the Forth Valley, Scotland. Journal of Quaternary Science 13, 171-176.

Pérez-Arlucea, M. and Smith, N.D., 1999. Depositional patterns following the 1870s avulsion of the Saskatchewan River (Cumberland Marshes, Saskatchewan, Canada). Journal of Sedimentary Research 69, 62-73.

Petrone, R.M., Devito, K.J., Silins, U., Mendoza, C., Brown, S.C., Kaufman, S.C. and Price, J.S., 2008. Transient peat properties in two pond-peatland complexes in the sub-humid Western Boreal Plain, Canada: Mires and Peat 3, 1-13.

Pizzuto, J.E. and Schwendt, A.E., 1997. Mathematical modeling of autocompaction of a Holocene transgressive valley-fill deposit, Wolfe Glade, Delaware. Geology 25, 57-60.

Poelman, J.N.B., 1975 (in Dutch). Dichtheid van de vaste delen van rivierkleigronden. Boor en spade: verspreide bijdragen tot de kennis van de bodem van Nederland, p. 32-38.

Pouya, A., Djeran-Maigre, I., Lamoureux-Var, V. and Grunberger, D., 1998. Mechanical behaviour of fine grained sediments: experimental compaction and three-dimensional constitutive model. Marine and Petroleum Geology 15, 129-143.

Price, J. S., Cagampan, J. and Kellner, E., 2005. Assessment of peat compressibility: is there an easy way? Hydrological Processes 19, 3469-3475.

Rajchl, M. and Uličný, D., 2005. Depositional record of an avulsive fluvial system controlled by peat compaction (Neogene, Most Basin, Czech Republic). Sedimentology 52, 601-626.

Reimer, P., Baillie, M., Bard, E., Bayliss, A., Beck, J., Bertrand, C., Blackwell, P., Buck, C., Burr, G., Cutler, K., Damon, P.E., Edwards, R., Fairbanks, R., Friedrich, M., Guilderson, T., Hogg, A., Hughen, K., Kromer, B., McCormac, G., Manning, S., Ramsey, C., Reimer, R., Remmele, S., Southon, J., Stuiver, M., Talamo, S., Taylor, F., van der Plicht, J. and Weyhenmeyer, C., 2004. IntCal04 terrestrial radiocarbon age calibration, 0 – 26 cal kyr BP. Radiocarbon 46, 1029-1058.

Rieke, H.H. and Chilingarian, G.V., 1974. Compaction of argillaceous sediments. Developments in Sedimentology 16, Amsterdam, Elsevier, p. 424.

Rijkswaterstaat-AGI, 2005 (in Dutch). Actueel Hoogtebestand van Nederland. Revised version. Rijkswateraat, Adviesdienst Geo-infomratie en ITC, Delft.

Rodolfo, K.S. and Siringan, F.P., 2006. Global sea-level rise is recognized, but flooding from anthropogenic land subsidence is ignored around northern Manila Bay, Philippines. Disasters 30, 118-139.

Roulet, N.T., 1991. Surface level and water table fluctuations in a subarctic fen: Arctic and Alpine Research 23, 303-310.

Rogers, K., Wilton K.M. and Saintilan, N., 2006. Vegetation change and surface elevation dynamics in estuarine wetlands of southeast Australia. Estuarine, Coastal and Shelf Science 66, 559-569.

Saxton, K.E., Rawls, W.J., Romberger, J.S. and Papendick, R.I., 1986. Estimating generalized soil-water characteristics from texture: Soil Sciences Society of America Journal 50, 1031-1036.

Schothorst, C. J., 1977. Subsidence of low moor peat soils in the western Netherlands. Geoderma 17, 265-291.

Schreiner, B.T., 1983. Lake Agassiz in Saskatchewan. In: Teller, J.T., and Clayton, L. (eds.) Glacial Lake Agassiz: Geological Association of Canada Special Paper 26, p. 75-96.

Sclater, J.G. and Christie, P.A.F., 1980. Continental stretching: explanation of post-mid-Cretaceous subsidence of the central North Sea Basin. Journal of Geophysical Research 85, 3711-3939.

SCPS – Swedish Committee on Piston Sampling, 1961. Standard piston sampling: Proceedings of the Swedish Geotechnology Institute 19, Stockholm.

Seber, G.A.F. and Wild, C.J., 2003. Nonlinear regression. Wiley, New York.

Sheldon, N.D. and Retallack, G.J., 2001. Equation for compaction of paleosols due to burial. Geology 29, 247-250.

Shennan, I. and Horton, B., 2002. Holocene land-and sea-level changes in Great Britain. Journal of Quaternary Science 17, 511-526.

Skempton, A.W., 1944. Notes on compressibility of clays. Quaternary Journal Geological Society of London 100, 119-135.

Skempton, A.W., 1970. The consolidation of clays by gravitational compaction. Quaternary Journal of the Geological Society of London 125, 373-411.

Smith, N.D., Cross, T.A., Dufficy, J.P. and Clough, S.R., 1989. Anatomy of an avulsion. Sedimentology 36, 1-23.

Smith, N.D., Slingerland, R.L., Pérez-Arlucea, M. and Morozova, G.S., 1998. The 1870s avulsion of the Saskatchewan River: Canadian Journal of Earth Sciences 35, 453 – 466.

Smith, N.D. and Pérez-Arlucea, M., 2004. Effects of peat on the shapes of alluvial channels: examples from the Cumberland Marshes, Saskatchewan, Canada. Geomorphology 61, 323-335.

Spijker, J., 2005. Geochemical patterns in the soils of Zeeland. Netherlands Geographical Studies 330/KNAG, Utrecht.

Stout, S.A. and Spackman, W., 1989. Notes on the compaction of a Florida peat and the Brandon lignite as deduced from the study of compressed wood. International Journal of Coal Geology 11, 247-256.

Stouthamer, E., 2001. Holocene avulsions in the Rhine-Meuse delta, The Netherlands. PhD thesis, Universiteit Utrecht. Netherlands Geographical Studies 283.

Stouthamer, E., 2005. Reoccupation of channel belts and its influence on alluvial architecture in the Holocene Rhine-Meuse delta, The Netherlands. In: Giosan, L. and Bhattacharya, J.P. (eds.) River Deltas – Concepts, models, and examples, SEPM Special Publication 83, 319-339.

Stouthamer, E. and Berendsen, H.J.A., 2000. Factors controlling the Holocene avulsion history of the Rhine-Meuse delta (The Netherlands). Journal of Sedimentary Research 70, 1051-1064.

Stouthamer, E. and Berendsen, H.J.A., 2007. Avulsion: the relative roles of autogenic and allogenic processes. Sedimentary Geology 198, 309-325.

Syvitski, J.P.M., 2008. Deltas at risk. Sustainable Science 3, 23-32.

Syvitski, J.P.M., Kettner, A.J., Overeem, I., Hutton, E.W.H., Hannon, M.T., Brakenridge, G.R., Day, J., Vörösmarty, C., Saito, Y., Giosan, L. and Nicholls, R.J., 2009. Sinking deltas due to human activities. Nature Geoscience 2, 681-686.

Teatini, P., Ferronato, M., Gambolati, G. and Gonella, M., 2006. Groundwater pumping and land subsidence in the Emilia-Romagna coastland, Italy: Modeling the past occurrence and the future trend. Water Resources Research 42, 1-19.

Termaat, R. and Topolnicki, M., 1993. Biaxial tests with natural and artificial peat. In: Proceedings of International Workshop on Advances in understanding and modelling the mechanical behaviour of peat, April 1993.

Terzaghi, K., 1943. Theoretical Soil Mechanics. John Wiley and Sons, New York.

Tooth, S. and McCarthy, T.S., 2004. Controls on the transition from meandering to straight channels in the wetlands of the Okavango Delta, Botswana. Earth Surface Processes and Landforms 29, 1627-1649.

Törnqvist, T.E., 1993a. Fluvial sedimentary geology and chronology of the Holocene Rhine-Meuse delta, The Netherlands. PhD Thesis, Utrecht University. Netherlands Geographical Studies 166.

Törnqvist, T.E., 1993b. Holocene alternation of meandering and anastomosing fluvial systems in the Rhine-Meuse Delta (central Netherlands) controlled by sea-level rise and subsoil erodibility. Journal of Sedimentary Petrology 63, 683-693.

Törnqvist, T.E. and Van Dijk, G.J., 1993. Optimizing sampling strategy for radiocarbon dating of Holocene fluvial systems in a vertically aggrading setting. Boreas 22, 129-145.

Törnqvist, T.E., Van Ree, M.H.M., Van 't Veer, R. and Van Geel, B., 1998. Improving methodology for high-resolution reconstruction of sea-level rise and neotectonics by paleoecological analysis and AMS ^{14}C dating of basal peats. Quaternary Research 49, 72-85.

Törnqvist, T.E. and Bridge, J.S., 2002. Spatial variation of overbank aggradation rate and its influence on avulsion frequency. Sedimentology 49, 891-905.

Törnqvist, T.E., Wallace, D.J., Storms, J.E.A., Wallinga, J., van Dam, R.L., Blaauw, M., Derksen, M.S., Klerks, C.J.W., Meijneken, C. and Snijders, E.M.A., 2008. Mississippi Delta subsidence primarily caused by compaction of Holocene strata. Nature Geoscience 1, 173-176.

Tovey, N.K. and Paul, M.A., 2002. Modelling self-weight consolidation in Holocene sediments. Bulletin of Engineering Geology and the Environment 61, 21-33.

Turner, R.E. 2004. Coastal wetland subsidence arising from local hydrologic manipulations. Estuaries 27, 265-273.

Van Asselen, S., Stouthamer, E. and Van Asch, Th.W.J., 2009. Effects of peat compaction on delta evolution: a review on processes, responses, measuring and modeling: Earth-Science Reviews 93, 35-51.

Van Asselen, S., and Roosendaal, C., 2009. A new method for determining the bulk density of uncompacted peat from field settings. Journal of Sedimentary Research 79, 918-922.

Van Asselen, S., Stouthamer, E and Smith, N.D., 2010. Factors controlling peat compaction in alluvial floodplains: a case study in the cold-temperate Cumberland Marshes, Canada. Journal of Sedimentary Research, 80, 155-166.

Van der Meulen, M., Van der Spek, A., De Lange, G., Gruijters, S., Van Gessel, S., Nguyen, B.-L., Maljers, D., Schokker, J., Mulder, J. and Van der Krogt, R., 2007. Regional Sediment Deficits in the Dutch Lowlands: Implications for Long-Term Land-Use Options. Journal of Soils and Sediments 7, 9-16.

Van Dijk, G.J., Berendsen, H.J.A. and Roeleveld, W., 1991. Holocene water level development in The Netherlands' river area; implications for sea-level reconstruction. Geologie en Mijnbouw 70, 311-326.

Vos, P.C. and Van Heeringen, R.M., 1997. Holocene geology and occupation history of the province of Zeeland (SW Netherlands). Mededelingen – Nederlands Instituut voor Toegepaste Geowetenschappen TNO 59, 5-109.

Wardenaar, E.C.P., 1987. A new hand tool for cutting peat profiles: Canadian Journal of Botany 65, 1772 – 1773.

Watters, J.R. and Stanley, E.H., 2007. Stream channels in peatlands: The role of biological processes in controlling channel form. Geomorphology 89, 97-110.

Whittington, P.N. and Price, J.S., 2006. The effects of water table draw-down (as a surrogate for climate change) on the hydrology of a fen peatland, Canada. Hydrological Processes 20, 3589-3600.

Wright, H.E., Jr., Mann, D.H. and Glaser, P.H., 1984. Piston corers for peat and lake sediments. Ecology 65, 657-659.

Żurek, S., 1984. Relief, geologic structure and hydrograph of the Biebrza ice-marginal valley. Polish Ecological Studies 10, 239-251.

Appendix 1

The dry bulk density (ρ_{dry}), loss on ignition (LOI) and calculated amount of compaction measured at 5-cm-intervals in cores obtained from the North Angling Channel study site (chapter 4).

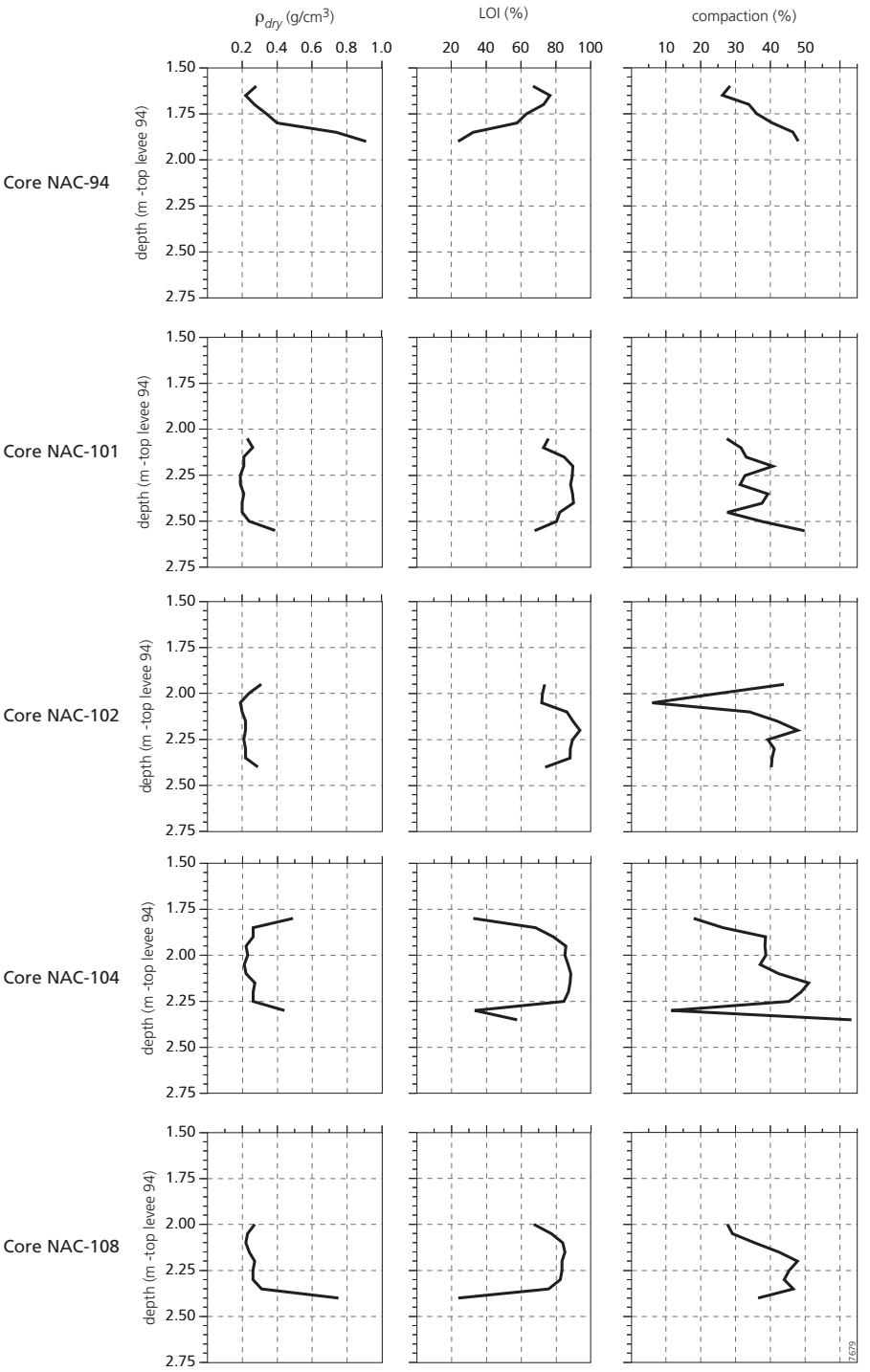
ρ_{dry} (g/cm^3)
0.2 0.4 0.6 0.8 1.0
LOI (%)
20 40 60 80 100
compaction (%)
10 20 30 40 50
depth (m -top levee 94)
1.50 1.75 2.00 2.25 2.50 2.75
Core NAC-94
Core NAC-101
Core NAC-102
Core NAC-104
Core NAC-108
7679

Appendix 2

The dry bulk density (ρ_{dry}), loss on ignition (LOI) and calculated amount of compaction measured at 5-cm-intervals in cores obtained from the Mossy River study site (chapter 4).

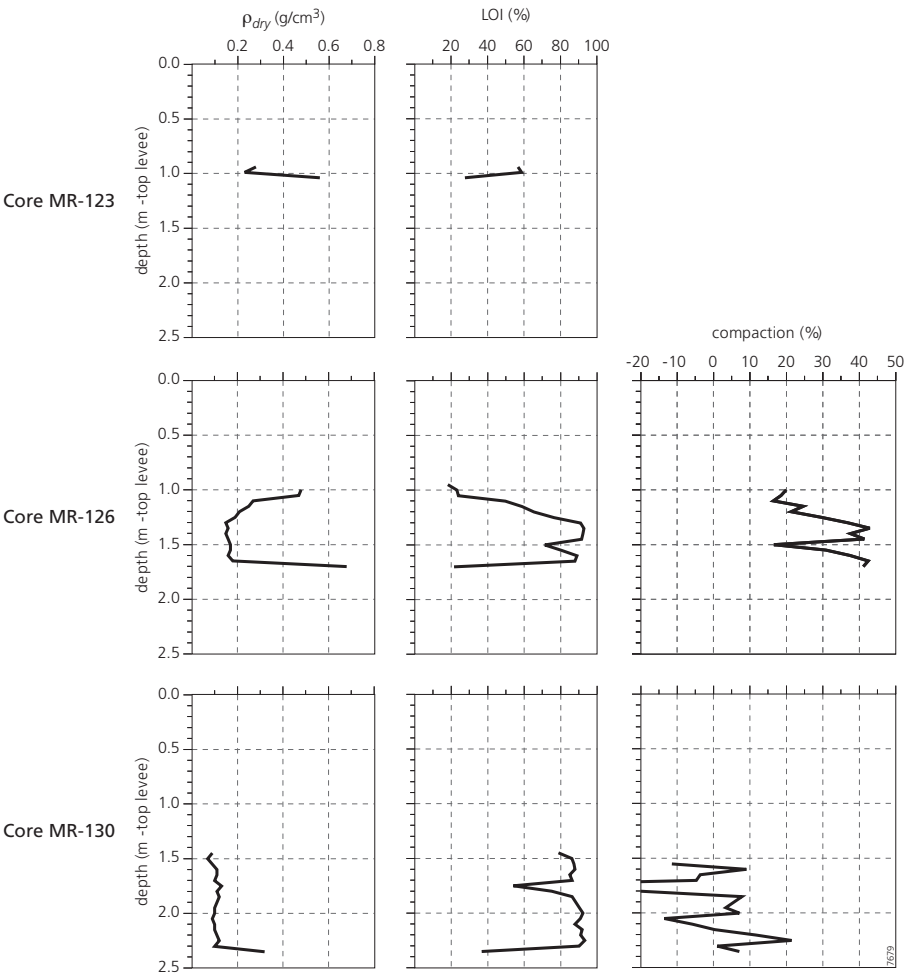

Appendix 3

The dry bulk density (ρ_{dry}), loss on ignition (LOI) and calculated amount of compaction measured at 5-cm-intervals in cores obtained from the James Bond River study site.

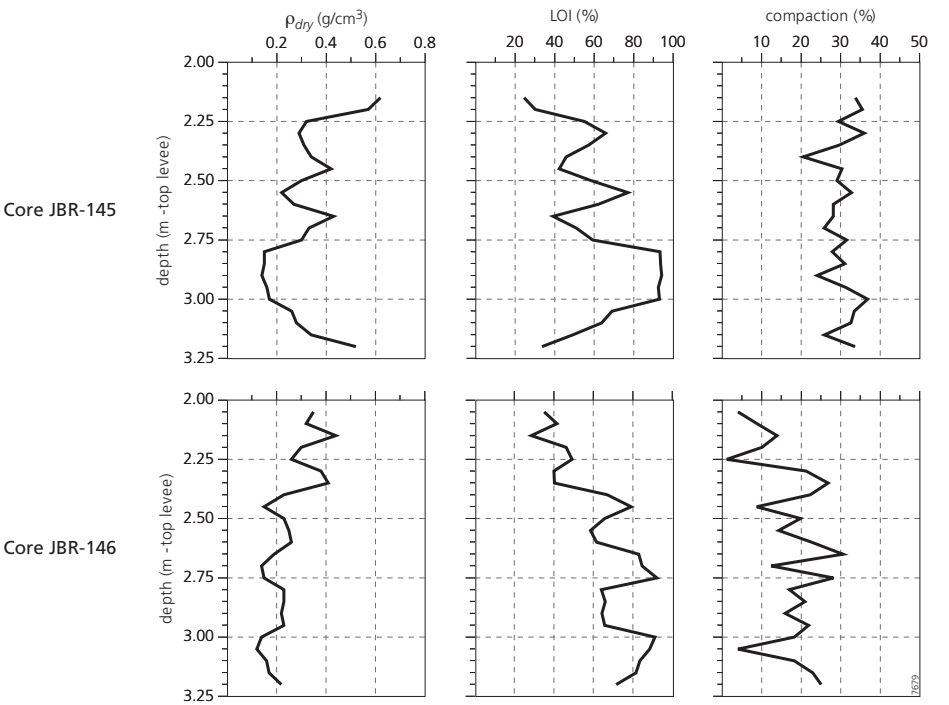

Appendix 4

Detailed information of radiocarbon-dated samples used in chapter 5. Paper code numbers correspond with those used in chapter 5. I=method 1 (groundwater table reconstruction) has been applied to sample, II=method 2 (dry bulk density measurements) has been applied to sample (core), TBM=Terrestrial Botanical Macrofossils.

Paper code	Lab nr.	Sample name	^{14}C age ± σ (yr BP)	Calendar age (cal yr BP)	Depth below surface (cm)	Coordinates (km)/Surface elevation (m ±O.D.)	Dated material	Source
1 (I/II))	UtC-14349	Lange Avontuur I	2584±46	2735	100-101	141.807-438.329/+0.34	27 Carex sect. Acutae, 0.5 Stachys palustris	Gouw (2007)
2 (I)	UtC-14275	Lange Avontuur II	4047 ± 47	4470	194-196	141.807-438.329/+0.34	192 Typha, 2 Carex biconvex nutlets, 1.33 Carex, trigonous nutlets, 2.5 Alisma plantago-aquatica, 0.5 Oenanthe aquatica, 13 Lythrum salicaria	Gouw (2007)
3 (I)	UtC-14276	Lange Avontuur III	5022 ± 50	5740	305-306	141.807-438.329/+0.34	2 Frangula alnus, 2 Lychnis flos-cuculi, Alnus: 1 fruit, 3 male catkin scales; 2 Rubus sp.	Gouw (2007)
4 (I/II)	UtC-14350	Lange Avontuur V	6980±50	7820	514-516	141.807-438.329/+0.34	5.5 Alnus fruits, 3 Carex biconvex nutlets, 1 Carex trigonous nutlet, 2 Alisma plantago-aquatica, 1 Pragmites australis, 1.25 Stachys pa ustris, 1 Mentha aquatica, 1 Oenanthe aquatica	Gouw (2007)
5 (I)	UtC-13504	De Woerd-5	4240 ± 90	4835	110-111	143.375-437.003/+1.26	TBM	Unpublished (Stouthamer). First published: Berendsen and Stouthamer (2001)
6 (I)	UtC-13505	De Woerd-6	4480 ± 120	5000	130-131	143.375-437.003/+1.26	TBM	Unpublished (Stouthamer). First published: Berendsen and Stouthamer (2001)
7 (I)	UtC-13506	De Woerd-7	4520 ± 130	5390	160-161	143.375-437.003/+1.26	TBM	Unpublished (Stouthamer). First published: Berendsen and Stouthamer (2001)
8 (I)	UtC-13507	De Woerd-8	4910 ± 80	5620	250-255	143.375-437.003/+1.26	TBM	Unpublished (Stouthamer). First published: Berendsen and Stouthamer (2001)
9 (I)	UtC-13508	De Woerd-9	5440 ± 100	6245	282-286	143.375-437.003/+1.26	TBM	Unpublished (Stouthamer). First published: Berendsen and Stouthamer (2001)

Paper code	Lab nr.	Sample name	^{14}C age ± σ (yr BP)	Calendar age (cal yr BP)	Depth below surface (cm)	Coordinates (km)/Surface elevation (m ±O.D.)	Dated material	Source
10 (I)	UtC-13509	De Woerd-10	5590 ± 90	6380	310-315	143.375-437.003/+1.26	TBM	Unpublished (Stouthamer). First published: Berendsen and Stouthamer (2001)
11 (I)	UtC-13510	De Woerd-1	6170 ± 150	6670	340-345	143.375-437.003/+1.26	TBM	Unpublished (Stouthamer). First published: Berendsen and Stouthamer (2001)
12 (I)	UtC-13511	De Woerd-2	5840 ± 80	6710	370-375	143.375-437.003/+1.26	TBM	Unpublished (Stouthamer). First published: Berendsen and Stouthamer (2001)
13 (I)	UtC-13762	Wijngaarden 1	2640 ± 70	2790	055-059	107.874-431.816/-1.69	TBM	Unpublished (Stouthamer). First published: Berendsen and Stouthamer (2001)
14 (I)	UtC-13763	Wijngaarden 2	3010 ± 60	3175	110-114	107.874-431.816/-1.69	TBM	Unpublished (Stouthamer). First published: Berendsen and Stouthamer (2001)
15 (I)	UtC-13764	Wijngaarden 3	3380 ± 70	3635	160-161	107.874-431.816/-1.69	TBM	Unpublished (Stouthamer). First published: Berendsen and Stouthamer (2001)
16 (I)	UtC-13765	Wijngaarden 4	3849 ± 47	4260	210-211	107.874-431.816/-1.69	TBM	Unpublished (Stouthamer). First published: Berendsen and Stouthamer (2001)
17 (I)	UtC-13766	Wijngaarden 5	4090 ± 50	4585	260-261	107.874-431.816/-1.69	TBM	Unpublished (Stouthamer). First published: Berendsen and Stouthamer (2001)
18 (I)	UtC-13767	Wijngaarden 6	4406 ± 45	4902	310-311	107.874-431.816/-1.69	TBM	Unpublished (Stouthamer). First published: Berendsen and Stouthamer (2001)
19 (I)	UtC-13768	Wijngaarden 7	4330 ± 60	4935	362-364	107.874-431.816/-1.69	TBM	Unpublished (Stouthamer). First published: Berendsen and Stouthamer (2001)

Paper code	Lab nr.	Sample name	^{14}C age ± σ (yr BP)	Calendar age (cal yr BP)	Depth below surface (cm)	Coordinates (km)/Surface elevation (m ±O.D.)	Dated material	Source
20 (I)	UtC-13799	Wijngaarden 8	4410 ± 60	5010	411-412	107.874-431.816/-1.69	TBM	Unpublished (Stouthamer). First published: Berendsen and Stouthamer (2001)
21 (I)	UtC-13800	Wijngaarden 9	4500 ± 60	5210	460-461	107.874-431.816/-1.69	TBM	Unpublished (Stouthamer). First published: Berendsen and Stouthamer (2001)
22 (I)	UtC-13801	Wijngaarden 10	4630 ± 50	5415	510-511	107.874-431.816/-1.69	TBM	Unpublished (Stouthamer). First published: Berendsen and Stouthamer (2001)
23 (I)	UtC-13802	Wijngaarden 11	4960 ± 60	5675	560-561	107.874-431.816/-1.69	TBM	Unpublished (Stouthamer). First published: Berendsen and Stouthamer (2001)
24 (I)	UtC-13803	Wijngaarden 12	5090 ± 50	5885	611-612	107.874-431.816/-1.69	TBM	Unpublished (Stouthamer). First published: Berendsen and Stouthamer (2001)
25 (I)	UtC-13804	Wijngaarden 13	5280 ± 50	6050	660-661	107.874-431.816/-1.69	TBM	Unpublished (Stouthamer). First published: Berendsen and Stouthamer (2001)
26 (I)	UtC-13805	Wijngaarden 14	5600 ± 70	622	700-701	107.874-431.816/-1.69	TBM	Unpublished (Stouthamer). First published: Berendsen and Stouthamer (2001)
27 (I)	UtC-13808	Wijngaarden 17	6080 ± 80	6940	860-864	107.874-431.816/-1.69	TBM	Unpublished (Stouthamer). First published: Berendsen and Stouthamer (2001)
28 (I)	UtC-13809	Wijngaarden 18	6850 ± 80	7530	910-911	107.874-431.816/-1.69	TBM	Unpublished (Stouthamer). First published: Berendsen and Stouthamer (2001)
29 (I)	GrN-9403	Polsbroek I	3995 ± 40	4493	208-210	118.500-444.475/-1.56	Wood peat	Bosch and Kok (1994):
30 (I)	GrN-9404	Polsbroek II	4650 ± 40	5415	403-405	118.500-444.475/-1.56	Wood peat with gyttja	Bosch and Kok (1994):
31 (I)	GrN-9405	Polsbroek III	5810 ± 40	6610	526-528	118.500-444.475/-1.56	Phragmites peat	Bosch and Kok (1994):

Paper code	Lab nr.	Sample name	^{14}C age ± σ (yr BP)	Calendar age (cal yr BP)	Depth below surface (cm)	Coordinates (km)/Surface elevation (m ±O.D.)	Dated material	Source
32 (I/II)	UtC-14351	Zeedijk I	4240±60	4835	77-79	143.792-437.415/+0.53	4 Valeriana sp., 1 Stachys palustris, 5 Mentha aquatica, 0.5 Ranunculus acris/repens, 6 Lythrum salicaria	Gouw (2007)
33 (I/II)	UtC-14532	Zeedijk II	5210±60	5925	195-196	143.792-437.415/+0.53	1.33 Carex trigonous nutlets, 30 Lythrum salicaria, 1 Stachyspalustris, 59 Typha, 3 Alnus fruits, 2.5 Lycopus europaeus, 2 Mentha aquatica, 8 Berula erecta	Gouw (2007)
34 (I/II)	UtC-14353	Zeedijk III	5220±90	5975	260-262	143.792-437.415/+0.53	1 Alnus fruit, 107 Lythrum salicaria, 5 Carex trigonous nutlets, 0.25 Stachys palustris	Gouw (2007)
35 (I/II)	UtC-14277	Zeedijk IV	5830 ± 60	6650	307-308	143.792-437.415/+0.53	1 Alnus twig	Gouw (2007)
36 (I/II)	UtC-14278	Zeedijk V	6010 ± 60	6860	451-452	143.792-437.415/+0.53	Alnus: 2 twigs, 3 budscales, 5 fruits, 1 fragment male catkin, 3 male catkin scales	Gouw (2007)
37 (I/II)	UtC-14354	Zeedijk VI	7620±70	8410	562-563	143.792-437.415/+0.53	36 Urtica dioica, 6 Oenanthe aquatica, 2 Solanum dulcamara, 4 Alnus fruits	Gouw (2007)
38 (I)	UtC-01187	Ochten M10	3400 ± 300	4000	300	162.650-434.920/+5.60	TBM	Unpublished (A.F.M. de Jong); first published: Berendsen & Stouthamer (2001)
39 (I)	UtC-01188	Ochten M13	4860 ± 190	5080	380	162.650-434.920/+5.60	TBM	Unpublished (A.F.M. de Jong); first published Berendsen & Stouthamer (2001)
40 (I)	UtC-01189	Ochten M14	4360 ± 160	5210	410	162.650-434.920/+5.60	TBM	Unpublished (A.F.M. de Jong); first published Berendsen & Stouthamer (2001)
41 (I)	UtC-01190	Ochten M15	4914 ± 160	5640	430	162.650-434.920/+5.60	TBM	Unpublished (A.F.M. de Jong); first published Berendsen & Stouthamer (2001)

Paper code	Lab nr.	Sample name	^{14}C age ± σ (yr BP)	Calendar age (cal yr BP)	Depth below surface (cm)	Coordinates (km)/Surface elevation (m ±O.D.)	Dated material	Source
42 (I)	UtC-01191	Ochten M16	5260 ± 160	6060	450	162.650-434.920/+5.60	TBM	Unpublished (A.F.M. de Jong); first published Berendsen & Stouthamer (2001)
43 (I)	UtC-01192	Ochten M17	5890 ± 200	6600	480	162.650-434.920/+5.60	TBM	Unpublished (A.F.M. de Jong); first published Berendsen & Stouthamer (2001)
44 (I)	UtC-01235	Ochten M18	6060 ± 190	6900	510	162.650-434.920/+5.60	TBM	Unpublished (A.F.M. de Jong); first published Berendsen & Stouthamer (2001)
45 (I)	GrA-04184	Vlaardingen 20A	4830 ± 50	5600	655-657	084.150-435.950/-0.50	TBM	Unpublished (O. v.d. Plassche); first published: Berendsen & Stouthamer (2001)
46 (I)	GrA-04185	Vlaardingen 26A	5220 ± 130	5950	809-811	084.150-435.950/-0.50	TBM	Unpublished (O. v.d. Plassche); first published: Berendsen & Stouthamer (2001)
47 (I)	GrA-04186	Vlaardingen 27A	5780 ± 170	6320	816-818	084.150-435.950/-0.50	TBM	Unpublished (O. v.d. Plassche); first published: Berendsen & Stouthamer (2001)
47 (I)	GrA-05214	Vlaardingen 27B	5490 ± 80	6320	816-818	084.150-435.950/-0.50	TBM	Unpublished (O. v.d. Plassche); first published: Berendsen & Stouthamer (2001)
48 (I)	GrA-04189	Vlaardingen 28A	5900 ± 70	6745	826-828	084.150-435.950/-0.50	TBM	Unpublished (O. v.d. Plassche); first published: Berendsen & Stouthamer (2001)
49 (I)	GrA-05210	Vlaardingen 30A	5880 ± 50	6692	836-837	084.150-435.950/-0.50	TBM	Unpublished (O. v.d. Plassche); first published: Berendsen & Stouthamer (2001)
50 (I)	GrA-05211	Vlaardingen 19A	4780 ± 50	5542	650-652	084.150-435.950/-0.50	TBM	Unpublished (O. v.d. Plassche); first published: Berendsen & Stouthamer (2001)

Paper code	Lab nr.	Sample name	^{14}C age ± σ (yr BP)	Calendar age (cal yr BP)	Depth below surface (cm)	Coordinates (km)/Surface elevation (m ±O.D.)	Dated material	Source
51 (I)	GrA-05212	Vlaardingen 21A	5040 ± 50	5750	669-671	084.150-435.950/-0.50	TBM	Unpublished (O. v.d. Plassche); first published: Berendsen & Stouthamer (2001)
52 (I)	GrN-10102	Middelkoop 4	4090 ± 60	4580	112-114	132.712-437.390/-0.25	Slightly clayey amorphous peat	Törnqvist and Van Dijk (1993)
53 (I)	GrN-10103	Middelkoop 5	2880 ± 50	3020	79-81	132.712-437.390/-0.25	Slighly clayey Alnus peat	Törnqvist and Van Dijk (1993)
54 (I)	GrN-10104	Noordeloos 1	6310 ± 60	7180	468-471	123.193-435.132/-1.40	Alnus peat	Van Dijk et al. (1991)
55 (I)	GrN-10105	Noordeloos 2	5350 ± 50	6130	372-375	123.193-435.132/-1.40	Alnus peat	Törnqvist (1993a)
56 (I)	GrN-10108	Noordeloos 5	3570 ± 70	3900	98-101	123.193-435.132/-1.40	Slightly clayey Alnus peat	Törnqvist (1993a)
57 (I)	GrN-10114	Leerdam.12	5300 ± 80	5960	271-274	135.170-435.665/-0.04	Slightly clayey Phragmites peat	Van Dijk et al. (1991)
58 (I)	GrN-10116	Leerdam 11	4800 ± 80	5580	248-251	135.170-435.665-0.04	Slightly clayey Phragmites peat	Van Dijk et al. (1991)
59 (I)	GrN-10117	Leerdam 9	4730 ± 70	5340	240-243	135.170-435.665-0.04	Slightly clayey Phragmites peat	Van Dijk et al. (1991)
60 (I)	GrN-10118	Leerdam 8	2860 ± 60	2960	111-114	135.170-435.665-0.04	Slightly clayey Alnus peat	Van Dijk et al. (1991)
61 (I)	GrN-10119	Leerdam 7	2510 ± 60	2700	86-90	135.170-435.665-0.04	Slightly clayey Alnus peat	Van Dijk et al. (1991)
62 (I)	GrN-9152	HoonkomLeebrug I	3795 ± 55	4200	160-165	139.948-447.305/+0.40	peat	Berendsen (1982)
63 (I)	GrN-9153	HoonkomLeebrug V	6900 ± 90	7680	515-520	139.948-447.305/+0.40	peat	Berendsen (1982)
64 (I)	GrN-9351	HoonkomLeebrug II	5040 ± 85	5805	255-260	139.948-447.305/+0.40	Peat	Berendsen (1982)
65 (I)	GrN-9352	HoonkomLeebrug III	5975 ± 45	6800	425-430	139.948-447.305/+0.40	Peaty clay	Berendsen (1982)
66 (I)	UtC-01141	Schelluinen.I-1a	4580 ± 110	5410	311-314	123.805-429.645/-0.80	TBM	Törnqvist (1993a)
66 (I)	UtC-01142	Schelluinen.I-1b	4740 ± 160	5410	311-314	123.805-429.645/-0.80	20 Allisma plantago-aquatica fruits	Törnqvist (1993a)
67 (I)	UtC-01143	Schelluinen.I-2a	5490 ± 100	5950	480-483	123.805-429.645/-0.80	TBM	Törnqvist (1993a)
67 (I)	UtC-01144	Schelluinen.I-2b	5100 ± 110	5950	480-483	123.805-429.645/-0.80	2 Scirpus lacustris nuts	Törnqvist (1993a)
67 (I)	UtC01300	Schelluinen I-2c	4980 ± 130	5950	480-483	123.805-429.645/-0.80	2 Scirpus lacustris nuts	Törnqvist (1993a)

Paper code	Lab nr.	Sample name	^{14}C age ± σ (yr BP)	Calendar age (cal yr BP)	Depth below surface (cm)	Coordinates (km)/Surface elevation (m ±O.D.)	Dated material	Source
68 (I)	UtC-01297	Bazeldijk.I-2a	5440 ± 50	6140	343-345	128.030-432.750/-1.10	TBM	Törnqvist (1993a)
68 (I)	UtC-01396	Bazeldijk I-2C	5330 ± 70	6140	343-345	128.030-432.750/-1.10	Fragments of Coleoptera	Törnqvist (1993a)
68 (I)	Utc-01397	Bazeldijk I-2b	5240 ± 70	6140	343-345	128.030-432.750/-1.10	2 Scirpus Lucustris nuts	Törnqvist (1993a)
69 (I)	UtC-01410	Bazeldijk.I-1b	3630 ± 40	3840	95-96	128.030-432.750/-1.10	1Sparganium erectum	Törnqvist (1993a)
69 (I)	UtC-01479	Bazeldijk.I-1a	3380 ± 60	3840	95-96	128.030-432.750/-1.10	TBM	Törnqvist (1993a)
70 (I)	UtC-04643	Schoonrewoerdse 7	3818 ± 42	4225	226-228	148.865-437.940/+2.50	TBM	Makaske (1998)
71 (I)	UtC-04644	Schoonrewoerdse 8	5170 ± 110	5930	324-325	148.865-437.940/+2.50	TBM	Makaske (1998)
72 (I)	UtC-04645	Schoonrewoerdse 9	6220 ± 70	7060	570-571	148.865-437.940/+2.50	TBM	Makaske (1998)
73 (I)	UtC-13501	DeTreeft. 1	4020 ± 70	4520	196-197	148.579-436.198/+2.73	TBM	Unpublished (Stouthamer). First published: Berendsen and Stouthamer (2001)
74 (I)	UtC-13502	DeTreeft. 2	4210 ± 70	4820	218-221	148.579-436.198/+2.73	TBM	Unpublished (Stouthamer). First published: Berendsen and Stouthamer (2001)
75 (I)	UtC-13503	DeTreeft. 4	5030 ± 80	5680	292-293	148.579-436.198/+2.73	TBM	Unpublished (Stouthamer). First published: Berendsen and Stouthamer (2001)
76 (I)	UtC-13769	DeTreeft.-A	4850 ± 60	5510	261-262	148.579-436.198/+2.73	TBM	Unpublished (Stouthamer). First published: Berendsen and Stouthamer (2001)
76 (I)	UtC-13770	DeTreeft.-B	4680 ± 70	5510	261-262	148.579-436.198/+2.73	TBM	Unpublished (Stouthamer). First published: Berendsen and Stouthamer (2001)
76 (I)	UtC-13771	DeTreeft.-C	4780 ± 60	5510	261-262	148.579-436.198/+2.73	TBM	Unpublished (Stouthamer). First published: Berendsen and Stouthamer (2001)

Paper code	Lab nr.	Sample name	^{14}C age ± σ (yr BP)	Calendar age (cal yr BP)	Depth below surface (cm)	Coordinates (km)/Surface elevation (m ±O.D.)	Dated material	Source
76 (I)	UtC-13772	DeTreeft.-D	4740 ± 140	5510	261-262	148.579-436.198/+2.73	TBM	Unpublished (Stouthamer). First published: Berendsen and Stouthamer (2001)
77 (I)	UtC-14214	Opheusden 1	2873±48	3010	205-209	174.348-439.194/+6.72	1 Hippuris vulgaris, 19 Ranunculus sceleratus, 1.5 Urtica dioica, 14 Alisma plantago-aquatica, 2.5 Eleocharis palustris, 1 Potentilla sp., 1 Rorippa amphibium, 2 Poaceae caryopsis, 8 Mentha aquatica	Gouw (2007a)
78 (I)	UtC-14215	Opheusden 2	4454±49	5010	295-296	174.348-439.194/+6.72	Alnus: 6 fruits, 1 female catkin scales, 46 male catkin scales, 2 female catkin axis, 1 budscale	Gouw (2007)
79 (I)	UtC-14216	Opheusden 3	5210±49	5960	368-369	174.348-439.194/+6.72	Alnus: 13 budscales, 5 fruits, 6 male catkin scales, 1 female catkin scale, 1 bud; 2 Sparganium erectum	Gouw (2007)
80 (I)	UtC-14217	Opheusden 4	5820±70	6630	481-482	174.348-439.194/+6.72	Alnus: 1.5 fruits, 1 twig, 3 male catkin scales, 2 female catkin scales, 1 budscale; Carex: 6 trigonous nutlets, 4 biconvex nutlets	Gouw (2007)
81 (I)	UtC-14271	Zoowijk 2B	5077±41	5790	240-242	140.317-439.896/+0.64	1 Alnus female catkin	Gouw (2007)
82 (I)	UtC-14272	Zoowijk 1A	4099±47	4600	204-207	140.421-439.11/+0.88	7 Carex trigonous nutlets, 1 Sium latifolium, 2 Oenanthe, aquatica, 5 Alisma plantago-aquatica, 1.5 Ranunculus, acris/repens, 1 Phragmites australis, 2 Rorippa amphibia	Gouw (2007)
83 (I)	UtC-14273	Zoowijk 1C	4383±50	4900	334-336	140.421-439.11/+0.88	5.5 Oenanthe aquatica, 1 Solanum dulcamara, 1 Rorippa amphibia	Gouw (2007)

Paper code	Lab nr.	Sample name	^{14}C age ± σ (yr BP)	Calendar age (cal yr BP)	Depth below surface (cm)	Coordinates (km)/Surface elevation (m ±O.D.)	Dated material	Source
84 (I)	UtC-14279	Voetakkers IV	5340±50	6155	341-342	144.750-430.729/+1.18	12 Alnus fruits	Gouw (2007)
85 (I)	UtC-14280	Voetakkers V	5540±60	6345	450-451	144.750-430.729/+1.18	50 Alisma plantago-aquatica	Gouw (2007)
86 (I)	UtC-14281	Voetakkers VI	6100±50	6955	523-524	144.750-430.729/+1.18	3 Oenanthe aquatica, 25 Lythrum salicaria, 12 Carex, trigonous nutlets, 2 Scirpus lacustris, 3 Mentha aquatica, 0.5 Stachys palustris, 1 Berula erecta, 1 Lycopus europaeus	Gouw (2007)
87 (I)	UtC-14284	Regterweide I	5270±50	5950	453-455	144.941-427.549/+2.25	8 Alisma plantago-aquatica, 5.25 Carex trigonous nutlets, 8 Berula erecta, 5 Alnus fruits	Gouw (2007)
88 (I)	UtC-14285	Regterweide II	5224±49	6165	470-471	144.941-427.549/+2.25	Alnus: 3 fruits, 3 twigs, 3 budscales, 3 male catkin scales	Gouw (2007)
89 (I)	UtC-14286	Regterweide III	5820±60	6585	591-592	144.941-427.549/+2.25	Alnus: 2 twigs, 19 male catkin scales, 2.5 fruits, 1 female catkin scales	Gouw (2007)
90 (I)	UtC-14343	Zoowijk 2A	4525 ± 47	5125	145-146	140.317-439.896/+0.64	9 Carex biconvex nutlets	Gouw (2007)
91 (I)	UtC-14344	Zoowijk 1B	4350 ± 70	4875	290-294	140.421-439.11/+0.88	4 Rorippa amphibia, 9 Typha sp., 0.5 Ranunculus sceleratus, 0.2 Stachys palustris, 1 Phragmites australis, 1 Solanum dulcamara	Gouw (2007)
92 (I)	UtC-14355	Voetakkers I	3100±50	3320	120-122	144.750-430.729/+1.18	Alnus: 1.5 fruit, 8 male catkin scales; 5 Alisma plantago-aquatica 0.5 Carex biconvex nutlet	Gouw (2007)
93 (I)	UtC-14356	Voetakkers VIII	3230±70	3435	183-185	144.750-430.729/+1.18	3 Alisma plantago-aquatica, 12 Urtica, 1 Carex biconvex nutlet, 0.5 Oenanthe aquatica, 1 Carex trigonous nutlet	Gouw (2007)
94 (II)	GrA-24210	Veldwijk 1.1	3200±90	3440	286-290	123.830-456.504/-0.7	6 Carex trig., 2 Stachys palustris, 6 Lythrum	Chapter 5, this thesis

Paper code	Lab nr.	Sample name	^{14}C age ± σ (yr BP)	Calendar age (cal yr BP)	Depth below surface (cm)	Coordinates (km)/Surface elevation (m ±O.D.)	Dated material	Source
95 (II)	GrA-24212	Veldwijk 1.2	4080±95	4550	358-364	123.830-456.504/-0.7	1 Ranuculus acris/repens,1 Alopecurus, 5 Lythrum, 2 Typha, 3 Mentha, 1 Carex bic. (coalified), 8 Carex bic.	Chapter 5, this thesis
96 (I/II)	GrA-24213	Veldwijk 1.3	4670±95	5400	421-427	123.830-456.504/-0.7	4 (1 coalified) Scirpus sylvestris, 9 Mentha, 1 Scirpus lacustris, 2 Eupatorium cannabinum, 1 Carex paniculata sp., 1 Valeriana, 1 Lysimachia	Chapter 5, this thesis
97 (I/II)	GrA-24215	Veldwijk 1.4	5840±95	6580	486-488	123.830-456.504/-0.7	16 1/2 Carex bic., 1 Alnus, 1 1/2 Berula erecta, 9 Typha, 1 Mentha	Chapter 5, this thesis
98 (II)	GrA-24216	Veldwijk 1.5	5890±100	6730	502-506	123.830-456.504/-0.7	4 Berula erecta, 16 Carex bic., 3 Alnus, 1 Lythrum, 1/3 Carex trig., 1 embryo Carex	Chapter 5, this thesis
99 (II)	GrA-42418	Veldwijk 2.1	2825±110	2900	70-76	123.761-456.086/-1.25	3 Mentha, 12 Lythrum, 1 Carex trig., 1/2 Carex bic., 1/3 Caryophyllaceae	Chapter 5, this thesis
100 (II)	GrA-42981	Veldwijk 2.2	3375±40	3600	169-172	123.761-456.086/-1.25	1 1/4 Stachys palustris, 1 Carex trig., 12 Lythrum salicaria, 2 Typha sp., 1 Thalictrum flavum, 1 Viola cf. odorata, 1 galium sp., 6 Ranunculus lingua	Chapter 5, this thesis
101 (II)	GrA-43062	Veldwijk 2.3	4350±45	4870	299-300	123.761-456.086/-1.25	3 Carex bic., 1 Carex trig., 1 Lythrum salicaria, 4 Galium, 1 Mentha aquatica/arvensis	Chapter 5, this thesis
102 (I/II)	GrA-43063	Veldwijk 2.4	5150±60	5910	416-419	123.761-456.086/-1.25	7 Mentha aquatica/arvensis, 2 Lythrum salicaria, 6 Carex trig., 1 Carex bic., 4 Typha sp., 1 Berula erecta	Chapter 5, this thesis
103 (II)	GrA-43068	Veldwijk 2.5	6660±45	7525	527-528	123.761-456.086/-1.25	1 coalified but, 1 but, 2 Galium sp., 1 Berula erecta, 3 Carex bic., 1 Alnus fruit, 2 leave fragments	Chapter 5, this thesis

Appendix 5

Depth-age plots representing Holocene groundwater table rise at core locations *CB-II*, *WO*, *WG*, *PB*, *CB-I* and *OC* (for core locations see Fig. 5.1). Vertical lines denote the standard deviation of the reconstructed groundwater tables. Numbers of samples (dots indicate present-day depth) for which subsidence has been calculated correspond with numbers in Fig. 5.3.

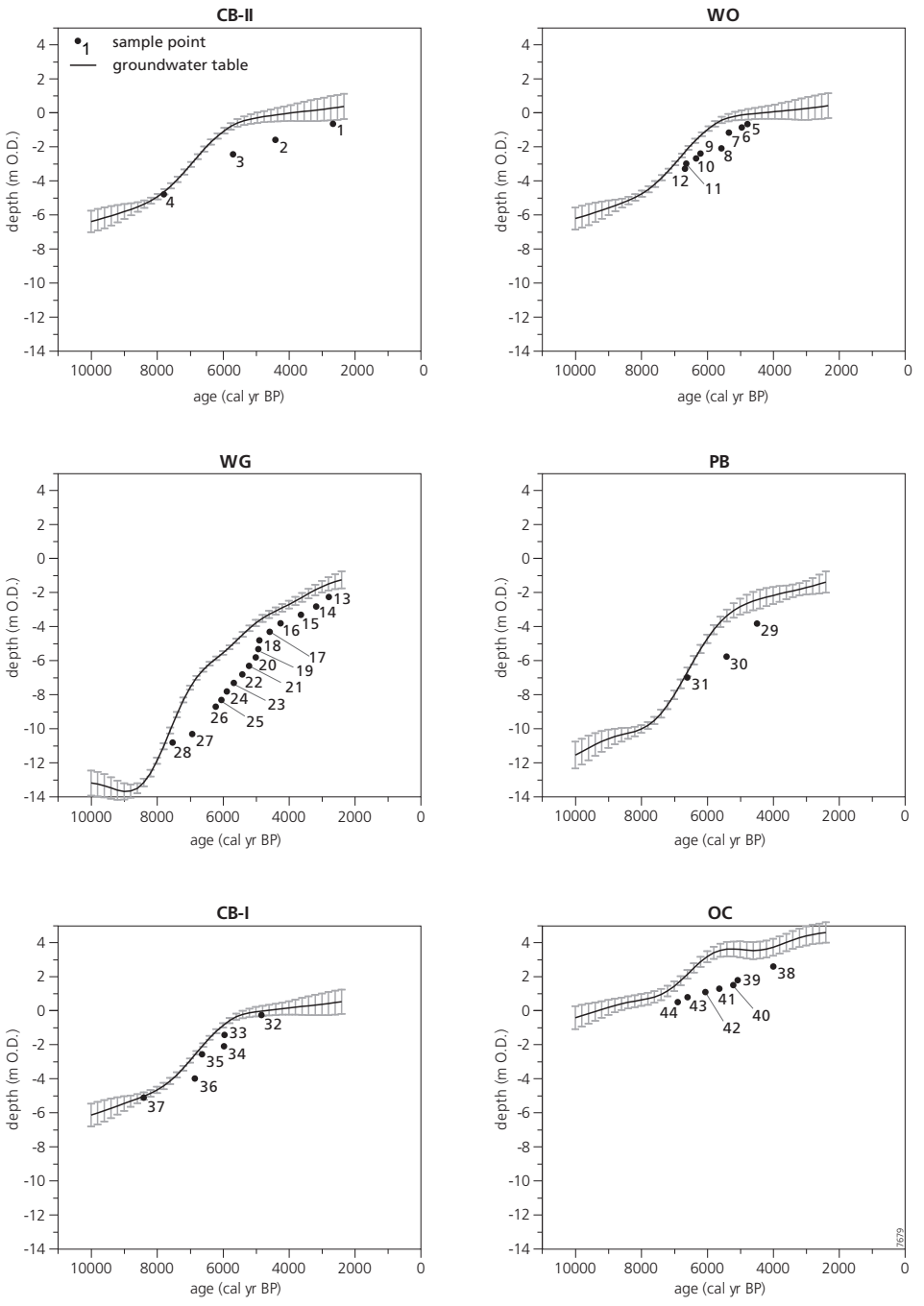
CB-II
sample point
groundwater table
depth (m O.D.)
age (cal yr BP)
WO
WG
PB
CB-I
OC
7679

Appendix 6

Supplementary information for chapter 6 (peat compaction model).

Appendix 6a

Primary compression describes the process during which excess pore water pressure, due to an increase in effective stress, is completely dissipated. Secondary compression, or creep, describes continuing settlement after dissipation of the excess pore pressure under a constant effective stress.

Appendix 6b

Natural strain (ε), also called logarithmic or Hencky strain, is defined as:

$$\varepsilon = -\int_{i=1}^{i=n} \frac{-dh}{h} = -\ln \frac{h}{h_0} \tag{A.1}$$

in which h_0 is the initial thickness (m), h is the current thickness (m) and dh is the change in thickness (m) of layer i (see also Fig. 2.18).

Appendix 6c

The most important assumptions in Equation 6.2 are:

1. The initial effective stress (σ'_0) is assumed to be 1 kPa, and $\sigma' > 1$ kPa. This relatively low value is derived from the assumption that the peat layer is near full saturation throughout the year during time of formation, and that only small groundwater table fluctuations occur. The reference value for t (t_0) is set to 1.
2. Considering the high permeability of recently formed peat, it is assumed that overpressured pore water is fully dissipated at the end of each timestep (in the calibration dataset on average ~115 years, in the model prediction runs usually 50 years).

Appendix 6d

The effective stress of one layer at a certain moment in time is calculated based on Terzaghi's principle of effective stress ($\sigma' = \sigma - u$), in which the total stress (σ; kPa) is calculated by:

$$\sigma = h_{sed}\, \rho_s g \tag{A.2}$$

and the pore water pressure (u; kPa) by:

$$u = h_{water}\, \rho_w g \tag{A.3}$$

with h, the thickness of the overlying sediment (suffix *sed*) or water (suffix *water*) column (m), ρ_s, saturated density of a texture class (kg/m^3), ρ_w, density of water (=1000 kg/m^3) and g, the gravity constant (= 9.81 m/s^2). The ρ_s of a texture class is calculated as:

$$\rho_s = \rho_d + (S\phi\rho_w) \tag{A.4}$$

in which ρ_d is the dry bulk density (g/cm^3), S is the degree of saturation (fraction: taken 0.98 for peat and clay, 0.99 for loamy deposits and 1.0 for sandy deposits) and $\varnothing$ is the porosity, calculated as $\varnothing = 1-(\rho_d/\rho_{mass})$, where ρ_{mass} is the mass density (g/cm^3), calculated using:

$$\rho_{mass} = \frac{1}{\left(f_{org}/1470\right) + \left(f_{clas} f_{clay}/2700\right) + \left(f_{clas} f_{silt}/2650\right) + \left(f_{clas} f_{sand}/2650\right)} \quad \text{(A.5)}$$

in which f_{org}, f_{clas}, f_{clay}, f_{silt} and f_{sand}, fraction of organics, clastics, clay, silt and sand respectively, which were estimated from the American soil texture triangle (www.pedosphere.com). The ρ_d (Equation A.4) of different texture classes was estimated based on field measurements of the dry bulk density (Van Asselen et al., 2010), or, if this data was not available, derived from soil porosity (n) and soil mass density (ρ_{mass}) estimates, using $\rho_d = (1-n)\cdot \rho_{mass}$ (Saxton et al., 1986).

Appendix 6e

I) The model was run for 125000 combinations of the parameters *b*, *c* and *d* (50 different values for each parameter; dots in figures below). The values of parameter *b* ranged from 0 to 0.049, with increments of 0.001, and values of parameters *c* and *d* ranged from 0 to 0.49 with increments of 0.01. Contours of different outcomes of the objective function are indicated with black lines. Parameter combinations within contour 0.00256 (shaded area) are used in model scenarios.

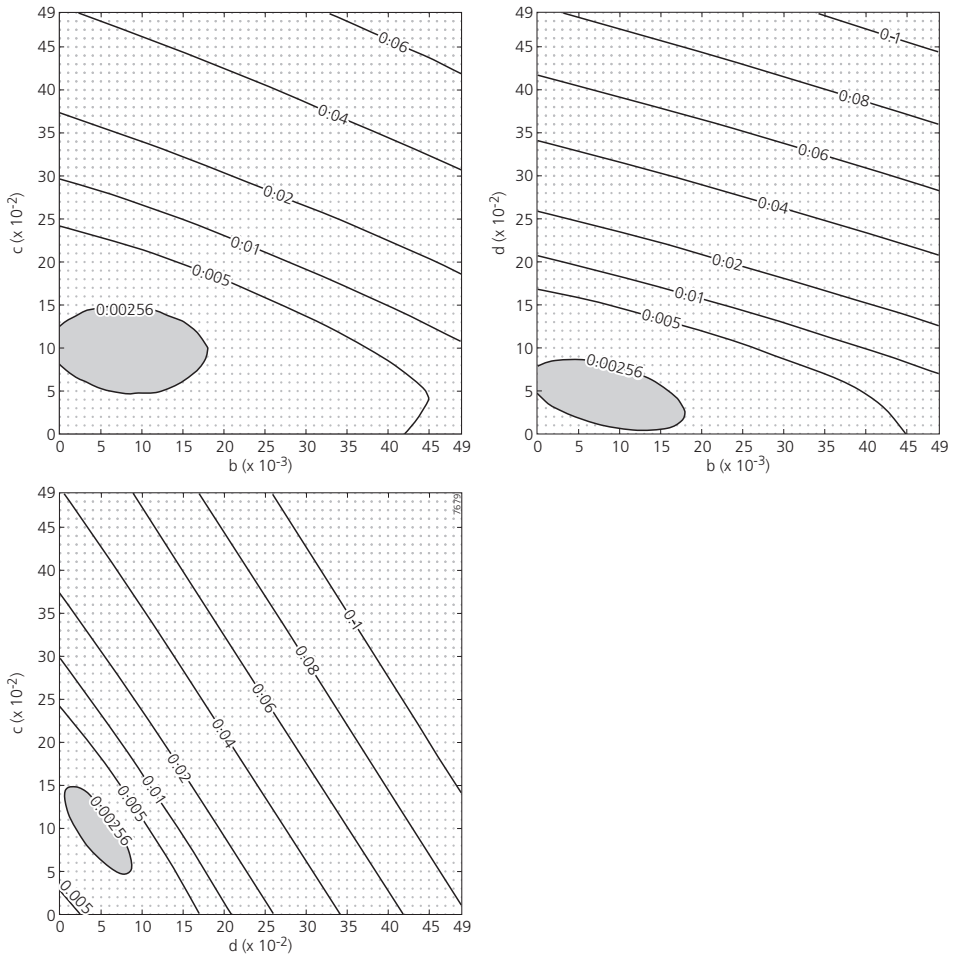

II) The 95% confidence interval was calculated as model outcomes from parameter sets lying within the Φ_{min}+ δ contour in parameter space, where Φ_{min} is the lowest objective function value and δ is (Seber and Wild, 2003; Doherty, 2004):

$$\delta = ns^2F_{\alpha}(n,m-n) \quad \text{(A.6)}$$

in which n is the number of parameters, m is the number of observations in the calibration field dataset, $s^2 = \Phi_{min}/(m-n)$ and F_α is the F-distribution with probability interval $\alpha = 0.05$. For this calibration, $\Phi_{min} + \delta = 0.00252 + 3 \cdot 0.00236/(100-3) \cdot 2.7 = 0.00252 + 0.000197 = 0.00256$. This range comprises a set of 240 parameter combinations, which were used in subsequent model runs. The highest and lowest outcomes of these 240 model predictions for a particular scenario are the boundaries of the 95% confidence interval of the prediction for that scenario. The shaded areas in the plots in Appendix 6e-I define areas in the parameter space where $(\Phi_{min} + \delta) < 0.00256$.

III) The following table presents the lowest objective function resulting from calibration using the field dataset for different equations relating stress and time with natural strain, and using the same ranges of parameter values as outlined in Appendix 6e-I.

Compaction equation	*a*	*b*	Φ_{min}
$\varepsilon = a \cdot \ln(\sigma') + b \cdot \ln(t)$	0.09·LOI+0.05	0.009	0.00236
$\varepsilon = a \cdot (\sigma') + b \cdot (t)$	0.01·LOI+0.006	0.00009	0.00382
$\varepsilon = a \cdot \ln(\sigma') + t^{-b}$	0.1·LOI+0.06	0.7	0.00252
$\varepsilon = \sigma'^{-a} + t^{-b}$	0.25	5.6	0.04122

Appendix 6f

Plot of the modeled vs. observed compaction of all 5-cm-thick peat samples obtained from the 6 cores (core codes in legend) used for calibration, using the parameter set c=0.09, d=0.05 and b=0.009.

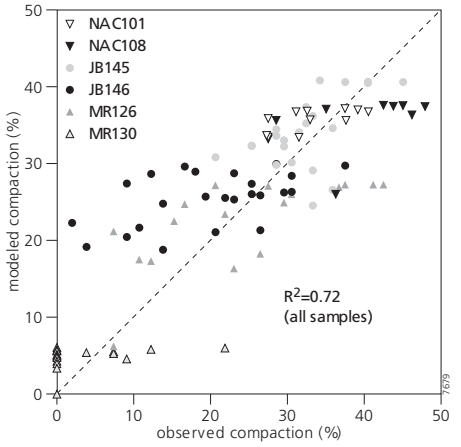

Appendix 6g

Each model run starts with a time period of peat formation, resulting in a peat sequence, followed by a time period of overburden (clay) deposition (both in situation 1; constant base-level rise). Each timestep, a peat or clay layer with an initial uncompacted thickness of 0.05 m is added to the aggrading sequence. With a base-level rise of 0.001 m/yr, the accumulation time of one layer becomes 50 years. In the scenarios presented in this paper, the peat sequence has an *LOI* of 0.5 or 0.8, and the percentage of intercalated 5-cm-thick clay layers is 0% or 20%, which means that respectively none or every fifth layer within the peat sequence is clay. The amount of compaction of a peat sequence is calculated as:

$$compaction = \frac{dh}{h_0} \tag{A.7}$$

in which dh (m) is the total amount of subsidence of the top level due to compaction of the peat sequence and h_0 is the initial thickness of the peat sequence (m; base-level rise multiplied by duration of accumulation of the peat sequence).

During constant-base-level-rise (situation 1; Figure below), accommodation space (acc.sp.) created by compaction of one or more peat layers with thickness h (dark grey) and by a rise of the base level during a timestep (BL_t) is filled up by increased sedimentation of clay (s; grey). During constant-aggradation-rate (situation 2), a constant amount of sediment is deposited at each timestep. If this amount of sediment is not sufficient to fill up the amount of accommodation space created by subsidence due to peat compaction and base-level rise, the new surface elevation is lower than the new base-level height.

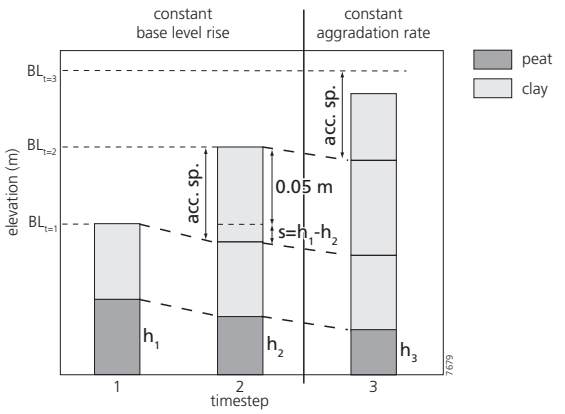

Appendix 6h

Plots of the amount of subsidence or rise versus aggradation rate after 100 years of constant aggradation, in an 8 (a) and 3 (b) meter thick peat layer (*LOI* 0.8) covered by clay deposited over different time periods (t_c=duration of clay deposition).

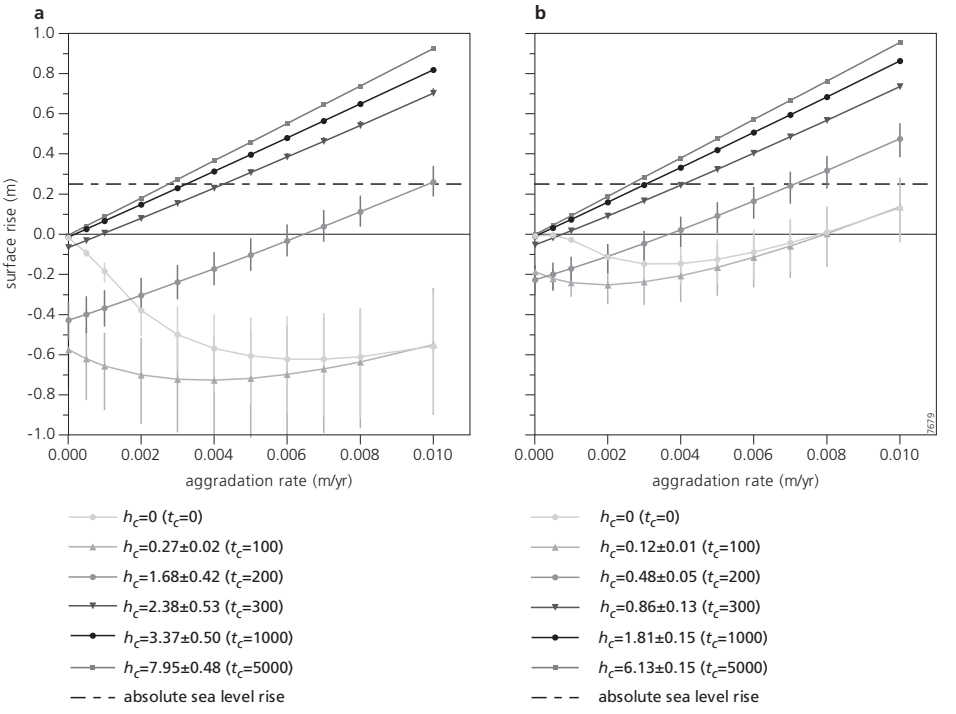

Color figures

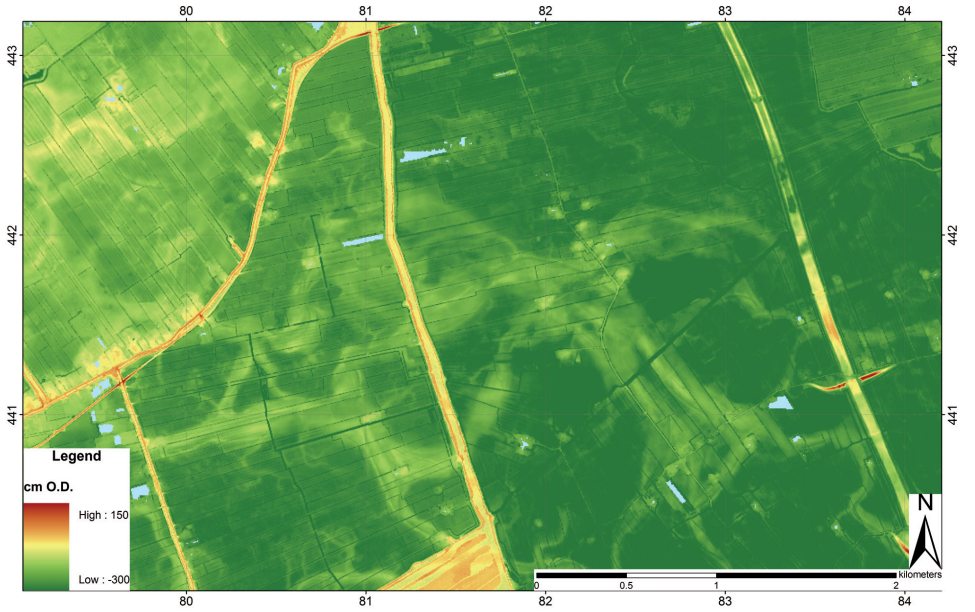

Figure 2.8. Digital Elevation Model (DEM; 5 m resolution). Levees appear as ridges in the landscape after compaction of peat and clay in the floodbasins (near Rotterdam, western Netherlands) (Rijkswaterstaat-AGI, 2005). See also Berendsen and Volleberg (2007).

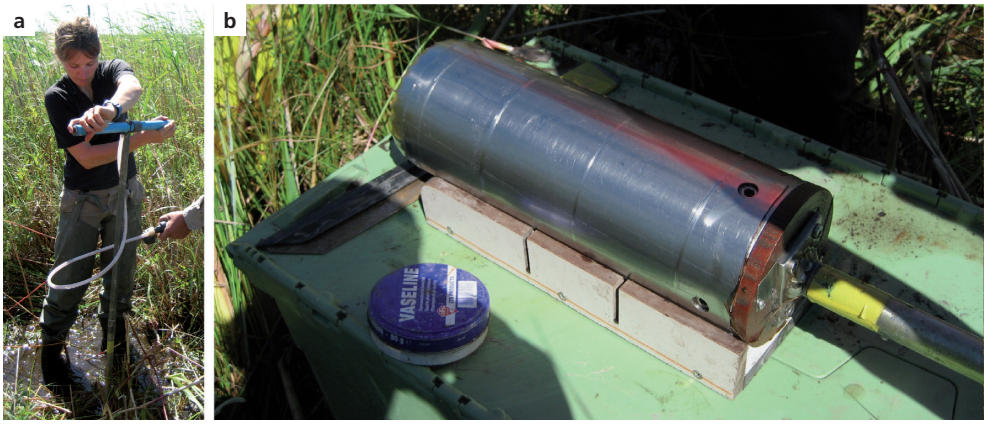

Figure 3.3. a) Coring in a wet fen: the corer is turned to detach the peat sample while using a vacuum pump to create a partial vacuum inside the sampler. b) The corer with fitting device and extension rod still attached, stabilized in a three-sided cradle.

Figure 3.4. Individual liners are separated by using a very thin and sharp knife. The liners are stabilized in the sample cradle.

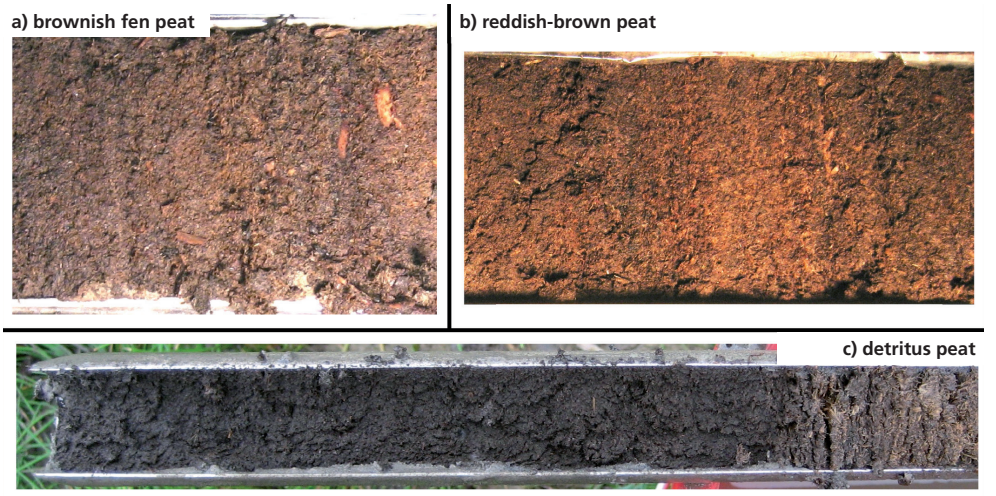

Figure 4.3. Photographs of the main peat types: a) brownish-fen peat, b) reddish-brown peat and c) detritus peat.

NEDERLANDSE GEOGRAFISCHE STUDIES / NETHERLANDS GEOGRAPHICAL STUDIES

360 T VAN DER VALK Technology dynamics, network dynamics and partnering; The case of Dutch dedicated life sciences firms -- Utrecht 2007: Knag/Copernicus Institute. 143 pp, 23 figs, 25 tabs. ISBN: 978-90-6809-402-2, Euro 15,00

361 M A SCHOUTEN Patterns in biodiversity; Spatial organisation of biodiversity in the Netherlands -- Utrecht 2007: Knag/Copernicus Institute. 152 pp, 16 figs, 20 tabs. ISBN: 978-90-6809-403-9, Euro 20,00

362 M H J W VAN AMSTEL – VAN SAANE Twilight on self-regulation; A socio-legal evaluation of conservation and sustainable use of agrobiodiversity by industry self-regulation -- Utrecht 2007: Knag/Copernicus Institute. 167 pp, 15 figs, 13 tabs, 5 box. ISBN: 978-90-6809-404-6, Euro 20,00

363 S MUHAMMAD Future urbanization patterns in the Netherlands, under the influence of information and communication technologies -- Utrecht 2007: Knag/Faculteit Geowetenschappen Universiteit Utrecht. 187 pp, 82 figs, 20 tabs. ISBN: 978-90-6809-405-3, Euro 20,00

364 M GOUW Alluvial architecture of the Holocene Rhine-Meuse delta (The Netherlands) and the Lower Mississippi Valley (U.S.A.) -- Utrecht 2007: Knag/Faculteit Geowetenschappen Universiteit Utrecht. 192 pp, 55 figs, 14 tabs. ISBN: 978-90-6809-406-0**,** Euro 22,00

365 E HEERE & M STORMS Ormeling's cartography; Presented to Ferjan Ormeling on the occasion of his 65th birthday and his retirement as Professor of Cartography -- Utrecht 2007: Knag/Faculteit Geowetenschappen Universiteit Utrecht. ISBN: 978-90-6809-407-7, Euro 20,00

366 S QUARTEL Beachwatch; The effect of daily morphodynamics on seasonal beach evolution -- Utrecht 2007: Knag/Faculteit Geowetenschappen Universiteit Utrecht. 125 pp, 39 figs, 7 tabs. ISBN: 978-90-6809-408-4, Euro 12,50

367 R O VAN MERKERK Intervening in emerging nanotechnologies; A CTA of Lab-on-a-chip technology regulation -- Utrecht 2007: Knag/Copernicus Institute. 206 pp, 19 box, 35 figs, 12 tabs. ISBN: 978-90-6809-409-1, Euro 20,00

368 R M FRINGS From gravel to sand; Downstream fining of bed sediments in the lower river Rhine -- Utrecht 2007: Knag/Faculteit Geowetenschappen Universiteit Utrecht. ISBN: 978-90-6809-410-7**,** Euro 25,00

369 W IMMERZEEL Spatial modelling of the hydrological cycle, climate change and agriculture in mountainous basins -- Utrecht 2008: Knag/Faculteit Geowetenschappen Universiteit Utrecht. 147 pp, 54 figs, 12 tabs. ISBN: 978-90-6809-411-4, Euro 25,00

370 D S J MOURAD Patterns of nutrient transfer in lowland catchments; A case study from northeastern Europe -- Utrecht 2008: Knag/Faculteit Geowetenschappen Universiteit Utrecht. 176 pp, 44 figs, 19tabs. ISBN: 978-90-6809-412-1**,** Euro 20,00

371 M M H CHAPPIN Opening the black box of environmental innovation; Governmental policy and learning in the Dutch paper and board industry -- Utrecht 2008: Knag/Copernicus Institute. 202 pp, 41 figs, 30 tabs. ISBN: 978-90-6809-413-8, Euro 22,50

372 R P ODDENS & M VAN EGMOND Ormelings atlassen; Catalogus van atlassen geschonken aan de Universiteit Utrecht door de hoogleraren F.J. Ormeling sr. en jr. – Utrecht 2008: Knag/Faculteit Geowetenschappen Universiteit Utrechts. ISBN: 978-90-6809-415-2, Euro 15,00

373 R VAN MELIK Changing public space; The recent redevelopment of Dutch city squares – Utrecht 2008: Knag/Faculteit Geowetenschappen Universiteit Utrecht. 323 pp, 47 figs, 32 tabs. ISBN: 978-90-6809-416-9, Euro 20,00

374 E ANDRIESSE Institutions and regional development in Southeast Asia; A comparative analysis of Satun (Thailand) and Perlis (Malaysia) -- Utrecht 2008: Knag/Faculteit Geowetenschappen Universiteit Utrecht. 250 pp, 42 figs, 43 tabs, 18 box. ISBN: 978-90-6809-417-6, Euro 25,00

375 E HEERE GIS voor historisch landschapsonderzoek; Opzet en gebruik van een historisch GIS voor prekadastrale kaarten -- Utrecht 2008: Knag/Faculteit Geowetenschappen Universiteit Utrecht. 231 pp, 73 figs, 13 tabs. ISBN: 978-90-6809-418-3, Euro 30,00

376 V D MAMADOUH, S M DE JONG, J F C M THISSEN & J A VAN DER SCHEE Dutch windows on the Mediterranean; Dutch Geography 2004-2008 -- Utrecht 2008: Knag/International Geographical Union Section The Netherlands. 104 pp + cd-rom, 38 figs, 9 tabs. ISBN: 978-90-6809-419-0, Euro 10,00

377 E VAN MARISSING Buurten bij beleidsmakers; Stedelijke beleidsprocessen, bewonersparticipatie en sociale cohesie in vroeg-naoorlogse stadswijken in Nederland -- Utrecht 2008: Knag/Faculteit Geowetenschappen Universiteit Utrecht. 230 pp, 6 figs, 31 tabs. ISBN: 978-90-6809-420-6, Euro 25,00

378 M DE BEER, R C L BUITING, D J VAN DRUNEN & A J T GOORTS (Eds.) Water Wegen; Op zoek naar de balans in de ruimtelijke ordening -- Utrecht 2008: Knag/VUGS/Faculteit Geowetenschappen Universiteit Utrecht. 91 pp, 18 figs, 1 tab. ISBN: 978-90-6809-421-3, Euro 10,00

379 J M SCHUURMANS Hydrological now- and forecasting; Integration of operationally available remotely sensed and forecasted hydrometeorological variables into distributed hydrological models -- Utrecht 2008: Knag/Faculteit Geowetenschappen Universiteit Utrecht. 154 pp, 65 figs, 12 tabs. ISBN 978-90-6809-422-0, Euro 15,00

380 M VAN DEN BROECKE Ortelius' *Theatrum Orbis Terrarum* (1570-1641); Characteristics and development of a sample of *on verso* map texts -- Utrecht 2009: Knag/Faculteit Geowetenschappen Universiteit Utrecht. 304 pp + cd-rom, 9 figs, 65 tabs. ISBN 978-90-6809-423-7, Euro 30,00

381 J VAN DER KWAST Quantification of top soil moisture patterns; Evaluation of field methods, process-based modelling, remote sensing and an integrated approach -- Utrecht 2009: Knag/Faculteit Geowetenschappen Universiteit Utrecht. 313 pp, 108 figs, 47 tabs. ISBN 978-90-6809-424-4, Euro 30,00

382 T J ZANEN 'Actie, actie, actie…'; De vakbeweging in regio Noord-Nederland, 1960-1992 -- Utrecht/ Groningen 2009: Knag/Faculteit Ruimtelijke Wetenschappen Rijksuniversiteit Groningen. ISBN 978-90-6809-425-1, Euro 30,00

383 M PERMENTIER Reputation, neighbourhoods and behaviour -- Utrecht 2009: Knag/Faculteit Geowetenschappen Universiteit Utrecht. 146 pp, 10 figs, 19 tabs. ISBN 978-90-6809-426-8, Euro 15,00

384 A VISSER Trends in groundwater quality in relation to groundwater age -- Utrecht 2009: Knag/Faculteit Geowetenschappen Universiteit Utrecht. 188 pp, 47 figs, 24 tabs. ISBN 978-90-6809-427-5, Euro, 20,00

385 B A FURTADO Modeling social heterogeneity, neighborhoods and local influences on urban real estate prices; Spatial dynamic analyses in the Belo Horizonte metropolitan area, Brazil -- Utrecht 2009: Knag/Faculteit Geowetenschappen Universiteit Utrecht. 236 pp, 50 figs, 48 tabs. ISBN 978-90-6809-428-2, Euro 25,00

386 T DE NIJS Modelling land use change; Improving the prediction of future land use patterns -- Utrecht 2009: Knag/Faculteit Geowetenschappen Universiteit Utrecht. 206 pp, 59 figs, 32 tabs. ISBN 978-90-6809-429-9, Euro 25,00

387 I J VISSEREN-HAMAKERS Partnerships in biodiversity governance; An assessment of their contributions to halting biodiversity loss -- Utrecht 2009: Knag/Copernicus Institute. 177 pp, 4 figs, 4 tabs. ISBN 978-90-6809-430-5, Euro 20,00

388 G ERKENS Sediment dynamics in the Rhine catchment; Quantification of fluvial response to climate change and human impact -- Utrecht 2009: Knag/Faculteit Geowetenschappen Universiteit Utrecht. 278 pp + addendum, 59 figs, 27 tabs. ISBN 978-90-6809-431-2, Euro 30,00

389 M HIJMA From river valley to estuary; The early-mid Holocene transgression of the Rhine-Meuse valley, The Netherlands -- Utrecht 2009: Knag/Faculteit Geowetenschappen Universiteit Utrecht. ISBN 978-90-6809-432-9, Euro 25,00

390 N L M B VAN SCHAIK The role of Macropore Flow from PLOT to catchment scale; A study in a semi-arid area -- Utrecht 2010: Knag/Faculteit Geowetenschappen Universiteit Utrecht. 174 pp, 65 figs, 26 tabs. ISBN 978-90-6809-433-6, Euro 20,00

391 B DOUCET Rich cities with poor people; Waterfront regeneration in the Netherlands and Scotland -- Utrecht 2010: Knag/Faculteit Geowetenschappen Universiteit Utrecht. 208 pp, 49 figs, 13 tabs. ISBN 978-90-6809-434-3, Euro 25,00

392 L PAPE Predictability of nearshore sandbar behaviour -- Utrecht 2010: Knag/ Faculteit Geowetenschappen Universiteit Utrecht. 157 pp, 36 figs, 5 tabs. ISBN 978-90-6809-435-0, Euro 17,50

393 M M VAN HUIJSTEE Business and NGOs in interaction; A quest for corporate social responsibility -- Utrecht 2010: Knag/Copernicus Institute. 176 pp, 4 figs, 8 tabs. ISBN 978-90-6809-436-7, Euro 24,00

394 A KOKX Between dreams and reality; Urban governance in the process of Dutch urban restructuring -- Utrecht 2010: Knag/Faculteit Geowetenschappen Universiteit Utrecht. 172 pp, 6 figs, 4 tabs. ISBN 978-90-6809-437-4, Euro 20,00

395 S VAN ASSELEN Peat compaction in deltas; Implications for Holocene delta evolutions -- Utrecht 2010: Knag/Faculteit Geowetenschappen Universiteit Utrecht. ISBN 978-90-6809-438-1, Euro 17,50

For a complete list of NGS titles please visit www.knag.nl. Publications of this series can be ordered from KNAG / NETHERLANDS GEOGRAPHICAL STUDIES, P.O. Box 80123, 3508 TC Utrecht, The Netherlands (E-mail info@knag.nl; Fax +31 30 253 5523). Prices include packing and postage by surface mail. Orders should be prepaid, with cheques made payable to "Netherlands Geographical Studies". Please ensure that all banking charges are prepaid. Alternatively, American Express, Eurocard, Access, MasterCard, BankAmericard and Visa credit cards are accepted (please specify card number, name as on card, and expiration date with your signed order).